Technische Universität München

Fakultät für Medizin

Klinik für Herz- und Gefäßchirurgie des Deutschen Herzzentrums München

Characterization of miR-128a in early cardiac development

Sarah Catherine Hölscher

Vollständiger Abdruck der von der Fakultät für Medizin der Technischen Universität München zur Erlangung des akademischen Grades eines

Doktors der Naturwissenschaften (Dr. rer. nat.)

genehmigten Dissertation.

Vorsitzende/r: Prof. Dr. Dr. Stefan Engelhardt

Prüfer der Dissertation:

1. apl. Prof. Dr. Markus Krane
2. Prof. Angelika Schnieke, Ph.D.

Die Dissertation wurde am 23.06.2020 bei der Fakultät für Medizin der Technischen Universität München eingereicht und durch die Fakultät für Medizin am 29.12.2020 angenommen.

“**Science will never be a finished book**.”

- Albert Einstein (1879-1955) -

Publication

Parts of the presented work have been published as:

Hoelscher, S. C., Stich, T., Diehm, A., Lahm, H., Dressen, M., Zhang, Z., Neb, I., Aherrahrou, Z., Erdmann, J., Schunkert, H., Santamaria, G., Cuda, G., Gilsbach, R., Hein, L., Lange, R., Hassel, D., Krane, M., and Doppler, S. A. (2020). miR-128a Acts as a Regulator in Cardiac Development by Modulating Differentiation of Cardiac Progenitor Cell Populations. *Int J Mol Sci, 21*(3). doi:10.3390/ijms21031158 (Hoelscher *et al.*, 2020).

Table of Contents

List of Abbreviations and Acronyms

‘	minutes
“	seconds
%	percentage
°C	degree Celsius
~	approximately
3p (3’)	3 prime
5p (5’)	5 prime
ATP	adenosine triphosphate
AU	arbitrary units
bHLH	basic helix-loop-helix
bp	base pairs
bpm	beats per minute
BSA	bovine serum albumin
BSL-2	biosafety level 2
cDNA	complementary DNA
CE	cardiac enhancer
CF	cardiac fibroblast
CHD	congenital heart disease
CM	cardiomyocytes
CMV	cytomegalovirus
Comp	fluorescence compensation
CPCs	cardiac progenitor cells
Cre	Cre recombinase
Ct	threshold cycle value
Ctr	control
CyTUM	flow cytometry unit of the TUM
D	day(s)
d.p.c.	days post coitum
DAPI	4,6-Diamidino-2-phenylindol
dATP	deoxyadenosine triphosphate
dCTP	deoxycytidine triphosphate

DEPC	diethyl pyrocarbonate
dGTP	deoxyguanosine triphosphate
dH_20	distilled water
DMEM	Dulbecco's Modified Eagle Medium
DMSO	dimethyl Sulfoxide
DNA	deoxyribonucleic acid
DNase	deoxyribonuclease
dNTP(s)	deoxynucleotide triphosphate(s)
dox	doxycycline
DTT	1,4-Dithiothreitol
dTTP	deoxythymidine triphosphate
E	embryonic day
E. coli	Escherichia coli
EB	embryoid body
EC	endothelial cell
EDTA	ethylenediaminetetraacetic acid
eGFP	enhanced GFP
EMT	epithelial-mesenchymal transition
ESC	embryonic stem cells
FACS	fluorescent activated cell sorting (flow cytometry)
FC	fold change
FCS	fetal calf serum
FHF	first heart field
FITC	Fluorescein-5-isothiocyanat
for	forward
FSC	forward scatter light
GFP	green fluorescent protein
GTP	guanosine 5'-triphosphate
h	hours
HBSS	Hank's Balanced Salt Solution
HEK	human embryonic kidney cells
hiPSC(s)	human iPSC(s)
hpf	hours post fertilization
ICC	Immunocytochemistry
IFT	inflow tract
IgG	Immunoglobulin G
iITG	induced Isl1Cre/$R26^{mTmG}$ pluripotent stem cells

IMDM	Iscove’s Modified Dulbecco’s Medium
iPSC(s)	induced pluripotent stem cell(s)
IRES	internal ribosome entry site
kb	kilobase
KO	knockdown
LB	lysogen broth
LIF	leukemia inhibitory factor
LNA	locked nucleotide acid
loxP	locus of X-over P1
LTR	long terminal repeat
LV	lentivirus
M-MLV	moloney murine leukemia virus
MEF	murine embryonic fibroblasts
mG	membrane tagged GFP
miR(s)	microRNA(s)
ml	milliliter
MO(s)	morpholino-modified oligonucleotide(s)
mRNA	messenger RNA
mT	membrane tagged tdTomato
MTT	3-(4,5-Dimethylthiazol-2-yl)-2,5-Diphenyltetrazoliumbromid
mu	murine
n.a.	not available
NCBI	National Center for Biotechnology Information
NEAA	non-essential amino acids
Neo	neomycin
NkxCE	Nkx2.5 cardiac enhancer
nm	nanometer
nt	nucleotide
OE	overexpression
OFT	outflow tract
p	passage
P21	postnatal day 21
PB	polybrene
PBMCs	peripheral blood mononuclear cells
PBS	phosphate buffered saline
PBS-T	phosphate buffered saline w/Triton-X
PCR	polymerase chain reaction

PE	Phycoerythrin
Pen/Strep	Penicillin/Streptomycin
pre-miR	precursor miR
pri-miR	primary miR
PS	primitive streak
puro	puromycin
qRT-PCR	quantitative real time PCR
R26	ROSA26 (reverse oriented splice acceptor lone 26)
R3HDM1	R3H domain containing 1
rev	reverse
RFP	red fluorescent protein
RISC	RNA-induced silencing complex
RNA	ribonucleic acid
RNAseq	RNA Sequencing
rpm	revolutions per minute
RRE	Reverse Response Element
RT	room temperature
rtTA	reverse tetracycline transcriptional activator
S.E.M	standard error of the mean
S.O.C	super optimal broth
SAN	sinoatrial node
SHF	second heart field
SMC	smooth muscle cells
SSC	side scatter light
STEMCCA	stem cell cassette
SV	sinus venosus
SV40	simian virus 40
TBE	TRIS-Borat-EDTA
td	tandem dimer
TE	TRIS-EDTA
tet	tetracycline
tet-on	tetracycline inducible
tetO	tetracycline operator
TF(s)	transcription factor(s)
tRFP	turbo red fluorescent protein
TRIS	tris(hydroxymethyl)aminomethane
TTF	tail tip fibroblasts

TU	transduction unit
U	units
UTR	untranslated region
v/v	volume by volume
w/	with
w/o	without
w/v	weight by volume
wk(s)	weeks
WPRE	woodchuck hepatitis posttranscriptional regulatory element
Δ	delta
µ	micro
µl	microliter

List of Figures

List of Tables

Abstract

MicroRNAs (miRs) are major players in regulatory networks guiding cardiogenesis. However, the impact of a large number of miRs on heart development is yet poorly understood. In our study, we sought to identify miRs with unknown functions during cardiac development and analyzed the microRNA profile of a specific multipotent cardiac progenitor cell (CPC) population that is marked by GFP upon the activation of a 2.1kb Nkx2.5 cardiac enhancer element (NkxCE). Besides well-known candidates like miR-1 and miR-133a, we found 40 miRs highly enriched in these NkxCE-GFP CPCs. Among those were miR-20b, miR-30a, miR-30b, as well as miR-128a which were chosen for further analysis based on literature research, evaluation of evolutionary conservation and expression kinetics. Morpholino (MO)-induced knockdown of these candidate miRs in zebrafish revealed that miR-128a knockdown robustly affected cardiac development causing significantly smaller ventricles, abnormal heart looping and impaired cardiac function. To analyze the role of miR-128a during early cardiogenesis in more detail, we further conducted loss- and gain-of-function experiments during *in vitro* differentiations of different transgenic murine embryonic and induced pluripotent stem cell lines (ESCs/iPSCs). We demonstrated that (1) miR-128a knockdown increased the expression of cardiac transcription factors (TFs) such as *Isl1*, *Sfrp5,* and *Hcn4* but reduced *Irx4* at the onset of cardiogenesis. (2) *Isl1*-positive CPCs were upregulated whereas above-mentioned NkxCE-GFP CPCs were downregulated. (3) The downregulation of miR-128a was associated with increased expression of the ventricular cardiomyocyte marker *Myl2* and attended by a reduced beating frequency of early cardiomyocytes (4) Overexpression of miR-128a diminished the expression of *Isl1, Sfrp5, Nkx2.5, Mef2c* but increased *Irx4* (5) The NkxCE-GFP CPC population was enhanced and (6) *Tnnt2, Myh6* and *Shox2* expression was favored (nodal-type-like cardiomyocytes) upon miR-128a overexpression accompanied by increased beating frequencies. Conclusively, our study demonstrated, for the first time, that miR-128a plays a so far unknown role in early cardiac development by regulating CPC specification and CPC differentiation. Our results contribute to a more complete picture of miRs involved in cardiac development and by this provide a basis to identify further new strategies for regenerative approaches to treat cardiac disease in future.

1 Introduction

The heart is an indespensible organ that ensures overall survival in mammals. By pumping blood through the circulatory system, it provides oxygen and nutrition to all organs as well as assistance in the removal of metabolic waste (Harvey, 2002).

While sharing those important functions, the hearts of vertrebrates come in different shapes that became more and more complex throughout evolution. Whereas fish such as the zebrafish (*Danio rerio*) have two-chambered hearts with only one ventricle and atrium, most amphibians and reptiles display a three-chambered heart that has one ventricle and two atria. This evolutionary step naturally coincided with the development of the lungs and led to a first separation of pulmonary and systemic circulation which, at least in part, led to further improved oxygenation capacity (Jensen *et al.*, 2013). The most efficient cardiovascular system is found in higher vertebrates such as most birds and mammals including mice (*Mus musculus*) or humans *(Homo sapiens)* and is characterized by four-chambered hearts with two ventricles and two atria, respectively. It enables a fully closed, so called “double circulatory system” that completely separates pulmonary from systemic circulation (Harvey, 2002; Jensen *et al.*, 2013). Given its extraordinary importance, the heart is the first functional organ that develops during the embryogenesis of vertebrates (Hoelscher *et al.*, 2017; Zaffran and Frasch, 2002).

1.1 Early cardiac development

Despite the striking differences described in size and shape of hearts, especially between lower vertebrates (fish) and higher vertebrates (mouse, humans), the basic building plan of all vertebrate hearts is remarkably well conserved throughout evolution (Jensen *et al.*, 2013). In fact, most of the below described milestones of cardiogenesis including their underlying signaling pathways and transcriptional machineries, are highly similar and highly conserved between vertebrate species (Fishman and Chien, 1997; Poon and Brand, 2013).

In most vertebrates, early cardiogenesis starts with gastrulation, one of the hallmarks of embryogenesis that is defined as a dynamic cellular process that ultimately results in the formation of the three germ layers: ectoderm, mesoderm, and endoderm (Van Vliet *et al.*, 2012).

The beginning is marked by the generation of a transient structure in the epiblast, the so-called primitive streak (PS), which ultimately forms the posterior end of the embryo (Tam and Behringer, 1997). After undergoing epithelial-mesenchymal transition (EMT), a subset of epiblast cells ingresses through the PS and then further egresses either as mesodermal or endodermal derivatives (Duelen and Sampaolesi, 2017). The time as well as location of cell ingression through the PS mainly determines the fate of the cells. Since the heart is the first functional organ during development, cells with cardiac commitment are among the first to migrate through the PS during gastrulation (Brade *et al.*, 2013). They further egress to their designated topographical position to an anterior lateral region relative to the streak, where they finally build the cardiac mesoderm around embryonic day 6.5 (E6.5) in mice and roughly embryonic day 15 in humans. Cardiac mesoderm contains specific cell populations that will develop into the inner lining of the heart (endocardium) and heart muscle (myocardium) (Brade *et al.*, 2013; Van Vliet *et al.*, 2012). The induction of cardiac mesoderm is controlled by complex interaction of molecular networks including noncanonical Wnt and Wnt/β-catenin signaling which are both among the most essential regulatory pathways guiding cardiogenesis (Cohen *et al.*, 2008; Sklepkiewicz *et al.*, 2015). Wnt signaling not only regulates the induction of cardiac mesoderm but also subsequent steps when the migration of endocardial and myocardial progenitor cells into the medial region of the embryo begins. There, they form the so-called cardiac crescent, a crescent-shaped area that becomes visible at E7.5 in mice and around day 17 in humans (Brade *et al.*, 2013; Ivanovitch *et al.*, 2017). At this stage, the cardiac fate of these cardiac progenitor cells (CPCs) gets further specified. CPCs will later form the heart by differentiating into various types of cardiac lineages.

The first wave of cells undergoing differentiation is positioned in the anterior region at the outmost rim of the cardiac crescent and referred to as first heart field (FHF) progenitors. The induction process of these cells might be due to its exposed position in the embryo in which they encounter immediate contact with cytokines and inhibitors of the Wnt signaling pathway (Brade *et al.*, 2013; Marvin *et al.*, 2001; Noseda *et al.*, 2011; Reifers *et al.*, 2000; Schneider and Mercola, 2001; Schultheiss *et al.*, 1997; Tzahor and Lassar, 2001). While FHF-CPCs further build a linear heart tube by cell fusion to the midline of the embryo at E8 in mice (around day 17-19 in humans), other progenitor cells yet remain undifferentiated at this stage referred to as second heart field (SHF) progenitors. They gradually migrate into the heart tube at later stages during cardiac looping taking place around E8.5 in mice and around day 19-20 in humans (Kelly *et al.*, 2014) and then differentiate into cardiac lineages. The induction of SHF progenitors also relies on several signaling pathways not only including noncanonical Wnt signaling but also Notch signaling, another essential pathway that coordinates cell fate decisions during heart development (de la Pompa and Epstein, 2012; Pedrazzini, 2007).

In vivo lineage tracing and fate mapping studies revealed that after specification and differentiation, FHF and SHF progenitor populations will contribute to different structures of the heart. While FHF progenitors mainly develop into cardiac lineages of the left ventricle and the cardiac conduction system (Buckingham *et al.*, 2005; Domian *et al.*, 2009), SHF progenitors mainly contribute to the right ventricle, the outflow tract (OFT), the atria and the inflow tract (IFT)(Colombo *et al.*, 2018).

However, the specification process is not only dependent on above-mentioned pathways but also relies on spatiotemporal activation of molecular and transcriptional networks and regulators. These become activated, in part, by crosstalk interactions with these pathways (Boni et al., 2008; Gessert and Kuhl, 2010). This happens already at very early stages of cardiogenesis and is necessary to further define progenitor cell specification and cardiac fate (Cambier *et al.*, 2014). Among those regulators are specific sets of transcription factors (TFs) such as members of the Nkx-, Gata-, Tbx- and Mef2 families including *Gata4, Tbx5 and Mef2c* and others like *Isl1, Irx4*, *Sfrp5 or Hcn4* that are dynamically expressed as early as E7.5 in the cardiac crescent by FHF and SHF progenitors (Fujii *et al.*, 2017; Laugwitz *et al.*, 2008; Nelson *et al.*, 2016; Rana *et al.*, 2013; Spater *et al.*, 2013).

While some TFs including *Gata4, Nkx2.5, Mef2c* and *Isl1* and *Sfpr5* are temporarily expressed in both heart fields (Dodou *et al.*, 2004; Fujii *et al.*, 2017; Ivanovitch *et al.*, 2017; Laugwitz *et al.*, 2008; Molkentin *et al.*, 1997), the expression of other TFs such as *Tbx5, Hcn4* and *Irx4* are restricted predominantly to progenitors of the FHF or other ventricular-specific progenitor cell pools (Bruneau *et al.*, 1999; Nelson *et al.*, 2016; Spater *et al.*, 2013).

Given this dynamic expression pattern of TFs, FHF and SHF progenitors cannot be unambiguously identified depending on their gene expression pattern. However, at the same time, the transcriptional signature of progenitors undoubtable defines their cardiac fate, thus, to some extent TFs do serve as marker genes that also indicate cardiac commitment of CPCs (Clark *et al.*, 2013; Zhang *et al.*, 2014). Together, the well-orchestrated and tightly regulated interactions of cardiac TFs and signaling pathways ultimately ensure proper cardiac development including processes such as the induction, specification and differentiation of cardiac progenitors.

Ultimately, this leads to a defined chambered heart morphology that can be seen starting at E10.5 of murine development and around day 32 in humans which further evolves into an organ that shows fully-septated chambers and outflow tracts at E14.5 (around day 42 in humans) (Brade *et al.*, 2013).

Three major cardiac cell lineages can be distinguished that include endothelial cells (ECs), smooth muscle cells (SMCs) and several subtypes of cardiomyocytes (CMs). ECs predominately form the interior lining of the heart and blood vessels where they, in support of SMCs, fulfill essential functions of cardiovascular homeostasis such as the regulation of

vascular permeability or the diameter of blood vessels in response to changing demands (Brutsaert, 2003).

CMs make up most of the cardiac mass and are crucial for contractile performance. While most atrial and ventricular CMs are part of the so called “working myocardium” that inherit basic contractile functions, some specialized CMs referred to as “nodal -like CMs” form the conduction system which is essential for the generation and coordinated spread of electrical activity (Sedmera and McQuinn, 2008).

Over the last decades, many of the networks that guide cardiac development have been uncovered, not at least due to increasing numbers of elegant transgenic models that have been used to investigate nearly every facet of cardiogenesis (1.2).

1.2 Model organisms to study early cardiac development

Studying normal cardiac development is crucial to understand how malfunctions during embryogenesis can lead to cardiac disease such as congenital heart disease (CHD) that are still the leading cause of infant’s death (Hoelscher *et al.*, 2017).

Since early cardiogenesis is highly conserved in vertebrate species, genetic approaches, especially in mice (Sperling, 2011), have made significant contributions to a deeper understanding of the mechanisms guiding heart formation of vertebrates, including humans. Other model organisms such as the zebrafish have entered the field of cardiovascular research not at least due to their easy genetic tractability, external fertilization and optical transparency (Bakkers, 2011; Nguyen *et al.*, 2008; Stainier, 2001; Tu and Chi, 2012). Given the complexity of interacting genes, proteins, cells and signaling pathway, however, a full picture of cardiogenesis is still evolving.

A range of transient knockdown or overexpression strategies as well as stable knock in or deletion of genes in animal models has been applied successfully to study their impact on cardiogenesis *in vivo* (Hoelscher *et al.*, 2017).

In addition, reporter systems enable the tracking of specific cell populations (e.g. CPCs) to determine their fate or investigate their impact after genetic manipulations. Here, reporters such as the green or red fluorescent protein (*GFP* or *RFP*) are utilized which are introduced into specific genetic loci. Reporter gene expression is, in most cases, controlled by an upstream located regulatory element or gene that is spatiotemporal activated throughout cardiogenesis (Lien *et al.*, 1999; Wu *et al.*, 2006).

Since CPC populations are characterized by dynamic expression of cardiac TFs, many reporter systems have used their regulatory elements (promoters, enhancer) to label specific cell pools.

By this, tracking of *Srfp5*-, *Irx4*, *Hcn4, Isl1- or Nkx2.5*- expressing cells is enabled, amongst others (Andersen *et al.*, 2018; Fujii *et al.*, 2017; Moretti *et al.*, 2006; Muzumdar *et al.*, 2007; Nelson *et al.*, 2016). However, although all the above-mentioned TFs mark specific CPC populations, not all of them are exclusively expressed in the developing heart. The expression domain of murine *Nkx2.5*, for instance, encompasses many tissues, including the thyroid, pharynx, stomach, and spleen (Moses *et al.*, 2001; Wu *et al.*, 2006), conclusively also labelling cells that reside in other organs and tissues.

To achieve cardiac-specific labelling, an *Nkx2.5* cardiac enhancer-eGFP (NkxCEeGFP) reporter mouse was developed by the use of a 2.1 kb *Nkx2.5* enhancer element located 9.5 kb upstream of the translation start site (ATG-site) of *Nkx2.5* along with a 500 bp base promoter followed by an eGFP (Figure 1). The enhancer is able to fully recapitulate the expression pattern of the endogenous *Nkx2.5* gene exclusively in the heart (Lien *et al.*, 1999; Wu *et al.*, 2006). It thereby labels, upon activation, a specific pool of multipotent CPCs (NkxCE-GFP CPCs) in the embryonic heart at E8.5 - E15.5 (Wu *et al.*, 2006) (Figure 1).

In accordance with the endogenous *Nkx2.5* expression, CPCs marked by the activated NkxCE have been shown to contribute to different structures of the heart that include the left ventricle but also parts of the right ventricles and atria (Domian *et al.*, 2009). However, since many of those progenitors largely contribute to the left ventricle, NkxCE-GFP CPCs are often referred to as a pool of FHF progenitors.

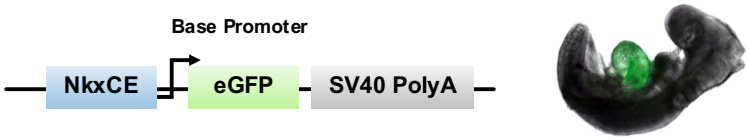

Figure 1 Nkx2.5 cardiac enhancer eGFP (NkxCE-GFP) reporter. The cardiac-specific 2.1kb Nkx2.5 cardiac enhancer (NkxCE: ~9.5kb upstream of Nkx2.5-ATG site) along with a 500bp base promoter exclusively marks cardiac progenitor cells (CPCs) in embryonic hearts by GFP expression (left panel) from E8.5-E15.5 as shown in an E9.5 mouse embryo (right panel). Adapted from Figure 1A, B from Hoelscher et al. miR-128a Acts as a Regulator in Cardiac Development by Modulating Differentiation of Cardiac Progenitor Cell Populations. Int. J. Mol. Sci. 2020, 21, 1158 (Hoelscher *et al*., 2020).

Furthermore, the Cre/loxP reporter system has become one of the most commonly used approaches to generate conditional animal reporter strains. In such systems, the first gene is flanked by two loxP sites (floxed) facing the same direction, followed by a second gene, which is often a fluorescent reporter (Li *et al.*, 2018; S. Li *et al.*, 2014). The first gene is expressed before Cre-mediated excision, while the second gene will be expressed after Cre-mediated excision (Li *et al.*, 2018; S. Li *et al.*, 2014).

One example, used in this work, is the Isl1Cre-R26^{mTmG} double-fluorescent Cre reporter mouse line (Figure 2). The R26^{mTmG} mouse carries a floxed membrane-tagged tandem dimer Tomato (mT) as first gene and a membrane-tagged green fluorescent protein (mG) as second gene (Muzumdar *et al.*, 2007). It was crossed with an *Isl1*-Cre mouse line (Muzumdar *et al.*, 2007; Yang *et al.*, 2006). Upon Cre-mediated excision of mT, *Isl1*-positive CPCs will be marked by GFP expression at E8.5 - E11.5 during murine embryonic development. *Isl1*-expressing CPCs are predominantly considered part of the SHF progenitor pool given their major contributions to the outflow region, right ventricular structures and parts of the atria. However, *Isl1*-expressing CPCs are also found in the FHF, thus, also contributing to small parts of left ventricle (Cai *et al.*, 2003).

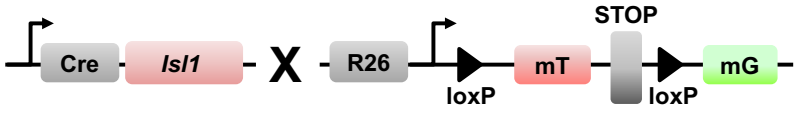

Figure 2 Isl1Cre-R26^{mTmG} transgenic construct. The Isl1Cre-R26^{mTmG} is a double-fluorescent Cre reporter mouse line, which includes membrane-targeted tandem dimer Tomato (mT) and membrane-targeted green fluorescent protein (mG). Upon Cre-mediated excision of mT, GFP-positive *Isl1*-expressing CPCs will be marked on E8.5-11.5 of embryonic development. Adapted from Figure S7A from Hoelscher *et al.* miR-128a Acts as a Regulator in Cardiac Development by Modulating Differentiation of Cardiac Progenitor Cell Populations. *Int. J. Mol. Sci.* 2020, *21*, 1158 (Hoelscher *et al.*, 2020).

Besides *in vivo* models, the use of *in vitro* models is indispensable for a detailed analysis of underlying mechanisms of cardiogenesis. Pluripotent stem cells, such as embryonic stem cells (ESCs) or induced pluripotent stem cells (iPSCs), are able to recapitulate all crucial steps of cardiogenesis during *in vitro* differentiation, including mesoderm formation, CPC specification and CPC differentiation into all cardiac lineages (CMs, SMCs and ECs) (Li *et al.*, 2015; Van Vliet *et al.*, 2012; Wu *et al.*, 2006).

By utilizing ESCs/iPSC from appropriate reporter mouse strains fluorescent labeling of e.g. various CPC populations, further enables easy tracking of the cells of interest.

Nevertheless, cardiogenesis remains one of the most complex tasks to be accomplished during embryogenesis. Besides the previously described interactions of various genes, proteins, cells and signaling pathways, great interest has grown in epigenetic control mechanisms that include tiny RNAs such as microRNAs which have been shown to fundamentally influence many aspects of heart development (Thum *et al.*, 2007; Wong *et al.*, 2016).

1.3 MicroRNAs

MicroRNAs (miRs) are small, 20 to 24 nucleotide (nt) long, endogenous non-coding regulatory RNAs, that act as post-transcriptional regulators in animals and plants by targeting mRNAs for cleavage or translational repression (Bartel, 2004).

The first miR was detected back in 1993 in *C. elegans* as a heterochronic gene called *lin-4* that unexpectedly did not encode for a protein but rather for a small RNA that showed antisense complementarity to multiple sites in the 3' untranslated region (UTR) of the *LIN-14* gene. By demonstrating that *lin-4* expression substantially reduced the amount of LIN-14 protein synthesis, however, without any changes in the *LIN-14* mRNA levels, it became clear that this tiny RNA led to a specific translational repression of the LIN-14 protein synthesis as part of regulatory events in larval stages of *C. elegans* (Lee *et al.*, 1993; Wightman *et al.*, 1993). These tiny RNAs were subsequently termed microRNAs (miRs) (Lagos-Quintana *et al.*, 2001; Lau *et al.*, 2001). Since then the interest in them grew exponentially and already a decade later many new miRs with regulatory functions have been described in flies (Brennecke *et al.*, 2003; Johnston and Hobert, 2003) and mammals (Chen *et al.*, 2004).

Like protein coding genes, miRs are of genomic origin and are usually transcribed by RNA Polymerase II as a primary transcript that forms an imperfect stem loop structure, the so-called pri-miR (Lee *et al.*, 2004). They can be subdivided into 'intronic' or 'exonic' transcription classes (Rodriguez *et al.*, 2004).

After transcription, the pri-miR is then, in most cases, cleaved in the nucleus by Drosha, an RNAse III enzyme, that results in an approximately 70 nt long precursor miR (pre-miR) with a 3' overhang. An alternative way to generate a pre-miR is the splicing of introns during mRNA processing. These short hairpin introns use splicing to bypass Drosha cleavage and are called 'Mirtrons' (Berezikov *et al.*, 2007; Winter *et al.*, 2009). The pre-miR is then further exported to the cytoplasm by exportin 5, a RanGTP-dependent double-strand binding protein (Bohnsack *et al.*, 2004). The next cleavage step of the pre-miRNA is then performed by DICER, an adenosine triphosphate (ATP)-dependent RNase III. This RNAse recognizes the 3' overhang of the pre-miR and cleaves it 21 to 23 nt downstream of the 5' end, thus producing a shorter double-stranded miR/miR RNA complex (Lee *et al.*, 2002).

One strand of the RNA duplex (either 3' to 5' (miR-3p) or 5' to 3' (miR-5p)) then further assembles with the RNAse Argonaut to the RNA-induced-silencing complex (RISC) and is processed into a mature, single-stranded and regulatory miR of about 20 to 24 nt. The remaining strand is released and degraded (Khvorova *et al.*, 2003; Kim *et al.*, 2009). The strand 'selection' seems to be dependent on the thermodynamic stability of the strands and leads in most cases to an incorporation of the strand which is positioned in forward direction (5'→ 3'; miR-5p), thus, leading to a degradation of the 3'→ 5' (miR-3p) strand (Khvorova *et al.*, 2003).

However, also the reverse miR-3p strands can be integrated into the RISC complex and be further processed into a functional miR (Bhayani *et al.*, 2012).

After incorporation, the miR/RISC complex binds to complementary mRNA sequences (especially to regions in the 3' UTR) of target genes through the 'seed region' of the miR that is defined as the 2nd to 7th nt at the 5' end of the sequence. In case of perfect base pairing to the 3'UTR region, the targeted mRNA is mostly degraded, whereas imperfect binding leads to translational repression (Winter *et al.*, 2009).

1.4 MiRs in early cardiac development

The requirement of miRs for normal cardiac development was initially revealed by a tissue-specific deletion of DICER in mice. Lethal phenotypes have been observed at E16 to E17 associated with extensive internal hemorrhage due to thin-walled blood vessels (Albinsson *et al.*, 2010; Hoelscher *et al.*, 2017). Additionally, cardiac-specific disruption of DICER led to embryonic lethality due to dilated cardiomyopathy (Chen *et al.*, 2008). Both studies indicated the great importance of miRs during embryogenesis and cardiac development already a decade ago (Hoelscher *et al.*, 2017).

With continuing research in the field, numerous miRs have been identified as indispensable regulators of heart development including miRs such as miR-1, miR-133a, miR-208, miR-499, miR-142 and the 17~92 cluster (Ai *et al.*, 2016; Chen *et al.*, 2017; Gu *et al.*, 2017; Ivey *et al.*, 2008; Wang *et al.*, 2012). They have been shown to be involved in nearly all steps of early cardiogenesis including mesodermal induction, progenitor cell specification and differentiation by regulating underlying molecular networks. Further, most of them have also been shown to be highly preserved across all vertebrate species not only in regard of their sequence but also their inherited functions (Hoelscher *et al.*, 2017).

Among the first relevant miRs that were identified were miR-1 and miR-133 (Zhao *et al.*, 2005). These miRs belong to a group of the so-called myo-miRs due to their particular enrichment in cardiac tissue (van Rooij *et al.*, 2009). MiR-133a-1/miR-1-2 and miR-133a-2/miR-1-1 which are transcribed from the same locus in a bicistronic manner, have been shown to promote early mesoderm formation but have opposing effects during further development steps where they in fact suppress progenitor cell specification and cardiomyocyte proliferation (Ivey *et al.*, 2008). In part, this functions have been attributed to the targeting of *Delta-like 1* (*Dll-1*) by miR-1, a prominent factor in the Notch signaling pathway regulating mesoderm formation as well as the targeting of *Hand2*, a bHLH transcription factor involved in cardiomyocyte expansion (Chen and Wang, 2012).

Just as miR-1 and miR-133, also miR-208 and miR-499 belong to the myo-miR group and represent mayor players in heart development. Being 'hidden' in the intronic sequences of the myosin heavy chain (*MHC*) genes *Myh6* (*α-MHC*) and *Myh7* (*β-MHC*), they mediate important functions in cardiomyocyte differentiation by being expressed in parallel to their host genes, respectively (van Rooij *et al.*, 2009). By targeting important cardiac genes such as *Gata4* (early cardiac TF) as well as transcriptional repressors of *Myh7* (structural CM protein) as well as *Sox6* (factor of muscle differentiation) (Callis *et al.*, 2009; Cohen-Barak *et al.*, 2003; Sluijter *et al.*, 2010; van Rooij *et al.*, 2009) they are indispensable players of cardiogenesis by forming the identity of cardiac lineages.

Furthermore, miR-142 inherits functional relevance especially in progenitor cell specification by directly targeting *Mef2c*, an early progenitor marker. In addition, the expression of this miR has been shown to cause downregulation of further cardiac progenitor-specific genes such as *Mesp1, Nkx2.5* and *Tbx5*, thus, contributing significantly to early cell fate decisions (Chen *et al.*, 2017).

Another yet well-studied subset of miRs is encoded within the 17~92 cluster and includes the six miRs, miR-17, miR-18a, miR-19a, miR-20a, miR-19b-1 and miR-92-1 (Chen and Wang, 2012). Besides miR-1 and miR-133, the 17~92 cluster and its members are probably one of the most extensively studied clusters with functional relevance to heart development (Ai *et al.*, 2016; Gu *et al.*, 2017). Among a multiplicity of functions, it has been demonstrated that in particular miR-17 and miR-20a are able to mediate cardiac lineage differentiation of SHF progenitors through direct translational repression of the early cardiac TFs *Isl1* and *Tbx1* (Wang *et al.*, 2010). Furthermore, miR-19 has been shown to regulate Wnt-signaling by targeting important molecules of this pathway.

All these studies demonstrated that miRs affect multiple signaling pathways and transcriptional networks to modulate heart development. And although dozens of miRs have been identified so far (Cordes *et al.*, 2010), the exact roles of many miRs in cardiac development still remain elusive and will be matter of future research.

1.5 MiR-128a

MiR-128a, also commonly referred to as miR-128-1, is an intronic miR that is embedded in the intron of the *R3HDM1* (R3H domain containing 1) gene which is located on chromosome 2 (2q21.3) in humans, chromosome 1 in mice and chromosome 22 in zebrafish (Bruno *et al.*, 2011; Li *et al.*, 2013).

Highly expressed in the brain, miR-128 is primarily known for its functional role in neurogenesis (Krichevsky *et al.*, 2003; Krichevsky *et al.*, 2006; Persengiev *et al.*, 2012).

Besides, miR-128 has been linked to the development of gliomas. MiR-128 acts as a tumor suppressor and its downregulation increases neural stem cell proliferation thereby initiating brain tumor growth (Ciafre *et al.*, 2005; Zhang *et al.*, 2009).

The role of miR-128 in the cardiac context has so far only been marginally investigated. The first publication about a functional role of miR-128 in the heart was published in 2013 (Witman *et al.*, 2013) and showed that miR-128 harbors a role in cardiac regeneration in lower vertebrates. The authors demonstrated that miR-128 was differentially expressed after resection injury in the regeneration zone in newt hearts and regulates the proliferation especially of non-cardiomyocyte populations. Furthermore, they identified *Isl1* as a direct target of miR-128 and showed that this interaction is predominantly evident during the hyperplastic response of newt cardiac regeneration (Witman *et al.*, 2013).

Moreover, a very recent publication in 2018 attributed miR-128 with a functional role in postnatal heart growth in mice (Huang *et al.*, 2018). They showed that miR-128 was robustly enriched in one-week old postnatal cardiac ventricles when compared to those analyzed one day after birth and showed that loss of miR-128 promoted postnatal cardiomyocyte proliferation and regeneration (Huang *et al.*, 2018).

1.6 Aim

MiRs are important for many aspects of cardiac development and homeostasis but also play pivotal roles in cardiac disease development including congenital heart disease (CHD). Studying the roles of miRs in early cardiac development therefore helps to understand how dysregulations of miRs may contribute to the development of cardiac disease. In this work we sought to identify yet uncharacterized miRs with functions in early cardiogenesis. To realize this goal, different approaches were applied:

(1) MicroArray analysis was performed to identify new miR candidates highly enriched in a pool of cardiac progenitors (namely NkxCE-GFP CPCs) which would indicate their potential developmental relevance.
(2) *In vivo* loss-of-functions studies in zebrafish were performed to preselect miR candidates with cardiac impact.
(3) Finally, detailed functional analysis of selected miRs (miR-128a) was performed with loss-of-function as well as gain-of-function studies conducted in various murine transgenic ESC and iPSC lines.

2 Material

2.1 Chemicals

Table 1 List of used chemicals

Chemical/Reagent	Manufacturer	Catalogue#	Headquarter
1-Thioglycerol	Sigma-Aldrich	M6145	St. Louis, MO, USA
2-propanol ROTIPURAN® ≥99.8 % (Isopropanol)	Carl Roth	6752	Karlsruhe, Germany
2-propanon ROTISOLV ® (Aceton) ≥99.8 %	Carl Roth	5025	Karlsruhe, Germany
Agar-agar, bacteriological	Carl-Roth	2266.3	Karlsruhe, Germany
ampicillin sodium salt BioChemica	AppliChem	A0839	Darmstadt, Germany
Bovine Serum Albumin	Thermo Fisher Scientific	B14	Waltham, MA, USA
Chloroform	Sigma Aldrich	C2432	St. Louis, MO, USA
DAPI 5mg/ml	BioLegend	422801	San Diego, CA, USA
Deoxyadenosine triphosphate (dATP)	Thermo Fisher Scientific	R0141	Waltham, MA, USA
Deoxycytidine triphosphate (dCTP)	Thermo Fisher Scientific	R0161	Waltham, MA, USA
Deoxyguanosine triphosphate (dGTP)	Thermo Fisher Scientific	R0151	Waltham, MA, USA
Deoxythymidine triphosphate (dTTP)	Thermo Fisher Scientific	R0171	Waltham, MA, USA
DMSO ≥ 99,5 %	Carl Roth	A994.1	Karlsruhe, Germany
DNAse away	Thermo Fisher Scientific	7010	Waltham, MA, USA
Doxycycline hyclate	Sigma-Aldrich	D9891	St. Louis, MO, USA
Dulbecco's MEM (w. 3,7 g/l Na-HCO_3, 4,5 g/l D-Glucose, stabile glutamine; w/o Na-Pyruvate; low endotoxin	Biochrom AG	FG0435	Billerica, MA, USA
EDTA ≥99 %	Carl Roth	CN 06.1	Karlsruhe, Germany
Ethanol ROTIPURAN® ≥99.8 %	Carl Roth	9065.1	Karlsruhe, Germany
Fluoroshield Mounting Medium w/ DAPI	Abcam	Ab104139	Cambridge, UK
Fugene® HD Transfection Reagent	Promega	E2311	Madison, WI, USA
Gel loading Dye,Blue (6x)	New England BioLabs	B7021S	Ipswich, MA, USA
Gelatin Type B (bovine)	Sigma-Aldrich	G9391	St. Louis, MO, USA
Collagenase Typ II	Worthington	LS0004174	Columbus, OH, USA

Chemical/Reagent	Manufacturer	Catalogue#	Headquarter
	(PAN Biotech)		
Gibco™ Fetal calf serum (FCS)	Thermo Fisher Scientific	10270-106	Waltham, MA, USA
Gibco™ MEM Non-Essential Amino Acids (NEAA), 100x	Thermo Fisher Scientific	1140-50	Waltham, MA, USA
Gibco™Sodium Pyruvate 100 mM (100x)	Thermo Fisher Scientific	700211360-039	Waltham, MA, USA
Gibco™Trypsin-EDTA 0,25% (1x)	Thermo Fisher Scientific	25200-056	Waltham, MA, USA
Glycerol ≥ 99,5 %	Sigma-Aldrich	56815	St. Louis, MO, USA
Hank's Balanced Salt Solution (HBSS)	Biochrom AG	L2035	Billerica, MA, USA
IMDM (w/ 2,024 g/l NaHCO3, stabile glutamine, low endotoxin)	Biochrom AG	FG0465	Billerica, MA, USA
Invitrogen™ 1kb DNA marker	Thermo Fisher Scientific	10787018	Waltham, MA, USA
Invitrogen™ 50bp DNA marker	Thermo Fisher Scientific	10416014	Waltham, MA, USA
Invitrogen™ 5x First Strand Buffer	Thermo Fisher Scientific	Y02321	Waltham, MA, USA
Invitrogen™ DTT	Thermo Fisher Scientific	Y00147	Waltham, MA, USA
Invitrogen™ Random Primers (250ng/µl)	Thermo Fisher Scientific	48190-011	Waltham, MA, USA
Invitrogen™ UltraPure™ TRIS-borate-EDTA (TBE) buffer, 10X	Thermo Fisher Scientific	15581028	Waltham, MA, USA
Isofluran (2-chloro-2-(difluoromethoxy)-1,1,1-trifluoro-ethane Baxter vet 100mg/g	Baxter	HDG9623V	Deerfield, IL, USA
L-Ascorbic acid	Sigma-Aldrich	A4544-25G	St. Louis, MO, USA
Magnesium sulphate hydrate ($MgSO_4$) ≥ 99%	Carl Roth	0261.1	Karlsruhe, Germany
Mitomycin C, 2mg	Sigma-Aldrich	10107409001	St. Louis, MO, USA
murine Leukemia inhibitory factor (LIF) ESGRO ® supplement	Merck Millipore	ESG1107	Billerica, MA, USA
3-(4,5-Dimethylthiazol-2-yl)-2,5-Diphenyltetrazoliumbromid (MTT)	Sigma Aldrich	M5655	St. Louis, MO, USA
Normal goat serum	Abcam	Ab7481	Cambridge, UK
Penicillin/Streptomycin (Pen/Strep) 100x	Thermo Fisher Scientific	15140163	Waltham, MA, USA
peqGREEN DNA, RNA Dye	VWR		Erlangen, Germany
PeqLab DEPC-water (RNAse-free)	VWR	4034	Erlangen, Germany
Phosphate buffered saline (PBS) 10x	Biochrom AG	L1835	Billerica, MA, USA
Phenol ≥96 %	Sigma Aldrich	16018	St. Louis, MO, USA
Polybrene	Sigma Aldrich	H9268	St. Louis, MO, USA
Potassium chloride (KCl) ≥ 99,5 %, p.a., ACS, ISO	Carl Roth	6781.3	Karlsruhe, Germany
Power SYBR™ Green PCR Master Mix	Thermo Fisher Scientific	4367659	Waltham, MA, USA

Chemical/Reagent	Manufacturer	Catalogue#	Headquarter
Puromycin	GE Healthcare (ehem. PAA-Laboratories)	P11-019	Chicago, IL, USA
Red Blood Cell Lysis Solution (10x)	Miltenyi Biotech GmbH	130-094-183	Bergisch Gladbach, Germany
RNase AWAY	Thermo Fisher Scientific	7002	Waltham, MA, USA
Sodium chloride (NaCl), ≥ 99,5 %, p.a., ACS, ISO	Carl Roth	3957.1	Karlsruhe, Germany
tetracycline-free FCS	Biochrom AG	S0115	Billerica, MA, USA
TRIS 1M, pH 7, RNAse-free	Thermo Fisher Scientific	AM9850G	Waltham, MA, USA
Triton-X-100	Carl Roth	3051.3	Karlsruhe, Germany
Trypanblue 0,5 %	Biochrom AG	L6323	Billerica, MA, USA
Trypton/Pepton ex casein	Carl Roth	8952.3	Karlsruhe, Germany
UltraPure® 0.5M EDTA pH 8	Thermo Fisher Scientific	15575020	Waltham, MA, USA
Universal agarose, peqGOLD	VWR	732-2789P	Erlangen, Germany
Yeast extract	Carl Roth	2363.3	Karlsruhe, Germany
β-Mercaptoethanol	Sigma-Aldrich	M6250	St. Louis, MO, USA

2.2 Solutions, buffers and media

2.2.1 Standard solutions and buffers

Table 2 Standard solutions and buffers

Solution/Buffer	Application	Composition	Note/Storage
TE buffer	Dilutions , Elution	1ml UltraPure® 0.5M EDTA pH 8, 5ml TRIS 1M, pH 7, RNAse-free ad 500ml Millipore® (Final concentration 10mM Tris pH 7.5, 1mM EDTA)	Storage at RT
1x TBE buffer	Gelelektrophorese	100ml 10X Invitrogen™ UltraPure™ TRIS-borate-EDTA (TBE) buffer *ad* 1000ml Millipore® (Final concentration 0.1 M Tris, 90 mM boric acid, 1 mM EDTA, pH 8.3)	Storage at RT
70% v/v ethanol	Disinfection	35ml ethanol ROTIPURAN® ≥99.8 % *ad* 50ml Millipore®	Storage at RT
1x Phosphate buffered saline (PBS)	Cell culture, ICC	100ml Phosphate buffered saline (PBS) 10x *ad* 1000ml Millipore®	Autoclave 20’ 121°C, storage at RT

2.2.2 Buffers and solutions for Immunocytochemistry (ICC)

Table 3 ICC buffers and solutions

Solution/Buffer	Application	Composition	Note/Storage
0.1 % v/v PBS-T	Washing, Dilutions	100µl Triton-X-100, *ad* 100ml 1x PBS	Storage at RT
0.25 % v/v PBS-T	Permeabilization	250µl Triton-X-100, *ad* 100ml 1x PBS	Storage at RT
1 % v/v PBS-T (1x PBS-T)	Dilutions	1ml Triton-X-100, *ad* 100ml 1x PBS	Shortly incubate at 37°C in a water bath to dissolve, storage at RT
1.5% v/v goat serum in 1x PBS-T	Dilutions	150µl normal goat serum *ad* 10ml 1x PBS-T	Prepare fresh before use
5% v/v goat serum in 1x PBS-T	Blocking	500µl normal goat serum *ad* 10ml 1x PBS-T	Prepare fresh before use

2.2.3 Cell culture solutions and media

Table 4 Solution and media used for cell culture

Solution/Media	Application	Composition	Note/Storage
0.1% w/v gelatin	Cell culture plate coating	1g Gelatin Type B *ad* 1000ml Millipore®	Autoclave 20' 121°C, storage at 4°C
Collagenase II Solution I	Dissociation	Final concentration 10.000U/ml Hank's Balanced Salt Solution (HBSS)	Calculation dependent on units of shipped Collagenase II lot.
Collagenase II Dissociation Solution	Dissociation of EBs, Tail tip digestion	100µl Collagenase II Solution I (10.000U/ml), 10µl DNase I Recombinant, RNAse-free (10.000U/ml) *ad* 2ml HBSS	Storage at 4°C, storage no longer than one week
Polybrene	Viral transduction	Stock solution 0.8mg/ml, 0.8mg polybrene *ad* 1ml Millipore®	Sterile filtrate through 0.22µm syringe, aliquot and store at -20°C until use in final conc. 6-8µg/ml
Puromycin	ESC culture	Stock solution 1mg/ml, 1mg puromycin ad 1ml 1x PBS	Aliquot and store at -20°C until use in final conc. 1µg/ml (Dilution factor 1000)
Mitomycin C	Inactivation of MEF feeder layer	Stock solution 0.5mg/ml, 2mg Mitomycin C *ad* 4ml 1x PBS	Sterile filtrate through 0.22µm syringe, aliquot and store at -20°C until use in final conc. of 10µg/ml (Dilution factor 50)

Solution/Media	Application	Composition	Note/Storage
MEF Inactivation Medium	Inactivation of MEF feeder layer	10ml MEF medium, 200µl 0.5mg/ml Mitomycin C (final conc. 10µg/ml)	Storage at 4°C, up to 4 weeks. Several usages possible if filtrated before use (0.22µm syringe)
L-Ascorbic acid	ESC differentiation medium	Stock solution 5mg/ml, 0.5g L-ascorbic acid *ad* 100ml Millipore®	Sterile filtrate through 0.22µm syringe, aliquot and store at -20°C until use in final conc. of 0.05mg/ml (Dilution factor 100)
Doxycycline	Viral induction	Stock solution 1mg/ml, 1mg Doxycycline hyclate *ad* 1ml Millipore®	Aliquot and store at -20°C until use in final conc. 1-2µg/ml (dilution factor 500-1000)
Leukemia inhibitory factor (LIF)	ESC culture	Stock solution 10^7 U/ml, 1 vial of murine Leukemia inhibitory factor (LIF) ESGRO® supplement, add 1ml 1x PBS	Aliquot and store at -20°C until use in final conc. 10^3 U/ml (Dilution factor 10.000)
MTT Solution	MTT assays	Stock solution 5mg/ml, 5mg 3-(4,5-Dimethylthiazol-2-yl)-2,5-Diphenyltetrazolium-bromid (MTT) *ad* 1ml 1x PBS	Aliquot and store at -20°C. Short term storage at 4°C, no longer than three days in the dark.
MEF medium	HEK293 FT, Fibroblast culture	500ml DMEM, 50ml Gibco™ FCS (w/o heat inactivation), 5ml Pen/Strep (100x), 5ml Sodium Pyruvate (100mM)	Storage at 4°C
CJ7 medium*	ESC/iPSC culture	500ml DMEM, 100ml Gibco™ FCS (w/o heat inactivation), 12.5ml Pen/Strep (100x), 6.25ml NEAA (100x), 4.4µl β-Mercaptoethanol, LIF (10^3 U/ml, 1x)	Aliquot in 40ml, store at -20°C. Before use add LIF (4µl of 10^7 U/ml stock solution per 40ml). CJ7 Medium w/ LIF can be stored at 4°C up to 7 days.
IMDM-ES medium*	Preparation of ESC/iPSC for differentiation	500ml IMDM, 100ml Gibco™ FCS (w/o heat inactivation), 12.5ml Pen/Strep (100x), 6.5µl 1-Thioglycerol, LIF (10^3 U/ml)	Aliquot in 40ml, store at -20°C. Before use add LIF (4µl of 10^7 U/ml stock solution per 40ml). IMDM-ES Medium w/ LIF can be stored at 4°C up to 7 days.
Differentiation medium*	ESC/iPSC differentiation	500ml IMDM, 100ml Gibco™ FCS (w/ heat inactivation), 12.5ml Pen/Strep (100x), 6.5µl 1-Thioglycerol, 6,25ml L-Ascorbic acid	Inactivate FCS for 30' at 56°C in the water bath before use. Aliquot medium in 40ml, store at -20°C.
Transduction medium	Viral transduction	CJ7 Medium (s. above), w/o FCS, w/o Pen/Strep	Storage at 4°C.

*if required for corresponding overexpression experiments, medium was supplied with tetracycline-free FCS (Biochrom AG) and additionally supplied with 1-2µg/ml doxycycline and/or 1µg/ml puromycin.

2.2.4 Buffers and solutions for bacterial growth and selection

Table 5 Buffers and solutions for bacterial growth and selection

Solution	Application	Composition	Note/Storage
Ampicillin	Bacterial selection	Stock solution 50mg/ml, 50mg ampicillin *ad* 1ml H_2O	Store stock solution at -20°C until final use in a conc. of 100µg/ml (dilution factor 500)
Lysogeny broth (LB medium)	Bacterial growth	5g Trypton/Pepton, 2.5g NaCl, 2.5g Yeast extract *ad* 500ml H_2O	Autoclave 20' 121°C before usage, storage at RT.
LB agar plates w/ ampicillin	Bacterial plating	5g Trypton/Pepton, 2.5g NaCl, 2.5g Yeast extract, 7.5 g agar-agar (CarlRoth) *ad* 500ml H_2O	Autoclave 20' 121°C, let it cool down until hand warm, then add ampicillin in a final conc. of 100µg/ml and plate on 100x15mm petri dishes (~20ml on each plate). Store agar plates upside down at 4°C.
S.O.C-medium (0.5% w/v yeast extract, 2% w/v Trypton/Pepton, 10mM NaCl, 2.5mM KCL, 20mM $MgSO_4$, 20mM Glucose)	Bacterial transformation, growth	5g Yeast extract, 20g Trypton/Pepton, 0.584g NaCl, 0.186g KCl, 2.4g $MgSO_4$ *ad* 1liter H_2O	Autoclave 20' 121°C, cool down and add 20ml of 20% glucose solution. Long term storage at -20°C, short term storage at 4°C.
1 % or (2%) w/v agarose gel	Gel electro-phoresis	0.5g or (1g) universal agarose (peqGOLD) *ad* 50ml 1x TBE buffer	Microwave for 5' until agarose is dissolved, add 2.5µl/50ml gel of peqGREEN DNA, RNA Dye and transfer into a gel slide with the required comb for hardening. Place the gel into the electrophoresis system and fill with 1x TBE as running buffer and apply samples.

2.2.5 Flow cytometry buffer and solutions

Table 6 Solutions, buffers for flow cytometry

Solution	Application	Composition	Note/Storage
FACS buffer (0.5% w/v BSA, 4mM EDTA, 1x PBS)	Flow cytometry	0.5g Bovine Serum Albumin (BSA), 0.11g EDTA *ad* 100ml 1x PBS	Storage at 4°C
DAPI	Flow cytometry, nuclear counterstain	Stock solution 5mg/ml, 10mg DAPI *ad* 2ml Millipore®, working solution 0.1mg/ml (10µl of 5mg/ml solution w/ 490µl Millipore®)	Aliquot stock solution and store at -20°C. Before use dilute to working solution and use final conc. of 1µg/ml (Dilution factor 100), storage at 4°C.

2.3 Plasmids

2.3.1 Used lentiviral plasmids

The lentiviral plasmid pHAGE-STEMCCA was kindly provided by Sommer and colleagues on filter paper (Sommer *et al.*, 2009). FUdeltaGW-rtTA, pCMV-VSV-G and pCMV-dR8.2 dvpr were purchased from Addgene in bacterial stabs. The detailed vector maps are attached as Appendix Figures A1-A4.

Table 7 Lentiviral plasmids

Name	Plasmid specification	Addgene Plasmid#	Bacterial host	References
muSTEMCCA	pHAGE-STEMCCA	-	XL10	(Sommer *et al.*, 2009)
rtTA	FUdeltaGW-rtTA*	19780	Stbl3	(Maherali *et al.,* 2008)
VSV-G	pCMV-VSV-G#	8454	DH5alpha	(Stewart *et al.*, 2003)
dR8.2	pCMV-dR8.2 dvpr#	8455	DH5alpha	(Stewart *et al.*, 2003)

*was a gift from Konrad Hochedlinger (Addgene plasmid # 19780; http://n2t.net/addgene:19780; RRID: Addgene 19780), # were a gift from Bob Weinberg (Addgene plasmid # 8454; http://n2t.net/addgene:8454; RRID:Addgene 8454) and (Addgene plasmid # 8455 ; http://n2t.net/addgene:8455; RRID:Addgene_8455).

2.4 Competent bacteria

Table 8 Chemically competent bacteria

Enzyme	Manufacturer	Catalogue#	Headquarter
XL10-Gold® Ultracompetent Cells	Agilent Technologies	as part of 200522	Santa Clara, CA, USA

2.5 Enzymes

2.5.1 Restriction enzymes

Table 9 Restriction enzymes

Enzyme	Manufacturer	Catalogue#	Headquarter
BamHI (10U/µl)	Thermo Fisher Scientific	ER0051	Waltham, MA, USA
NotI (10U/µl)	Thermo Fisher Scientific	ER0591	Waltham, MA, USA
NdeI (10U/µl)	Thermo Fisher Scientific	ER0581	Waltham, MA, USA
PstI (10U/µl)	Thermo Fisher Scientific	ER0661	Waltham, MA, USA
EcoRI (10U/µl)	Thermo Fisher Scientific	ER0271	Waltham, MA, USA

2.5.2 Further enzymes

Table 10 Further enzymes

Enzyme	Manufacturer	Catalogue#	Headquarter
DNase I Recombinant, RNAse-free (10.000U/ml)	Sigma-Aldrich	04716728001	St. Louis, MO, USA

2.6 Primer

LNA™ miR Primer sets (2.6.1) for *in vitro* analysis were purchased from Exiqon (Vedbaek, Denmark) and dissolved in 220µl of DNAse/RNAse-free dH_20. Primers for endpoint PCR (2.6.2) as well as quantitative real-time PCR (qRT-PCR) (2.6.3) were ordered from Ella Biotech (Munich, Germany) and were both resuspended to a stock concentration of 100µM with DNAse/RNAse-free dH_20. Before use, endpoint PCR primers were diluted to a final concentration of 2µM. For final qRT-PCR, a working solution of 5µM was diluted freshly each time. All primer stocks were stored at -20°C.

2.6.1 qRT-PCR primer sets for miRs

Table 11 MicroRNA primer for qRT-PCR

Primer specification	Accession (Exiqon)	Catalogue#	Target sequence (5'- 3')
hsa-miR-128-3p LNA™ PCR primer set, UniRT	MIMAT0000424	202143	UCACAGUGAACCGGUCUCUUU
hsa-miR-1 LNA™ PCR primer set, UniRT	MIMAT0000416	202106	UGGAAUGUAAAGAAGUAUGUAU
hsa-miR-133a-5p LNA™ PCR primer set, UniRT	MIMAT0026478	202145	AGCUGGUAAAAUGGAACCAAAU
hsa-miR-20b-5p LNA™ PCR primer set, UniRT	MIMAT0001413	202257	CAAAGUGCUCAUAGUGCAGGUAG
hsa-miR-30b-5p LNA™ PCR primer set, UniRT	MIMAT0000420	202014	UGUAAACAUCCUACACUCAGCU
hsa-miR-30a-5p LNA™ PCR primer set, UniRT	MIMAT0000087	202120	UGUAAACAUCCUCGACUGGAAG

Primer specification	Accession (Exiqon)	Catalogue#	Target sequence (5'- 3')
U6 snRNA LNA™ PCR primer set, UniRT (Reference RNA)	without MIMAT #	203907	GUGCUCGCUUCGGCAGCACAUAUA CUAAAAUUGGAACGAUACAGAGAAG AUUAGCAUGGCCCCUGCGCAAGGA UGACACGCAAAUUCGUGAAGCGUUC CAUAUUUU

2.6.2 Endpoint PCR primer for mRNA

Table 12 Primer for Endpoint PCR

Gene	Direction	NCBI Reference Sequence*/ Further Reference#†	Sequence (5'- 3')
cMyc	for	NM_001177352*	TCAAGCAGACGAGCACAAGC
	rev		TACAGTCCCAAAGCCCCAGC
Oct3/4	for	NM_013633*	CCAACGAGAAGAGTATGAGGC
	rev		CAAAATGATGAGTGACAGACAGG
Klf4	for	NM_010637*	GGCGAGAACCTTACCACTGT
	rev		TACTGAACTCTCTCTCCTGGCA
Sox2	for	NM_011443*	TCTGTGGTCAAGTCCGAGGC
	rev		TTCTCCAGTTCGCAGTCCAG
cMyc/Sox2 (exogene)	for	see above*	AGGGCGCCCTGCCAGGC
	rev		GGGAAGCAGCTCGAATTTCTT
DR4_Puro/Neo	for	JAX protocol#	ATGACCGAGTACAAGCCCAC
	rev		GCGTGAGGAAGAGTTCTTGC
DR4_Hygro	for	JAX protocol#	TGAACTCACCGCGACGTCTG
	rev		GCAGTTCGGTTTCAGGCAGG
NkxCEeGFP	for	Kindly given by Sean M. Wu†	TAGGTGACGCAGAACTGCCC
	rev		CTCCTCGCCCTTGCTCACCA

* Data adopted from https://www.ncbi.nlm.nih.gov/nuccore/ (NCBI Nucleotide), # Sequences obtained from section "Genotyping Protocols" from https://www.jax.org/strain/003208, †Cardiovascular Institute, Institute for Stem Cell Biology and regenerative Medicine, Stanford University of Medicine, Stanford, USA.

2.6.3 qRT-PCR primer for mRNA

Table 13 Primer for qRT-PCR

Gene	Direction	NCBI Reference Sequence*	Sequence (5'- 3')
β-Actin	for	NM_007393.5	CCAACCGTGAAAAGATGACC
	rev		ACCAGAGGCATACAGGGACA
Isl1	for	NM_021459.4	CCACGATGTGGTGGAGAGA
	rev		CTAGCCGAGATGGGTTCG
Nkx2.5	for	NM_008700.2	GAGCCTACGGTGACCCTGA
	rev		GTGGTCTCTCGGCGCCAT
Mef2c	for	NM_025282.3	ATGGGCGGAGATCTGACA
	rev		TTCTTGTTCAGGTTACCAGGTG
Acta2	for	NM_007392.3	CCAACCCGGGAGAAAATGAC
	rev		CAGTTGTACGTCCAGAGGCATA

Gene	Direction	NCBI Reference Sequence*	Sequence (5'- 3')
Tbx5	for	NM_011537.3	GGATGTCTCGGATGCAAAGT
	rev		GGTTGGAGGTGACTTTGTGC
Tnnt2	for	NM_011619.3	TTCGACCTGCAGGAAAAAGTT
	rev		CTTCCCAGGAGTTTTGGAGA
Pecam1	for	NM_008816.3	GTTGCAGCCAAATGCTACTT
	rev		GAAATCTTCTCGCTGTTGGA
Myh6	for	NM_010856.4	CCTATGCTTCTGCTGATACCG
	rev		TCATCAGCTTGTTCAGATTTTCC
Cited2	for	NM_010828.3	GTTTAACAACTCCCAGTTCATGG
	rev		AATACTGGTTGTTGAGCTTCTGC
Hcn4	for	NM_001081192.2	CGCATTGTCCGTTTCACTAA
	rev		CAGGTCATAGGTCATGTGGAAG
Myl2	for	NM_010861.4	GACTGAGCCCTGAACCACAG
	rev		ACATCATCAACTTGCGGTCA
Shox2	for	NM_013665.1	CCCACTATCCAGACGCTTTC
	rev		TCGATTTTGAAACCAAACCTG
Myl7	for	NM_022879.2	CCCATCAACTTCACCGTCTT
	rev		AGGCACTCAGGATGGCTTC
Sfrp5	for	NM_018780.3	GATCTGTGCCCAGTGTGAGA
	rev		TTAATGCGCATCTTGACCAC
Ki67	for	NM_001081117.2	CCAGGAAAGTCCCTTGGAA
	rev		CATTTTTGAAGCTTTGGTATCTTG
Irx4	for	NM_018885.2	GATGAGAAGCGCCCCTATG
	rev		GTCTTTGCCAGCATGACCTT
Neurod1	for	NM_010894.2	CGCAGAAGGCAAGGTGTC
	rev		TTTGGTCATGTTTCCACTTCC
Nanog	for	NM_028016.3	TTCTTGCTTACAAGGGTCTGC
	rev		AGAGGAAGGGCGAGGAGA
Gata4	for	NM_008092.3	GGAAGACACCCCAATCTCG
	rev		CATGGCCCCACAATTGAC
Hand1	for	NM_008213.2	CAAGCGGAAAAGGGAGTTG
	rev		GTGCGCCCTTTAATCCTCTT
Nestin	for	NM_016701.3	TGCAGGCCACTGAAAAGTT
	rev		TTCCAGGATCTGAGCGATCT
Ncam1	for	NM_001081445.1	ACCTGAAACCTGAGACGAGGT
	rev		CTTGGGTGCACTGGGTTC
Afp	for	NM_007423.4	GCTTATCTCTAAATCCAAGCCAGT
	rev		AGGAAGGTTGGGGTGAGTTC
Sox17	for	NM_011441.5	CAACGCAGAGCTAAGCAAGA
	rev		TTGTAGTTGGGGTGGTCCTG

*Data adopted from https://www.ncbi.nlm.nih.gov/nuccore/ (NCBI Nucleotide).

2.7 LNA probes

All used LNA probes were purchased from Exiqon (Vedbaek, Denmark) and diluted to a stock solution of 25µM with nuclease-free, sterile TE buffer (200µl TE buffer to 5nmol LNA probe). Stock solutions were aliquoted and stored at -20°C until use.

Table 14 LNA probes used for *in vitro* miR-128a knockdown

LNA probes	Accession (Exiqon)	Catalogue#	Target sequence (5'-3')
mmu-miR-128-3p miRCURY LNA miRNA Inhibitor	MIMAT0000140	4101052-101	UCACAGUGAACCGGUCUCUUU
miRCURY LNA miRNA inhibitor control A	n.a.	199006-101	no hits of >70% homology to any sequence in any organism in the NCBI and miRBase databases (Exiqon)

2.8 Lentiviruses

Dharmacon™ shMIMIC Inducible Lentiviral microRNA particles were purchased from Dharmacon, Lafayette, CO, USA, (SO-2593614G) The below listed (Table 15) lentiviral particles were used for transduction of NkxCE-GFP ESCs to generate the miR-128a and miR-Ctr overexpression ESC lines (OE-128, OE-Ctr).

Table 15 Lentiviruses used for generation of miR overexpression ESC lines

Lentiviruses	Sample name	Order Nr.	clone ID	Lot Nr.#	Titer
shMIMIC™ mouse inducible microRNA mmu-miR-128-3p mCMV-TurboRFP	OE-128	VSM6922-224657152	V2ISMMMCR_3972553	V17022305	$3.32*10^8$ TU/ml
SMARTvector inducible Non-targeting Control mCMV/TurboRFP	OE-Ctr	VSC6571	-	V16090805	$1.19*10^8$ TU/ml

2.9 Antibodies

2.9.1 Primary antibodies

Table 16 List of primary antibodies

Antibody	Manufacturer	Catalogue#	Headquarter
Anti-Sox2 (rabbit polyclonal IgG)	Abcam	ab137385	Cambridge, UK
Anti-Nanog (rabbit polyclonal IgG)	Abcam	ab80892	Cambridge, UK
Anti-sarcomeric α-Actinin (Actn) (mouse monoclonal IgG1)	Abcam	ab9465	Cambridge, UK

Antibody	Manufacturer	Catalogue#	Headquarter
Anti-αMHC mouse (Myh6) monoclonal IgG2b	R&D Systems	MAB4470	Minneapolis, MN, USA
Anti-αSMA (Acta2) mouse monoclonal IgG	Santa Cruz Biotechnology	sc-53142	Santa Cruz, CA, USA
Anti-CD31 (Pecam1) rabbit polyclonal IgG	Abcam	ab28364	Cambridge, UK

2.9.2 Secondary antibodies

Table 17 List of secondary antibodies

Antibody	Manufacturer	Catalogue#	Headquarter
Goat anti-mouse IgG H&L Alexa Fluor® 555	Abcam	ab150114	Cambridge, UK
Goat anti-rabbit IgG H&L Alexa Fluor® 488	Abcam	ab150077	Cambridge, UK
Goat anti-rabbit IgG H&L Alexa Fluor® 555	Abcam	ab150078	Cambridge, UK

2.10 Cells and Cell lines

2.10.1 Murine non-transgenic pluripotent stem cell lines

Table 18 Murine non-transgenic pluripotent stem cells

ESC line	Manufacturer	Catalogue#	Headquarter
V6.5 ESCs	Novus Biologicals	NBP1-41162	Centennial. CO, USA

2.10.2 Murine transgenic pluripotent stem cell lines

Table 19 Murine transgenic pluripotent stem cells

ESC/iPSC lines	Application	Source
NkxCE-GFP ESC line	miR knockdown	Kindly provided by Sean M. Wu*
NkxCE-GFP ESC miR-Ctr overexpression line (OE-Ctr)	miR overexpression	Self-generated from NkxCE-GFP ESCs
NkxCE-GFP ESC miR-128a overexpression line (OE-128)	miR overexpression	Self-generated from NkxCE-GFP ESCs
Isl1Cre-R26^{mTmG} iPSC line (iITG-iPSC)	miR knockdown	Self-generated from Isl1Cre-R26^{mTmG} tail tip fibroblasts (TTFs)

*Cardiovascular Institute, Institute for Stem Cell Biology and regenerative Medicine, Stanford University of Medicine, Stanford, USA. Abbreviations: ESC, embryonic stem cells; iPSC, induced pluripotent stem cells; OE, overexpression.

2.10.3 Murine transgenic fibroblasts

Table 20 Transgenic fibroblasts

Transgenic fibroblasts	Application	Source
Murine embryonic fibroblasts (MEFs)	Feeder layer for ESCs/iPSCs lines	Self-generated from DR4 transgenic mouse embryos
Isl1Cre-R26^{mTmG} tail tip fibroblasts (TTFs)	Reprogramming to iPSCs	Self-generated from Isl1Cre-R26^{mTmG} mouse tail tips*
NkxCEeGFP tail tip fibroblasts (TTFs)	MicroArray analysis	Self-generated from NkxCEeGFP mouse tail tips
NkxCEeGFP cardiac fibroblasts (CFs)	MicroArray analysis	Self-generated from NkxCEeGFP mouse hearts

*tail tips of 8-week old mice were kindly provided by AG Laugwitz at Klinikum rechts der Isar, Technical University Munich.

2.10.4 293FT cells

The below listed 293FT cells were used for production of lentiviral particles which were used for the generation of the Isl1Cre-R26^{mTmG} iPSC lines (iITG-iPSCs).

Table 21 Purchased 293FT cell line

Cell line	Manufacturer	Catalogue#	Headquarter
293FT cell line	Thermo Fisher Scientific	R700-07	Waltham, MA, USA

2.11 Transgenic mice

Mice were housed in Makrolon® cages type III H in an accredited facility at the German Heart Center Munich in compliance with the European Community Directive related to laboratory animal protection (2010/63/EU). All experiments including mice conformed to the essential ethical rules and current applicable legislations (European regulations for animal care and handling 2010/63/EU) and have been approved by the Regierung von Oberbayern.

Table 22 Used transgenic mice

Mice	Stock number	Source
NkxCEeGFP transgenic mice	-	Kindly given by Sean M. Wu*
DR4 transgenic mice	003208	The Jackson Laboratory#

*Cardiovascular Institute, Institute for Stem Cell Biology and regenerative Medicine, Stanford University of Medicine, Stanford, USA. # (Tucker *et al.*, 1997)

2.12 Commercially available kits

Table 23 Commercially purchased kits

Kit	Manufacturer	Catalogue#	Headquarter
HotStar Taq® DNA Polymerase	Qiagen	203205	Hilden, Germany
ExiLENT SYBR® Green Master Mix	Exiqon	203401	Vedbaek, Denmark
Invitrogen™ M-MLV Reverse Transcriptase	Thermo Fisher Scientific	28025-013	Waltham, MA, USA
PeqGOLD DNase I Digest Kit	VWR	12-1091-01	Erlangen, Germany
PeqGOLD total RNA Kit	VWR	12-6834-02	Erlangen, Germany
Universal cDNA synthesis kit II	Exiqon	203301	Vedbaek, Denmark
QIAGEN® Plasmid Midi Kit	Qiagen	12143	Hilden, Germany
QIAGEN® Plasmid Mini Kit	Qiagen	12125	Hilden, Germany
QIAGEN® DNeasy Blood and Tissue Kit	Qiagen	69506	Hilden, Germany
*miR*Vana™ miRNA Isolation Kit	Thermo Fisher Scientific	AM1561	Waltham, MA, USA

2.13 Consumables

Table 24 List of consumables

Consumables	Manufacturer	Catalogue#	Headquarter
Applied Biosystems™ MicroAmp® fast optical 96 well reaction plate, 0.1ml	Thermo Fisher Scientific	4346907	Waltham, MA, USA
Applied Biosystems™ MicroAmp® optical adhesive film	Thermo Fisher Scientific	4311971	Waltham, MA, USA
Rotilabo® Filters, sterile (0.22µm)	Carl Roth	KH54.1	Karlsruhe, Germany
Rotilabo® Filters, sterile(0.45µm)	Carl Roth	KH55.1	Karlsruhe, Germany
Falcon™ Cell Strainers (70µm)	Corning	352350	Corning, NY, USA
30µm (30G) Syringe Falcons Non- sterile	BD Biosciences	340599	Franklin Lakes, NJ, USA
Corning® Cell scraper	Sigma Aldrich	CLS3010	St. Louis, MO, USA
Nunc™ Cryo tubes	Thermo Fisher Scientific	377224	Waltham, MA, USA
Falcon® High-Clarity Polypropylene Conical Tube (15ml/50ml)	Corning	352096/ 352070	Corning, NY, USA
Falcon® Polystyrene Round-Bottom Tube (5ml/ 14ml)	Corning	352052/ 352057	Corning, NY, USA
Falcon® 8-well Culture Slide	Corning	354118	Corning, NY, USA

Consumables	Manufacturer	Catalogue#	Headquarter
Falcon®Disposable Polystyrene Serological Pipets, sterile (2ml 5ml, 10ml, 2ml, 50ml)	Corning	356507 357543 356551 357525 356543	Corning, NY, USA
Greiner CELLSTAR® multiwell culture plates (6 well, 12 well, 24 well. 48 well, 96 well)	Greiner Bio-One	657160 665180 662160	Kremsmünster, Austria
SPL Cell Culture flasks (75cm^2, T75)	SPL Life science	70075	Pocheon, South Korea
SPL Cell Culture flasks (25cm^2, T25)	SPL Life science	70025	Pocheon, South Korea
SPL Cell Culture dishes, 100x20mm, sterile (10cm culture plate)	SPL Life science	20101	Pocheon, South Korea
SPL Cell Culture dishes, 150x25mm, sterile (15cm culture plate)	SPL Life science	20150	Pocheon, South Korea
Falcon® Disposable petri dishes, 100x15mm, sterile	Corning	25373-100	Corning, NY, USA
Eppi™ Safe-Lock Tubes (1.5ml, 2ml)	Eppendorf	0030120086 0030120094	Hamburg, Germany
PCR reaction tube strips (0.2ml)	Weber Scientific Inc.	3189-10	Hamilton Township, NJ, USA
Inoculating loop 1mm Ø	NeoLab	1-2115	Heidelberg, Germany
SafeSeal SurPhob tips, sterile (10µl, 100µl, 1250µl)	Biozym Scientific GmbH	VT0200 VT0230 VT0270	Hessisch Oldendorf, Germany
SFM disposable syringes	SFM Hospital Products GmbH	534201	Berlin, Germany

2.14 Equipment and Devices

Table 25 Equipment/devices and applications

Equipment/device	Application	Manufacturer	Headquarter
Milli-Q ® Reference	Millipore water	Merck Millipore	Billerica, MA, USA
Nikon Eclipse Ts2	Inverted microscopy	Nikon	Tokyo, Japan
Neubauer chamber	Cell count	VWR	Erlangen, Germany
Axiovert 200M w/ AxioCam MRm	Inverted/fluorescence microscopy	Zeiss	Oberkochen, Germany
NanoDrop™2000 Spectralphotometer	Nucleotide quantification	Thermo Fisher Scientific	Waltham, MA, USA
Tecan Safire 2 Multimode Microplate Reader	MTT assays	Tecan Group	Männedorf, Schwitzerland

Equipment/device	Application	Manufacturer	Headquarter
BD LSRFortessa™	Flow cytometry	BD Bioscience	Franklin Lakes, NJ, USA
BioRad Thermocycler C1000	Endpoint PCR, cDNA synthesis	BioRad	Hercules, CA, USA
Horizontal electrophoresis system	Agarose gel electrophoresis	BioRad	Hercules, CA, USA
GelDoc™ XR documentation system	Documentation gel electrophoresis	BioRad	Hercules, CA, USA
QuantStudio™ 3 Real-Time PCR System	qRT-PCR	Thermo Fisher Scientific	Waltham, MA, USA
Thermomixer® R, dry block heating and cooling shaker	Tail tip digestion	Eppendorf	Hamburg, Germany
Pipets	Pipetting	Eppendorf	Hamburg, Germany
Eppendorf Research ® Plus Multi Channel pipet	EB forming	Eppendorf	Hamburg, Germany
Fisher Bioblock Top Mix 11118	Vortex	Thermo Fisher Scientific	Waltham, MA, USA
Heracell 240i	Incubation for cell growth	Thermo Fisher Scientific	Waltham, MA, USA
GFL Hybridization incubator 7601	Incubation for cell dissociation (e.g. EBs)	GFL Gesellschaft für Labortechnik mbH	Burgwedel, Germany
Safe2020	Laminar Flow Bank	Thermo Fisher Scientific	Waltham, MA, USA
Ecotron (Bacteria incubator)	Bacterial growth	Infors HT	Bottmingen, Switzerland
Hettich MIKRO 200	Centrifugation	Hettich	Beverly, MA, USA
Megafuge™ 1.0R	Bacterial centrifugation	Thermo Fisher Scientific	Waltham, MA, USA
Campingaz CV 470 Plus w/ Twister® Plus (Bunsen burner)	Sterilization	Campingaz	Newell Brands, France
Mini plate spinner mps1000	Centrifugation	Labnet International	Edison, NJ, USA
HICLAVE Autoclave HI-50	Sterilization	HMC Europe GmbH	Tüßling, Germany
DNA/RNA UV-Cleaner Workstation I	Pipetting PCR/qRT-PCR reactions	Kisker Biotech GmbH & Co. KG	Steinfurt, Germany

2.15 Software

Table 26 Software and applications

Software	Application	Manufacturer	Headquarter
TiControl Ver. 4.4.2	Nikon Inverted microscopy	Nikon	Tokyo, Japan

Software	Application	Manufacturer	Headquarter
AxioVision Rel 4.8 software version 2.0	Inverted/flourescence microscopy	Zeiss	Oberkochen, Germany
NanoDrop 1000 Software 3.71	Nucleotide quantification	Thermo Fisher Scientific	Waltham, MA, USA
XFLUOR4 version 4.51	MTT assays	Tecan Group	Männedorf, Schwitzerland
BD FACS Diva software version 6.2	Flow cytometry	BD Bioscience	Franklin Lakes, NJ, USA
FlowJo 7.6.5 software	analysis Flow cytometry	FlowJo, LLC	Ashland, OR, USA
BioRad C1000 Thermo Cycler	Endpoint PCR, cDNA synthesis	BioRad	Hercules, CA, USA
Image Lab Software version 5.2.1	Documentation gel electrophoresis		Hercules, CA, USA
QuantStudio™ Design and Analysis Software v1.4	qRT-PCR analysis	Thermo Fisher Scientific	Waltham, MA, USA
GraphPad Prism® Software version 8.0.2 for Mac OS X	Graphs	GraphPad Software	La Jolla, CA, USA
SPSS Statistics Software version 25	Statistical analysis	SPSS Inc	Chicago, IL, USA

2.16 Databases and Online Tools

Table 27 List of databases and online tools

Database	Link
National Center for Biotechnology Information (NCBI)	https://www.ncbi.nlm.nih.gov/
miRbase	http://www.mirbase.org/
NEB Cutter v2.0 (New England Biolabs)	http://nc2.neb.com/NEBcutter2/
BioRender	BioRender.com

3 Methods

3.1 Cells and cell culture

All experiments with cells and cell lines were performed under sterile conditions in the Thermo Fisher Scientific™ Safe2020 laminar flow bank. Before cells were seeded, all cell culture plates were coated with gelatin to improve cell attachment. Therefore, each well was covered with an adequate amount of autoclaved 0.1% gelatin and incubated for 30' at 37°C. The gelatin was aspired, and plates could be used immediately. All cells were incubated at 37°C and 5% CO_2 in a Heracell 240i incubator.

3.1.1 293FT cells

293FT cells were used for production of lentiviral particles. Originally derived from primary human embryonic kidney cells (HEK293) (Graham *et al.*, 1977; Harrison *et al.*, 1977), 293FT cells are derivates of 293F cells, a fast-growing ("F") variant of HEK293 cells originally obtained by Robert Horlick at Pharmacopeia. In addition, this cell line expresses high levels of the SV40 large T antigen ("T") under the control of the human cytomegalovirus (CMV) promoter. This makes them a particularly well-suited host for virus productions since the large T antigen binding to the SV40 enhancer of expression vectors enables high protein production (Naldini *et al.*, 1996).

For maintenance/expansion, 293FT cells were cultured in T75 culture flasks with MEF medium and split/seeded once a week with a cell number of $1x10^6$ per flask. Usually, after 7 days of culture, one confluent T75 culture flask roughly yielded $2x10^7$ cells. For splitting, cells were washed once with 1x PBS and incubated for 3' at 37°C with 2ml of a 1:3 diluted 0.25% Gibco™ Trypsin-EDTA solution (w/ 1 x PBS) until detached. Then the trypsin was neutralized with 6ml MEF medium and cells were transferred into 14ml round bottom tubes and centrifuged for 5' at 300 x *g*. The pellet was resuspended in 1ml fresh MEF medium, counted (3.1.2.3.2) and split in the required amount to the needed numbers of flasks. To maintain lower passages, 293FT cells were frozen regularly as a backup with a cell number of $1x10^6$ per Nunc™ Cryo tube as described in 3.1.2.3.3. 293FT cells were thawed and seeded into one T75 culture flask per Nunc™ Cryo tube with MEF medium when fresh cells were needed.

3.1.2 Murine embryonic fibroblasts (MEFs)

MEFs are embryonic connective tissue cells which support the growth and pluripotency of stem cells by secretion of important metabolites while co-cultured. MEFs were generated from embryos of genotyped pregnant transgenic DR4 mice (3.1.2.1 & 3.1.2.2). They exhibit resistance for neomycin, hygromycin, puromycin and 6-thioguanine which makes them an optimal source for the stem cell culture in which several antibiotics were used for selection or induction.

After MEF generation, DR4 MEFs in passage 2 (p2) were frozen for long-term backup. To prepare MEFs as feeder layers (3.1.2.3), they were expanded until p5 (3.1.2.3.1), subsequently counted (3.1.2.3.2) and frozen as stocks (3.1.2.3.3). When needed for murine pluripotent stem cell culture (3.1.4), MEFs stocks at p5 were freshly thawed and inactivated (3.1.2.3.4).

3.1.2.1 Generation of MEFs

For MEF generation, pregnant transgenic DR4 mice were euthanized with isoflurane (2-chloro-2-(difluoromethoxy)-1,1,1-trifluoro-ethane) by cervical dislocation on day 13 to 14 d.p.c. (days post coitum) and embryos were collected in ice-cold 1x PBS. In addition, an ear biopsy was conducted for genotyping (3.1.2.2). After washing the embryos again in 1x PBS twice, all organs (e.g. liver, heart, visceral organs) and the head (kept for genotyping 3.1.2.2) were removed. The remaining tissue was put into a 6cm petri dish, covered by approximately 2ml of 0.25% Gibco™Trypsin-EDTA solution and finely cut by a scalpel. The tissue/trypsin mixture was then transferred to 14ml round bottom tubes with a 10ml pipette. Up- and down-pipetting for several times ensured further breakup of tissue chunks. The petri dish was rinsed with an additional 4ml of 0.25% Gibco™Trypsin-EDTA solution and added to the mixture in the tube (total volume per embryo/tissue ~5-6 ml). Then the mixture was incubated for 25’ at 37°C and was gently shacked by hand every ~5’. After that, the mixture was again gently pipetted up and down several times. Fifteen ml of MEF medium were added to the cell suspension to neutralize the trypsin. Continued disaggregation was obtained by further pipetting with a 10ml pipette. The tubes were subsequently stored vertically at RT for 5-10’ under the flow bank until cell debris has settled to the bottom. The supernatant, containing connective tissue cells (p0), was transferred to gelatin coated T75 culture flasks at a density equal to one embryo per flask and incubated for 24h. The cells in each flask were then detached as described in 3.1.2.3.2 and split 1:3 into p1 and further cultivated until fully confluent. On day 4 or day 5 freshly produced MEFs were again detached and frozen for long term backup in p2. Here, one T75 culture flask of MEFs was frozen into three Nunc™ Cryo tubes without counting the cell number according to the protocol described in 3.1.2.3.3.

3.1.2.2 Genotyping

3.1.2.2.1 Isolation of genomic DNA

Isolation of genomic DNA was conducted from ear biopsies for adult mice or heads for mouse embryos using the QIAGEN® DNeasy Blood and Tissue Kit. Biopsies/heads were placed in a 1.5ml Eppi™ Safe-Lock Tube and mixed with 180µl of ATL buffer and 20µl of Proteinase K for cell lysis which was conducted overnight at 56°C in a Thermomixer® (shaking at 1.000 rpm). The next morning, the lysates were vortexed for 15" and 200µl AL buffer as well as 200µl of ROTIPURAN® ethanol (≥99.8 %) were added. After another vortex step of 15", the lysates were pipetted into the DNeasy Mini spin column which was placed in a 2ml collection tube and centrifuged for 1' at 6.000 x *g*. The flow-through was discarded and the DNeasy Mini spin column was placed onto a new collection tube. Five hundred µl of buffer AW1 were added to the column and centrifuged again for 1' at 6.000 x *g*. The flow-through was discarded and the DNeasy Mini spin column was again placed onto a new collection tube. Then, 500µl AW2 buffer were added to the membrane and centrifuged for 3' at 20.000 x *g* to wash and dry the membrane. The flow-through was discarded again and the DNeasy Mini spin column was placed onto a fresh 1.5ml Eppi™ Safe-Lock Tube. Finally, 200µl AE buffer were added to the membrane and incubated for 1' at RT before the DNA was eluted by centrifugation for 1' at 6.000 x *g*. The eluted DNA was stored at -20°C until being used for genotyping as described below (3.1.2.2.2).

3.1.2.2.2 Endpoint PCR for genotyping

Endpoint PCR for genotyping was performed using the HotStar Taq® DNA Polymerase Kit with correspondent primer pairs of DR4_Puro/Neo and DR4_Hygro as listed in Table 12. The isolated genomic DNA, reagents as well as primers were pipetted in a 200µl PCR reaction tube stripe according to Table 28. Each primer pair was used in a separate reaction tube and endpoint thermocycling profile for the Thermocycler C1000 is listed in Table 29. For analysis, PCR products were separated on a 2% w/v agarose gel as described in 3.1.2.2.3. As positive controls, already genotyped samples were used whereas water (replacing the genomic DNA) served as negative control.

Table 28 Reagents for endpoint PCR for genotyping

Reagents	Final concentration	Volume (µl)
Genomic DNA	<10ng/µl	1
dNTPs (1mM each)	200µM of each dNTP	4
Primer forward (2µM)	0.2µM	2
Primer reverse (2µM)	0.2µM	2
PCR Buffer (10x)*	1x	2
Q-Solution (5x)	1x	4
HotStarTaq DNA Polymerase	2.5 units/reaction	0.1
Aqua bidest.		4.9
Total volume		**20**

*contains 15mM $MgCl_2$

Table 29 Thermocycling profile for endpoint PCR for genotyping

Reaction step	Duration	Temperature	
Initial activation	15‘	95°C	
Denaturation	60”	94°C	**3-step cycling** (40 cycles)
Annealing	45”	60°C	
Extension	60”	72°C	
Final extension	10’	72°C	
Cooling	∞	4°C	

3.1.2.2.3 Agarose gel electrophoresis

Horizontal agarose gel electrophoresis of PCR products was conducted in a 2% w/v agarose gel that was prepared as described in Table 5. The PCR products (20µl) were mixed with 4µl of a 6x blue gel loading dye and an appropriate DNA marker was prepared to identify DNA fragment sizes. Therefore, 19µl of H_2O, 1µl of Invitrogen™ 50bp DNA marker and 4µl of 6x blue gel loading dye were mixed. All samples were then applied to the slots of the gel that was placed in the electrophoresis system filled with 1x TBE as running buffer. After running for 40 to 45’ at 120V, the gel was photographed under UV light in the GelDoc™ XR documentation system using the Image Lab Software version 5.2.1.

3.1.2.3 Preparation of MEFs as feeder layers

3.1.2.3.1 Expansion

For expansion of MEFs, one Nunc™ Cryo tube of frozen MEFs p2 (3.1.2.1) was thawed/seeded as described in 3.1.2.3.4 to one gelatin coated 15cm culture plate with MEF medium (~15ml). Once the MEFs were grown confluent after a few days in culture, they were detached as described in 3.1.2.3.2 and split in a 1:4 ratio to new 15cm culture plates (MEFs p3) with fresh MEF medium.

After reaching confluence, they were once more split in a 1:4 ratio, to new 15cm plates (MEFs p4). When reaching confluence, MEFs were detached, counted (3.1.2.3.2) and frozen as feeder layer stocks (p5) (3.1.2.3.3).

3.1.2.3.2 Cell counting

MEFs were washed with 1x PBS and detached from the culture plates using 4ml of a 1:3 diluted 0.25% Gibco™Trypsin-EDTA solution (w/ 1x PBS). After incubation for 3' to 5' at 37°C, the trypsin was neutralized with 10ml MEF medium and the cells were transferred into a 14ml round bottom tube. Centrifugation for 5' at 300 x *g* was followed by aspiration of the supernatant. The remaining cell pellet was resuspended in 1ml fresh MEF medium and 10µl of the cell solution was transferred into a 1.5ml Eppi™ Safe-Lock Tube and mixed with 90µl of 0.5% trypan blue (dilution factor 10) to stain dead cells. Approximately 20µl of the cell/trypan blue solution was pipetted into a Neubauer chamber and vital cells (appear white under a phase contrast microscope) were counted in all four quadrants. The number of cells per ml was calculated using the following equation:

$$\frac{\text{number of cells}}{\text{ml}} = \frac{\text{counted cells (vital)}}{\text{counted quadrants (4)}} \times \text{chamber factor (10.000)} \times \text{dilution factor (10)}$$

3.1.2.3.3 Freezing of MEF stocks

Based on the number of counted cells per ml (3.1.2.3.2), the volume of MEF suspension for freezing was calculated. A total of $2.5*10^6$ MEFs p5 in MEF medium, were frozen in one Nunc™ Cryo tube supplied with 10% DMSO and 10% FCS. For preparation, a 1:1 mixture of DMSO/FCS was prechilled on ice for 10' due to its exothermic reaction when combined. Afterwards, each tube received 200µl of the 1:1 DMSO/FCS mixture followed by 800µl of $2.5*10^6$ cells in MEF medium (total volume of 1000µl per Nunc™ Cryo tube). Inverting the tubes 4 to 5 times ensured equal cell distribution. Then, cells were stored at -80°C for a minimum of 3 days to avoid cell damage due to fast temperature drop. For long term storage, MEF stocks were transferred to N_2 tanks until required for seeding as feeder layers (3.1.2.3.4).

3.1.2.3.4 Thawing, Seeding and Inactivation of MEFs

One day before use as feeder layer for stem cell culture, one tube of frozen MEFs p5 ($2.5x10^6$,3.1.2.3.3) was thawed and seeded to one gelatin coated culture plate (either one full 6 well, 12 well, 24 well or 48 well culture plate). MEFs were thawed in the water bath at 37°C for 2', supplied with ~ 3ml of fresh MEF medium and transferred into a 14ml round bottom tube for centrifugation for 5' at 300 x *g*.

The supernatant was discarded, the pellet was resuspended in the required amount of fresh MEF medium and cells were seeded into cell culture plates. After 24h, MEFs became confluent and were inactivated by Mitomycin C to avoid further proliferation. For this propose, the medium was exchanged by fresh MEF medium supplied with 10µg/ml Mitomycin C and incubated for 2.5 h at 37°C, 5% CO_2. Subsequently, inactivated cells were washed twice with 1x PBS and supplied with the required amount of fresh MEF medium.

3.1.3 Murine adult fibroblasts

Two different murine fibroblast populations from the transgenic NkxCEeGFP mouse line were used in this study (Table 22). For MicroRNA Array analysis (3.3), cardiac fibroblasts (CF) as well tail tip fibroblasts (TTF) were isolated. Before cell isolation, NkxCEeGFP mice (~8 weeks old) were anesthetized with isoflurane (2-chloro-2-(difluoromethoxy)-1,1,1-trifluoro-ethane) and euthanized by cervical dislocation. Ear biopsies were taken for genotyping which was conducted as described in 3.1.2.2 with correspondent primer pairs for NkxCEeGFP listed in Table 12.

In addition, transgenic TTFs were generated from Isl1Cre-R26^{mTmG} mice (Muzumdar *et al.*, 2007; Yang *et al.*, 2006) for reprogramming into induced pluripotent stem cells (iPSCs) (3.5). Therefore, tail tips of 8 weeks old Isl1Cre-R26^{mTmG} mice were kindly gifted by AG Laugwitz at Klinikum rechts der Isar, Technical University Munich. Genotyping of Isl1Cre-R26^{mTmG} mice was kindly performed by Tatjana Dorn (AG Laugwitz) before tail tips were transferred to our institute in 1x PBS on ice for TTF isolation. The protocols of CF and TTF isolation of both transgenic mice are described below in 3.1.3.1 and 3.1.3.2.

3.1.3.1 Isolation of cardiac fibroblasts (CF)

For CF isolation, hearts of NkxCEeGFP mice were collected in petri dishes with ice-cold 1x PBS. To remove remaining blood, the organ was thoroughly flushed several times with 1x PBS by a 30G syringe which was injected into the ventricle. After transfer to a new petri dish, the heart was minced into small pieces with a scalpel and collected in a 14ml round button tube for digestion. Therefore, 4ml of freshly prepared Collagenase II Dissociation Solution were added and incubated for 2h at 37°C in a hybridization incubator. After a filter step through a 70µM Falcon™ Cell Strainer as well as centrifugation of 10’ at 300 x *g*, cells were resuspended in 1ml fresh 1x PBS. To clean cells from remaining erythrocytes, erythrocyte lysis was performed. Therefore, 10x Red Blood Cell Lysis Solution was diluted 1:10 with aqua bidest., and a final volume of 10ml was added to the cells of one heart. After a short vortex, the lysis was conducted by incubation for 2’ at RT and centrifuged for 10’ at 300 x *g*.

Subsequently, cells were resuspended in 2ml of MEF medium and finally plated on one well of a gelatin coated 6 well plate. After 24h, the medium was replaced and if necessary, again after a few days to ensure optimal growth. When cells were finally confluent (~one week), they were detached with 500µl of a 1:3 diluted 0.25% Gibco™Trypsin-EDTA solution (w/ 1x PBS), incubated for 3' to 5' at 37°C and stopped with 2ml of MEF medium. Followed by a centrifugation step of 5' at 300 x *g*, the cells were freshly resuspended in MEF medium and seeded into one T25 culture flask in a total volume of 5ml. Subsequently, isolated CFs required for MicroRNA Array analysis (3.3) were harvested in Lysis/Binding Solution for miR isolation as described in 3.3.2.

3.1.3.2 Isolation of tail tip fibroblast (TTF)

Tail tips of NkxCEeGFP (self-collected) and Isl1Cre-R26^{mTmG} mice (provided by colleagues, AG Laugwitz) were collected in ice-cold 1x PBS and washed once in 70% ethanol, then rinsed again with 1x PBS and transferred into a 2ml Eppi^{TM} Safe-Lock Tube for digestion with 300µl Collagenase II Dissociation Solution in a Thermomixer® under the conditions described above (3.1.3.1). The digested tail tips were centrifuged for 10' at 300 x g and resuspended in a total of 2ml of fresh MEF medium. Each digested tail tip was then seeded onto one well of a gelatin coated 6 well plate. Medium was replaced with fresh MEF medium after 24h of cultivation. After about one week, when TTFs became confluent, they were passaged once into T25 culture flasks as described above (3.1.3.1).

For MicroRNA Array analysis, the TTFs of NkxCEeGFP mice were subsequently harvested in Lysis/Binding Solution for miR isolation (3.3.2). Isl1Cre-R26^{mTmG}-derived TTFs were directly used for transduction as described in 3.5.3. at this low passage to avoid replicative senescence which could influence reprogramming efficiency.

3.1.4 Murine pluripotent stem cell lines

Two different murine transgenic stem cell lines were used for miR knockdown experiments including the NkxCE-GFP ESC line as well as the self-generated Isl1Cre-R26^{mTmG} iPSC (iITG-iPSC) line (3.5). For overexpression studies, the self-generated miR overexpressing NkxCE-GFP ESC lines (OE-ESCs), referred to as OE-Ctr and OE-128 (3.6), were utilized. Additionally, the non-transgenic murine ESC line V6.5 was used for evaluation of miR kinetics during *in vitro* differentiation (3.4). All utilized murine pluripotent stem cell lines are listed in Table 18 and Table 19.

3.1.4.1 Culturing and passaging

All murine ESC/iPSC lines were cultured on gelatin coated 6 well plates on mitomycin-inactivated MEFs as feeder layer in CJ7 medium in the presence of leukemia inhibitory factor (LIF) to maintain their pluripotent stage (Hopfl *et al.*, 2004). For culture of the self-generated miR overexpressing NkxCE-GFP ESC lines (OE-Ctr, OE-128), CJ7 medium was supplied with tetracycline-free FCS due to the integrated, doxycycline-inducible lentiviral tet-on system (see 3.6.1, Appendix Figure A6A). Doxycycline belongs to the family of tetracycline antibiotics.

In addition, 1µg/ml puromycin was added to the medium to increase the selection pressure on miR expressing ESC clones. If required for experiments, 2µg/ml doxycycline were added to the medium to induce miR expression. Medium was changed every day and ESC/iPSC lines were passaged every other day. Therefore, cells were incubated with 500µl 0.25% Gibco™ Trypsin-EDTA solution for 3' to 5' at 37°C until fully detached. Cells were then transferred into a 14ml round button tube containing 3ml CJ7 medium w/o LIF and centrifuged for 5' at 300 x *g*. The supernatant was removed, and the cells were resuspended in CJ7 medium with the required supplements as described above. ESCs/iPSCs were generally split at a ratio from 1:3 to 1:6 onto new MEF feeder layers on 6 well plates dependent on their confluency.

3.1.4.2 Freezing and thawing of ESCs/iPSCs

For freezing, ESCs/iPSCs were detached and centrifuged for 5' at 300 x *g* as described above (3.1.4.1). In general, one confluent well of a 6 well plate was frozen into four to six Nunc™ Cryo tubes in a mixture of 90% FCS (standard or tetracycline-free, depending on the ESC/iPSC line) and 10% DMSO. Cells were stored at -80°C for a minimum of 3 days to avoid cell damage due to fast temperature drop. Long term storage was conducted in a N_2 tank.

For thawing, ESCs/iPSCs were incubated for 2' in a water bath at 37°C before they were centrifuged in a 14ml round button tube that was supplied with ~ 3ml of CJ7 medium for 5' at 300 x g. After resuspension in fresh CJ7 medium, in general one Nunc™ Cryo tube of ESCs/iPSCs was seeded on one well of a gelatin coated 6 well plate on mitomycin-inactivated MEFs.

3.2 *In vitro* differentiation of murine pluripotent stem cell lines

In vitro differentiations of murine pluripotent ESCs/iPSCs were conducted for several experimental purposes. First, NkxCE-GFP ESCs were differentiated for isolation of cells for MicroArray analysis (3.3). Further, NkxCE-GFP ESCs were differentiated for the analysis of kinetics of TFs (3.4.1). Kinetics of miRs was evaluated on differentiating non-transgenic murine V6.5 ESCs (3.4.1). The self-generated iITG-iPSCs (3.5) and OE-ESCs (3.6) were first differentiated for characterization.

Finally, fully characterized iITG-iPSCs as well as the transgenic NkxCE-GFP ESCs were differentiated for miR-128a knockdown experiments (3.8), where they were transfected with LNA probes for inhibition of miR function as described in 3.8.1. For miR overexpression studies (3.9), corresponding OE-ESCs were differentiated under dissenting medium conditions to induce miR expression as described in (3.9.1).

Regardless of the different purposes of experiments, all murine ESCs/iPSCs were differentiated using the a standard differentiation method: the “hanging drop method” (Huang and Wu, 2010; Wang and Yang, 2008) as explained in detail below (3.2.1).

3.2.1 Hanging drop method

The hanging drop method which had first been developed by Robert Koch to study bacteria (Sakula, 1979), is nowadays widely used for stem cell research, especially to investigate early embryogenesis. By forming stem cell-containing single hanging droplets that subsequently form three-dimensional structures by gravity (in the following referred to as embryoid bodies (EBs)), EBs are able to differentiate into more or less mature cells of all three germ layers (endoderm, ectoderm and mesoderm) thus recapitulating crucial aspects of early mammalian cell differentiation *in vitro* (Desbaillets *et al.*, 2000; Hopfl *et al.*, 2004).

Subsequently, three of the main cardiac subpopulations including cardiomyocytes (CMs), endothelial cells (ECs) and smooth muscle cells (SMCs) can be observed during differentiation after two to three weeks, also verified by immunocytochemistry (ICC) (3.2.2.1).

3.2.1.1 Formation of EBs

Before starting *in vitro* differentiation experiments, all murine ESCs/iPSCs were cultured under normal growth conditions as described in 3.1.4.1. At the beginning of *in vitro* differentiation, all murine ESCs/iPSCs lines were replated on gelatin coated 6 well plates without MEF feeders for 48h in IMDM-ES medium supplied with 1x LIF to reduce MEFs from the ESCs/iPSCs culture which may negatively impact the differentiation.

To start the differentiation, the cells were then detached as described in 3.1.4.1 and counted with the “Neubauer chamber” method described in 3.1.2.3.2. Dependent on the ESC/iPSC line used, single hanging droplets (11µl) with a cell number of either 1000 or 2000 cells per droplet in differentiation medium were formed on 15cm culture plates using a multi-channel pipet (~300 drops/plate). The used numbers of cells per droplet (EB) and ml are indicated in Table 30 below.

Table 30 Number of ESC/iPSC for EB formation

ESC/iPSC	Cells per droplet (EB)	Cells per ml
NkxCE-GFP ESCs	1000	$0.9x10^5$
non-transgenic V6.5	1000	$0.9x10^5$
NkxCE-GFP ESC miR-Ctr overexpression line (OE-Ctr)	1000	$0.9x10^5$
NkxCE-GFP ESC miR-128a overexpression line (OE-128)	1000	$0.9x10^5$
Isl1Cre-R26^{mTmG} iPSC line (iITG-iPSC)	2000	$1.8x10^5$

To enable the building of EBs, plates were stored up-side down in the incubator at 37°C for two days (48h). Afterwards, EBs were flooded with about 20ml of differentiation medium and dependent on the experiment either cultured on 15cm culture plates or replated as described below (3.2.1.2).

3.2.1.2 Replating of EBs

For isolation of cells (cell sorting) for MicroArray analysis (3.3), evaluations of kinetics (3.4), and characterization of self-generated ESC/iPSC lines (3.5.5, 3.6.3), ESCs/iPSCs were not replated at day 2 but further cultured in 15cm culture plates until analysis.

For knockdown and overexpression experiments (3.8, 3.9), EBs were replated on 12 well plates. Therefore, EBs from 3 to 4 15cm culture plates were carefully collected with a 10ml serological pipet and transferred to a 14ml round button tube followed by a centrifugation step at 130 x *g* for 1’. The supernatant was aspirated, and after careful resuspension in fresh differentiation medium (only tapping with fingers), EBs were transferred to four wells of a gelatin coated 12 well plate where they started to adhere and differentiate.

For ICC experiments performed during differentiations (3.2.2.1), one single EB was collected with a 1ml pipette and directly transferred into one well of a gelatin coated 96 well plate where it was further differentiated until staining.

For MTT assays performed during *in vitro* differentiation, a different replating strategy into a 48 well plate was applied, explained in detail in 3.7.1.

In general, the duration of each differentiation assay was dependent on the experimental purpose and varied between 1 and 4 weeks. During that time the medium was replaced when it was necessary according to the experimental setup (3.9.1) or if the medium was consumed due to cell growth.

3.2.2 Analysis of differentiation capacity and maturation of ESCs

3.2.2.1 ICC for cardiac lineages

To verify the differentiation and maturation capacity of ESCs into cardiac lineages, the NkxCE-GFP ESCs were differentiated up to three weeks (day 20) using the standard protocol with the replating approach as described above (3.2.1.2). The staining was conducted with below mentioned diluted antibodies and the protocol (buffers, chemicals and times) as described in 3.5.5.5. For staining of CMs, the mouse monoclonal antibody against sarcomeric α-Actinin (Actn) was diluted 1:200 whereas the mouse monoclonal anti-αMHC (Myh6) antibody was diluted 1:100. SMCs were stained by a mouse monoclonal anti-αSMA (Acta2) antibody at a dilution 1:20 and ECs were stained for CD31 with a rabbit polyclonal anti-CD31 (Pecam1) antibody at a dilution 1:50. For staining of CMs as well as SMCs, the goat anti-mouse Alexa Fluor® 555 labelled secondary antibody was used at a concentration of 1:500. Labeling of ECs was conducted with a 1:500 diluted Alexa Fluor® 488 coupled goat anti-rabbit secondary antibody. As negative controls for unspecific binding of the secondary antibodies, NkxCE-GFP ESCs were stained with the correspondent secondary antibody only. A full list of the used first and secondary antibodies can be found in Table 16 and Table 17.

3.3 MicroRNA Array

MicroRNA Array analysis was conducted using a Taqman™ Array Rodent MicroRNA A+B Card Set (Thermo Fisher Scientific) in cooperation with Jeanette Erdmann and Zouhair Aherrahrou (Institute for Cardiogenetics, University of Lübeck, Lübeck, Germany) to establish a miR expression profile of a distinct, multipotent NkxCE-GFP CPC population. Therefore, the expression of about 750 known miRs was evaluated in four different murine cell populations including (1) above-mentioned cardiac-specific NkxCE-GFP CPCs, (2) their correspondent GFP-negative cell fractions (both isolated from embryos (*in vivo*) and ESC differentiations (*in vitro*)), (3) adult CFs as well as (4) adult TTFs as a non-cardiac cell population.

By comparative analysis of miR profiles, differentially expressed miRs (potential candidates) within the targeted CPC population were identified and further selected for *in vivo* and *in vitro* studies.

All sample preparations, including the isolation of cell populations (1)-(4) and miR isolations were conducted in our facility as described in 3.3.1 & 3.3.2 and transferred to Jeanette Erdmann und Zouhair Aherrahrou for final MicroRNA Array analysis. The received raw expression data were then analyzed by Gianluca Santamaria (Medical Department 1, Cardiology, Klinikum rechts der Isar, Technical University Munich) (3.3.3).

3.3.1 Isolation of cell populations

NkxCEeGFP transgenic TTFs and CFs required for analyses were generated as described under the section 3.1.3. NkxCE-GFP CPCs and correspondent GFP-negative fractions were isolated *in vivo* from NkxCEeGFP transgenic embryonic hearts and *in vitro* differentiated NkxCE-GFP ESCs as described below in 3.3.1.1.

3.3.1.1 NkxCE-GFP CPCs and negative fractions

In vivo NkxCE-GFP CPCs as well as their correspondent GFP-negative fractions were isolated from NkxCEeGFP embryonic mice hearts at E9.5. Mouse embryos derived from timed mating whereas a positive mating plug indicated E0.5. After animals were euthanized as described in 3.1.3, embryos were collected, directly placed in ice-cold 1x PBS and first mechanically dissociated using a scalpel. Then, they were further digested by Collagenase II Dissociation Solution for 1h at 37°C in a hybridization incubator. After 5' centrifugation at 300 x *g*, the remaining dissociation solution was aspirated, and digested tissue including isolated cells was resuspended in 1ml FACS buffer for fluorescent activated cell sorting (FACS, flow cytometry) which was conducted on a BD FACSARIA III (BD Biosciences) by Lynette Henkel at the flow cytometry unit of the Technical University Munich (CyTUM) in cooperation with Dr. Schiemann at the Institut für Medizinische Mikrobiologie, Immunologie und Hygiene (MIH). Both fractions were directly sorted into Lysis/Binding Solution for subsequent miR isolation (3.3.2).

Additionally, NkxCE-GFP CPCs and GFP-negative fractions were isolated from seven days (D7) *in vitro* differentiated NkxCE-GFP ESCs. For this, ESCs were differentiated without replating according to the standard protocol described in 3.2 until day 7. Then, the cells were scraped mechanically from the culture plate using a Corning® Cell scraper and digested with Collagenase II Dissociation Solution for 1h at 37°C before being resuspended in 1ml FACS buffer and sorted by mentioned colleagues into Lysis/Binding Solution for miR isolation (3.3.2).

3.3.2 Isolation of miRs for MicroRNA Array

The isolation of miRs for microRNA Array analysis was conducted with the *miR*Vana™ miRNA Isolation Kit according to the manufacturer's instructions. Thus, the isolated cell populations (3.3.1) were either harvested or sorted in 600µl of Lysis/Binding Solution in a 1.5ml Eppi™ Safe-Lock Tube and vigorously vortexed to ensure a homogenous lysate. Then, 1/10 of the volume (60µl) of miRNA Homogenate Additive was added to each cell lysate, the tubes were inverted several times and incubated for 10' on ice. 600µl of a 1:1 Phenol: Chloroform solution (equal to the initial lysate volume) was added and the tubes were vortexed for 30 to 60". A centrifugation step of 5' at maximum speed (10.000 x *g*) at RT followed to separate the aqueous and the organic phase. The aqueous upper phase was removed, the volume was noted and transferred to a fresh 1.5ml Eppi™ Safe-Lock Tube. Then, 1.25 volumes of 100% ethanol were added to the aqueous phase (e.g. if 300µl were removed, 375µl ethanol was added). The lysate/ethanol mixture was then applied to a filter cartridge that was placed into a collection tube and centrifuged for 15" at 10.000 x *g*. The flow-through was discarded and the filter was washed once with 700µl miRNA Wash Solution 1 by centrifugation for 5 to 10" at 10.000 x *g*. Then two subsequent washing steps with each 500µl of Wash Solution 2/3 (5 to 10" at 10.000 x *g*) followed. After removing the last flow-through, the filter cartridge in the collection tube was centrifuged for 1' at 10.000 x *g* to remove all residual fluid. The filter cartridge was then transferred to a new collection tube and 100µl of pre-heated (95°C) DNase/RNase-free dH_20 was added and centrifuged for 1' at 10.000 x *g* for miR elution. The samples were then transferred on dry ice to the mentioned colleagues for final MicroRNA Array analysis.

3.3.3 Comparative analysis of microRNA profiles

The microRNA Array raw data (Ct values) were analyzed by Gianluca Santamaria as stated above. For comparative analysis of miR expression profiles, U6 expression was used as an internal control (ΔCt = Ct (Target) - Ct (Reference)) and the fold change (FC) was calculated by the $2^{-\Delta\Delta Ct}$ method (Schmittgen and Livak, 2008).

MiRs were considered to be differentially expressed using a threshold of a |1.5| fold change (FC) and two-sided Student's t-test *p*-value ≤ 0.05 between cell populations of interest. By this, significantly enriched miRs (potential candidate miRs) within the targeted CPC population could be identified for further analysis.

3.4 Analysis of expression kinetics

Kinetics of candidate miRs as well as selected cardiac transcriptions factors (TFs) were evaluated during *in vitro* differentiation of two different murine pluripotent stem cells lines including the non-transgenic V6.5 ESC line or the transgenic NkxCE-GFP ESC line, respectively, as described in 3.4.1. Additionally, candidate miR expression was analyzed during *in vitro* differentiation of human iPSCs (hiPSCs) as stated in 3.4.2 to evaluate miR kinetics in a different species.

3.4.1 Kinetics during *in vitro* differentiation of murine ESCs

For analysis of miR and TF kinetics, non-transgenic V6.5 as well as NkxCE-GFP ESCs were differentiated with the standard protocol without replating as described in 3.2 until day 10. RNA was isolated (3.5.5.1) from both lines every other day from day 0 to day 10. RNA derived from V6.5 ESC differentiations was reverse transcribed (3.6.3.2) for final qRT-PCR analysis of candidate miRs (3.6.3.3). RNA samples derived from NkxCE-GFP ESC differentiations were used for cDNA synthesis of mRNA (3.5.5.2) and qRT-PCR analysis (3.5.5.4) of TFs like *Gata4, Nkx2.5* and *Hand1* (Table 13).

3.4.2 Kinetics during *in vitro* differentiation of hiPSCs

The generation of hiPSCs by reprogramming from peripheral blood mononuclear cells (PBMCs) of a healthy individual with Sendai virus, the characterization (*unpublished data*) as well as culture and *in vitro* differentiation was kindly conducted in our faculty by colleagues, namely Martina Dreßen, Harald Lahm and Irina Neb (German Heart Center Munich, Department of Cardiovascular Surgery, Institute Insure) under the approval of the Ethikvotum ”Die Einrichtung einer kardiovaskulären Biobank innerhalb des Deutschen Herzzentrums Münchens (KaBi/DHM 5943/13). HiPSCs were differentiated by manipulating the Wnt-signaling pathway according to the protocol of Burridge *et al*. (Burridge *et al.*, 2014). RNA samples were isolated every other day beginning on day 0 until day 14 and were kindly provided for cDNA synthesis of miRs and qRT-PCR analysis (3.6.3.2 & 3.6.3.3).

3.5 Generation of Isl1Cre-R26^{mTmG} iPSC line (iITG-iPSC)

The Isl1Cre-R26^{mTmG} iPSC line was generated by reprogramming Isl1Cre-R26^{mTmG} transgenic murine TTFs by co-transducing them with a polycistronic doxycycline-inducible murine "stem cell cassette" (muSTEMCCA) containing lentivirus expressing the four "Yamanaka factors" *Oct-4, Klf4, Sox-2*, and *c-Myc* (Takahashi and Yamanaka, 2006) and a lentivirus expressing a reverse tetracycline transcriptional activator (rtTA) element (3.5.3). By constitutive expression of rtTA, which binds to the tetO operator of the muSTEMCCA cassette under the presence of doxycycline, this element enables the induction of the tet-on system throughout reprogramming.

Both lentiviruses were generated under Biosafety level 2 (BSL-2) in our laboratory and continuative reprogramming protocols were approved by the "Regierung von Oberbayern". The muSTEMCCA and rtTA lentiviruses were produced by 293FT cells which were transfected with either the pHAGE-STEMCCA expression vector or the FUdeltaGW-rtTA plasmid in addition to the pCMV-VSV-G plasmid which expresses the required viral envelope protein as well as pCMV-dR8.2 dvpr harboring the packaging protein.

Before being used for viral production (3.5.2), the purchased plasmids (2.3.1, Table 7) had to be processed as described below (3.5.1) dependent on the form of delivery (either as bacterial stab or purified DNA). The detailed vector maps of all plasmids are attached as Appendix Figures A1-A4.

3.5.1 Preparation of lentiviral plasmids

The pHAGE-STEMCCA plasmid was received as purified plasmid DNA on filter paper. The plasmid DNA was then eluted in aqua bidest. and was transformed into competent *XL10 E. coli* for amplification and purification (3.5.1.1). The other plasmids purchased from Addgene were obtained as bacterial agar stabs either in competent DH5alpha *E. coli* (pCMV-R8.2 and pCMV-VSV-G) or Stbl3 *E. coli* (FUdeltaGW-rtTA) and were streaked on agar plates for isolation of single colonies and further amplification (3.5.1.2).

3.5.1.1 Transformation of pHAGE-STEMCCA into *XL10 E-coli*

For transformation, one vial containing 50µl of chemically competent *XL10* bacteria was thawed on ice for 5' and 1µl of pHAGE-STEMCCA plasmid DNA (~1pg -100ng) was added to the vial and further incubated on ice for 30'. After incubation, heat shock was conducted at 42°C by placing the vial into the Thermomixer® for exactly 30".

After an incubation for 5' on ice, 600µl of S.O.C medium was added to the bacteria/DNA mixture. For initiating bacterial growth, the vial was incubated for 1h at 37°C in a shaking Thermomixer® (~250 rpm).

Finally, 5µl or 50µl of the transformed bacteria were plated on prewarmed LB agar plates containing 100µg/ml ampicillin for selection. After incubating the plates up-side down for 24h at 37°C in the bacterial incubator, single colonies were picked for overnight culture (3.5.1.3).

3.5.1.2 Streak of pCMV-R8.2, pCMV-VSV-G and FUdeltaGW-rtTA

The bacterial agar stocks for pCMV-R8.2, pCMV-VSV-G and FUdeltaGW-rtTA were plated on prewarmed LB agar plates containing 100µg/ml ampicillin with the help of sterile inoculation loops. For preparation, the inoculating loop was flamed over the Bunsen burner until sterile. After cooling the loop, it was dipped into the agar stab and streaked on the agar plates. The agar plates were put in the incubator up-side down overnight at 37°C until single colonies were visible. Subsequently, single colonies were picked for amplification (3.5.1.3).

3.5.1.3 Inoculating overnight cultures of bacteria

After receiving single colonies from overnight incubated agar plates (3.5.1.1 & 3.5.1.2), the plasmid-containing bacteria were first amplified in a small scale, also called "Miniprep-culture", predominantly as a quality control step to ensure that the right plasmid was amplified. Therefore, a single colony was picked with the help of a sterile pipette tip from the agar plate and transferred to a 14ml round button containing 3ml of LB medium supplemented with 6µl of ampicillin (final concentration 100µg/ml). Bacteria were incubated overnight at 37°C in the shaking bacterial incubator (250 rpm). Plasmid DNA was subsequently isolated as described in 3.5.1.4 and digested for quality control (3.5.1.6) on the next day.

For large scale plasmid purification, needed for virus production, a so-called "Midiprep-culture" was inoculated. For this, 50µl of the previously described "Miniprep-culture" were inoculated with 100ml LB medium containing 200µl ampicillin (final concentration 100µg/ml) in a 500ml Erlenmeyer flask. Bacterial cultures were incubated over night at 37 °C at 250 rpm and large-scale plasmid isolation (3.5.1.5) as well as enzymatic control digest was conducted the next day (3.5.1.6).

3.5.1.4 Small-scale isolation of plasmid DNA from *E. coli*

For small-scale DNA isolation, also referred to as Miniprep, the QIAGEN® Plasmid Miniprep Kit was used according to the manufacturer's protocol.

In brief, 2ml from an overnight “Miniprep-culture” (3.5.1.3) was transferred into an 2ml Eppi™ Safe-Lock Tube and centrifuged at maximum speed (~17.900 x *g*) for 3’ at 4°C. The supernatant was discarded, and the bacterial pellet was homogenously resuspended in 250µl buffer P1 (supplied with RNAse A and LyseBlue) until no cell clumps remained. Then, 250µl of buffer P2 were added and the tubes were vigorously mixed by inverting them 4-6 times until the solution became blue as a sign of cell lysis. Finally, 350µl of buffer N3 were added and tubes were vortexed until solution became white again and cloudy (efficient SDS precipitation). In order to separate phases, the tubes were then centrifuged at maximum speed for 10’ at 4°C and the cleared supernatant containing the plasmid DNA was transferred directly to the membrane of a QIAprep 2.0 spin column. After a centrifugation step for 1’ at maximum speed, the flow-through was discarded and the membrane binding the DNA was washed with 750µl buffer PE (centrifuged for 1’ at maximum speed). Another centrifugation step for 1’ at maximum speed followed to ensure that all residual washing buffer was removed. The washed and dried QIAprep 2.0 spin column was now transferred to a fresh 1.5ml Eppi™ Safe-Lock Tube. To elute the plasmid DNA, 50µl of buffer EB were directly applied to the column membrane, incubated for 1’ at RT to enhance DNA yield, and finally centrifuged at maximum speed for 1’. The eluted plasmid DNA was then used for control digests as described in 3.5.1.6.

3.5.1.5 Large-scale isolation of plasmid DNA from *E. coli*

Large-scale DNA isolation of plasmid DNA (Midiprep), was conducted with the QIAGEN® Plasmid Midiprep Kit which was used according to manufacturer’s recommendations. The inoculated 100ml of overnight cultures (described in 3.5.1.3) were first allocated to two 50ml Falcon® High-Clarity Polypropylene Conical Tubes and then centrifuged for 30’ at 4000 x *g* at 4°C. After the supernatant was discarded, the bacterial pellets were resuspended in a total of 4ml P1 buffer including RNase A and LyseBlue. After 4ml of P2 buffer were added, the tubes were mixed by inverting them several times. Then, they were incubated for 5’ at RT. Additionally, 4ml of prechilled P3 buffer were added, gently mixed by inversion and incubated on ice for 15’. Then, the tubes were centrifuged for 30’ to 45’ at 4000 x *g* to separate phases followed by a filtration step (30µm) to ensure that all remaining precipitates are removed. Meanwhile, the QIAtip was equilibrated with 4ml QBT and the filtrated lysate was directly applied to the QIAtip. After the lysate passed the resin by gravity flow, two washing steps with each 10ml of buffer QC followed to remove all remaining contaminants. The DNA-containing QIAtip was now transferred onto a new tube and 5ml of prewarmed Buffer QF were applied to elute DNA. DNA was precipitated with 3.5ml of 100% v/v isopropanol and subsequent centrifugation at 4000 x *g* for 1h at 4°C. The supernatant was carefully removed, and DNA was washed by 2ml of 70% v/v ethanol (centrifuged for 1h at 4°C and 4000 x *g*). Again, the supernatant was removed, and the pellet was air dried for 30’.

To resolve the DNA, 100µl TE buffer were added to the pellet and tubes were stored overnight at 4°C to enhance DNA yield. The plasmid DNA was further used for control digests as described in 3.5.1.6 and stored at -20°C until needed for 293FT cell transfection for virus production (3.5.2). Before usage, the DNA concentration was measured with the NanoDrop™2000.

3.5.1.6 Control digests of plasmid DNA

Control digests were performed as quality control for all plasmid DNA isolated with small- as well as large-scale isolation protocols (3.5.1.4 & 3.5.1.5). For enzymatic restriction digest, either 1µl of small-scale isolated plasmid DNA from Miniprep or 0.5µl of Midiprep DNA (~1µg) were digested with 0,5µl enzyme (5U) and 2µl of the respective 10x buffer in a total volume of 20µl in a 1.5ml Eppi™ Safe-Lock Tube. The required restriction enzymes were determined with the help of the online platform NEB Cutter v2.0 (New England Biolabs). The plasmid sequences were uploaded, and the restriction sites of enzymes computed. Two-, three- or four-times cutting enzymes were selected, and the resulting fragments were calculated by self-made plasmid maps. A list of used restriction enzymes can be found in Table 9. A list of the plasmids with corresponding restriction enzymes, buffers as well as resulting fragments are listed below (Table 31).

Table 31 Enzymes, buffers and resulting fragments of plasmid digestion

Plasmid	Enzyme	Buffer	Fragment sizes (bp*)
pHAGE-STEMCCA	BamHI/NotI	Buffer EcoRI	10000, 2600
	BamHI/NdeI	Buffer EcoRI	10000, 600
pCMV-R8.2,	PstI	Buffer O	10455, 1424, 1501
pCMV-VSV-G	EcoRI	Buffer EcoRI	4791, 1668, 24, 24
FUdeltaGW-rtTA	PstI	Buffer O	1422,8525

*Abbreviation: bp, base pairs

Digests were incubated at 37°C in the Thermomixer® for 1h and further separated on a 1% w/v agarose gel with the Invitrogen™ 1kb DNA marker as described in 3.1.2.2.3.

3.5.1.7 Bacterial glycerol stocks for long-term storage

To ensure long-term storage, all lentiviral plasmids were stored as bacterial glycerol stocks in our facilities. Therefore, 700µl of bacteria culture obtained from overnight Miniprep culture (3.5.1.3) were mixed (vortexed) with 300µl Glycerol in a 2ml Eppi™ Safe-Lock Tube and stored at -80°C.

3.5.2 Production of muSTEMCCA and rtTA lentiviruses

3.5.2.1 Seeding of 293FT cells

One day before transfection with lentiviral expression plasmids, confluent 293FT cells from maintenance culture (T75 culture flasks) (3.1.1) were detached and counted as described in 3.1.2.3.2. Since transfection reagents increase cell permeability and a higher uptake of penicillin/streptomycin during transfection could result in toxic effects influencing transfection efficiency, cells were seeded in a total of 10ml antibiotic-free MEF medium on gelatin coated 10cm culture plates with $5x10^6$ cells per plate. After incubation of 24h to 30h at 37°C and 5% CO_2, the cells reached 70-80% confluency and were ready for transfection for virus production (3.5.2.2).

3.5.2.2 Transfection of 293FT cells

The transfection mixture contained 11µg of lentiviral plasmid DNA (either pHAGE-STEMCCA or FUdeltaGW-rtTA), 5.5µg of pCMV-VSV-G as well as 8.25µg of pCMV-R8.2 which were diluted in a total volume of 600µl serum-free (pure) DMEM. The transfection reagent Fugene was vortexed for 1" and 50µl (at a ratio of 4:2, meaning 50µl Fugene to 25µg total DNA) were added to the DNA/DMEM mixture (w/o touching the walls of the 1.5ml Eppi™ Safe-Lock Tube). The tubes were shortly vortexed and incubated for 15' at RT. Then, the transfection mixture was added dropwise to the 293FT cells and incubated for 72h at 37°C and 5% CO_2 until the viruses were harvested (3.5.2.3).

3.5.2.3 Harvest of lentiviruses

The conditioned 293FT medium containing the infectious lentiviral particles of muSTEMCCA and rtTA was harvested 72h post transfection (day 3). Visually, the morphology of lentivirus-producing 293FT cells appeared macerated/swollen in comparison to non-transfected 293FT cells indicating a sufficient virus production and viral shedding. Medium was collected in a 15ml Falcon® High-Clarity Polypropylene Conical Tube and centrifuged for 10' at 300 x *g* at 4°C. The supernatant was then filtered through a 0.45µm filter to remove cell debris and further aliquoted into 1.5ml Eppi™ Safe-Lock Tube with each 500µl of lentivirus supernatant. Until usage (3.5.3), the virus was stored at -80°C in the BSL-2 laboratory.

3.5.3 Transduction of Isl1Cre-R26^{mTmG} TTFs

On the day of reprogramming, a confluent T25 culture flask with isolated Isl1Cre-R26^{mTmG}-derived TTFs (3.1.3.2, Appendix Figure A5A) was washed once with 1x PBS and treated with 500µl of a 1:3 diluted 0.25% Gibco™ Trypsin-EDTA solution (w/ 1 x PBS) for 3' at 37°C until detachment. Trypsin was stopped with MEF medium, cells were centrifuged for 5' at 300 x *g* and the pellet was resuspended in 1ml antibiotic-free MEF medium. After counting the number of cells as described in 3.1.2.3.2, 2x10^5 TTFs in a total volume of 500µl antibiotic-free MEF medium supplemented with polybrene (PB) at a final concentration of 8µg/ml were transferred into a 14ml round button tube and further mixed with 1000µl of each muSTEMCCA and rtTA lentivirus for reprogramming.

Polybrene, as a cationic polymer, has been shown to be able to neutralize e.g. the charge repulsion of viruses and target cells thereby enhancing transduction efficiency (Davis *et al.*, 2002; Davis *et al.*, 2004).

To exclude influence of polybrene on normal cell physiology, a control with 8µg/ml polybrene only (PB-Ctr) was conducted. The detailed reaction setup is listed in Table 32 below.

Table 32 Viral transduction scheme of Isl1Cre-R26^{mTmG} TTFs

Sample	TTFs (2x10^5)	Polybrene (0.8mg/ml)	muSTEMCCA lentivirus	rtTA lentivirus	Antibiotic-free MEF medium
Reprogramming	500µl	25µl	1000µl	1000µl	-
PB-Ctr	500µl	25µl	-	-	2000µl

The cell/virus mixture was then directly seeded on one well of a gelatin coated 6 well plate and incubated at 37°C. After 24h, cells were washed twice with MEF medium and finally supplied with MEF medium with antibiotics additionally containing 2µg/ml doxycycline for induction of the muSTEMCCA cassette. At 80-90% confluency, the fibroblasts were split in a 1:3 ratio to three wells coated with mitomycin-inactivated MEF feeders with CJ7 medium supplemented with 2µg/ml doxycycline and double amount (2x) of LIF (10^6 U/ml). The medium was changed every day or every second day until iITG-iPSC clones started evolving.

The documentation of several evolving iITG-iPSC clones before picking (3.5.4) can be found in Appendix Figure A5B.

3.5.4 Picking of iITG-iPSC clones

After two weeks of reprogramming, several single clones were picked by a 100µl pipette tip, directly transferred into 50µl 0.25% Gibco™Trypsin-EDTA solution and incubated at 37°C for 5' to 10'.

Trypsin was stopped with 300µl CJ7 medium and clones were centrifuged for 5' at 300 x *g*. Then, each clone was resuspended in 500µl CJ7 medium supplemented with 1µg/ml doxycycline and 1x LIF and seeded into one well of a 24 well plate on inactivated MEF feeders. Medium was changed every day and iPSCs were further cultured until 90% confluence and then split at appropriate ratios onto inactivated MEF feeders either on 24 well, 12 well or 6 well plates. With each passage doxycycline was subsequently removed from the medium, so that the cells were cultivated doxycycline-free from passage 4 (stable reprogramming occurred).

From now on, cells were passaged and cultured as described in 3.1.4.1. Before utilized for knockdown differentiation experiments (3.8), generated iITG-iPSCs were characterized as described below (3.5.5).

3.5.5 Characterization of iITG-iPSC clones

For verification of reprogramming and induced pluripotency, several passages of generated iITG-iPSC clones were analyzed regarding their pluripotency potential during expansion culture. Therefore, total RNA (3.5.5.1) and cDNA (3.5.5.2) for endpoint (3.5.5.3) and qRT-PCR (3.5.5.4) (between p1-p18) as well as iITG-iPSCs for ICC (3.5.5.5) (p24) were prepared.

In addition, selected iITG-iPSC clones were *in vitro* differentiated using the standard protocol and corresponding replating approach as described in 3.2. RNA (3.5.5.1) was isolated at different timepoints between day 5 (0.75wks) and day 19 (2.75wks) and cDNA produced (3.5.5.2) to evaluate differentiation/pluripotency potential with the use of qRT-PCR (3.5.5.4).

After full characterization, iITG-iPSC clone 15 was used for final miR knockdown experiments (3.8) (Appendix Figure A5B, lower panel).

3.5.5.1 Isolation of total RNA

Total RNA was isolated using the peqGOLD total RNA Kit according to manufacturer's instructions. In brief, cells were resuspended in 400µl of lysis buffer, transferred to the DNA Removing Column and centrifuged for 1' at 12.000 x *g*. After adding an equal volume of 70% ethanol, the lysate was vortexed, transferred to the PerfectBind RNA Column and centrifuged for 1' at 10.000 x *g*. The flow-through was discarded and the membrane was washed once by 500µl RNA Wash Buffer I (centrifuged 1' at 10.000 x *g*) followed by DNAse I Digestion. For this, the PeqGOLD DNase I Digest Kit was used with 73.5µl DNAse I Digestion Buffer and 1.5µl DNAse I (20U/µl) per column. The 75µl mixture was directly pipetted to the membrane and incubated at RT for 15'. Afterwards, 400µl Wash Buffer I was applied to each column, incubated for 5', and then centrifuged for 15" at 10.000 x *g*.

Two washing steps with 600µl of Wash Buffer II each followed before the membrane was finally centrifuged for 2' at 10.000 x *g* to remove all remaining ethanol. RNA was eluted with 50µl sterile RNAse-free dH_20 which was applied directly to the binding matrix and centrifuged for 1' at 5.000 x *g*. Total RNA concentration was measured using the Nanodrop™ 2000 and stored at -20°C or 80°C until used for cDNA synthesis.

3.5.5.2 cDNA synthesis of total RNA

cDNA first strand synthesis was performed using the Invitrogen™ M-MLV Reverse Transcriptase Kit with a mixture of dNTPs and random primers. In a first step (STEP 1), 100ng of isolated RNA, RNAse-free dH_20, dNTPs and random primers were mixed and incubated for 5' at 65°C in the Thermocycler C1000 for denaturation. The mixture was quickly chilled on ice before the 5x First strand buffer and DTT was added to the reaction in a second step (STEP 2) to loosen possible secondary structures of the RNA and to facilitate enzyme initiation.

After incubation for 2' at 37°C, the M-MLV reverse transcriptase was finally added at STEP 3 for starting the actual cDNA synthesis including steps of annealing, strand synthesis and enzyme inactivation. The used reagents and concentrations for STEP 1-3 are listed in Table 33 and correspondent temperatures and times for cDNA synthesis are listed in Table 34 below. Until required for further usage, the generated cDNA was stored at -20°C.

Table 33 Reaction setup of cDNA synthesis of total RNA

Reaction step	Reagents	Final concentration	Volume (µl)
STEP 1	RNA	100ng	*variable*
	dNTPs (10mM)	0.5mM	1.5
	random hexamer primers (250ng/µl)	375ng	1.5
	RNAse-free dH_20	-	*ad* 20.25
STEP 2	5x First strand buffer*	1x	6
	DTT (0.1M)	10mM	3
STEP 3	M-MLV reverse transcriptase (200U/µl)	5U	0.75
Total volume			**30**

*contains 250mM Tris-HCl, 375 mM KCl, 15mM $MgCl_2$.

Table 34 Thermocycler protocol for cDNA synthesis of total RNA

Reaction step			Duration	Temperature
STEP 1	**Denaturation**		5'	65°C
STEP 2	**Loosen secondary structures**		2'	37°C
STEP 3	Primer annealing	**cDNA synthesis**	10'	25°C
	Strand synthesis		50'	37°C
	Enzyme inactivation		15'	75°C
	Cooling		∞	4°C

3.5.5.3 Endpoint PCR of pluripotency markers

Conventional endpoint PCR was performed as described in 3.1.2.2.2 to qualitatively determine the expression of pluripotency markers. Here, the template (cDNA), reagents and correspondent primers (Table 12) for endogenous expression of *c-Myc, Oct3/4*, *Klf4* and *Sox2* as well as *c-Myc/Sox2* for exogenous expression were mixed as shown below in Table 35 in separate 200µl PCR reaction tube stripes. cDNA generated from NkxCE-GFP ESCs served as a positive control for endogenous expression of pluripotency genes and the muSTEMCCA plasmid DNA (3.5.1) as a positive control for the exogenous marker. For negative controls, the template was replaced with sterile aqua bidest. PCR products were visualized by agarose gel electrophoresis on a 2% w/v agarose gel with the Invitrogen™ 50bp DNA marker as described in 3.1.2.2.3.

Table 35 Reaction setup for endpoint PCR of pluripotency markers

Reagents	Final concentration	Volume (µl)
Template (cDNA)	0.5-1ng	1
dNTPs (1mM each)	200µM of each dNTP	4
Primer forward (2µM)	0.1µM	1
Primer reverse (2µM)	0.1µM	1
PCR Buffer (10x)*	1x	2
Q-Solution (5x)	1x	4
HotStarTaq DNA Polymerase	2.5 units/reaction	0.1
Aqua bidest.		6.9
Total volume		**20**

*contains 15mM $MgCl_2$

Table 36 Thermocycling profile for endpoint PCR of pluripotency markers

Reaction step	Duration	Temperature	
Initial activation	15‘	95°C	
Denaturation	60”	94°C	**3-step cycling** (40 cycles)
Annealing	60”	60°C	
Extension	120”	72°C	
Final extension	10’	72°C	
Cooling	∞	4°C	

3.5.5.4 qRT-PCR of cDNA

qRT-PCR was used for quantification of PCR products by fluorescence measurement (SYBR™ Green) during PCR reaction. For this, the template cDNA, Power SYBR™ Green PCR Master Mix and correspondent primer pairs (Table 13) were pipetted as listed below (Table 37) in an Applied Biosystems™ MicroAmp® fast optical 96 well reaction plate.

As a negative control, the template cDNA was replaced by PCR-grade water. Each cDNA was analyzed as single sample (no technical replicate) but as experimental triplicates from three independent experiments.

Table 37 Reaction setup for qRT-PCR of cDNA

Reagents	Final concentration	Volume (µl)
Template cDNA	-	1
Power SYBR™ Green PCR Master Mix	1x	10
Primer forward (5µM)	0.3µM	1.2
Primer reverse (5µM)	0.3µM	1.2
PCR grade water	-	6.6
Total volume		**20**

*contains SYBR® Green 1 Dye, AmpliTaq Gold® DNA Polymerase LD, dNTPs with dUTP/dTTP blend and optimized buffer components.

After pipetting, the 96 well plate was sealed with the Applied Biosystems™ MicroAmp® optical adhesive film and shortly spinned by a Mini plate spinner mps1000 for 1' at 300 x *g*. The plate was transferred into the QuantStudio™ 3 Real-Time PCR System with the QuantStudio™ Design and Analysis Software v1.4 and the following PCR conditions were applied:

Table 38 Thermocycling profile for qRT-PCR of cDNA

Reaction step	Duration	Temperature	
Initial activation	2'	50°C	
	10'	95°C	
Denaturation	15"	95°C	**2-step cycling** (40 cycles)
Annealing/Extension	60"	60°C	
Melting curve	15"	95°C	
3-step cycling	60"	60°C	
	1"	95°C	
Cooling	∞	4°C	

Melting curve analysis as a quality step for template duplex hybridization was included after each PCR reaction for each primer pair and plate. Additionally, all PCR products of new primer sets were separated on a 2% w/v agarose gel with the Invitrogen™ 50bp DNA marker as described in 3.1.2.2.3 to ensure a correct PCR product size and exclude non-specific amplification. Data analysis was performed with the use of the "standard curve method" as described in 3.5.5.4.1.

3.5.5.4.1 Analysis of qRT-PCR data with the standard curve method

For expression analysis, the “standard curve method” was used where Ct values are assigned to correspondent arbitrary units (AU) with the help of standard curves specific for each primer pair.

To generate a standard curve for each gene, an appropriate template cDNA was serially diluted and pipetted in an Applied Biosystems™ MicroAmp® fast optical 96 well reaction plate with the correspondent primer pair for each gene and Power SYBR™ Green PCR Master Mix as described in Table 37, Table 38 for qRT-PCR analysis. Each cDNA was analyzed as technical replicate. After receiving the Ct value for each cDNA dilution, they were subsequently assigned to AUs as shown exemplary for the primer pair of β-actin in Table 39.

Table 39 Exemplary assignment of AUs to Ct values of β-actin

Ct value	Serial dilution	Assigned AU
18.732	undiluted	1.000.000
18.442	undiluted	1.000.000
21.113	1:5	200.000
20.915	1:5	200.000
23.674	1:25	40.000
23.590	1:25	40.000
26.321	1:125	8.000
26.324	1:125	8.000
29.050	1:625	1.600
29.111	1:625	1.600
32.371	1:3.125	320
32.282	1:3.125	320
35.582	1:15.625	64
35.473	1:15.625	64

The standard curve for each gene (primer set) was then calculated with the following equation: $y= m \cdot \ln(x) + b$. Here, y describes the mean Ct value, x represents the AUs, b the y-axis section (also referred to as “zp” value) and m describes the slope. With the help of these standard curves, the gene-specific AUs of obtained Ct values were subsequently calculated by solving the above-mentioned equation for x ($x = e^{y-b/m}$).

Relative gene expression was then calculated by normalization of the AUs of the gene of interest against the AUs of the housekeeping gene β-actin. If required for analysis, fold changes (FC), e.g. against a control group, were calculated.

3.5.5.5 ICC of pluripotency markers

Pluripotency on protein level was verified by staining with anti-Sox2 and anti-Nanog antibodies which are listed in Table 16.

First ESCs/iPSCs were seeded on gelatin coated 8 well chamber slides on mitomycin-inactivated MEF feeders in CJ7 medium without doxycycline (150µl total volume) and incubated at 37°C for 24h to 48h until they reached about 80% confluence. Then, the medium was removed, and after a washing step with 1x PBS, the cells were fixed with ice-cold acetone for 10' at -20°C. The slides were subsequently washed twice with 1x PBS. Permeabilization was conducted by incubation with 0.25% v/v PBS-T for 10'. After another washing step with 0.1% v/v PBS-T, blocking was conducted by incubation with 5% v/v goat serum in 0.1% v/v PBS-T (1x PBS-T) for 30' at RT. The first antibodies anti-Sox2 and anti-Nanog were diluted (anti-Sox2, 1:250; anti-Nanog, 1:100) in 1.5% v/v goat serum in 1x PBS-T and applied to the chamber slides for 1h at 37°C. After washing twice with 1x PBS-T, the goat anti rabbit Alexa Fluor® labeled 488 secondary antibody (Table 17) was diluted 1:500 in 1.5% v/v goat serum in 1x PBS-T and incubated for 1h at RT in the dark. To ensure that no unspecific binding happens for secondary antibodies, ESCs/iPSCs were stained with correspondent secondary antibody only as negative controls. NkxCE-GFP ESCs served as positive controls. Nuclear staining was conducted by covering the dried chamber slides in Fluoroshield Mounting Medium w/ DAPI. Correspondent fluorescent pictures were made as described in 3.10.

3.6 Generation of miR overexpressing NkxCE-GFP ESC lines (OE-ESCs)

3.6.1 Lentiviral constructs

OE-ESC lines were generated by transduction of transgenic murine NkxCE-GFP ESCs with Dharmacon™ shMIMIC Inducible Lentiviral microRNA particles (Table 15). Upon doxycycline induction, the constructs express either the murine miR-128-3p (OE-128) or a non-targeting control miR (OE-Ctr) which is accompanied by red fluorescent protein (tRFP) expression. Additionally, lentiviral transduced NkxCE-GFP-ESCs exhibit constitutive puromycin resistance driven by a mCMV promoter (Appendix Figure A6A).

3.6.2 Transduction of the NkxCE-GFP ESC line

NkxCE-GFP ESCs were cultured as described (3.1.4). Before transduction, they were detached from culture flasks as described in 3.1.4.1, counted with the "Neubauer chamber" method (3.1.2.3.2), and $2x10^5$ ESCs were resuspended in a total of 50µl transduction medium in a 1.5ml Eppi™ Safe-Lock Tube.

Then, the correspondent volume of lentiviruses (starting (LV start) and final concentrations (LV final) listed below) and polybrene (PB) at a final concentration of 6µg/ml were added. If required, the mixtures were replenished to a total volume of 150µl with transduction medium. ESCs with polybrene only (PB-Ctr) and ESCs only (Ctr) served as controls. The detailed reaction setup is listed in Table 40 below.

Table 40 NkxCE-GFP ESCs transduction scheme with miR lentiviruses

Sample	ESCs ($2x10^5$)	LV volume	Polybrene (0.8mg/ml)	Transduction medium	Total volume	LV start	LV final
OE-128	50µl	100µl	1.13µl	-	150µl	$3.32x10^8$ TU/ml	$3.32x10^7$ TU/150µl
OE-Ctr	50µl	25µl	1.13µl	75µl	150µl	$1.19x10^8$ TU/ml	$2.9x10^6$ TU/150µl
PB-Ctr	50µl	-	1.13µl	100µl	150µl		
Ctr	50µl	-	-	100µl	150µl		

The ESC/virus mixture was directly seeded in one well of a 48 well plate on inactivated MEF feeders and incubated at 37°C. After 24h, the cells were washed twice with transduction medium and fresh CJ7 medium supplemented with tetracycline-free FCS in addition to 2µg/ml doxycycline for viral induction was added. After another 24h (day 2), CJ7 medium with tetracycline-free FCS and doxycycline (2µg/ml) was additionally supplied with 1µg/ml puromycin for selection of transduced ESCs. Medium was changed every day until day 7 when each well of the 48 well plate was transferred to one well of a 6 well plate on inactivated MEF feeders. Transduced ESCs were further cultured with daily medium change (tetracycline-free CJ7 with doxycycline and puromycin) until control ESCs without virus (Ctr and PB-Ctr) died due to their sensitivity to puromycin (week two to three). Surviving, and therefore potentially efficiently transduced, single ESC clones from OE-128 and OE-Ctr lines were then picked (as previously described in 3.5.4) based on their RFP expression. A selection of RFP-positive ESC clones under doxycycline from both generated lines (before picking) is attached as Appendix Figure A6B.

All picked ESC clones were further cultured as described in 3.1.4 in tetracycline-free CJ7 medium with puromycin (in addition to doxycycline, if required for induction).

RFP-positive cells within some picked OE-clones were additionally sorted by flow cytometry as described in 3.6.3.4 (Appendix Figures 7A-F).

3.6.3 Verification of OE-ESCs

Selected RFP-positive ESC clones picked from both lines were analyzed at different passages (between p1-p35) maintained either with or without doxycycline.

For measurement of miR-128a expression levels, total RNA including miRs was isolated (3.6.3.1) and miRs were further quantified by qRT-PCR (3.6.3.3).

The percentage of RFP-positive ESCs was accessed by flow cytometry (3.6.3.4). MTT assay for the evaluation of cell proliferation (3.6.3.5) and ICC for pluripotency markers (as described in 3.5.5.5) were performed to exclude an influence on proliferation or pluripotency capacity by overexpression of miRs in transduced NkxCE-GFP ESCs.

All selected clones were also *in vitro* differentiated (with or without doxycycline as described in 3.9.1) and especially the OE-Ctr ESC line was further characterized concerning their frequency of GFP-positive cells and gene expression levels at day 9.5/10 (1.5wks) and day 14 (2wks). In addition, the beating frequencies of evolving early cardiomyocytes were evaluated (3.6.3.6) under both conditions.

After full verification, OE-Ctr clone 4 as well as two OE-128 clones (21 and 30) were used for final miR overexpression experiments (3.9).

3.6.3.1 Isolation of miRs

The Isolation of miRs was conducted according to the protocol used for the isolation of total RNA as described in 3.5.5.1.

3.6.3.2 cDNA synthesis of miRs

cDNA synthesis of miRs (miR-cDNA) was performed using the Universal cDNA synthesis kit II from Exiqon. During reverse transcription, a poly(A) tail is added to the mature miR sequence which is further amplified using poly(T) primer containing a 3' degenerative anchor as well as a 5' universal tag.

As reaction mixture, 100ng of isolated total RNA (3.5.5.1), the correspondent amounts of reaction buffer, enzyme mix as well as RNAse-free dH_20 were mixed (shown below in Table 41) and incubated in the Thermocycler C1000 with the protocol listed in Table 42. Until required for further usage, the generated miR-cDNA was stored at -20°C.

Table 41 Reaction setup for cDNA synthesis of miRs

Reagents	Final concentration	Volume (µl)
RNA	100ng	variable
5x Reaction buffer	1x	2
Enzyme mix	-	1
RNAse-free dH_20	-	*ad* 10
Total volume		**10**

Table 42 Thermocycler protocol for cDNA synthesis of miRs

Reaction step	Duration	Temperature
STEP 1 cDNA synthesis	60‘	42°C
STEP 2 Enzyme inactivation	5‘	95°C
STEP 3 Cooling	∞	4°C

3.6.3.3 qRT-PCR of miR-cDNA

qRT-PCR of miR-cDNA was performed with specific LNA™ PCR Primer sets (Table 11) and the ExiLENT SYBR® Green Master Mix from Exiqon according to the miRCURY LNA™ Universal RT protocol. For this, the generated miR-cDNA (3.6.3.2) was first diluted 1:80 with RNAse-free dH_20. Then, the miR-cDNA template, ExiLENT SYBR® Green Master Mix, and primer sets were pipetted as listed below (Table 43) in an Applied Biosystems™ MicroAmp® fast optical 96 well reaction plate. As a negative control, the template miR-cDNA was replaced by PCR-grade water. Each miR-cDNA was analyzed as single sample (no technical replicate) but as experimental triplicates from two to three independent experiments.

Table 43 Reaction setup for qRT-PCR of miR-cDNA

Reagents	Volume (µl)
Template miR-cDNA (1:80)	4
ExiLENT SYBR® Green Master Mix	5
LNA™ PCR Primer sets	1
Total volume	**10**

After pipetting, the 96 well plate was sealed with the Applied Biosystems™ MicroAmp® optical adhesive film and shortly spun by a of Mini plate spinner mps1000 for 1’ at 300 x *g*. The plate was transferred into the QuantStudio™ 3 Real-Time PCR System equipped with the QuantStudio™ Design and Analysis Software v1.4 and the following PCR conditions were applied (Table 44):

Table 44 Thermocycling profile for qRT-PCR of miR-cDNA

Reaction step	Duration	Temperature	
Initial activation	10‘	95°C	
Denaturation	10”	95°C	**2-step cycling** (40 cycles)
Annealing/Extension	60”	60°C	
Melting curve	15”	95°C	
3-step cycling	60”	60°C	
	1”	95°C	
Cooling	∞	4°C	

To ensure specification of LNA™ primer sets, 3-step cycling melting curve analysis was performed for all plates. Expression analysis of miRs was then conducted with the $2^{\wedge-\Delta\Delta Ct}$ method as described below 3.6.3.3.1.

3.6.3.3.1 Analysis of qRT-PCR data with the $2^{\wedge-\Delta\Delta Ct}$ method

For analysis of miR expressions, the comparative $2^{-\Delta\Delta Ct}$ method was used where the expression of a miR is determined relative to an internal control (Schmittgen and Livak, 2008). Therefore, the obtained Ct values of miRs (referred to as target) as well as the internal control U6 (referred to as reference) were used in first step to calculate ΔCt with the following equation: ΔCt = Ct (target) - Ct (reference).

Subsequently, ΔΔCt was determined by calculating the differences between all ΔCt values and the mean ΔCt value of a reference subgroup (e.g. OE-ESCs without doxycycline/LNA-Ctr) with the following equation: ΔΔCt = ΔCt - mean ΔCt (reference subgroup). Final relative expressions were then calculated with the $2^{-\Delta\Delta Ct}$ equation. If required for analysis, corresponded fold changes (FC) were calculated.

3.6.3.4 Flow cytometry (FACS)

For quantification of GFP-positive and RFP-positive cells, flow cytometry also referred to as FACS (Fluorescence Activated Cell Sorting) was conducted with the BD LSRFortessa™ using the BD FACS Diva software version 6.2 at our institute.

RFP-positive cell sorting was conducted on a BD FACSARIA III (BD Biosciences) by Lynette Henkel at the flow cytometry unit of the Technical University Munich (CyTUM) in cooperation with Dr. Schiemann at the Institut für Medizinische Mikrobiologie, Immunologie und Hygiene (MIH).

In brief, flow cytometry is based on an interaction between single cells and an excitation light source, specifically laser beam(s). Cell suspensions (prepared as described below) are pressurized and injected into a sheath core flow which passes a nozzle and is further directed to the laser beam(s).

While interacting with the cell, the laser beam(s) are refracted, and the resulting light diffusions and emissions are detected by an optical collection system. While small-angled light diffusions (forward-scatter light, FSC) are collected directly in the axis of the laser by a photodiode detector, larger and therefore side-angled diffusions of light (side-scatter light, SSC) are collected at a 90° angle of the laser beam. Since the magnitude of the FSC correlates to the relative-size of the cell and the occurring SSC is a combination of diffusion, reflection and refraction caused by the structural complexity of the cell, a conjunction of both allows, at least to some degree, a differentiation of cells within a heterogeneous cell population as a first step. Fluorescence emissions are also collected at a 90° angle and, equal to SSCs, filtered by dichroic mirrors and emission filters (bandpass filters) dependent on their range of wavelengths until directed to an adequate photomultiplier detector (Picot *et al.*, 2012). In some cases, however, especially when two types of fluorescence (e.g. RFP and GFP) are present in a sample, the emission spectra for those might overlap. This could lead to "false positive" results since for example the emission tail of GFP (normally detected by the FITC filter) lies within the detection range of the filter used for RFP emission (e.g. PE filter). However, with the help of the BD software the overlaps can be subtracted, a process referred to as "fluorescence compensation" ("Comp").

First, RFP-positive cells within picked OE-ESCs (Appendix Figure A6B) were sorted with the intension to increase the abundance of miR expressing cells within the generated OE-ESC lines. For this, OE-ESCs from 6 wells of a 6 well plate were detached (~$2x10^7$ cells) and centrifuged for 5' at 300 x *g*. After resuspension in 1000µl FACS buffer, cell samples were transferred on ice to the CyTUM-MIH Unit. Before flow cytometry, DAPI was added in a final concentration of 1µg/ml to exclude dead cells (e.g. BV421 filter). Cells were further filtered through a 30µm syringe to obtain single cell suspension. RFP-positive cells (~20-40%, depending on the OE-ESC line) were sorted each into one 1.5ml Eppi™ Safe-Lock Tube containing FCS and then finally seeded on one well of a 6 well plate with CJ7 medium (w/ doxycycline and puromycin) on inactivated MEF feeders. Cells were further cultured, and quantification of RFP-positive cells was determined again after a few passages in culture in comparison to unsorted OE-ESC clones in our laboratory on the BD LSR Fortessa™ (Appendix Figures A7A-F). For this, ESCs were treated as mentioned above, RFP-positive cells were detected by flow cytometry and finally analyzed by the FlowJo 7.6.5 software where single cells are represented in dot plots and subpopulations were identified ("gated") based on a negative control (samples without positive cells, e.g. without doxycycline, Appendix Figures A7A,B,D,E, each left panel). Due to the sorting results, both sorted and unsorted OE-ESC clones were combined for final analysis.

Exemplary dot plots illustrating the detailed selection of gates for RFP-positive cells in both OE-ESC lines (OE-Ctr and OE-128) with and without doxycycline are represented in (Appendix Figures A8A-B).

To examine the abundance (frequency) of RFP- as well as GFP-positive cells during *in vitro* differentiations, cells were scraped mechanically from the culture plate using a Corning® Cell scraper and additionally digested with Collagenase II Dissociation Solution for 1h at 37°C before being treated and quantified as described above. Representative dot plots including gate selection of RFP- and GFP-positive cells during *in vitro* differentiations of OE-ESC (day 5; 0.75wks) are shown in Appendix Figures A9A-B.

3.6.3.5 MTT assay for OE-ESC clones

To evaluate a potential altered proliferation capacity of OE-ESC clones, 3-[4.5-Dimethylthiazol-2-yl]-2.5-diphenyltetrazolium bromide (MTT) assays were performed. This colorimetric assay relies on the enzymatic reduction of yellow-colored MTT into purple-colored MTT-formazan by mitochondrial succinate dehydrogenases. Since the amount of MTT cleavage is dependent on mitochondrial respiration, it indirectly serves as a marker for the energy capacity of a cell and therefore also for cell viability (Stockert *et al.*, 2012).

For preparation, one confluent well of a 24 well plate with OE-ESCs was split into 16 wells of a gelatin coated 96 well plate (split 1:4) and further cultured either without or with doxycycline for three days as described in 3.1.4.1. After 72h, the medium was aspirated, and each well was incubated with 10µl of 5mg/ml MTT Solution diluted in 90µl pure DMEM medium (final concentration 0.5mg/ml) for 1h at 37°C. Then, the medium was carefully aspirated and 100µl of DMSO were added to each well to lyse the cells and to dissolve the purple MTT-formazan. After resuspension, the mixture was transferred to a fresh 96 well plate for final spectrometric analysis where the absorbance of the MTT-formazan was measured at 570 nm whereas the reference wavelength was set at 690nm. All measurements were conducted on the Tecan Safire 2 Multimode Microplate Reader equipped with the software XFLUOR4 version 4.51.

3.6.3.6 Beating frequencies

Beating frequencies of early cardiomyocytes (CMs) were evaluated at specific time points during *in vitro* differentiations (3.9.2) using the Nikon Eclipse Ts2 inverted microscope video feature in the TiControl Ver. 4.4.2. software. At each observation day, up to nine videos of nine different beating foci with a length of 20 seconds were recorded per condition and clone. The beats were counted visually by three independent observers and the beating rates (beats per minute) were subsequently calculated.

3.7 Analysis of influence of transient transfection on cell physiology

To analyze effects of transient transfection (e.g. the use the transfection reagent Fugene) on cell physiology, flow cytometry for quantification of GFP-positive cells (described in 3.6.3.4) was conducted after one week in differentiated NkxCE-GFP ESCs treated either with Fugene only (Control; Ctr) or with LNA miR inhibitor control A (LNA-Ctr).

Transfections were conducted according to the scheme described in 3.8.1. In addition, MTT assays were performed to evaluate impacts of transient transfections on cell proliferation as described below in 3.7.1 & 3.7.2.

3.7.1 Transfection with LNA probes for MTT assay

The possible impact of cell transfection on cell physiology during differentiation in general was first evaluated using MTT assays. Therefore, the NkxCE-GFP ESCs were differentiated using the standard hanging drop method (3.2), however, the replating strategy differed from that of knockdown experiments. Here, NkxCE-GFP ESC were directly seeded on gelatin coated 12 well plates with IMDM-ES medium on day -2 for preparation.

After 24h of cultivation (day -1), the ESCs were transfected according to the transfection protocol below (3.8.1) with the mixtures for LNA-Ctr and Ctr whereas the Ctr mixture was prepared without Fugene (Ctr w/o Fugene). EBs were then prepared normally on day 0, flooded at day 2 and further differentiated until day 7 (1wk) in 15cm culture plates. The differentiating EBs were then collected by scraping them mechanically from the plates followed by digestion with Collagenase II Dissociation Solution for 1h at 37°C. After counting the cells (3.1.2.3.2), $2x10^5$ differentiating ESCs were transferred into one well of a gelatin coated 48 well plate with differentiation medium. After another 24h of cultivation (day 8), the MTT assay was performed as described below 3.7.2.

3.7.2 MTT assay during *in vitro* differentiation

The MTT assay was performed in compliance with the general protocol described in 3.6.3.5. However, due to the use of 48 well plates for differentiated ESC cultivation, a total of 250µl of the diluted MTT Solution was used for the first incubation step (25µl of 5mg/ml MTT Solution diluted in 225µl pure DMEM medium (final concentration 0.5mg/ml)), and 250µl of DMSO for the second step of cell lysis and resuspension. Finally, an aliquot of 100µl was transferred into a fresh 96 well plate for final spectrometric analysis as described in 3.6.3.5.

3.8 LNA-mediated miR knockdown during *in vitro* differentiation

For knockdown experiments, the self-generated iITG-iPSCs as well as NkxCE-GFP ESCs were differentiated according to the protocol described in 3.2 including replating on 12 well plates at day 2. Both ESC and iPSC lines were transfected as described below (3.8.1) with mmu-miR-128a-3p LNA miR inhibitor (referred to as LNA-128) or an LNA miR inhibitor control A (LNA-Ctr) (Table 14). Effects of miR knockdown were analyzed at specific timepoints throughout differentiation as shown in 3.8.2.

3.8.1 Transfection with LNA probes for miR knockdown

For LNA-mediated miR knockdown, both ESC and iPSC lines were transfected twice throughout differentiation to ensure a stable knockdown. The NkxCE-GFP ESCs were transfected at day 3.5 and day 7 (1wk) and the iITG-iPSCs once at day 5 (0.75wks) and day 13 (2wks). Each well was transfected with a final concentration of 50nM (LNA final) of either LNA-128 or LNA-Ctr. As an additional negative control, ESCs/iPSCs were also differentiated with the transfection reagent Fugene only (referred to as Ctr).

Before transfection, the medium in each well was replaced by 500µl of differentiation medium without antibiotics. Then, the transfection mixture was prepared with the correspondent amounts of LNA stock probe (25µM), pure IMDM medium and Fugene transfection reagent. The reaction setup for each condition for one well of a 12 well plate is listed below in Table 45.

Table 45 Transfection mixture for miR knockdown with LNA probes

Sample name	Volume medium/well	LNA stock	IMDM	Fugene	Final volume/well	LNA stock	LNA final
Ctr	500µl	-	45µl	5µl	550µl	-	-
LNA-Ctr	500µl	2µl	43µl	5µl	550µl	25µM	50nM
LNA-128	500µl	2µl	43µl	5µl	550µl	25µM	50nM

After pipetting, the reaction mixture was incubated for 15’ at RT and then added dropwise to the well. After 36 to 48h of incubation, the medium was changed to fresh differentiation medium with antibiotics for further differentiation until the transfection procedure was repeated at above mentioned timepoints. NkxCE-GFP ESCs were differentiated until day 16 (2.25wks) and the iITG-iPSCs until day 22/23 (3wks). Effects of LNA-mediated knockdown were analyzed at several timepoints as described below in 3.8.2.

Exemplary fluorescence pictures of both differentiating ESC/iPSC lines under the three conditions described above (Ctr, LNA-Ctr and LNA-128) are attached as Appendix Figures A10A-C and Appendix Figures A11A-C.

3.8.2 Analysis of LNA-mediated miR knockdown effects

NkxCE-GFP ESCs were analyzed at timepoints between day 5 (0.75wks) and day 16 (2.25wks) whereas iITG-iPSCs were analyzed between week one (1wk) and three (3wks).

First, ESCs/iPSCs were lysed for RNA isolation (3.5.5.1), for analysis of miR-128a expression (3.6.3.2, 3.6.3.3) and gene expression evaluation (3.5.5.2. & 3.5.5.4).

Second, the abundance of GFP-positive cardiac progenitor cells (CPCs) was analyzed at different timepoints by flow cytometry (3.6.3.4).

And third, the beating frequency of early CMs was determined as described in 3.6.3.6. Table Table 46 and Table 47 provide a detailed overview of analysis of LNA-mediated knockdown during NkxCE-GFP ESC and iITG-iPSC differentiation including the evaluated timepoints.

Table 46 Analysis of LNA-mediated knockdown during NkxCE-GFP ESC *in vitro* differentiation

	Time of *in vitro* differentiation*					
	day 5 (0.75wks)	day 7 (1wk)	day 10 (1.5wks)	day 12 (1.75wks)	day 14 (2wks)	day 16 (2.25wks)
miR-128a expression	✓	✓	✓	-	✓	-
Gene expression	✓	✓	✓	-	✓	-
CPC abundance	-	✓	✓	-	✓	-
Beating frequency		✓	✓	✓	✓	✓

***** timepoints of *in vitro* differentiation marked with a check mark indicate that respective analysis (listed on left side) was conducted.

Table 47 Analysis of LNA-mediated knockdown during iITG-iPSC *in vitro* differentiation

	Time of *in vitro* differentiation*				
	day 8 (1wk)	day 13 (2wks)	day 16 (2.25wks)	day 19 (2.75wks)	day 22/23 (3wks)
miR-128a expression	✓	✓	✓	-	✓
Gene expression	✓	✓	-	-	✓
CPC abundance	-	✓	✓	-	✓
Beating frequency	-	✓	✓	✓	✓

***** timepoints of *in vitro* differentiation marked with a check mark indicate that respective analysis (listed on left side) was conducted

Dot plot examples of flow cytometry including the gates to quantify GFP-positive cells during differentiation is attached for both ESC/iPSC lines as Appendix Figures A12A-C & Appendix Figures A13A-C.

3.9 miR overexpression during *in vitro* differentiation

3.9.1 *In vitro* differentiation of OE-ESC lines

OE-ESC lines were differentiated with the hanging drop method as described in 3.2 either without or with doxycycline. For preparation, OE-ESCs were cultured in tetracycline-free IMDM-ES medium supplied with 1x LIF and 1µg/ml puromycin. After two days in culture, hanging drops (EBs) were prepared with differentiation medium either without doxycycline or medium containing 2µg/ml doxycycline for miR induction. OE-ESC clones were differentiated until day 14 (2wks). Medium was changed every 2-5 days, dependent on the medium consumption. Exemplary pictures of differentiating OE-ESC lines (OE-Ctr and OE-128) under both medium conditions are attached as Appendix Figure A14A-B.

After initially described characterization (especially the analysis of the OE-Ctr line) (3.6.3) which was *in vitro* differentiated under the above-mentioned conditions, the final evaluation of overexpression effects was conducted with both OE-ESCs (OE-Ctr, OE-128) differentiated without doxycycline only (3.9.2).

3.9.2 Analysis of miR overexpression effects

Analysis of OE-Ctr and OE-128 ESC lines followed the same course and techniques as described for miR knockdown experiments in 3.8.2. Table 48 gives an overview about conducted analysis at respective timepoints during *in vitro* differentiation of both OE-ESC lines without doxycycline (see also Appendix Figures A14A-B, each upper panel).

Table 48 Analysis of OE-ESCs during *in vitro* differentiation without doxycycline

	Time of *in vitro* differentiation*				
	day 5 (0.75wks)	day 7 (1wk)	day 9.5/10 (1.5wks)	day 12 (1.75wks)	day 14 (2wks)
miR-128a expression	✓	✓	✓	-	✓
Gene expression	-	✓	✓	-	✓
CPC abundance	-	✓	✓	-	✓
Beating frequency	-	✓	✓	✓	✓

* timepoints of *in vitro* differentiation marked with a check mark indicate that respective analysis (listed on left side) was conducted.

Exemplary dot plots of flow cytometry for RFP/GFP-positive cell quantification during *in vitro* differentiation without doxycycline can be found in previously mentioned Appendix Figure A9A-B, each upper panel).

3.10 Microscopic Imaging

All presented phase contrast and fluorescent images of fibroblasts, ESCs/iPSCs and immunostainings were taken with an AxioCam MR camera on an Axiovert 200M microscope equipped with 10x and 40x objectives, combined with a 10x ocular resulting in 100x to 400x magnification, supported by the AxioVison Rel 4.8 software. Scale bars are indicated within each single picture.

3.11 Data and Statistical Analysis

All graphs were processed using GraphPad Prism Software Version 7.0d. Explorative data analysis was performed by using IBM SPSS Statistics Version 22 SPSS. Comparisons between two groups were made with the two-tailed student's t-test or Mann-Whitney Rank Sum test in case the data did not approximate a normal distribution. Data are shown as mean values ± standard error of the mean (S.E.M). Values of $p \leq 0.05$ were considered to be statistically significant. Statistics is indicated in all figures as * $p \leq 0.05$, ** $p \leq 0.01$ and *** $p \leq 0.001$.

4 Results

4.1 Identification of miRs involved in early cardiac development

4.1.1 MicroRNA Array to identify potential miR candidates

MicroRNA Array analysis was performed in cooperation with Jeanette Erdmann und Zouhair Aherrahrou from the Institute of Cardiogenetics at the University of Lübeck and Gianluca Santamaria from the Cardiology Medical Department 1 at the Klinikum Rechts der Isar at the Technical University Munich.

The aim was to establish a miR expression profile of the previously described multipotent cardiac progenitor cell (CPC) population characterized by an active 2.1 kb *Nkx2.5* cardiac enhancer element (NkxCE-GFP CPC) (Lien *et al.*, 1999; Wu *et al.*, 2006) that exclusively marks the embryonic heart in the transgenic NkxCEeGFP mouse by GFP from E8.5 to E15.5 (Wu *et al.*, 2006) (1.2).

For miR profiling, the expression of about 750 known miRs was determined in several distinct cell populations by a Taqman™ Array Rodent miRNA Card Set. Therefore, above-mentioned NkxCE-GFP CPCs were isolated by FACS from (1) transgenic NkxCEeGFP mouse embryos at E9.5 and (2) from seven days (D7) *in vitro* differentiated murine NkxCE-GFP ESCs. In addition, their correspondent GFP-negative stage-mathed cell fractions (from E9.5 and D7) were collected. For further comparison to non-cardiac progenitor cells, murine cardiac fibroblasts (CFs) as well as tail tip fibroblasts (TTFs) were obtained from adult mice. Purified miRs from all isolated cell populations mentioned above were then forwarded to Jeanette Erdmann und Zouhair Aherrahrou to run the MicroRNA Array.

The MicroRNA Array data, which was analyzed by Gianluca Santamaria, showed that a total of 83 miRs were differentially regulated in D7 and/or E9.5 (D7/E9.5) isolated GFP-positive CPCs in comparison to their GFP-negative fractions (D7/E9.5), TTFs and CFs. (Appendix Figure A15). Among those 43 miRs were significantly downregulated (FC > 1.5, SD < FC, $p \leq 0.05$) and 40 miRs significantly upregulated (FC > 1.5, SD < FC, $p \leq 0.05$) in CPC populations.

The initial miR candidate selection was focused on upregulated miRs only (Figure 3A, B), since it has been shown previously that regulatory miRs usually become upregulated during early cardiogenesis (e.g. in CPC populations) (Ivey *et al.*, 2008; Shen *et al.*, 2016).

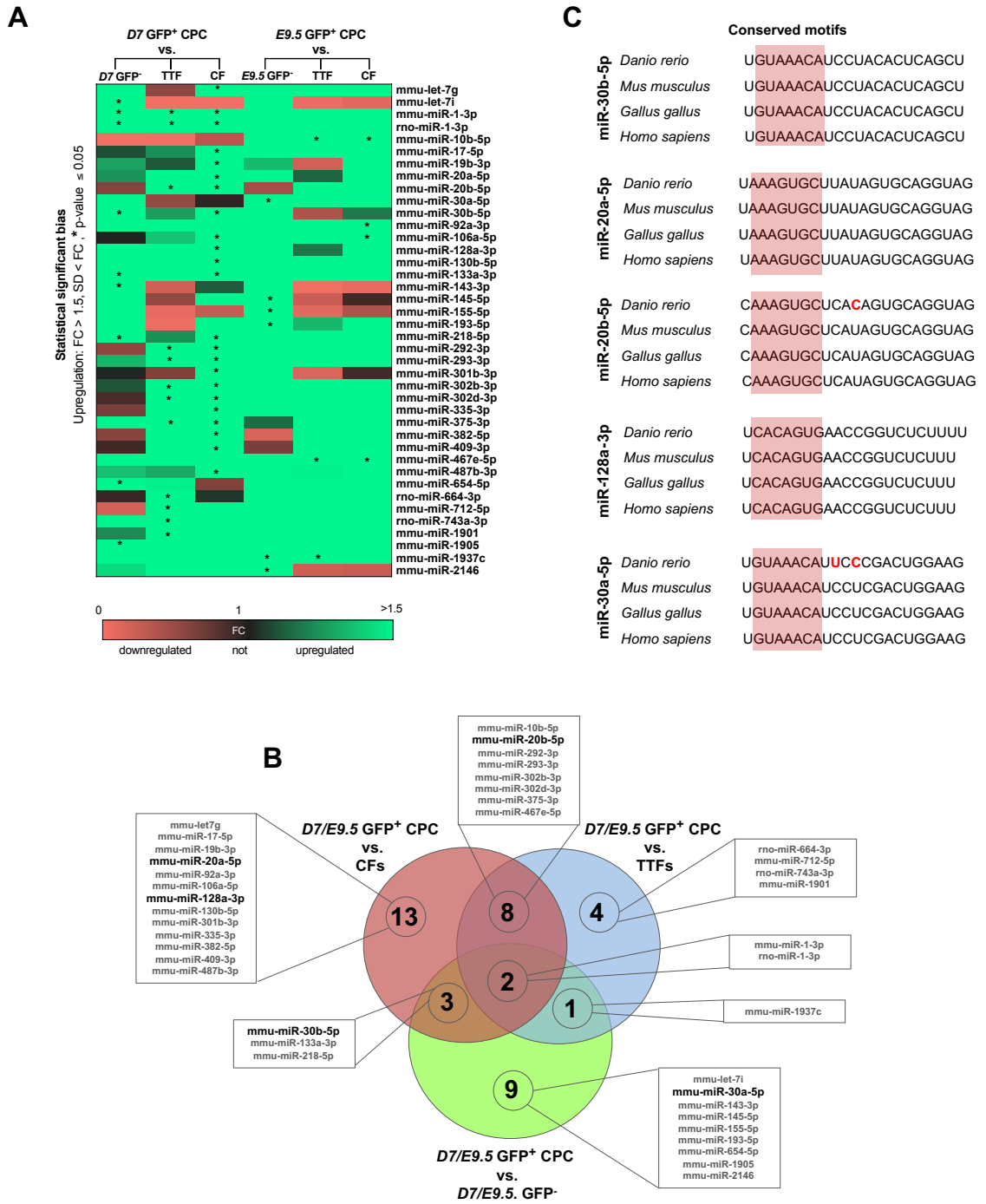

Figure 3 MicroRNA Array results of upregulated miRs in NkxCE-GFP CPCs. A. Heat map of top 40 significantly upregulated miRs in D7 and E9.5 isolated NkxCE-GFP CPCs (GFP$^+$ CPC) in comparison to GFP-negative fractions (GFP$^-$), TTFs and CFs. (bias: FC > 1.5, SD < FC, p ≤ 0.05 (two-sided Student's t-test), significant values are marked with *). **B.** Venn Diagram of significantly upregulated miRs in D7 and/or E9.5 (D7/E9.5) isolated GFP$^+$ CPCs. 25 miRs were significantly upregulated in D7/E9.5 GFP$^+$ CPCs compared to fibroblast populations. 9 miRs were found to be significantly higher expressed in GFP$^+$ CPCs (D7/E9.5) compared to GFP$^-$ cell fractions (D7/E9.5). Six miRs were upregulated in GFP$^+$ CPCs (D7/E9.5) compared to both groups **C.** Preservation analysis of candidate miR sequences using the miRbase online database (http://mirbase.org). Sequences and motifs (marked with red balks) of miR-30b-5p, miR-20a-5p, miR-20b-5p, miR-128a-3p and miR-30a-5p are highly conserved across species, including zebrafish (*Danio rerio*), mouse (*Mus musculus*), chicken (*Gallus gallus*) and human (*Homo sapiens*). Red bases represent non-homologous bases in comparison to human miR sequences. Analysis was conducted in cooperation with Jeanette Erdmann, Zouhair Aherrahrou and Gianluca Santamaria. Adapted from Figure S1E, F and 1D from Hoelscher *et al.* miR-128a Acts as a Regulator in Cardiac Development by Modulating Differentiation of Cardiac Progenitor Cell Populations. *Int. J. Mol. Sci.* 2020, *21*, 1158 (Hoelscher *et al.*, 2020). *Abbreviations: FC, fold change; SD, standard deviation.*

Within the upregulated miR-subgroup, 25 miRs were significantly upregulated in GFP-positive CPCs (D7/E9.5) compared to the fibroblast populations (vs. CFs: 13 miRs; vs. TTFs: 4 miRs and vs. CF and TTFs: 8 miRs) (Figure 3A, B). Nine miRs were found to be significantly higher expressed in GFP-positive CPCs (D7/E9.5) compared to their corresponding GFP-negative cell fractions (D7/E9.5) (Figure 3A, B). Six miRs were upregulated in GFP-positive CPCs (D7/E9.5) compared to both groups (vs. CFs and GFP-negative fractions (D7/E9.5): 3 miRs; vs. TTFs and GFP-negative fractions (D7/E9.5): 1 miR; vs. CF,TTFs and GFP-negative fractions (D7/E9.5): 2 miRs) (Figure 3A, B).

As the six miRs upregulated in CPCs in comparison to both groups (fibroblasts and GFP-negative fractions) we identified miR-1-3p (both *Mus musculus (mmu)* and *Rattus norvegicus (rno)* sequence), miR-133a-3p, and miR-218-5p, miR-30b-5p as well as miR-1937c (Figure 3A, B). Interestingly, miR-1-3p, miR-133a-3p, and miR-218-5p represent major key players during early cardiac development and have already been well-characterized in detail (Chen *et al.*, 2006; Chiavacci *et al.*, 2012; Fish *et al.*, 2011; Ivey *et al.*, 2008; Shen *et al.*, 2016; Zhao *et al.*, 2005). This indicated that the data from the MicroRNA Array analysis was sound. Since high cross-species conservation of these cardiac-specific miRs (miR-1, miR-133 and miR-218) has been described previously (Fish *et al.*, 2011; Lagos-Quintana *et al.*, 2002) we also performed preservation analyses for miR-30b-5p and miR-1937c with the help of the miRbase online database (http://mirbase.org). We found that the sequence as well as the seed region/motif of miR-30b-5p was indeed highly conserved across zebrafish *(Danio rerio),* mouse (*Mus musculus*), chicken (*Gallus gallus*) and human (*Homo sapiens*) (Figure 3C) making this miR an interesting candidate for further analysis. However, miR-1937c had only been described as a potential tRNA fragment that possibly does not exhibit any regulatory function as a miR and was therefore excluded as a potential candidate (Jovicic and Gitler, 2017).

To select further potential miR candidates from our MicroRNA Array data we next focused on miRs which had been found to be differentially expressed in comparison to only one other cell group (either fibroblasts or GFP-negative cell fractions). Here again, we analyzed the sequence homologies and found that among the 25 miRs significantly upregulated in comparison to fibroblast populations, miRs such as miR-20a-5p, miR-20b-5p and miR-128a-3p exhibited high sequence and motif conservation (Figure 3A-C). In addition, miR-30a-5p was identified as one of the conserved miRs amongst the 9 miRs upregulated more than 1.5-fold in comparison to the GFP-negative cell fractions (D7/E9.5) (Figure 3A-C).

After this preselection of potential miR candidates based on preservation analysis, we additionally conducted extensive literature research to gain further insights into these five miRs.

Interestingly, we found that all of these miRs (miR-30b-5p, miR-20a-5p, miR-20b-5p, miR-128a-3p, miR-30a-5p) have been associated with cardiac or at least skeletal muscle in some context before (Guess *et al.*, 2015; Huang *et al.*, 2018; Ketley *et al.*, 2013; Witman *et al.*, 2013; Zhu *et al.*, 2015).

This again supports the coherence of our MicroRNA Array data as well as our adequate candidate preselection. However, especially for miR-20a, which is transcribed from the miR-17~92 cluster, we found numerous publications that already characterized its distinct role during embryogenesis in detail, particularly in the context of cardiac development (Ai *et al.*, 2016; Gu *et al.*, 2017). On that account, miR-20a was excluded for further analysis.

Conclusively, as a result of the high cross-species sequence conservation as well as involvements in muscular settings, we finally selected miR-30b-5p, miR-20b-5p, miR-128a-3p as well as miR-30a-5p (further referred to as miR-30b, miR-20b, miR-128a and miR-30a) as the four candidates to be functionally analyzed in more detail (Figure 3A-C).

4.1.2 Kinetics during *in vitro* differentiations of ESCs/iPSCs

As described previously, miRs that play a role in early cardiogenesis, become typically upregulated at the onset of cardiogenesis to fulfil their specific functional roles (Ivey *et al.*, 2008; Shen *et al.*, 2016). This characteristic behavior has been demonstrated for cardiac-specific miRs, such as miR-1 and miR-133a (Ivey *et al.*, 2008), but also for other important cardiogenic transcriptional modulators like transcription factors (TFs) such as *Gata4, Nkx2.5* or *Hand1* (Holtzinger *et al.*, 2010; Nakashima *et al.*, 2014).

Since murine ESCs are able to recapitulate all crucial steps of early cardiac development when differentiated *in vitro* (Desbaillets *et al.*, 2000; Hopfl *et al.*, 2004) including the advent of CPCs around day 5/6 (0.75wks-0.85wks, Appendix Figure A10A), we next sought to investigate the expression kinetics of the four miR candidates during murine ESC *in vitro* differentiation to see their typical course of increased expression. For comparison, we also measured the kinetics of the above-mentioned TFs as well as miR-1 and miR-133a.

Therefore, non-transgenic V6.5 ESCs as well as NkxCE-GFP ESCs were spontaneously differentiated with the standard hanging drop method and cell lysates for RNA isolation were collected every other day between day 0 and day 10 for qRT-PCR analysis.

As expected, we found that the expressions of the cardiac TFs *Gata4, Nkx2.5* as well as *Hand1* started to rise upon the beginning of cardiomyogenesis between day 4 and day 6 of murine ESC *in vitro* differentiation (Figure 4).

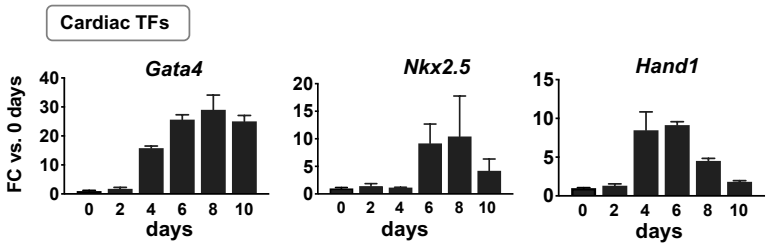

Figure 4 Kinetics of cardiac TFs during *in vitro* differentiations of murine ESCs. **A.** Expression kinetics of the cardiac transcription factors (TFs) *Gata4*, *Nkx2.5* and *Hand1* started to elevate at the onset of early cardiogenesis between day 4 and day 6 of *in* vitro differentiation of NkxCE-GFP ESCs. Data are represented as means ± SEM of two independent experiments with each one or three independent samples measured as singles (n=4). Adapted from Figure S2A from Hoelscher *et al.* miR-128a Acts as a Regulator in Cardiac Development by Modulating Differentiation of Cardiac Progenitor Cell Populations. *Int. J. Mol. Sci.* 2020, *21*, 1158 (Hoelscher *et al*., 2020).

Likewise, similar kinetics were found for previously described (Ivey *et al.*, 2008) miR-1 and miR-133a (Figure 5A) as well as three of our candidate miRs, namely miR-30a, miR-30b and miR-128a (Figure 5B). This again supported the idea that these three candidate miRs might play regulatory roles in early cardiogenic processes. However, for miR-20b we observed a different kinetic with an expression peak at day 4 and a second smaller peak at day 8 (Figure 5B). Interestingly, such a biphasic behavior has been previously demonstrated for cardiac transcription factors such as *Mzf1, D-mef2* or *Myf-6* with important roles in cardiac linage specification (Bober *et al.*, 1991; Doppler *et al.*, 2014; Nguyen *et al.*, 1994) indicating that miR-20b could possess functional relevance as well.

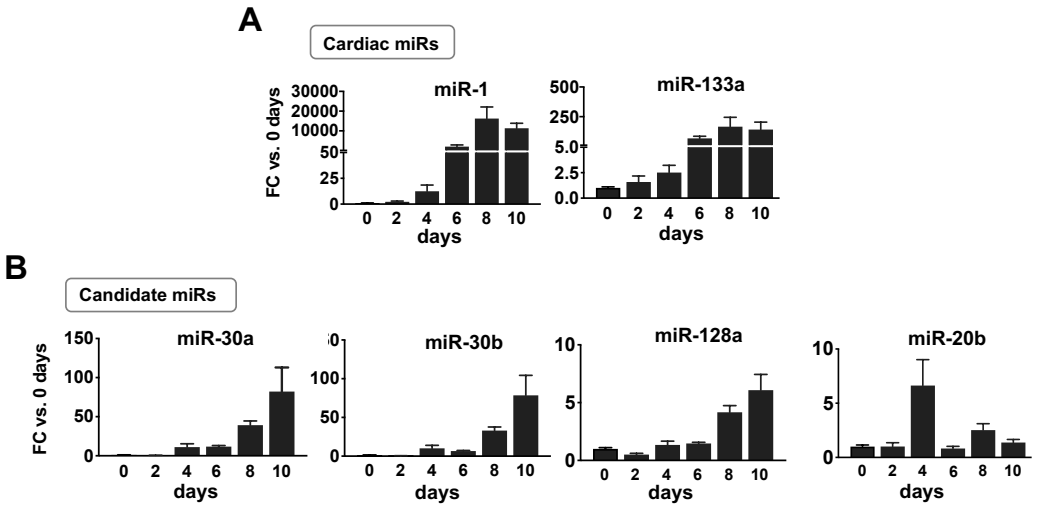

Figure 5 Kinetics of miRs during *in vitro* differentiations of murine ESCs. **A.** Expression of the cardiac-specific miR-1 and miR-133a rise upon the beginning of cardiomyogenesis around day 4 to day 6 of *in vitro* differentiation of V6.5 ESCs. **B.** Kinetics of three of the candidate miRs namely miR-30a, miR-30b and miR-128a followed the same trend starting to be expressed around day 4 to day 6. The kinetics of miR-20b appeared to be biphasic with a peak at day 4 as well as day 8. Data are represented as means ± SEM of three independent experiments with each three independent samples measured as duplicates (n=18). Adapted from Figure 1H from Hoelscher *et al.* miR-128a Acts as a Regulator in Cardiac Development by Modulating Differentiation of Cardiac Progenitor Cell Populations. *Int. J. Mol. Sci.* 2020, *21*, 1158 (Hoelscher *et al.*, 2020).

After showing the characteristic expression behavior during murine ESC differentiation, we next thought to investigate if our miRs also show typical kinetics in another species. Beside the previously shown concordances in miR sequences (Figure 3C), it has also been described that conserved miRs (e.g. miR-1 and miR-133a) in fact also share very similar underlying regulatory mechanisms across different species (Ivey *et al.*, 2008). Hence, an identical expression kinetic of our candidate miRs in diverse species could further indicate their relevance during early embryogenesis.

Therefore, we measured the expression of miR-1, miR-133a as well as our four candidate miRs in human induced pluripotent stem cells (hiPSCs) which were differentiated by our colleagues Martina Dreßen and Harald Lahm using a protocol that shifts hiPSCs into a cardiac direction by manipulating the Wnt-signaling pathway with small molecules (Burridge *et al.*, 2014). Total RNA samples isolated from cell lysates every other day were also kindly provided by above-mentioned colleagues. Since differentiation of human cells usually proceeds slower than in murine cells, *in vitro* differentiation and miR analysis was conducted until day 14.

Despite the fact, that pluripotent stem cell lines from different species do not necessarily behave equally *in vitro (*e.g. due to epigenomic and transcriptomic differences or variable differentiation abilities) (Bem *et al.*, 2018; Bober *et al.*, 1991; Bock *et al.*, 2011; Newman and Cooper, 2010; Schuster *et al.*, 2015), as well as the knowledge that miR chromosomal locations and expression profiles may vary between species (Bar *et al.*, 2008; Cao *et al.*, 2008; Chen *et al.*, 2007; Houbaviy *et al.*, 2003; Laurent *et al.*, 2008; Morin *et al.*, 2008; Razak *et al.*, 2013; Suh *et al.*, 2004; Tang *et al.*, 2006), we were able to confirm that the analyzed miRs indeed shared similar kinetics during *in vitro* differentiation regardless of the species.

The expression of miR-1, miR-133a as well as miR-30a, miR-30b and miR-128a started to rise upon day 8 to day 10 during human cardiac-directed differentiation (Figure 6A, B). Considering the earlier mentioned slower differentiation of hiPSCs *in vitro,* these results were comparable to previously described kinetics in murine spontaneous ESC *in vitro* differentiations (Figure 5A, B Figure 6A, B). Only miR-20b did not show a recognizable trend of upregulation during hiPSC *in vitro* differentiation (Figure 6B).

Conclusively, our first results supported the idea that the four selected miR candidates might have functional relevance in early cardiogenesis since they were found to be enriched in murine NkxCE-GFP CPCs, showed high sequence preservation across species and exhibited similar expression kinetics during *in vitro* differentiation of murine and human ESCs/iPSCs.

Thus, we next decided to analyze the impact of those miRs on cardiac development in zebrafish *in vivo* (4.2).

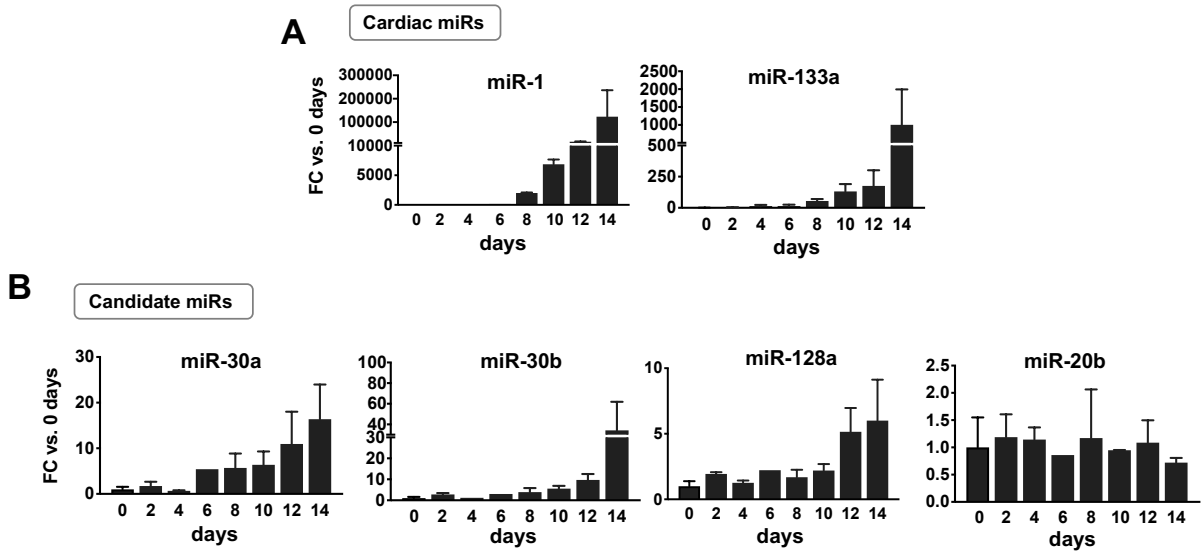

Figure 6 Kinetics of miRs during *in vitro* differentiations of hiPSCs. **A.** Expression of cardiac miRs miR-1 and miR-133a followed a typical course by rising upon the beginning of early cardiogenesis around day 8 to day 10. **B.** miR-30a, miR-30b and miR-128a also elevated around day 8 to day 10, whereas miR-20b showed no recognizable trend of upregulation throughout hiPSC *in vitro* differentiation. Total RNA samples from cell lysates taken during *in vitro* differentiations were kindly provided by Martina Dreßen and Harald Lahm. Data are represented as means ± SEM of one experiment with one probe measured as duplicates (n=2). Adapted from Figure S2C from Hoelscher *et al.* miR-128a Acts as a Regulator in Cardiac Development by Modulating Differentiation of Cardiac Progenitor Cell Populations. *Int. J. Mol. Sci.* 2020, *21*, 1158 (Hoelscher *et al.*, 2020).

4.2 Candidate miR function in zebrafish larvae *in vivo*

All zebrafish *in vivo* experiments stated below were performed by Dr. David Hassel and his team at the Department of Medicine III, Cardiology, Angiology, Pneumology at the University Hospital Heidelberg. However, the main results were included in this thesis since they were an indispensable part of this project.

First, candidate miR kinetics were analyzed during *in vivo* development of zebrafish larvae as a third species (4.2.1). Second, we wanted to evaluate if the candidate miRs were able to induce a cardiac phenotype *in vivo* in zebrafish larvae (4.2.2).

These experiments were crucial since they gave us a first idea of the impact of the candidate miRs *in vivo* and therefore allowed us to confine our miR candidate selection before we started to study their functions in more detail during murine ESC/iPSC differentiations in our laboratory (4.3-4.5).

4.2.1 Kinetics during *in vivo* development of zebrafish larvae

First, the expression kinetics of candidate miRs were evaluated during early zebrafish development to investigate whether they show similar upregulation in correlation with the onset of early cardiogenesis.

Therefore, expression of all candidate miRs was measured by qRT-PCR at specific timepoints between 0 hours post fertilization (hpf) until 72hpf (Figure 7).

Results showed, that all miRs (miR-30a, miR-30b, miR-128a and miR-20b) were induced at the beginning of heart morphogenesis in zebrafish larvae around 24hpf followed by a constant rise until 72hpf (Figure 7).

This matched our obtained results from murine ESC and hiPSC differentiations (Figure 5B, Figure 6B) and again verified high preservation of candidate miRs as well as potential functional relevance of those miRs across species.

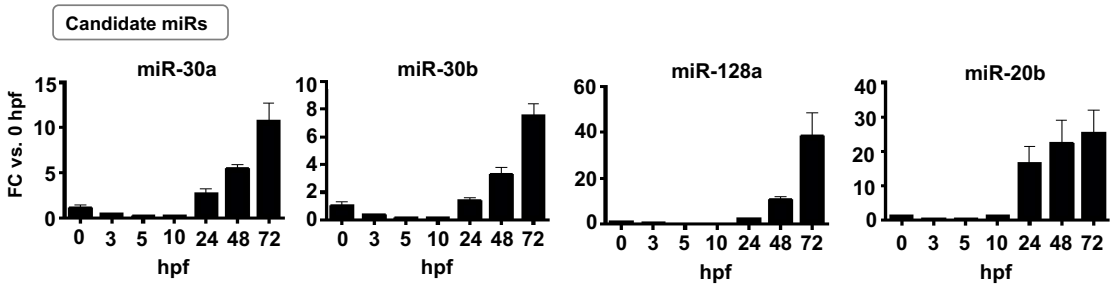

Figure 7 Kinetics of candidate miRs during *in vivo* development of zebrafish larvae. Expressions of miR-30a, miR-30b, miR-128a as well as miR-20b were upregulated in developing zebrafish larvae from 24hpf with further increase until 72hpf. Experiments were conducted by cooperation partner Dr. David Hassel and his team (University Hospital Heidelberg). Data are represented as means ± SEM. Adapted from Figure 2B from Hoelscher *et al.* miR-128a Acts as a Regulator in Cardiac Development by Modulating Differentiation of Cardiac Progenitor Cell Populations. *Int. J. Mol. Sci.* 2020, *21*, 1158 (Hoelscher *et al.*, 2020).

4.2.2 Morpholino-induced knockdown of candidate miRs during *in vivo* development of zebrafish larvae

Dr. Hassel and his team next investigated the cardiovascular impacts of the four miR candidates through knockdown experiments using antisense morpholino-modified oligonucleotides (MOs) complementary to the miR sequences.

MOs were injected at the one or two cell stage of developing transgenic zebrafish embryos in which GFP expression is driven by the *myl7* promoter, an early cardiac marker (Tg(myl7:ras-GFP)) (D'Amico *et al.*, 2007).

The efficiency of miR knockdown after MO injection was verified by qRT-PCR at 24hpf and showed that all candidate miRs were sufficiently downregulated by more than 85% (p≤0.05) after MO injection when compared to controls without MO injections (w/o MO) (Figure 8).

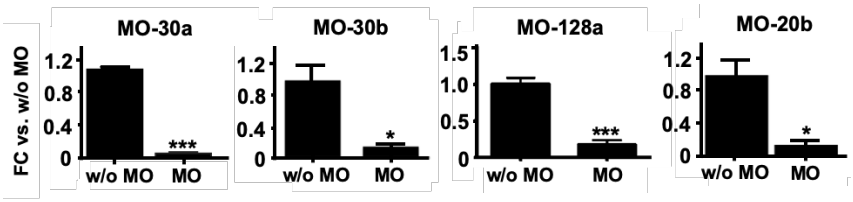

Figure 8 Knockdown efficiency of miR candidates *in vivo*. Morpholino (MO) injection sufficiently reduced the expression of all candidate miRs by more than 85% ($p \leq 0.05$) measured at 24hpf in zebrafish larvae in comparison to control larvae without MO injection (w/o MO). Experiments were conducted by cooperation partner Dr. David Hassel and his team (University Hospital Heidelberg). Data are represented as means ± SEM. Statistical significance was assessed by two-tailed student's t-test * $p \leq 0.05$, ***$p \leq 0.001$. Adapted from Figure 2D from Hoelscher *et al.* miR-128a Acts as a Regulator in Cardiac Development by Modulating Differentiation of Cardiac Progenitor Cell Populations. *Int. J. Mol. Sci.* 2020, *21*, 1158 (Hoelscher *et al.*, 2020).

As a next step, changes in larval phenotypes as well as parameters of cardiac function including fractional shortening (measured by Meazure™ v2.0 tool, C Thing Software, Mountain View, CA, USA) and heart rate (beats per minute (bpm) evaluated by video microscopy) were subsequently analyzed at 48hpf and 72hpf.

Results showed, that despite the sufficient knockdown of miR-30a, zebrafish larvae with MO-30a injection did neither exhibit morphological changes in general nor variations concerning cardiac morphology. In addition, no alteration of cardiac function was observed at 48hpf and 72hpf (*data from David Hassel not shown*). Since no cardiogenic relevance could be confirmed *in vivo*, miR-30a was excluded from further detailed functional studies. Interestingly, however, after knockdown of the other three miR candidates, various phenotypes were observed (Figure 9-11).

Morphants with miR-20b knockdown (MO-20b) exhibited severe brain hemorrhage (Figure 9A, red arrow, right panel) as well as edema in the eye region (Figure 9A, white arrow, right panel) at 48hpf. Additionally, MO-20b morphants appeared to have decreased body size when compared to control larvae (w/o MO) at 72hpf (Figure 9B). Interestingly, the observed hemorrhages and edema from 48hpf seemed to diminish at 72hpf (Figure 9B). Unfortunately, beside these general alterations in morphology, no obvious impact on the cardiac phenotype was observed at any timepoint. This was also reflected by the measurements of cardiac function at 72hpf where neither change in fractional shortening nor heart rate were detected in MO-20b larvae when compared to control larvae (w/o MO) (Figure 9C, D).

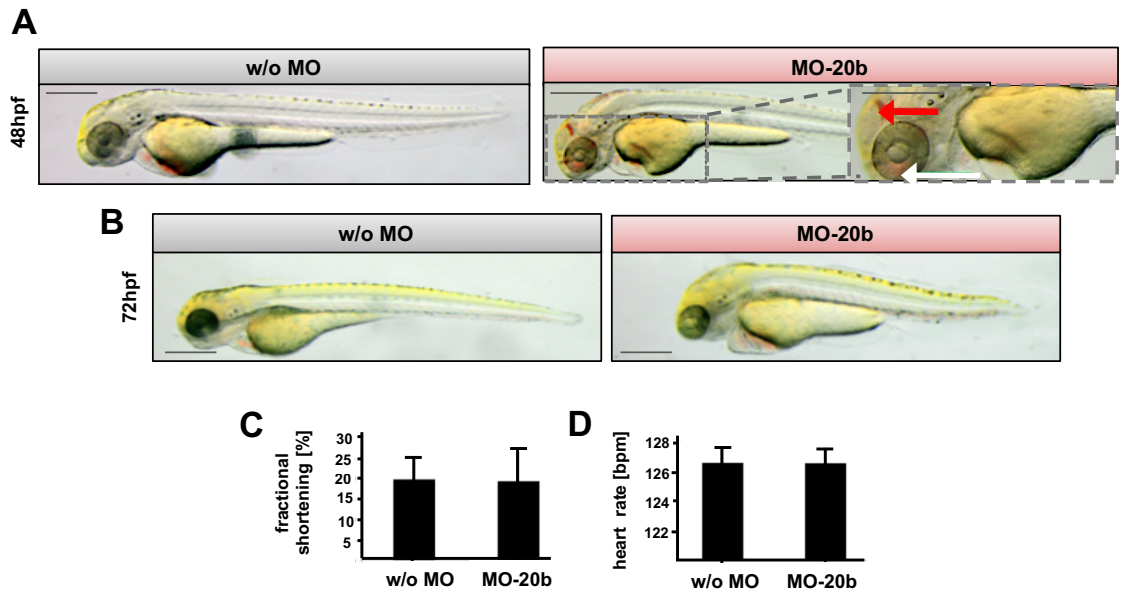

Figure 9 Phenotypes and cardiac functional parameters of MO-20b zebrafish larvae. A. MO-20b treated zebrafish larvae showed cerebral hemorrhage (red arrow, right panel) and edema in the eye region (white arrow, right panel) at 48hpf when compared to larvae w/o MO injection (w/o MO, left panel). **B.** At 72hpf, hemorrhages and edema diminished in MO-20b larvae (right panel), however, morphants appeared to develop decreased body size (right panel) in comparison to control larvae (w/o MO, left panel). **C.** MO-20b larvae did not show significant differences in fractional shortening compared to control larvae (w/o MO) at 72hpf **D.** Knockdown of miR-20b (MO-20b) had no significant impact on heart rate in zebrafish morphants at 72hpf compared to controls (w/o MO). All scale bars are 250µm. Experiments were conducted by cooperation partner Dr. David Hassel and his team (University Hospital Heidelberg). Data are represented as means ± SEM. Adapted from Figure 2E and S3A-C from Hoelscher *et al.* miR-128a Acts as a Regulator in Cardiac Development by Modulating Differentiation of Cardiac Progenitor Cell Populations. *Int. J. Mol. Sci.* 2020, *21*, 1158 (Hoelscher *et al.*, 2020)

Furthermore, morphants with MO injections for miR-30b knockdown (MO-30b) developed visible edema and enlarged hydrocephalus at 48hpf (Figure 10A, red arrow, right panel). Additionally, extreme blood stasis (Figure 10B, white arrow, lower panel) was observed in MO-30b at 72hpf which was accompanied by crimped tails (Figure 10B, red arrow, lower panel) and a severely shortened body length when compared to control larvae w/o MO (Figure 10A,B, each left panels). However, fractional shortening (Figure 10C) and even the reduced heart rate (Figure 10D) in MO-30b larvae at 72hpf did not reach significance when compared to controls w/o MO (Figure 10D).

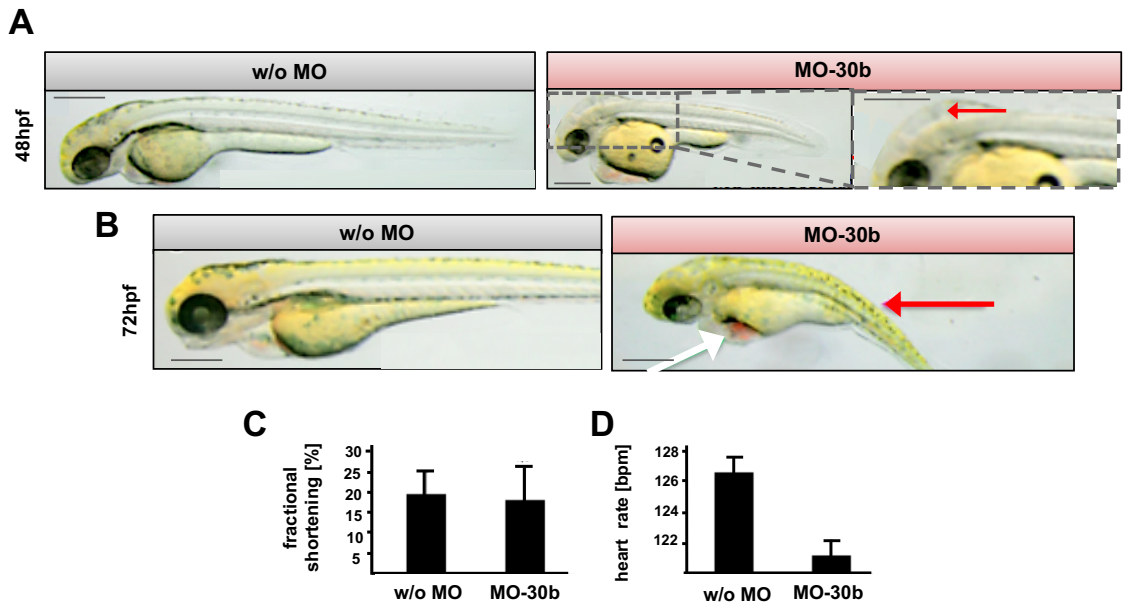

Figure 10 Phenotypes and cardiac functional parameters of MO-30b zebrafish larvae. A. At 48hpf, MO-30b morphants developed malformations and edema. The red arrow (right panel) highlights visible edema and enlarged hydrocephalus in MO-30b larvae compared to controls w/o MO (left panel). **B**. MO-30b morphants exhibited extreme blood stasis (white arrow, right panel) and crimped tails (red arrow, right panel) after 72hpf compared to control larvae w/o MO (left panel). **C.** No significant difference was observed in the percentage of fractional shortening in MO-30b morphants when compared to control larvae (w/o MO) at 72hpf. **D.** Knockdown of miR-30b had no significant effect on the heart rate (bpm) in zebrafish morphants at 72hpf when compared to controls w/o MO. However, the heart rate seemed to be reduced in MO-30b morphants. All scale bars are 250µm. Experiments were conducted by cooperation partner Dr. David Hassel and his team (University Hospital Heidelberg). Data are represented as means ± SEM. Adapted from Figure 2E and S3A-C from Hoelscher *et al.* miR-128a Acts as a Regulator in Cardiac Development by Modulating Differentiation of Cardiac Progenitor Cell Populations. *Int. J. Mol. Sci.* 2020, *21*, 1158 (Hoelscher *et al.*, 2020).

Even though the knockdowns of miR-20b and miR-30b caused morphological alterations, no obvious impact on cardiac structures or function was observed. Hence, these two miRs were also excluded for further analysis at this point.

Surprisingly, while evaluating zebrafish larvae with knockdown of miR-128a (MO-128a), several phenotypical alterations were found including a robust cardiac phenotype at 48hpf. Besides that, the eyes of MO-128a larvae (Figure 11A, right panel) appeared smaller in comparison to controls w/o MO injection at 48hpf (Figure 11A, left panel). In terms of cardiac malformations, MO-128a larvae developed pericardial edema (Figure 11A, red arrow, right panel) in addition to blood congestion in front of the right outflow tract (Figure 11A, white arrow, right panel) indicative for impaired heart function. In addition, smaller ventricles (Figure 11B, white arrow, right panel) as well as abnormalities in heart looping (Figure 11B) leading to an incorrect positioning of the heart, were frequently observed in MO-128a compared to controls (w/o MO, Figure 11B, left panel). The atrium seemed to be unaffected by downregulation of miR-128a (Figure 11B, right panel). Evaluation of cardiac functional parameters revealed that MO-128a larvae showed significant decreased fractional shortening (Figure 11C, $p \leq 0.05$) and heart rate (Figure 11D, $p \leq 0.001$).

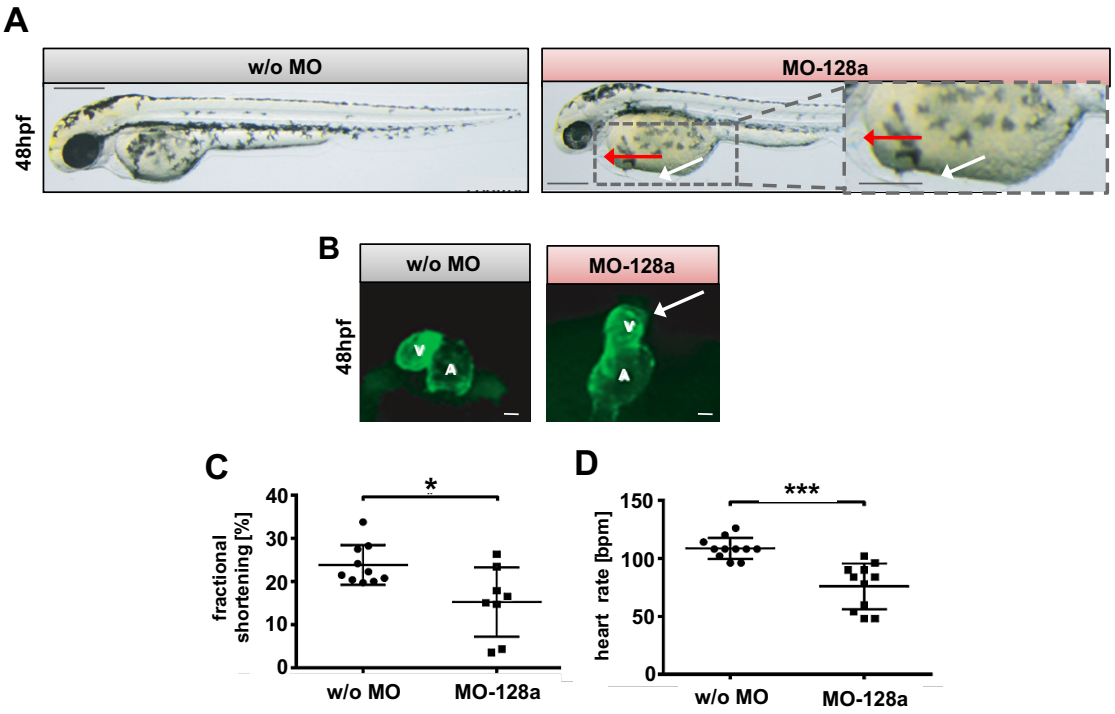

Figure 11 Phenotypes and cardiac functional parameters of MO-128a zebrafish larvae. A. MO-128a larvae exhibited robust pericardial edema (marked by red arrow, right panel) and blood congestion at the right outflow tract of the heart (indicated by white arrow, right panel) when compared to larvae w/o MO injection (left panel) at 48hpf. Scale bars are 250µm **B.** Evaluation of cardiac phenotype of Tg(my/7:ras-GFP) zebrafish larvae showed that larvae with miR-128a knockdown (MO-128a, right panel) exhibited smaller ventricles (marked by white arrow) as well as abnormalities in heart looping at 48hpf when compared to controls (left panel). Scale bars are 5µm **C.** MO-128a larvae showed a significantly reduced fractional shortening ($p \leq 0.05$, n=8) at 72hpf compared to non-treated larvae w/o MO (n=10) **D.** MO-128a morphants appeared to have a significantly reduced heart rate (bpm) ($p \leq 0.001$, n=11) at 72hpf compared to the control group w/o MO (n=11). Experiments were conducted by cooperation partner Dr. David Hassel and his team (University Hospital Heidelberg). Data are represented as means ± SEM. Statistical significance was assessed by two-tailed student's t-test. * $p \leq 0.05$, ***$p \leq 0.001$. Adapted from Figure 2E-H from Hoelscher *et al.* miR-128a Acts as a Regulator in Cardiac Development by Modulating Differentiation of Cardiac Progenitor Cell Populations. *Int. J. Mol. Sci.* 2020, *21*, 1158 ((Hoelscher *et al.*, 2020).

Altogether, *in vivo* knockdown experiments indicated that one of our miR candidates, miR-128a, had fundamental influence on early cardiogenesis in zebrafish development. Hence, we decided to focus on miR-128a and further study its function in detail during early development with the help of knockdown and overexpression experiments during *in vitro* differentiation with various transgenic murine ESC/iPSC lines as described in 4.3- 4.5.

4.3 LNA-mediated knockdown of miR-128a during *in vitro* differentiations of NkxCE-GFP ESCs

For *in vitro* knockdown experiments, we first utilized the previously described transgenic NkxCE-GFP ESC line as a CPC reporter line (1.2) to investigate the functional roles of miR-128a in more detail.

Therefore, NkxCE-GFP ESCs were differentiated by the standard hanging drop protocol and miR-128a knockdown was conducted by transfection with specific locked nucleic acid (LNA) probes (LNA-128) and LNA control probes (LNA-Ctr). Since LNA probes and transfection reagents might impact physiological processes of cells e.g. proliferation rates, we first sought to investigate this during *in vitro* differentiations (4.3.1).

This pre-evaluation was crucial for the selection of an adequate control (reference) and was thereby conducted prior to final knockdown experiments (4.3.2).

4.3.1 Analysis of influence of transient transfection on cell physiology

For analysis, NkxCE-GFP ESCs were either treated (day -1) with 50nM of an LNA control probe without homology to miRs of any species including Fugene transfections reagent (LNA-Ctr), with Fugene only (Ctr) or simply differentiated without LNA probe nor transfection reagent (Ctr w/o Fugene). After one week of *in vitro* differentiation, MTT assays to evaluate the cell proliferation as well as flow cytometry to quantify the amount of NkxCE-GFP CPCs were performed.

Interestingly, MTT assays revealed a significantly elevated proliferation rate ($p<0.001$) for LNA-Ctr transfected NkxCE-GFP ESCs (Figure 12A) when compared to Ctr w/o Fugene indicating that either the LNA probes or the transfection reagent Fugene influenced the proliferation rates of ESCs.

Additionally, GFP-positive CPCs were significantly increased in the LNA-Ctr group when compared to the control group with Fugene only (Ctr) ($p=0.0448$) showing that the transfection with LNA-Ctr alone was able to change the CPC abundance significantly (Figure 12B, C).

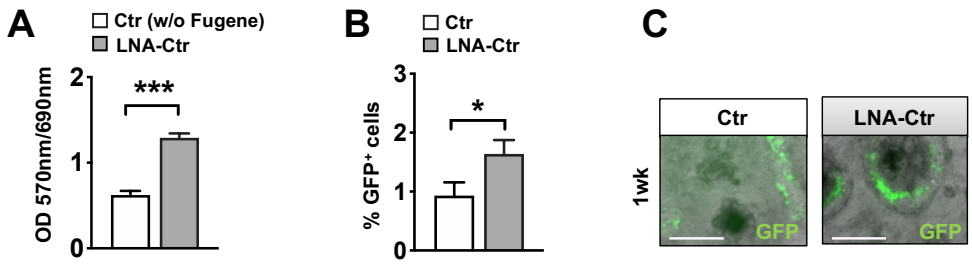

Figure 12 Influence of transient transfection during *in vitro* differentiations of NkxCE-GFP ESCs. A. MTT assay of NkxCE-GFP ESCs transfected with LNA-Ctr probes showed a significant upregulation of proliferation capacity ($p<0.001$, student's t-test) when compared to non-transfected ESCs (Ctr w/o Fugene) after one week of *in vitro* differentiation. **B.** Frequency of NkxCE-GFP CPCs was significantly enhanced ($p=0.0448$, student's t-test) after one week in LNA-Ctr transfected ESCs when compared to ESCs differentiated with Fugene only (Ctr) **C.** NkxCE-GFP CPCs after one week of NkxCE-GFP ESC differentiation when transfected with Fugene only (Ctr, left panel) or LNA-Ctr (right panel). Images are an overlay between phase contrast and fluorescent microscopic pictures. Scale bars are 500µm**.** Data are represented as means ± SEM of (A) one experiment with each sample measured in eight wells (n=8) and (B) three independent experiments with each three independent sample measured as singles (n=9). Statistical significance was assessed by two-tailed student's t-test as stated. * $p \leq 0.05$, *** $p \leq 0.001$. Adapted from Figure S4B, C and D from Hoelscher *et al.* miR-128a Acts as a Regulator in Cardiac Development by Modulating Differentiation of Cardiac Progenitor Cell Populations. *Int. J. Mol. Sci.* 2020, *21*, 1158 (Hoelscher *et al.*, 2020).

Hence, to ensure an evaluation of proper results without side effects related to the use of LNA probes or the transfection reagent Fugene we normalized all our results derived from *in vitro* knockdown experiments with LNA-128 probes to the respective LNA-Ctr transfected group.

4.3.2 Analysis of miR-128a knockdown effects during *in vitro* differentiations of NkxCE-GFP ESCs

To guarantee an efficient knockdown of miR-128a over the time course of two weeks, we performed two consecutive transient transfections during NkxCE-GFP ESC *in vitro* differentiation. Since we showed previously (Figure 5B) that the expression of miR-128a started to rise around day 4 to day 6 of *in vitro* differentiation, we decided to conduct the first LNA transfection (LNA-128 or LNA-Ctr) at day 3.5. Additionally, a second transfection was performed at day 7 (one week, 1wk) to ensure a stable knockdown until the experimental endpoint which was determined by day 16 (2.25wks).

As expected, the expression levels of miR-128a evaluated by qRT-PCR showed an efficient knockdown by more than 80% ($p<0.001$) from day 5 (0.75wks) until day 14 (2wks) during differentiation when compared to the correspondent LNA-Ctr group (Figure 13).

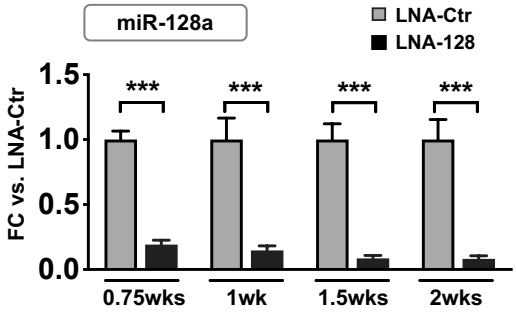

Figure 13 Knockdown efficiency of miR-128a during *in vitro* differentiations of NkxCE-GFP ESCs. The expression of miR-128a was efficiently downregulated from 0.75wks to 2wks (all timepoints p<0.001, Mann-Whitney) during *in vitro* differentiation of LNA-128 transfected NkxCE-GFP ESCs when compared to the respective LNA-Ctr group. Data are represented as means ± SEM of three to four independent experiments with each two to four independent samples measured as singles or duplicates (0.75wks n=16,17; 1wk n=7,6; 1.5wks n=7,6; 2wks n=14,12). Statistical significances were assessed by Mann-Whitney Rank Sum test as stated. *** p ≤ 0.001 Adapted from Figure 3B from Hoelscher *et al.* miR-128a Acts as a Regulator in Cardiac Development by Modulating Differentiation of Cardiac Progenitor Cell Populations. *Int. J. Mol. Sci.* 2020, *21*, 1158 (Hoelscher *et al.*, 2020).

Numerous miRs have been shown to harbor important regulatory functions during ESC differentiation such as cell fate decisions and lineage commitment including the specification of mesodermal cells into CPCs (Bondue *et al.*, 2011; Chen *et al.*, 2017; Ivey *et al.*, 2008; Wang *et al.*, 2012).

To see if miR-128a could be involved in the specification of NkxCE-GFP CPCs, we next analyzed the frequency of those GFP-positive CPCs after miR-128a knockdown by flow cytometry during *in vitro* differentiation of NkxCE-GFP ESCs (Figure 14).

Importantly, both LNA-treated ESC groups (LNA-Ctr and LNA-128) developed GFP-positive CPCs in embryoid bodies (EBs) in a regular manner beginning at day 6 (0.85wks) (Appendix Figures A10B, C) that was also accompanied by spontaneous beating. This observation indicated that at least the timing of NkxCE-GFP CPC appearance (day 6, 0.85wks) was not compromised by knockdown of miR-128a.

However, already one day later (1wk), we observed a slightly reduced amount of NkxCE-GFP CPCs in LNA-128 treated EBs in comparison to the LNA-Ctr group, although not yet significant (Figure 14A, B, representative FACS blots Appendix Figures A12B, C). Interestingly, this continued to a significant CPC reduction of 37% (p=0.001) after 10 days (1.5wks) of *in vitro* differentiation in LNA-128a treated EBs (Figure 14A, B). The CPC frequency after 2wks was not affected in the LNA-128 group when compared to LNA-Ctr-treated EBs (Figure 14A). Although, we saw a diminished percentage of GFP-positive CPCs in LNA-Ctr treated EBs (p<0.001 compared to 1.5wks) as well as in LNA-128 treated EBs (p=0.0141 compared to 1.5wks) after 2wks in general (Figure 14A).

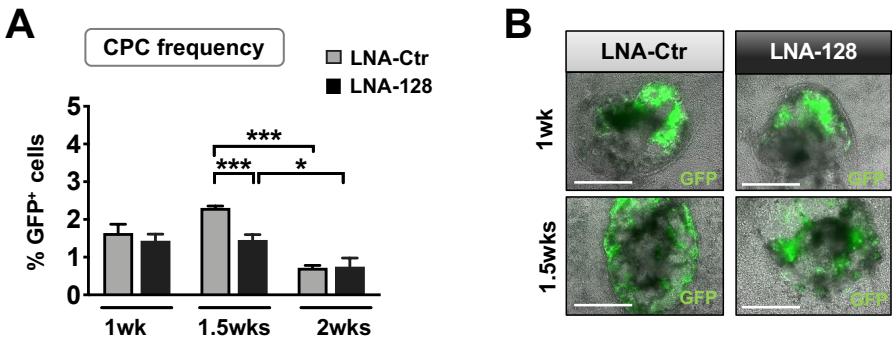

Figure 14 Frequency of NkxCE-GFP CPCs after miR-128a knockdown during *in vitro* differentiations. A. Flow cytometry showed that the percentage of NkxCE-GFP CPCs was significantly reduced (p=0.001, Mann-Whitney) after 1.5wks in LNA-128 treated NkxCE-GFP EBs in comparison to the LNA-Ctr group. In addition, CPCs were in general diminished after 2wks in LNA-Ctr treated EBs (p<0.001, student's t-test) as well as in LNA-128 treated EBs (p=0.0141, student's t-test) when being compared to their correspondent CPC frequency at 1.5wks. **B.** NkxCE-GFP CPCs after 1wk (upper panel) and 1.5wks (lower panel) of *in vitro* differentiation of LNA-Ctr or LNA-128 treated EBs. Images are an overlay between phase contrast and fluorescent microscopic pictures. Scale bars are 500µm. Data are represented as means ± SEM of two to three independent experiments with each three independent samples measured as singles (1wk n=9,9; 1.5wks n=5,9; 2wks n=6,6). Statistical significances were assessed by Mann-Whitney Rank Sum test or two-tailed student's t-test as stated. * p ≤ 0.05, *** p ≤ 0.001 Adapted from Figure 3C, D from Hoelscher *et al.* miR-128a Acts as a Regulator in Cardiac Development by Modulating Differentiation of Cardiac Progenitor Cell Populations. *Int. J. Mol. Sci.* 2020, *21*, 1158 (Hoelscher *et al*., 2020).

Typically, CPCs maturate continuously into cardiac lineages including cardiomyocytes (CMs), endothelial cells (ECs) and smooth muscle cells (SMCs) after 2-3wks of *in vitro* differentiation as shown below by ICC (Figure 15).

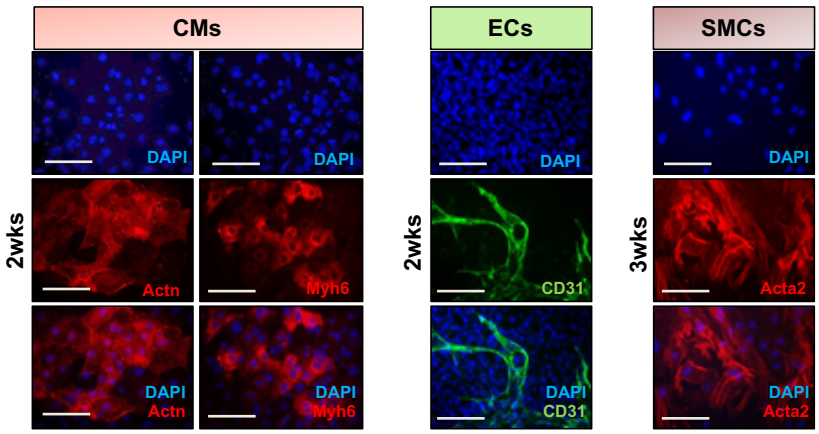

Figure 15 ICC of main cardiac lineages during *in vitro* differentiations of NkxCE-GFP ESCs. ICC staining showed that NkxCE-GFP ESCs differentiated into the three major cardiac cell types including cardiomyocytes (CMs, left two panels), endothelial cells (ECs, third panel from left) and smooth muscle cells (SMCs, right panel) after 2-3wks (2wks=13 days, 3wks=20 days of *in vitro* differentiation). CMs were stained with antibodies against sarcomeric α-Actinin (Actn) and αMHC (Myh6), ECs against CD31 (Pecam1) and SMCs against αSMA (Acta2). Nuclear staining was conducted with DAPI. Images are shown as single fluorescent pictures as well as an overlay between all fluorescent microscopic pictures. Scale bars are 100µm. Adapted from Figure S4E from Hoelscher *et al.* miR-128a Acts as a Regulator in Cardiac Development by Modulating Differentiation of Cardiac Progenitor Cell Populations. *Int. J. Mol. Sci.* 2020, *21*, 1158 (Hoelscher *et al*., 2020).

During this maturation process, the CPC-specific Nkx2.5CE becomes increasingly inactivated subsequently leading to a reduced and finally absent GFP expression. The seen reduction of GFP-positive CPCs after 2wks within both LNA treated groups is therefore an expected result which reflects functional maturation of NkxCE-GFP ESCs during *in vitro* differentiation after transfection.

Therefore, the significant reduction of GFP-positive CPCs in LNA-128 treated EBs after 1.5wks in comparison to the LNA-Ctr group could either point to an earlier differentiation of NkxCE-GFP CPCs into cardiac lineages as described above or could be a result of an enhancement of other progenitor cell populations (e.g. ectodermal progenitors or *Isl1*-positive CPCs).

To test the hypothesis that miR-128a knockdown could favor the abundance of other progenitor populations, we next performed gene expression analysis and measured several markers for CPC populations as well as other progenitors.

Characteristically, CPCs of the FHF and/or SHF start to express key TFs (markers) such as *Nkx2.5, Isl1, Sfrp5* or *Irx4* during very early murine embryonic heart development at the stage of the cardiac crescent (E7.5). By this they irreversibly commit to a cardiac fate and will later contribute to defined structures to the heart as previously described in detail (1.1) (Brade *et al.*, 2013; Fujii *et al.*, 2017; Moretti *et al.*, 2006; Wu *et al.*, 2006). Since E7.5 equals ~ 0.75wks of *in vitro* differentiations, we first checked that early timepoint for any changes of those CPC markers in LNA-Ctr and LNA-128 treated EBs.

Interestingly, we found a significant upregulation of *Isl1* ($p<0.01$), *Sfrp5* ($p<0.01$) and *Hcn4* ($p=0.0016$) as well as a significant downregulation of *Irx4* ($p=0.05$) in LNA-128 treated EBs when compared to correspondent LNA-Ctr group (Figure 16). Other CPC markers such as *Nkx2.5*, *Mef2c* and *Tbx5* showed a trend of upregulation at 0.75wks during *in vitro* differentiation after miR-128a knockdown (LNA-128) (Figure 16).

This indicated that miR-128a might indeed regulate CPC populations at the onset of cardiac development *in vitro* (0.75wks) by stimulating *Isl1/Sfrp5/Hcn4*-expressing cells which might also express *Nkx2.5*, *Mef2c* and *Tbx5* as well as inhibiting *Irx4*-expressing cells.

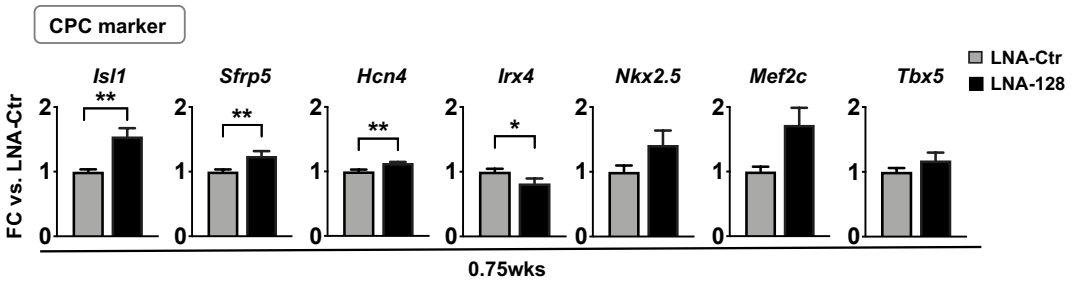

Figure 16 CPC marker expression in LNA-treated NkxCE-GFP EBs at 0.75wks of *in vitro* differentiations. Panels of early CPC markers show that the expression of *Isl1* ($p<0.01$), *Sfrp5* ($p<0.01$) as well as *Hcn4* ($p=0.0016$) (all student's t-test) were significantly upregulated in LNA-128 treated EBs when compared to LNA-Ctr group at 0.75wks. In addition, a slight upregulation was found for *Nkx2.5*, *Mef2c* and *Tbx5* at this timepoint. *Irx4* expression was found to be significantly downregulated ($p=0.05$, student's t-test) upon miR-128a knockdown (LNA-128) at 0.75wks when compared to LNA-Ctr. Data are represented as means ± SEM of three independent experiments with each three to four independent samples measured as singles (all n=11,11). Statistical significances were assessed by two-tailed student's t-test as stated. * $p \leq 0.05$, ** $p \leq 0.01$. Adapted from Figures 3E from Hoelscher *et al.* miR-128a Acts as a Regulator in Cardiac Development by Modulating Differentiation of Cardiac Progenitor Cell Populations. *Int. J. Mol. Sci.* 2020, *21*, 1158 (Hoelscher *et al*., 2020).

To further evaluate if other progenitor cells, e.g. ectodermal progenitors, were influenced by miR-128a knockdown at this stage, we measured the marker *Neurod1* that is known to be expressed by this cell type (Kamath *et al.*, 2005).

Indeed, *Neurod1* expression was significantly reduced ($p=0.0077$) in LNA-128 treated EBs at 0.75wks when compared to LNA-Ctr (Figure 17A). This observation could in fact promote our idea of an early stimulation of mesodermal CPCs as described above (Figure 16) since an enhancement of those CPCs could possibly be accompanied by reduced abundance of *Neurod1*-expressing ectodermal progenitors.

Recently, Huang and colleagues (Huang *et al.*, 2018) attributed a role to miR-128 in cell proliferation, although, in postnatal cardiomyocytes. Nonetheless, we next analyzed if the demonstrated changes in gene expression levels after miR-128 knockdown (Figure 16), might be caused by altered proliferation rates of cells.

Therefore, we evaluated the expression of a commonly used marker for cell proliferation (Sun and Kaufman, 2018), namely *Ki67*, at 0.75wks. Results showed, that both LNA-treated EB groups (LNA-128a and LNA-Ctr) expressed similar levels of *Ki67* (Figure 17B), implying that the enhanced or reduced expression levels (Figure 16, Figure 17A) were most likely not caused by any change of the proliferation rates of certain cell populations but rather due to other regulatory mechanisms linked to miR-128a knockdown.

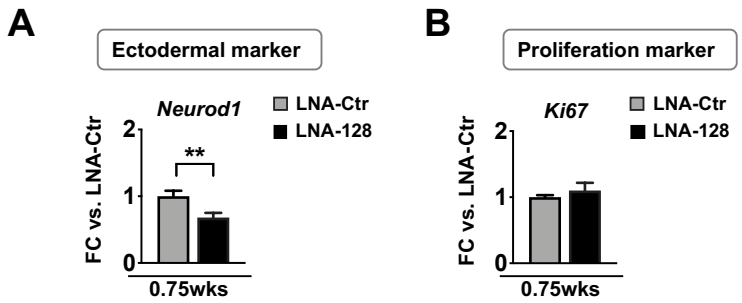

Figure 17 Ectodermal and proliferation marker expression in LNA-treated NkxCE-GFP EBs at 0.75wks of *in vitro* differentiations. **A.** The ectodermal marker *Neurod1* was significantly downregulated (p=0.0077, student's t-test) in LNA-128 treated EBs compared to LNA-Ctr EBs at 0.75wks of *in vitro* differentiation. **B.** The expression of the proliferation marker *Ki67* was not altered by miR-128a knockdown (LNA-128) at 0.75wks when compared to LNA-Ctr. Data are represented as means ± SEM of three independent experiments with each three to four independent samples measured as singles (all n=11,11). Statistical significance was assessed by two-tailed student's t-test as stated. ** p ≤ 0.01. Adapted from Figures 3G and H from Hoelscher *et al.* miR-128a Acts as a Regulator in Cardiac Development by Modulating Differentiation of Cardiac Progenitor Cell Populations. *Int. J. Mol. Sci.* 2020, *21*, 1158 (Hoelscher *et al*., 2020).

After showing that miR-128a was potentially able to influence early cardiogenesis by regulating the expression of several CPC markers at 0.75wks, we next aimed to investigate if we could also see such regulatory transcriptional effects at later timepoints (1wk, 1.5wks, 2wks) during *in vitro* differentiation of LNA-128 and LNA-Ctr treated NkxCE-GFP ESCs.

As shown below (Figure 18), almost none of the CPC markers including *Isl1, Nkx2.5, Mef2c, Tbx5, Hcn4* and *Irx4* were differentially expressed upon miR-128a knockdown (LNA-128) after 1wk (Figure 18A), 1.5wks (Figure 18B) or 2wks (Figure 18C). Only *Sfrp5* expression showed a continued trend of upregulation in LNA-128 treated EBs which was found to be significant until 1wk (p=0.0418) when compared to LNA-Ctr group (Figure 18A).

This implicated that miR-128a might only act as modulator during very early cardiogenesis (0.75wks) (Figure 16) and might not be involved in the regulation at later stages of cardiac development.

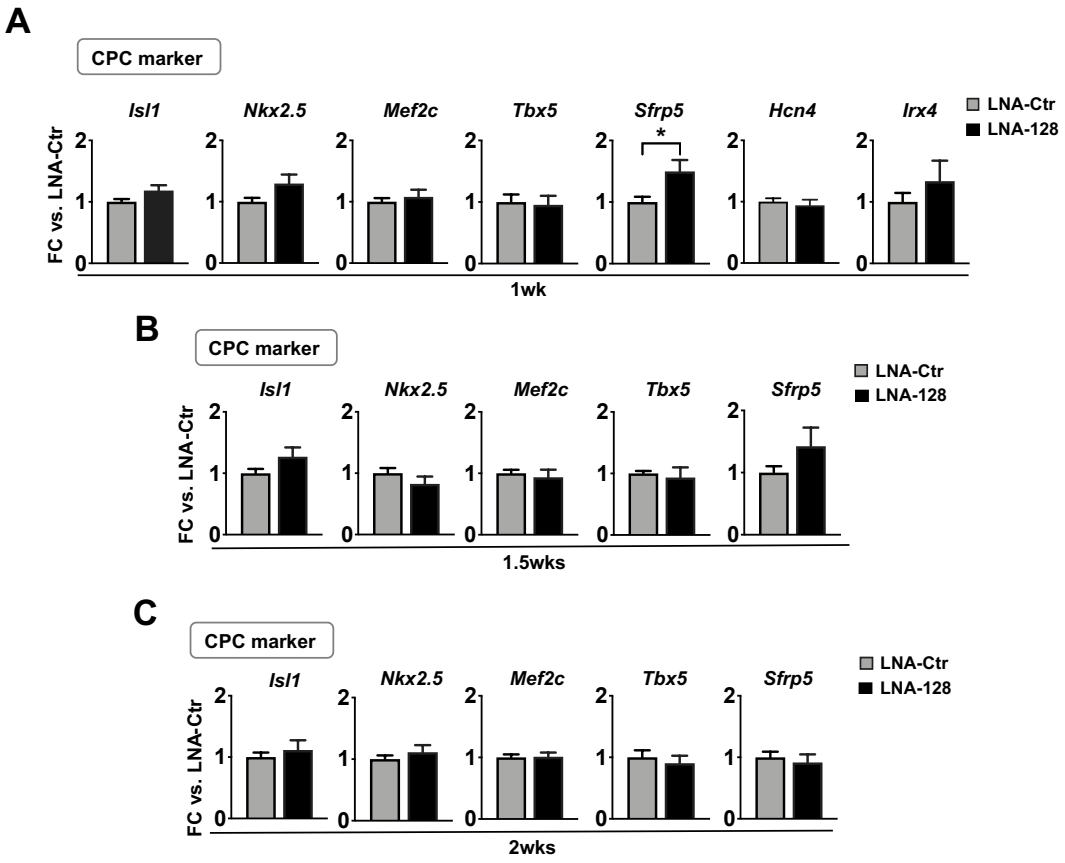

Figure 18 CPC marker expression in LNA-treated NkxCE-GFP EBs at 1wk, 1.5wks and 2wks of *in vitro* differentiations. A. The expression of CPC marker including *Isl1, Nkx2.5, Mef2c, Tbx5, Hcn4 and Irx4* were not significantly altered at 1wk of *in vitro* differentiation in LNA-128 treated EBs when compared to the LNA-Ctr group. Only *Sfrp5* was significantly enhanced at 1wk in the LNA-128 group (p=0.0418, student's t-test) **B-C.** Panels show that the expression of all CPC markers were not affected significantly after miR-128 knockdown (LNA-128) at (B) 1.5wks or (C) 2wks of *in vitro* differentiation. Data are represented as means ± SEM of (A, B) three independent experiments with each three independent samples measured as singles (all n=9,9) and (C) three independent experiments with each three to four independent samples measured as singles (all n=11,11). Statistical significance was assessed by two-tailed student's t-test as stated. * $p \leq 0.05$. (A) adapted from Figure 3F and (B, C) from Figures S5B, C from Hoelscher *et al.* miR-128a Acts as a Regulator in Cardiac Development by Modulating Differentiation of Cardiac Progenitor Cell Populations. *Int. J. Mol. Sci.* 2020, *21*, 1158 (Hoelscher *et al*., 2020).

Next, we aimed to test our second hypothesis in which we assumed that the reduction of GFP-positive CPCs in LNA-128 treated EBs after 1.5wks (Figure 14A) might be a result of an earlier differentiation of NkxCE-GFP CPCs into more mature cardiac lineages.

Therefore, we evaluated the expression of cardiac lineage markers including previously mentioned (Figure 15) markers for ECs (*CD31 (Pecam1)*), CMs (*αMHC (Myh6)*) and SMCs (*αSMA (Acta2*). In addition, we checked the expression of cardiac *Troponin-T (Tnnt*2) which is considered as a general marker for CMs. Since CPCs can maturate into all different kinds of CM populations, we also analyzed the expression of *Myl7* to identify atrial CMs as well as *Myl2* for the identification of ventricular CMs.

Cardiac lineage markers were measured at different timepoints during *in vitro* differentiation of LNA-128 as well as LNA-Ctr treated EBs according to previous analysis of CPC markers (1wk, 1.5wks, 2wks; Figure 20).

Although mature cardiac lineages finally develop after about 2wks of *in vitro* differentiation of ESCs (as demonstrated by ICC Figure 15), the onset of typical gene expression might in some cases start as early as day 5 (0.75wks) by this marking the beginning of cardiovascular lineage commitment. CM marker expression should be detectable at the latest from day 6 (0.85wks) when first beating clusters of early CM emerge.

Interestingly, two markers for SMCs (*Acta2*) and ECs (*Pecam1*), respectively, have been recently described to be highly expressed in NkxCE-GFP CPCs in the context of another project by one of our cooperation partners (Nothjunge *et al.*, 2017). By RNA sequencing (RNAseq) they showed that NkxCE-GFP CPCs from embryonic hearts (E9) expressed approximately 1000-fold higher levels of *Acta2* (p=0.0004) *(*Figure 19A, left panel) as well as about 60-fold higher levels of *Pecam1* (p=0.0123) *(*Figure 19A, right panel) in comparison to CMs which were isolated from adult mouse hearts at postnatal day 21 (P21).

Thus, changes of those markers at an early timepoint during *in vitro* differentiation (0.75wks) might indicate that also NkxCE-GFP CPC populations could be affected by a miR-128a knockdown. Before evaluating the above-mentioned other timepoints, we therefore first measured the expression of these marker genes at 0.75wks in LNA-128 and LNA-Ctr treated EBs.

Results showed that both, *Acta2* (Figure 19B, left panel, p<0.001) and *Pecam1* (Figure 19B, left panel, p=0.0357) were significantly enhanced upon miR-128a knockdown (LNA-128) when compared to LNA-Ctr at 0.75wks of *in vitro* differentiation. This supported the idea that miR-128a knockdown might be involved in the regulation of NkxCE-GFP CPCs by favoring their abundance at the very early onset of cardiac development (0.75wks).

In addition, the expression of *Acta2* and *Pecam1* at 0.75wks also reflected the multipotent character of NkxCE-GFP CPCs which finally differentiate into ECs and SMCs at later stages of development.

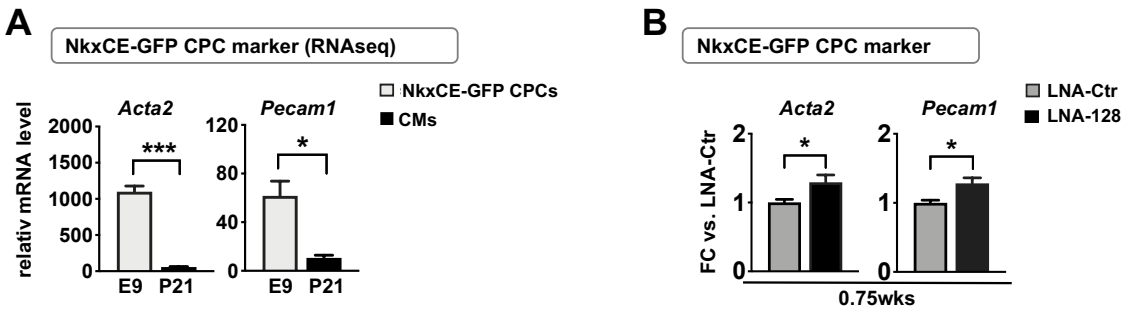

Figure 19 NkxCE-GFP CPC marker expressions. A. RNAseq data showed that NkxCE-GFP CPCs from E9 embryonic hearts expressed significantly higher levels of *Acta2* (p=0.0004, student's t-test, left panel) and *Pecam1* (p=0.0123, student's t-test, right panel) when compared to CMs from adult mouse hearts (postnatal day 21; P21). Data was obtained in the context of another cooperation project (Nothjunge *et al.*, 2017). **B.** Evaluation of *Acta2* and *Pecam1* at 0.75wks of *in vitro* differentiation of LNA-treated NkxCE-GFP ESCs showed that levels of *Acta2* ($p<0.001$, student's t-test, left panel) and *Pecam1* (p=0.0357, Mann-Whitney, right panel) were significantly elevated in LNA-128 EBs when compared to LNA-Ctr. Data are represented as means ± SEM of (A) two to three independent CPC and CM populations (n=2-3) and (B) three independent experiments with each three to four independent samples measured as singles (both n=11,11). Statistical significances were assessed by Mann-Whitney Rank Sum test or two-tailed student's t-test as stated. * $p \leq 0.05$, *** $p \leq 0.001$. (A) adapted from Figures S6D and (B) from Figure 3I from Hoelscher *et al.* miR-128a Acts as a Regulator in Cardiac Development by Modulating Differentiation of Cardiac Progenitor Cell Populations. *Int. J. Mol. Sci.* 2020, *21*, 1158 (Hoelscher *et al*., 2020).

We then further measured the expression of the different cardiac lineage markers at the above mentioned timepoints. Interestingly, neither *Acta2* nor *Pecam1* expression was significantly altered upon miR-128a knockdown in LNA-128 treated EBs when compared to LNA-Ctr at 1wk, 1.5wks and 2wks (Figure 20A-C, each two left panels) indicating that final EC as well as SMC lineage commitment might not be affected by miR-128a.

Additionally, no significant effect on the general CM markers *Tnnt2* and *Myh6* (Figure20A-C, each two middle panels) nor the atrial CM marker *Myl7* (Figure20A-C, each second right panel) was found upon miR-128 knockdown. However, the expression level of the ventricular CM marker *Myl2* started to rise at 1wk in LNA-128a treated EBs in comparison to LNA-Ctr (Figure 20A, right panel) becoming significantly upregulated at 1.5wks (p=0.05, Figure20B, right panel). A continued trend of upregulation was observed until 2wks of differentiation (Figure20C, right panel).

These results supported our second hypothesis that miR-128a might be involved in an earlier transdifferentiation of CPCs into cardiac lineages, in this case especially those expressing *Myl2.* Since we showed a significantly reduced abundance of our NkxCE-GFP CPC at the same timepoint (1.5wks) (Figure 14), it seemed likely that those *Myl2*-positive CMs derived from the NkxCE-GFP CPC pool.

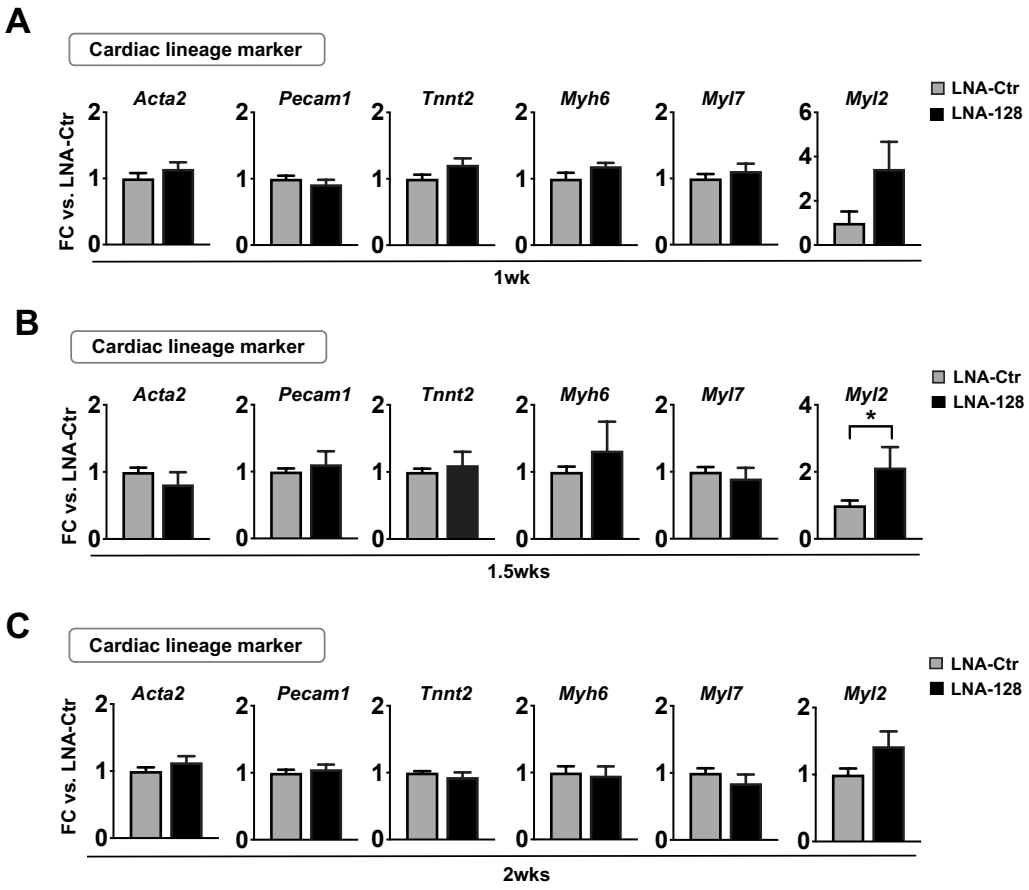

Figure 20 Cardiac lineage marker expression in LNA-treated NkxCE-GFP EBs at 1wk, 1.5wks and 2wks of *in vitro* differentiations. A. At 1wk none of the markers expressed by cardiac lineages such as SMCs (*Acta2,* left panel), ECs (*Pecam1,* second left panel), general CMs (*Tnnt2 and Myh6,* two middle panels) and atrial CMs (*Myl7,* second right panel) were significantly regulated after miR-128a knockdown (LNA-128), although a slight increase for the ventricular CM marker *Myl2* (right panel) was observed when compared to LNA-Ctr. **B.** At 1.5wks, the ventricular CM marker *Myl2* appeared to be significantly upregulated in the LNA-128 treated group when compared to LNA-Ctr (p=0.05, student's t-test). The expressions of all other cardiac lineage markers were unaffected in LNA-128 treated EBs (LNA-128) compared to LNA-Ctr **C.** At 2wks, cardiac lineages markers were not significantly differentially expressed in LNA-128 treated EBs, however, a slight increase was observed for the ventricular CM marker *Myl2* in comparison to LNA-Ctr. Data are represented as means ± SEM of (A, B) three independent experiments with each three independent samples measured as singles (all n=9,9) and (C) three independent experiments with each three to four independent samples measured as singles (all n=11,11). Statistical significance was assessed by two-tailed student's t-test as stated. * $p \leq 0.05$. Adapted from Figures S6A, B and C from Hoelscher *et al.* miR-128a Acts as a Regulator in Cardiac Development by Modulating Differentiation of Cardiac Progenitor Cell Populations. *Int. J. Mol. Sci.* 2020, *21*, 1158 (Hoelscher *et al*., 2020).

We next analyzed the beating frequency of beating foci ("beating rate") of early CMs by video microscopy at various timepoints of *in vitro* differentiations including 1, 1.5 and 2wks in addition to 1.75wks (day 12) and 2.25wks (day 16) (Figure 21) to evaluate if besides transcriptional changes also functional parameters were impacted by miR-128a knockdown.

Here we found a general reduction of the beating frequency of early CMs at all evaluated timepoints after miR-128a knockdown (LNA-128) which reached significance at 1wk (p=0.0027), 1.75wks (p=0.0028) and 2.25wks (p=0.0432) when compared to correspondent LNA-Ctr (Figure 21).

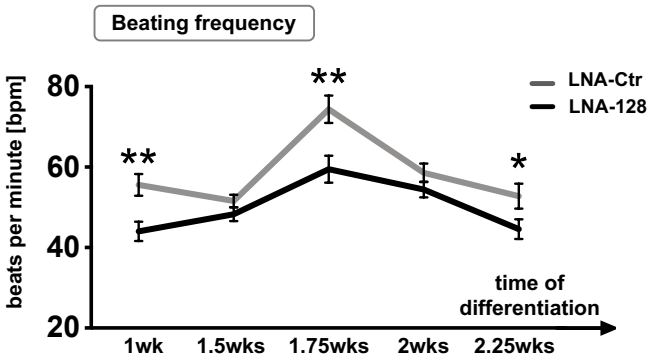

Figure 21 Beating frequency of early CMs during *in vitro* differentiations of NkxCE-GFP ESCs upon miR-128a knockdown. Beating frequency (beats per minute; bpm) of early CMs was downregulated from 1wk to 2.25wks upon miR-128a knockdown (LNA-128) when compared to LNA-Ctr with significances at 1wk (p=0.0027), 1.75wks (p=0.0028) and 2.25wks (p=0.0432) (all student's t-test). Data are represented as means ± SEM of two to six independent experiments with each six to eight independently recorded videos per condition evaluated by three independent observers (1wk n=23,24; 1.5wks (day 9/10 pooled) n=58,57; 1.75wks n=33,33; 2wks (day 13/14 pooled) n= 71,73; 2.25wks (day 15/16 pooled) n=32,30). Statistical significance was assessed by two-tailed student's t-test as stated. * $p \leq 0.05$, ** $p \leq 0.01$. Adapted from Figures 3J from Hoelscher *et al.* miR-128a Acts as a Regulator in Cardiac Development by Modulating Differentiation of Cardiac Progenitor Cell Populations. *Int. J. Mol. Sci.* 2020, *21*, 1158 (Hoelscher *et al*., 2020).

The heartbeat is normally controlled by fast-firing nodal cells at the sinoatrial node (SAN) which generally override electrical impulses of other cardiac cells with slower firing capacity (e.g. cells of the "working myocardium" including atrial and ventricular myocytes) (He *et al.*, 2003; van Weerd and Christoffels, 2016; Zhu *et al.*, 2010). Thus, we investigated if the observed slower beating frequency could be a result of a reduction of nodal-like cells caused by miR-128a knockdown. Therefore, we measured the expression of *Hcn4* and *Shox2,* markers that are known to be predominantly expressed by nodal-like CMs (Barbuti and Robinson, 2015).

However, neither *Hcn4* nor *Shox2* were significantly regulated in LNA-128 treated EBs after 1.5wks (Figure 22A) or 2wks (Figure 22B) when compared to LNA-Ctr (Figure 22). That made it rather unlikely that a reduction of nodal CMs was responsible for the reduction of the beating frequency upon miR-128a knockdown.

The slower beating frequency (Figure 21) might be rather due to the previously indicated increase of *Myl2*-positive CMs (Figure 20) as part of the ventricular "working myocardium".

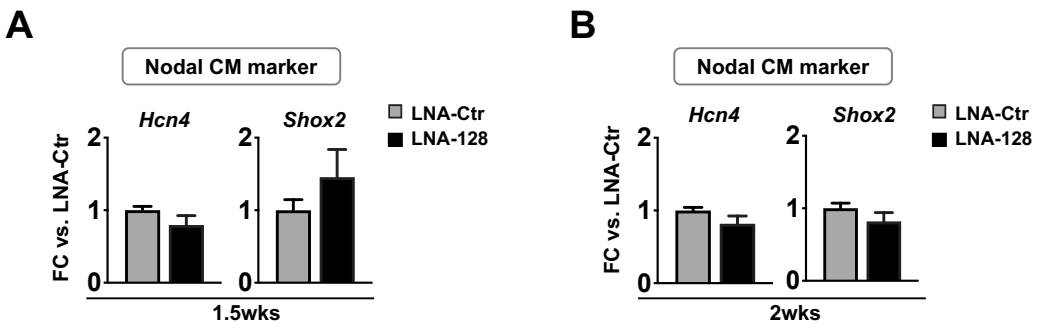

Figure 22 Nodal CM marker expression in LNA-treated NkxCE-GFP EBs at 1.5wks and 2wks of *in vitro* differentiations. **A-B**. Analysis of gene expression of nodal-like CM markers *Hcn4* and *Shox2* showed no significant alteration at (A) 1.5wks (left panel) and (B) 2wks (right panel) of *in vitro* differentiation in LNA-treated EBs (LNA-Ctr and LNA-128). Data are represented as means ± SEM of (A) three independent experiments with each three independent samples measured as singles (all n=9,9) and (B) three independent experiments with each three to four independent samples measured as singles (all n=11,11). Adapted from Figures S6E from Hoelscher *et al.* miR-128a Acts as a Regulator in Cardiac Development by Modulating Differentiation of Cardiac Progenitor Cell Populations. *Int. J. Mol. Sci.* 2020, *21*, 1158 (Hoelscher *et al*., 2020).

4.4 LNA-mediated knockdown of miR-128a during *in vitro* differentiations of iITG -iPSCs

We have shown that knockdown of miR-128a influenced early cardiogenesis, among others by modulating the expression of the CPC marker *Isl1* (Figure 16). Thus, we thought to confirm this result on a cellular level. Therefore, we generated the *Isl1*-reporter-iPSC line (iITG-iPSC line) by reprogramming transgenic Isl1Cre-R26^{mTmG} tail tip fibroblasts (TTFs) (Appendix Figure A5A) with the "Yamanaka factors" *Sox2, c-Myc, Oct4* and *Klf4* (Sommer *et al.*, 2009; Takahashi and Yamanaka, 2006).

The generated iITG-iPSCs are characterized by ubiquitous expression of membrane-tagged tdTomato in all cells (Figure 23A) and *Isl1*-expressing cells are labeled by membrane-tagged GFP upon Cre-mediated excision of tdTomato as previously described in detail (1.2) (Appendix Figure A11A) (Muzumdar *et al.*, 2007; Yang *et al.*, 2006). This enabled us to particularly track *Isl1*-positive CPCs upon miR-128a knockdown during *in vitro* differentiation.

4.4.1 Characterization of generated iITG-iPSCs

To select one appropriately reprogrammed iITG-iPSC clone for miR-128a knockdown experiments, we first characterized several promising picked iPSC clones (Appendix Figure A5B) on behalf of their pluripotency properties during expansion culture as well as during *in vitro* differentiation. Finally, we selected iITG-iPSC clone 15 for further investigation of miR-128a knockdown (Figure 23-26).

We first checked the induction of endogenous expression of the introduced “Yamanaka factors” in our iITG-iPSCs as well as the expression of the exogenously introduced construct (c-*Myc/Sox2* cassette from muSTEMCCA, Sommer *et al.*, 2009) by endpoint PCR analysis with different passages from p1 to p18 (exemplary passages are shown in Figure 23A, Figure 23B).

All passages of the generated iITG-iPSCs (lines 1-4 in Figure 23B) endogenously expressed *c-Myc, Oct3/4, Klf4* (upper three panels) as well as *Sox2* (lower left panel) at similar levels than NkxCE-GFP ESCs which were used as a positive control (line 5 in Figure 23B). In addition, we showed a declining expression of the exogenous c-*Myc/Sox2* cassette with increasing numbers of passages of the generated iITG-iPSCs (lines 1-4 in Figure 23B, lower right panel). The polycistronic muSTEMCCA construct was used as a positive control (line 6 in Figure 23B, lower right panel).

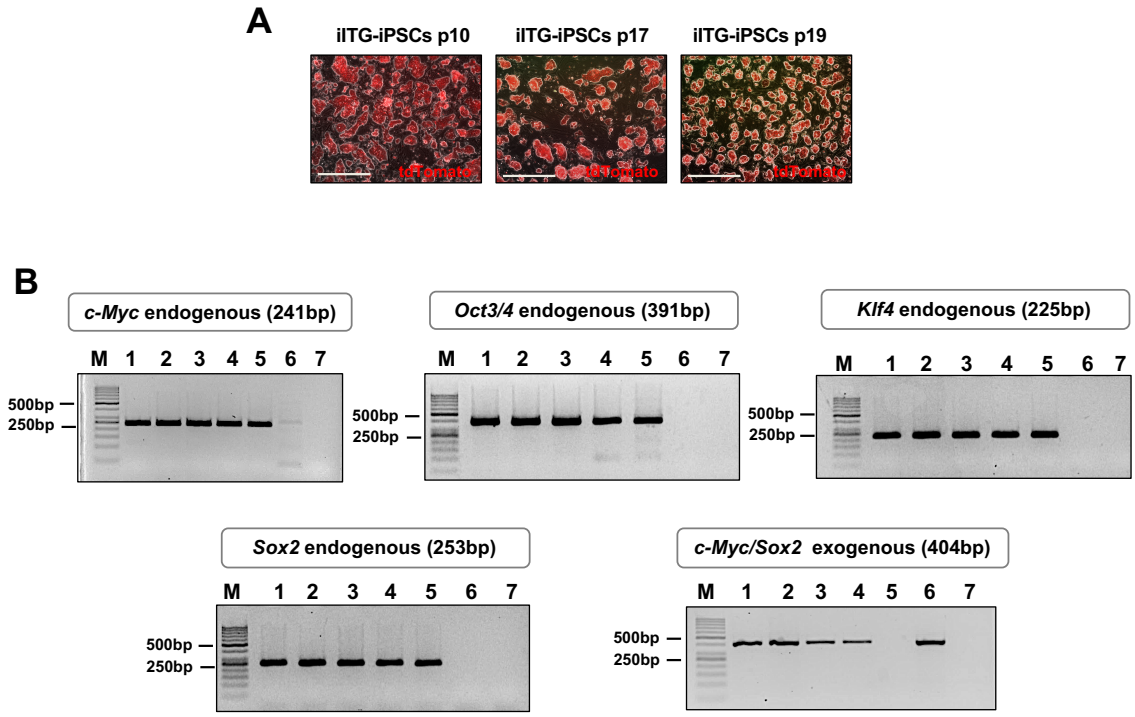

Figure 23 Induction of pluripotency in different passages of the generated iITG-iPSC clone 15. **A.** Exemplary microscopic images of the generated iITG-iPSC clone 15 at different passages during expansion culture (p, passage). Images are an overlay between phase contrast and fluorescent microscopic pictures. Scale bars are 500µm. **B**. Endpoint PCR results of endogenous expression of the “Yamanaka factors” at different passages (p1 to p18) of the iITG-iPSC clone 15. iITG-iPSCs expressed *c-Myc, Oct3/4, Klf4* (upper three panels) and *Sox2* (lower left panel) at a similar level than NkxCE-GFP ESCs used as positive control. Additionally, the generated iITG-iPSCs showed a decline of the exogenous *c-Myc/Sox2* expression cassette with increasing passages when compared to the positive control muSTEMCCA (Sommer *et al.*, 2009) which was used for reprogramming (lower right panel). PCR amplicon sizes are indicated above each panel. Caption indicates: (M) DNA marker 50bp; (1) iITG-iPSCs p1; (2) iITG-iPSCs p3; (3) iITG-iPSCs p13; (4) iITG-iPSCs p18; (5) NkxCE-GFP ESCs p28 (positive control for endogenous expression); (6) muSTEMCCA (positive control for exogenous expression); (7) H_2O (negative control). (B) Figure S7E from Hoelscher *et al.* miR-128a Acts as a Regulator in Cardiac Development by Modulating Differentiation of Cardiac Progenitor Cell Populations. *Int. J. Mol. Sci.* 2020, *21*, 1158 (Hoelscher *et al.*, 2020).

We further evaluated the expression of the pluripotency marker *Nanog* by qRT-PCR as and assessed Sox2 and Nanog protein expression by ICC (Figure 24). qRT-PCR results showed that the generated iITG-iPSCs expressed high levels of *Nanog* compared to TTFs ($p<0.0001$) (Figure 24A) confirming their pluripotency.

In addition, ICC revealed that iITG-iPSCs had similar protein levels of Sox2 and Nanog compared to the positive control NkxCE-GFP ESCs (Figure 24B, anti-Sox2, left two panels; anti-Nanog, two middle panels), again verifying the pluripotency of iITG-iPSCs.

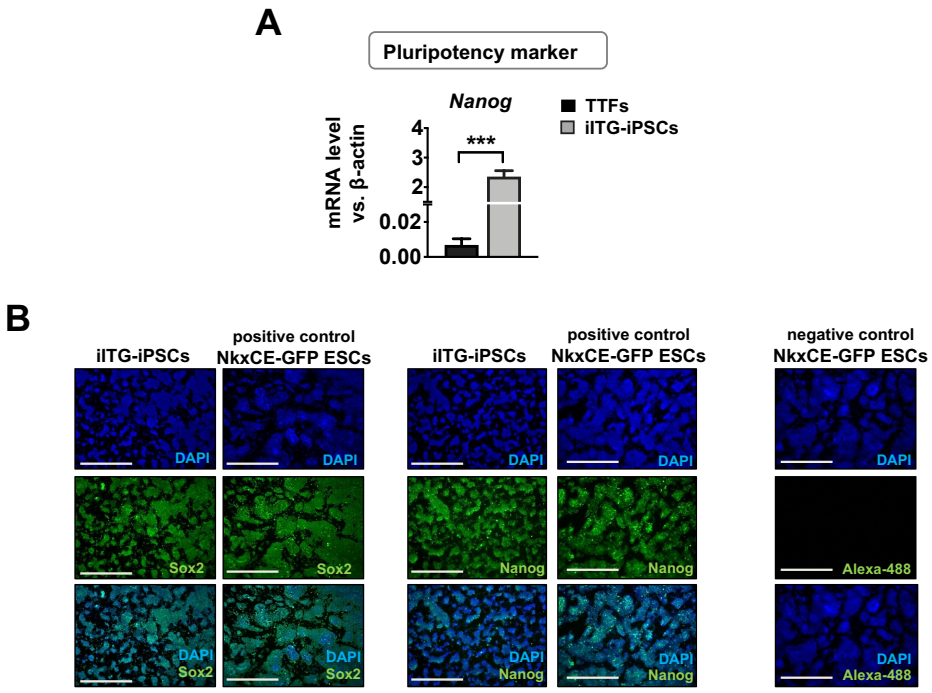

Figure 24 Pluripotency marker expressions on gene and protein level in iITG-iPSC clone 15. A. qRT-PCR results showed that the iITG-iPSCs expressed significant higher levels of *Nanog* compared to control TTFs ($p<0.0001$, student's t-test). **B.** ICC staining with anti-Sox2 (left two panel) as well as anti-Nanog (two middle panels) showed that iITG-iPSCs (p24) expressed both proteins at similar levels as the positive control NkxCE-GFP ESCs (p42). As a negative control NkxCE-GFP ESCs (p41) were stained with Alexa Fluor® 488 conjugated (Alexa-488) secondary antibodies only (right panel). Nuclear staining was conducted with DAPI. Images are shown as single fluorescent pictures as well as an overlay between all fluorescent microscopic pictures. Scale bars are 500µm. Data of (A) are represented as means ± SEM of six independently isolated TTF populations as well as three independent isolated iITG-iPSCs each measured as singles (n=6,3). Statistical significance was assessed by two-tailed student's t-test as stated. ***$p \leq 0.001$. Adapted from Figures S7F, G from Hoelscher *et al.* miR-128a Acts as a Regulator in Cardiac Development by Modulating Differentiation of Cardiac Progenitor Cell Populations. *Int. J. Mol. Sci.* 2020, *21*, 1158 (Hoelscher *et al*., 2020).

Furthermore, generated iITG-iPSCs were differentiated with the hanging drop method to ensure that they differentiate into all three germ layers. During that specification process, the expression of specific markers of all three germ layers are expected to rise at some point during *in vitro* differentiation, e.g. day 4 to day 6 for the cardiac TF *Nkx2.5* as an example of a mesodermal marker (see Figure 4).

This specification should be accompanied by declining expression of pluripotency markers such as *Nanog*.

Therefore, we measured *Nanog* as well as several germ layer markers by qRT-PCR at several timepoints from 0.75wks until day 19 (2.75wks) during iITG-iPSC differentiation to examine their expression kinetics (Figure 25). The expression of *Nanog* decreased throughout iITG-iPSC differentiation (Figure 25A), whereas the expressions of germ layer markers generally increased including *Nestin* and *Ncam1* as ectodermal markers (Figure 25B) *Afp and Sox17* as endodermal markers (Figure 25C) as well as previously mentioned *Isl1 and Nkx2.5* as mesodermal markers (Figure 25D).

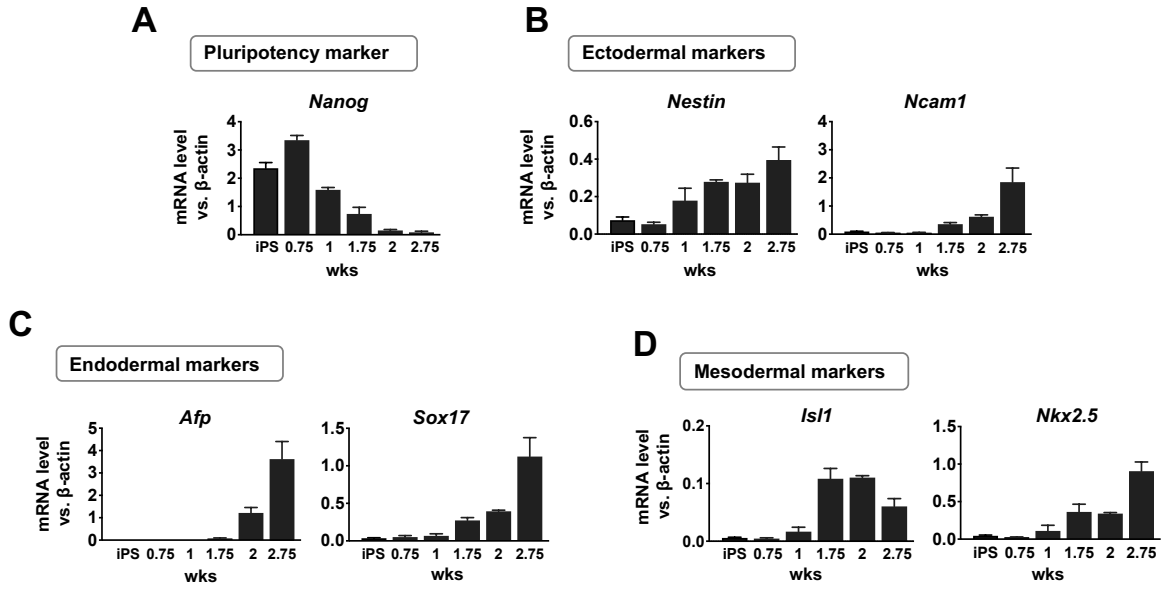

Figure 25 Kinetics of pluripotency and germ layer markers during *in vitro* differentiations of iITG-iPSC clone 15. **A.** The expression of *Nanog* decreased throughout *in vitro* differentiation of generated iITG-iPSCs. **B-D.** The expression of all three germ layers markers increased during *in vitro* differentiation of iITG-iPSCs including (B) *Nestin and Ncam1 as* ectodermal markers (C) *Afp and Sox17* as endodermal markers as well as (D) *Isl1 and Nkx2.5* as mesodermal makers. Data are represented as means ± SEM of one experiment with each three to four independent samples measured as singles (n=3-4). Adapted from Figure S8B from Hoelscher *et al.* miR-128a Acts as a Regulator in Cardiac Development by Modulating Differentiation of Cardiac Progenitor Cell Populations. *Int. J. Mol. Sci.* 2020, *21*, 1158 (Hoelscher *et al*., 2020).

Even though the generated *Isl1*-reporter-iPSC line showed all characteristics of fully reprogrammed iPSCs, we noted that the expression of the three germ layer markers (Figure 25B-D) started to rise with some delay, beginning between 1wk to 1.75wk, when compared to established NkxCE-GFP ESCs as previously described (Figure 4).

In fact, direct comparison of some markers in both ESCs and iPSCs at 1wk and 2wks *of in vitro* differentiation showed that the onset of expression of *Ncam1* (ectoderm, (Figure 26A)), *Sox17* (endoderm, (Figure 26B)) and *Nkx2.5* (mesoderm, (Figure 26C)) had a deferral of about one week in the iITG-iPSCs compared to NkxCE-GFP ESCs.

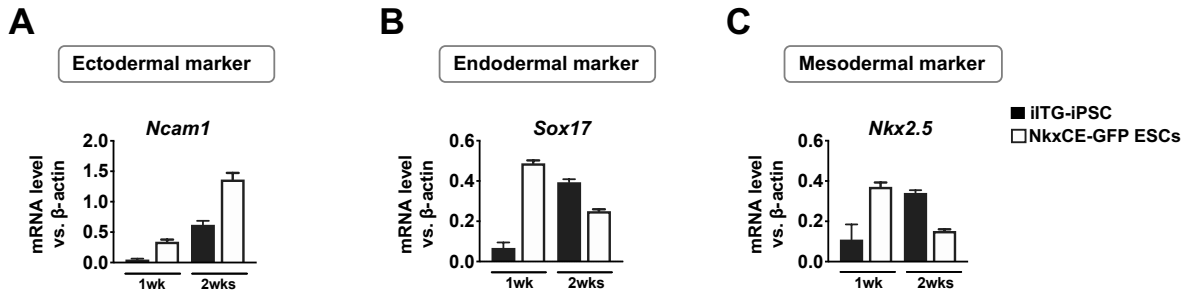

Figure 26 Comparison of kinetics of selected germ layer markers during *in vitro* differentiations of iITG-iPSCs and NkxCE-GFP ESCs. A-C. Kinetics of selected germ layer markers measured at 1wk and 2wks of *in vitro* differentiation of iITG-iPSCs and NkxCE-GFP ESCs showed that the onsets of expressions of (A) ectodermal marker *Ncam1*, (B) endodermal marker *Sox17* and (C) mesodermal marker *Nkx2.5* were approximately one week delayed in the generated iITG-iPSCs compared to established NkxCE-GFP ESCs. Data are represented as means ± SEM of one experiment with each three independent samples measured as singles (n=3). Adapted from Figure S8C from Hoelscher *et al.* miR-128a Acts as a Regulator in Cardiac Development by Modulating Differentiation of Cardiac Progenitor Cell Populations. *Int. J. Mol. Sci.* 2020, *21*, 1158 (Hoelscher *et al*., 2020).

GFP-positive *Isl1*-CPCs also occurred temporally delayed (around differentiation week 1 to 1.5) in comparison to NkxCE-GFP CPCs (representative fluorescence images can be found in Appendix Figure A10A (NkxCE-GFP ESC) and Appendix Figure A11A (iITG-iPSC). Beating clusters were observed shortly after the occurrence of *Isl1*-CPCs around 1.75wks of *in vitro* differentiation (Hoelscher *et al.*, 2020) which again reflected differentiation delay. At later stages of *in vitro* differentiation (2wks - 3wks (day 22/23)), iITG-iPSCs showed normal but still slightly delayed timing when compared to staged-matched NkxCE-GFP ESCs (Appendix Figure A10A &Appendix Figure A11A).

Despite several iITG-iPSC clones were analyzed, all of them showed a similar delayed *in vitro* differentiation which might be directly linked to the used Isl1Cre/R26$^{mT/mG}$ transgene in which Cre is directly knocked in into the endogenous *Isl1* locus, replacing the *Isl1* ATG start codon possibly leading to decreased expression of *Isl1* in iITG-iPSCs (Muzumdar *et al.*, 2007; Yang *et al.*, 2006) (Figure 2).

Conclusively, characterization results indicated that iITG-iPSCs were overall successfully reprogrammed. Thus, we subsequently used iITG-iPSCs for miR-128a knockdown experiments according to the experimental outline for NkxCE-GFP ESCs. Only, the timepoints for LNA transfections and final analysis were adjusted under consideration of the delayed differentiation capacity.

4.4.2 Analysis of miR-128a knockdown effects during *in vitro* differentiations of iITG-iPSCs

For miR-128a knockdown, iITG-iPSCs were transfected twice with LNA-probes (LNA-128 and LNA-Ctr) in accordance with the experimental outline of NkxCE-GFP ESCs. Due to the delay of iITG-iPSCs in differentiation capacity (4.4.1), we conducted the first transfection at 0.75wks followed by a second at 2wks of spontaneous *in vitro* differentiation. In addition, the timepoints of analysis were adjusted with a start at 1wk and a designated endpoint of 3wks.

By qRT-PCR evaluation, we confirmed that LNA-128 transfection led to a stable and sufficient knockdown of miR-128a during *in vitro* differentiation at all evaluated timepoints by more than 80% in comparison to LNA-Ctr transfected iITG-iPSCs (1wk, p=0.0289; 2wks, p=0.0037; 2.25wks, p=0.0002; 3wks, p=0.0065) (Figure 27).

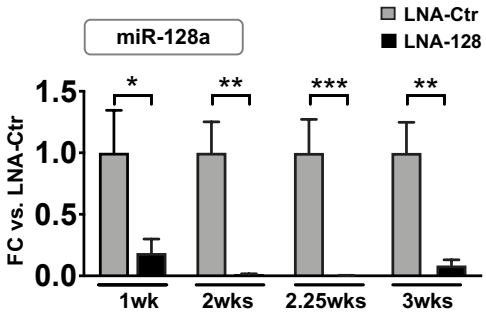

Figure 27 Knockdown efficiency of miR-128a during *in vitro* differentiations of iITG-iPSCs. The expression of miR-128a was significantly downregulated by more than 80% during iITG-iPSCs *in vitro* differentiations upon LNA-128 transfection at 1wk (p=0.0289, Mann-Whitney), 2wks (p=0.0037, Mann-Whitney), 2.25wks (p=0.0002, Mann-Whitney) and 3wks (p=0.0065, student's t-test) when compared to the correspondent LNA-Ctr group. Data are represented as means ± SEM of two independent experiments (one experiment with 2 different cell passages) with each three independent samples measured as singles (all timepoints n=8,7). Statistical significances were assessed by Mann-Whitney Rank Sum test or two-tailed student's t-test as stated. * $p \leq 0.05$, ** $p \leq 0.01$, *** $p \leq 0.001$. Adapted from Figure 4B from Hoelscher *et al.* miR-128a Acts as a Regulator in Cardiac Development by Modulating Differentiation of Cardiac Progenitor Cell Populations. *Int. J. Mol. Sci.* 2020, *21*, 1158 (Hoelscher *et al.*, 2020).

Both transfected iITG-iPSC EBs (LNA-Ctr and LNA-128) showed regular *in vitro* differentiation capacity (as described above in 4.4.1) with a first appearance of *Isl1*-positive CPCs around week 1 to 1.5 (Appendix Figures A11B-C) which was accompanied by spontaneous beating around 1.75wks (Hoelscher *et al.*, 2020).

To determine the frequency of GFP-positive *Isl1*-CPCs during *in vitro* differentiation, we conducted flow cytometry after 2, 2.25 and 3wks.

First, our results showed a steady increase (accumulation) of GFP-positive cells in both LNA-transfected iITG-iPSCs throughout differentiation from 2wks to 3wks (Figure 28A, B, representative FACS blots Appendix Figures A13B- C) since the excison of tdTomato in front of GFP by the Cre-recombinase led to a permanent labeling of *Isl1*-positive CPCs and their progeny (1.2).

Interestingly, the percentage of *Isl1*-positive CPCs was significantly elevated in LNA-128 transfected iITG-iPSCs when compared to LNA-Ctr after 2wks of *in vitro* differentiation (p=0.024) corresponding to early cardiac development in this iPSC line (Figure 28A).

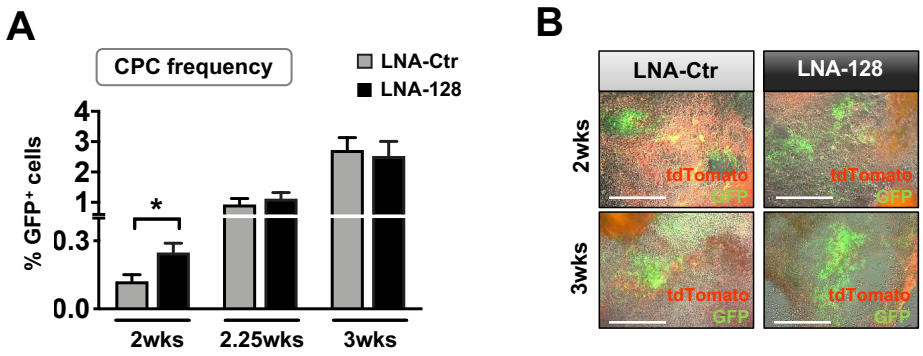

Figure 28 Frequency of GFP-positive, *Isl1*-CPCs after miR-128a knockdown during *in vitro* differentiations. **A.** Flow cytometry showed that the percentage of GFP-positive, *Isl1*-expressing CPCs was significantly enhanced in LNA-128 transfected iITG-iPSCs after 2wks of *in vitro* differentiation compared to correspondent iITG-iPSCs treated with LNA-Ctr (p=0.024, student's t-test). In addition, a general accumulation of GFP-positive, *Isl1*-CPCs was observed for both groups from 2wks to 3wks during *in vitro* differentiation. **B.** GFP-positive, *Isl1*-CPCs as well as cells ubiquitous expressing membrane-tagged tdTomato observed after 2wks (upper panel) and 3wks (lower panel) of *in vitro* differentiation of iITG-iPSCs after transfection with either LNA-Ctr or LNA-128. Images are an overlay between phase contrast and fluorescent microscopic pictures. Scale bars are 500µm. Data are represented as means ± SEM of one to two independent experiments (one experiment with 2 different cell passages) with each three independent samples measured as singles (2wks n=9,9; 2.25wks n=9,9; 3wks n=6,6). Statistical significance was assessed by two-tailed student's t-test as stated. * $p \leq 0.05$. Adapted from Figures 4C, D from Hoelscher *et al.* miR-128a Acts as a Regulator in Cardiac Development by Modulating Differentiation of Cardiac Progenitor Cell Populations. *Int. J. Mol. Sci.* 2020, *21*, 1158 (Hoelscher *et al*., 2020).

This strengthened our hypothesis that miR-128a might be involved in the promotion of *Isl1*-expressing CPCs at early cardiogenesis and confirmed previously shown expression results (Figure 16) on a cellular level (Figure 28A).

Additionally, we found that *Isl1* gene expression had a tendency of upregulation throughout *in vitro* differentiation (1wk, 2wks and 3wks) in LNA-128 transfected iITG-iPSCs in comparison to the LNA-Ctr treated control group, unfortunately without reaching significance (Figure 29).

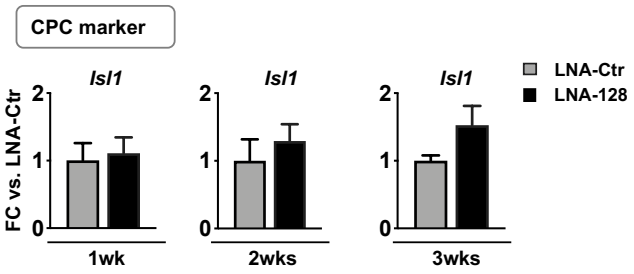

Figure 29 *Isl1* expression in LNA-treated iITG-iPSCs EBs at 1wk, 2wks and 3wks of *in vitro* differentiations. A tendency of increased *Isl1* expression is shown at 1wk (left panel), 2wks (middle panel) and 3wks of *in vitro* differentiation of LNA-128 treated iITG-iPSCs in comparison to the control group (LNA-Ctr). Data are represented as means ± SEM of one experiment with 2 different cell passages with each three independent samples measured as singles (all n=6,6). Adapted from Figure 4E from Hoelscher *et al.* miR-128a Acts as a Regulator in Cardiac Development by Modulating Differentiation of Cardiac Progenitor Cell Populations. *Int. J. Mol. Sci.* 2020, *21*, 1158 (Hoelscher *et al*., 2020)

Next, we evaluated beating frequencies of early CMs in the *Isl1*-reporter iPSC line upon miR-128 knockdown throughout *in vitro* differentiation (between 2 to 3wks) (Figure 30).

We found a constant decelerated beating capacity in LNA-128 transfected iITG-iPSC-derived CMs at all evaluated timepoints compared to the LNA-Ctr getting significant at 2.75wks (p=0.012) and 3wks (p=0.015) (Figure 30). This was in accordance with the data from NkxCE-GFP ESCs (Figure 21).

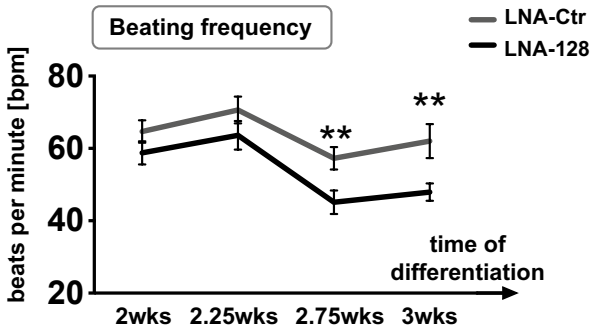

Figure 30 Beating frequency of early CMs during *in vitro* differentiations of iITG-iPSCs upon miR-128a knockdown. Beating frequency (beats per minute, bpm) of early CMs was constantly downregulated from 2wks to 3wks upon miR-128a knockdown (LNA-128) when compared to LNA-Ctr with significances at 2.75wks (p=0.012, student's t-test) and 3wks (p=0.015, Mann-Whitney). Data are represented as means ± SEM of one to two independent experiments (one experiment with 2 different cell passages) with each three to nine independently recorded videos per condition evaluated by three independent observers (2wk n=21,24; 2.25wks n=22,24; 2.75wks n=16,16; 3wks n=14,14). Statistical significance was assessed by Mann-Whitney Rank Sum test or two-tailed student's t-test as stated. ** p ≤ 0.01. Adapted from Figure 4F from Hoelscher *et al.* miR-128a Acts as a Regulator in Cardiac Development by Modulating Differentiation of Cardiac Progenitor Cell Populations. *Int. J. Mol. Sci.* 2020, *21*, 1158 (Hoelscher *et al*., 2020).

4.5 Overexpression of miR-128a during *in vitro* differentiations of NkxCE-GFP ESCs (OE-ESCs)

To gain a more complete picture of miR-128a function during early cardiogenesis, we next investigated the effect of miR-128a overexpression (OE) during *in vitro* differentiation of murine ESCs.

Therefore, we generated stable miR-OE lines that were generated by transduction of the transgenic NkxCE-GFP CPC reporter ESC line (1.2) with lentiviruses either overexpressing miR-128a (OE-128) or a non-targeting miR-Ctr (OE-Ctr). The activation of the integrated constructs was controlled by doxycycline (tet-on system) which should induce the expression of miR-Ctr or miR-128a accompanied by the expression of turbo red fluorescent protein (tRFP) that is located in front of miR-128a or miR-Ctr, respectively (Appendix Figures A6A-B).

4.5.1 Verification of generated OE-ESCs

Before usage for experiments, we first ensured that generated OE-ESC lines (OE-Ctr, OE-128) maintained their pluripotency after lentiviral transduction and verified a proper induction of the integrated tRFP (further also referred as only RFP) and miRs.

Therefore, several of the RFP-positive picked OE-Ctr and OE-128 ESC clones (Appendix Figure A6B) were analyzed during expansion culture and throughout *in vitro* differentiation either in addition or absence of doxycycline. Finally, we selected OE-Ctr clone 4 as well as two OE-128 clones (21 and 30) (Appendix Figure A6B, middle three panels; results are shown below in Figure 31-34) for final OE experiments.

For analysis of pluripotency, we first conducted ICC of Sox2 and Nanog in all OE-ESC clones cultured without doxycycline (Figure 31).

Results showed, that the OE-ESC clones exhibited similar protein levels of both pluripotency marker proteins as NkxCE-GFP ESCs which were used as a positive control (Figure 31) indicating that all the selected OE-ESCs maintained their pluripotency after lentiviral transduction.

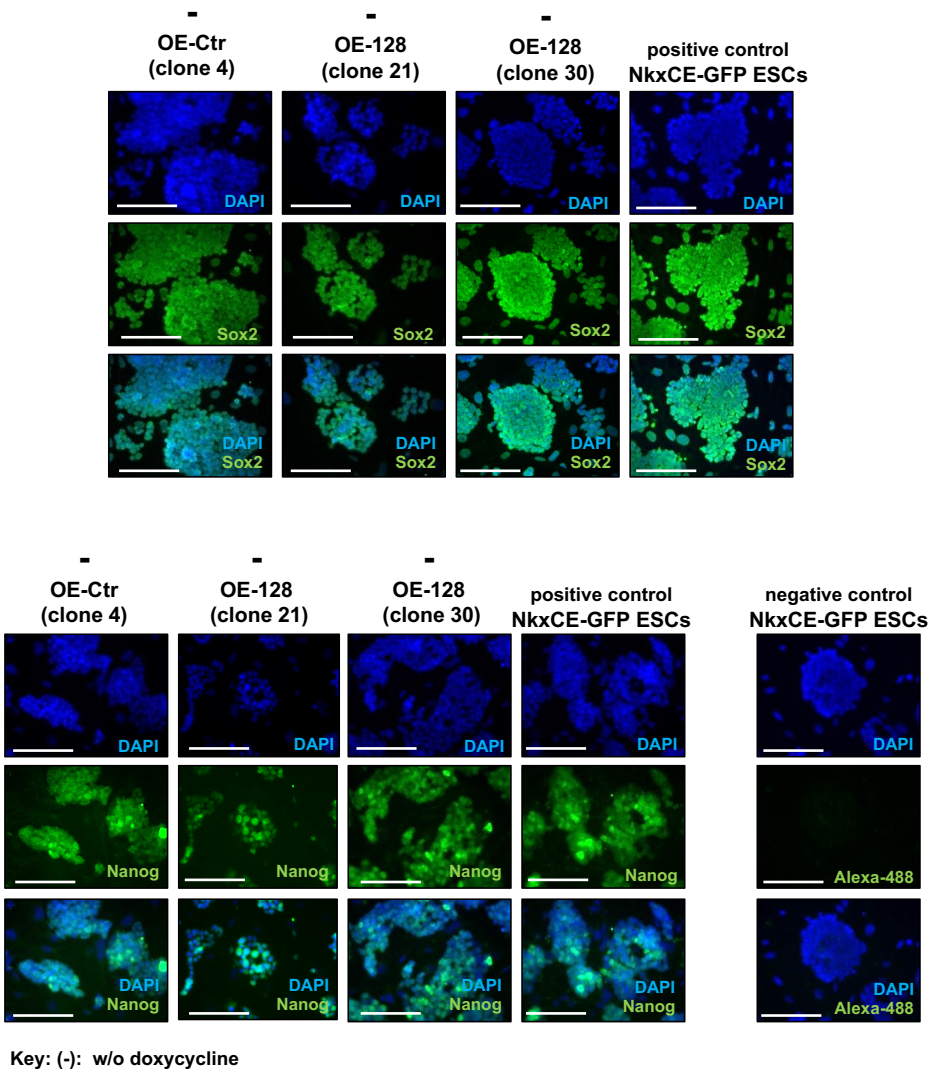

Figure 31 Pluripotency marker expressions detected by ICC in the generated OE-ESC lines. ICC staining with antibodies against Sox2 (upper panel) and against Nanog (lower panel) showed that OE-Ctr ESCs (clone 4, both ICCs p34), OE-128 ESCs clone 21 (both ICCs p34) and OE-128 ESCs clone 30 (anti-Sox2 ICC p35; anti-Nanog ICC p34) expressed pluripotency marker proteins at similar levels as the positive control NkxCE-GFP ESCs (both ICC p42). As a negative control NkxCE-GFP ESCs (p41) were stained with Alexa Fluor® 488 (Alexa-488) conjugated secondary antibodies only (lower right panel). Nuclear staining was conducted with DAPI. Images are shown as single fluorescent pictures as well as an overlay between all fluorescent microscopic pictures. Scale bars are 100µm. Adapted from Figure S9D from Hoelscher *et al.* miR-128a Acts as a Regulator in Cardiac Development by Modulating Differentiation of Cardiac Progenitor Cell Populations. *Int. J. Mol. Sci.* 2020, *21*, 1158 (Hoelscher *et al*., 2020).

Next, we investigated the functionality of the tet-on system and tested efficient induction of tRFP and miR expression upon doxycycline addition.

Therefore, OE-ESC lines were cultured either in the presence or absence of doxycycline for several days and were then analyzed by flow cytometry to determine the percentages of RFP-positive cells or by qRT-PCR analysis to quantify miR-128a expression (Figure 32A-C).

Microscopic assessment of fluorescence of OE-ESC lines showed an increase of RFP-positive cells upon the addition of doxycycline (Figure 32A) suggesting a functional tet-on system. This was further verified by flow cytometry results where the addition of doxycycline led to a significant increase of the amount of RFP-expressing cells in OE-Ctr ESCs ($p<0.001$) as well as the OE-128 ESCs ($p<0.001$) when compared to their correspondent counterparts cultured without doxycycline (Figure 32B, Appendix Figure A8A-B).

As expected, evaluation of miR-128a expression by qRT-PCR revealed no alteration upon doxycycline addition in the OE-Ctr ESCs (Figure 32C).

However, interestingly, miR-128a expression levels were already significantly elevated in OE-128 ESCs cultured without doxycycline when compared to OE-Ctr ESCs ($p=0.049$) (Figure 32C). Several tested OE-128 ESC clones showed a similar background expression of miR-128a.

Expression of miR-128a in the absence of doxycycline could be attributed to a leakiness of tet-on systems which has been described extensively before and is most likely due to basal regulation of the TRE3G-promoter (Garrick *et al.*, 1998; Meyer-Ficca *et al.*, 2004; Mizuguchi and Hayakawa, 2001).

In addition, miR-128a expression was unfortunately not significantly enhanced upon doxycycline addition in the OE-128 ESCs compared to OE-128 ESCs without doxycycline (Figure 32C), even if high doxycycline concentrations of 2 µg/ml were used.

Given the significantly enhanced number of RFP-positive cells in OE-128 ESCs with doxycycline compared to OE-128 ESCs without doxycycline (Figure 32B), it seemed that not all detected RFP-positive cells expressed miR-128a at a sufficient level upon doxycycline induction.

The reason for that might be the design of the lentiviral construct, where the tRFP gene is located in front of the miR-128a which are both controlled by the same TRE3G promoter (Appendix Figure A6A). Especially in constructs where two genes share one promoter, reduced expression of the second gene (here miR-128a) has been also commonly observed (Kim *et al.*, 2004).

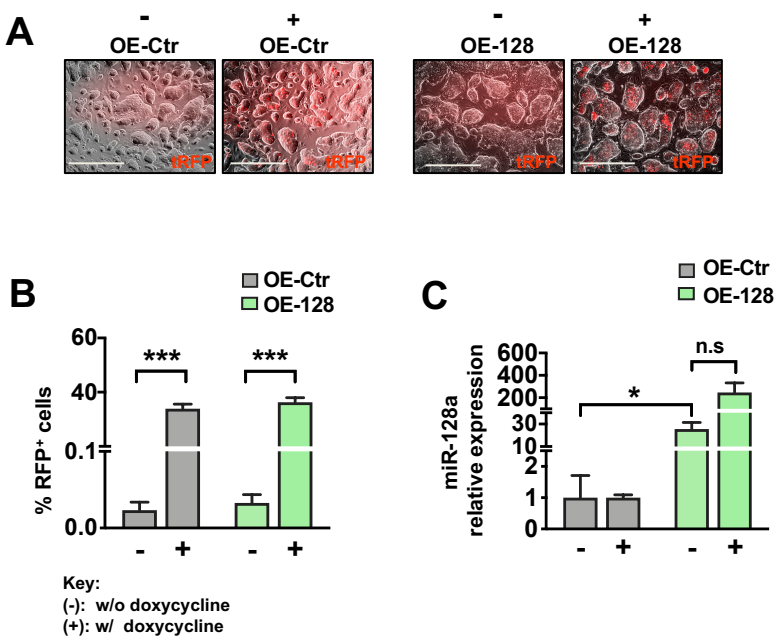

Figure 32 Frequency of RFP-positive cells and miR-128a expression in generated OE-ESC lines. A. Fluorescence images showed induction of RFP-positive cells in OE-Ctr ESCs (left panels) as well as OE-128 ESCs (right panels) upon addition of doxycycline compared to correspondent OE-ESCs without doxycycline. Images are an overlay between phase contrast and fluorescent microscopic pictures. Scale bars are 500µm. **B**. Flow cytometry showed that the percentage of RFP-positive cells was significantly enhanced upon doxycycline addition in OE-Ctr ESCs ($p<0.001$, Mann-Whitney) and OE-128 ESCs ($p<0.001$, Mann-Whitney) when compared to their counterpart OE-ESCs without doxycycline. **C.** Expression of miR-128a evaluated by qRT-PCR showed significantly elevated background expression of miR-128a in OE-128 ESCs without doxycycline ($p=0.049$, student's t-test) in comparison to OE-Ctr ESCs. No significant elevated induction of miR-128a expression could be achieved in OE-128 ESCs upon addition of doxycycline. Data are represented as means ± SEM of (B) two independent experiments (one with 2 different cell passages) with each two to three independent samples measured as singles (OE-Ctr (clone 4) n=8,8; OE-128 (clones 21/30 pooled) n=10,10) and (C) one experiment with each two to three independent samples measured as singles (OE-Ctr (clone 4) n=2,2; OE-128 (clones 21/30 pooled) n=3,3). Statistical significances were assessed by Mann-Whitney Rank Sum test or two-tailed student's t-test as stated. * $p \leq 0.05$, *** $p \leq 0.001$. (B) and (C) adapted from Figures S9E, F from Hoelscher *et al.* miR-128a Acts as a Regulator in Cardiac Development by Modulating Differentiation of Cardiac Progenitor Cell Populations. *Int. J. Mol. Sci.* 2020, *21*, 1158 (Hoelscher *et al.*, 2020).

Additionally, the use of tetracyclines (in our case doxycycline), has been controversially discussed due to potential impacts on cell metabolism, proliferation and even gene expression (Ahler et al., 2013; Moullan et al., 2015).

Hence, we first evaluated if doxycycline had an impact on the proliferation rate of our generated OE-ESCs.

Therefore, we performed MTT assays of OE-ESC lines cultured with or without doxycycline for three days. Neither OE-Ctr ESCs nor OE-128 ESCs showed changes in proliferation upon doxycycline treatment for three days (Figure 33).

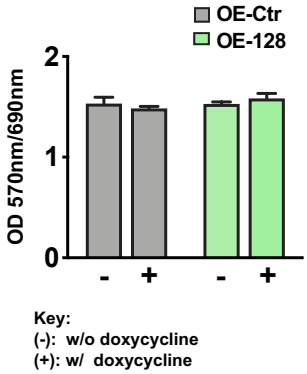

Figure 33 Influence of doxycycline on proliferation rate of generated OE-ESC lines. MTT assays of OE-Ctr ESCs as well as OE-128 ESCs cultured with or without doxycycline for three days. No significant impact on proliferation capacity was observed in OE-ESCs cultured with doxycycline compared to correspondent OE-ESCs cultured without doxycycline. Data are represented as means ± SEM of one experiment with each one sample measured in six wells (OE-Ctr (clone 4), OE-128 (clone 21), all n=6)). Adapted from Figure S9G from Hoelscher *et al.* miR-128a Acts as a Regulator in Cardiac Development by Modulating Differentiation of Cardiac Progenitor Cell Populations. *Int. J. Mol. Sci.* 2020, *21*, 1158 (Hoelscher *et al*., 2020).

We next sought to investigate if doxycycline altered the *in vitro* differentiation behavior of generated OE-ESC lines.

Therefore, both OE-ESCs were differentiated by the standard hanging drop method with or without doxycycline up to 2wks. First, it was noted that both OE-ESC lines seemed to differentiate, at least visually, in a regular manner independent of doxycycline addition. All OE-ESC lines developed GFP-positive CPCs around day 6 (0.85wks) to 7 (1wk) (Appendix Figures A14) and first beating clusters around day 7 to 8 (Hoelscher *et al.*, 2020).

However, compared to the originating NkxCE-GFP ESCs (typically develop CPCs and beating clusters as early as day 6 (0.85wks), Appendix Figure A10), the differentiation of the OE-ESCs (with and without doxycycline) happened to be slightly delayed by about one to two days.

Although no apparent visual impact of doxycycline was observed during differentiation, we further verified the amount of NkxCE-GFP CPCs by flow cytometry and analyzed gene expressions of selected CPC marker by qRT-PCR (Figure 34). To distinguish doxycycline-related effects miR-128a overexpression effects, only OE-Ctr ESCs were included into analysis.

Unfortunately, doxycycline significantly impacted *in vitro* differentiation of OE-Ctr ESCs, e.g. by raising the percentage of NkxCE-GFP CPCs after 2wks ($p=0.0018$, Figure 34A). In addition, doxycycline treatment led to significant downregulation of *Isl1* gene expression ($p=0.0251$) after 1.5wks as well as a significant upregulation of *Nkx2.5* ($p=0.0172$) and *Mef2c* ($p=0.0043$) after 2wks of OE-Ctr ESCs *in vitro* differentiation (Figure 34B). Merely the beating frequency of early CMs during *in vitro* differentiation was not altered upon doxycycline addition in OE-Ctr ESCs (Figure 34C).

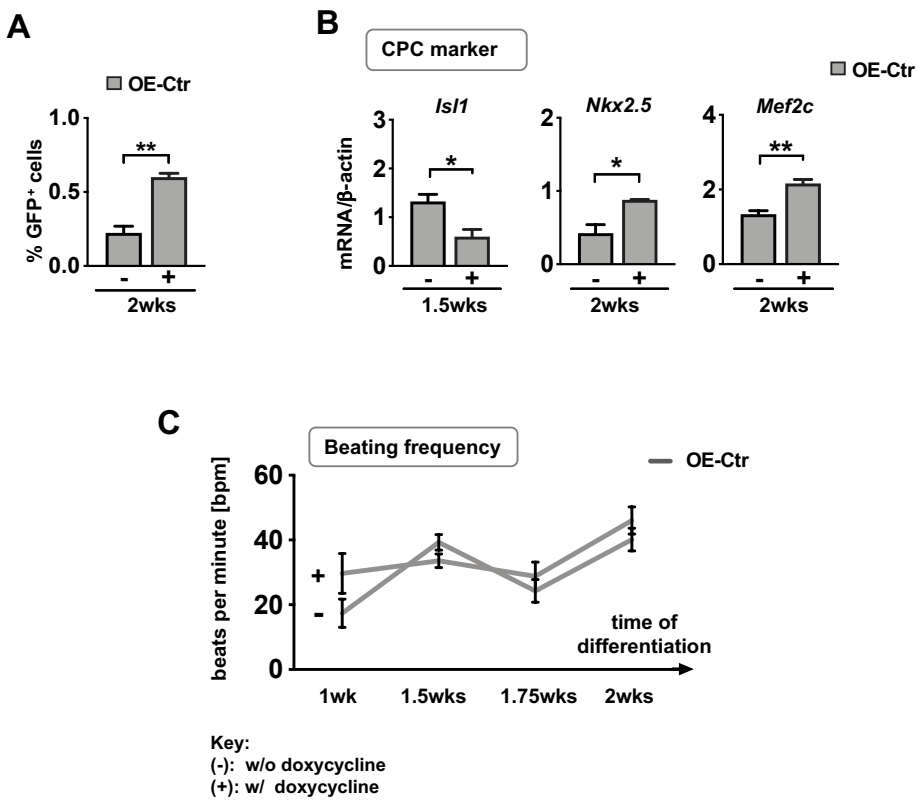

Figure 34 Influence of doxycycline during *in vitro* differentiations of OE-Ctr ESCs. A. Flow cytometry revealed that doxycycline significantly enhanced the abundance of NkxCE-GFP CPCs after 2wks of OE-Ctr ESC *in vitro* differentiation (p=0.0018, student's t-test). **B.** Gene expression of several early CPC markers was significantly altered in OE-Ctr ESCs differentiated with doxycycline including a downregulation of *Isl1* at 1.5wks (p=0.0251, student's t-test) as well as a upregulation of *Nkx2.5* (p=0.0172, student's t-test) and *Mef2c* p=0.0043, student's t-test) at 2wks. **C**. The beating frequency (beats per minute, bpm) of early CMs was not altered upon doxycycline addition in differentiating OE-Ctr ESCs between 1wk to 2wks. Data are represented as means ± SEM of (A, B) one experiment with each three independent samples measured as singles (OE-Ctr (clone 4) without and with doxycycline, all n=3,3)) and (C) one experiment with each three to nine independently recorded videos per condition evaluated by three independent observers (OE-Ctr (clone4) without and with doxycycline; 1wk n=5,3; 1.5wks (day 9/11 pooled) n=21,21; 1.75wks n=8,8; 2wks n=8,9). Statistical significances were assessed by two-tailed student's t-test as stated. * $p \leq 0.05$, ** $p \leq 0.01$. Adapted from Figures S10B, C from Hoelscher *et al.* miR-128a Acts as a Regulator in Cardiac Development by Modulating Differentiation of Cardiac Progenitor Cell Populations. *Int. J. Mol. Sci.* 2020, *21*, 1158 (Hoelscher *et al*., 2020).

Due to the leakiness of the promoter (tet-on system), the inefficient miR-128a induction upon doxycycline treatment (Figure 32), as well as the profound influences of doxycycline on *in vitro* differentiation (Figure 34), we finally decided to perform the following OE experiments without the addition of doxycycline to ensure rigorous result assessment.

4.5.2 Analysis of miR-128a overexpression effects during *in vitro* differentiations of OE-ESCs

For OE-experiments, generated OE-ESC lines (OE-Ctr and OE-128) were *in vitro* differentiated without the addition of doxycycline, due to above described reasons. Differentiations were conducted for 2wks and analysis of miR-128a effects was performed in accordance with knockdown experiments.

As previously demonstrated during verification of OE-ESC clones (Figure 32C), we also found elevated miR-128a expression throughout OE-128 ESC *in vitro* differentiation without doxycycline compared to OE-Ctr ESCs (Figure 35). Although robust overexpression of miR-128a was demonstrated at 1wk (p=0.0016) (Figure 35), sufficient overexpression was not maintained at later stages (1.5 and 2wks) in OE-128 ESCs compared to OE-Ctr ESCs. This might be caused by promoter methylation that has been described to occur during differentiations (Herbst *et al.*, 2012; Schlesinger and Goff, 2013) or other regulatory mechanisms impacting miR-128a expression itself.

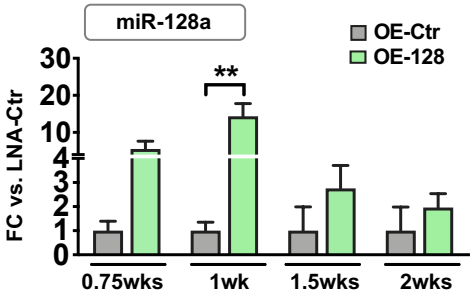

Figure 35 Overexpression of miR-128a during *in vitro* differentiations of OE-ESCs. Elevated overexpression of miR-128a was found throughout *in* vitro differentiation of OE-128 ESCs in comparison to OE-Ctr ESCs with significant upregulation at 1wk (p=0.0016, Mann-Whitney). Data are represented as means ± SEM of one to two independent experiments with each three independent samples measured as singles (OE-Ctr (clone4); OE-128 (clone 21/30 pooled); 0.75wks n=6,9; 1wk n=5,8; 1.5wks n=2,5; 2wks n=2,4). Statistical significance was assessed by Mann-Whitney Rank Sum test as stated. ** $p \leq 0.01$. Adapted from Figure 5B from Hoelscher *et al.* miR-128a Acts as a Regulator in Cardiac Development by Modulating Differentiation of Cardiac Progenitor Cell Populations. *Int. J. Mol. Sci.* 2020, *21*, 1158 (Hoelscher *et al*., 2020).

Next, we analyzed the frequency of NkxCE-GFP CPCs after 1, 1.5 as well as 2wks by flow cytometry (Figure 35A). As afore-mentioned, both OE-ESC lines (OE-Ctr, OE-128) showed normal differentiation behavior, however, with a slight delay of about one to two days in comparison to the originating NkxCE-GFP ESCs (Appendix Figures A10 &A14). This had to be considered for interpretation of results in comparison to miR-128a knockdown experiments.

After 1wk of *in vitro* differentiation the abundance of NkxCE-GFP CPCs appeared to be decreased by nearly 50% in OE-128 ESCs in comparison to OE-Ctr ESCs (Figure 36A).

This complemented our first results from miR-128a knockdown experiments where we found profound impact of miR-128a on the regulation of CPC marker gene expression (also indicating a possible increase of NkxCE-GFP CPCs) at the onset of cardiogenesis at 0.75wks (Figure16, Figure 19).

Interestingly, after 1.5wks of *in vitro* differentiation, twice as much NkxCE-GFP CPCs were observed in the OE-128 ESCs when compared to OE-Ctr ESCs and this effect became significant after 2wks (p=0.0088) (Figure 36A, B).

This increase of NkxCE-GFP CPCs pointed to a retarded differentiation capacity of CPCs which was in accordance with our results from miR-128a knockdown experiments where we showed a significant reduction of NkxCE-GFP CPCs frequency after 1.5wks (Figure 14A).

The idea of a retarded CPC differentiation upon miR-128a overexpression was further supported by the fact that the frequency of NkxCE-GFP CPCs in the OE-128 ESCs remained at rather high levels at all analyzed timepoints. This contrasted with the OE-Ctr ESCs that showed the expected steadily decrease in CPC abundance during *in vitro* differentiation (Figure 36A) caused by continuous maturation into cardiac lineages (as described earlier under 4.3.2, Figure 15).

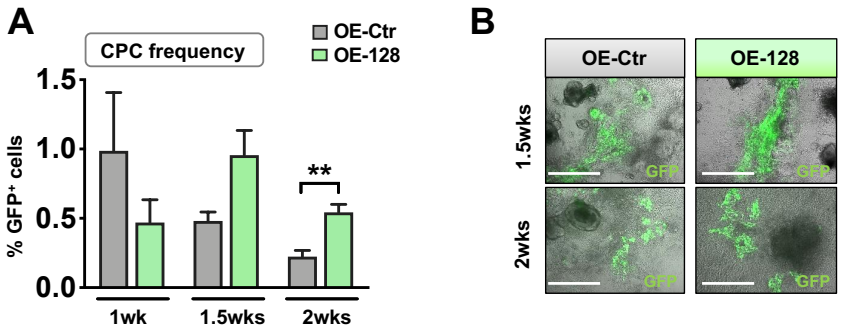

Figure 36 Frequency of NkxCE-GFP CPCs during *in vitro* differentiations of OE-ESCs. **A.** Flow cytometry showed that the percentage of NkxCE-GFP CPCs after miR-128a overexpression was reduced by nearly 50% after 1wk of *in vitro* differentiation of OE-128 ESCs compared to correspondent OE-Ctr ESCs. At 1.5 as well as 2wks, the percentage of GFP-positive CPCs increased in OE-128 ESCs in comparison to OE-Ctr ESCs, with detectable significance at 2wks (p=0.0088, student's t-test). **B.** NkxCE-GFP CPCs after 1.5wks (upper panel) and 2wks (lower panel) of *in vitro* differentiation of OE-Ctr or OE-128 ESCs. Images are an overlay between phase contrast and fluorescent microscopic pictures. Scale bars are 500µm. Data are represented as means ± SEM of one to two independent experiments with each three independent samples measured as singles (OE-Ctr (clone4); OE-128 (clone 21/30 pooled); 1wk n=6,9; 1.5wks n=3,6; 2wks n=3,6). Statistical significance was assessed by two-tailed student's t-test as stated. ** p ≤ 0.01. Adapted from Figures 5C, D from Hoelscher *et al.* miR-128a Acts as a Regulator in Cardiac Development by Modulating Differentiation of Cardiac Progenitor Cell Populations. *Int. J. Mol. Sci.* 2020, *21*, 1158 (Hoelscher *et al*., 2020).

Next, we analyzed gene expressions of several CPC markers during *in vitro* differentiation of OE-ESC lines by qRT-PCR.

Gene expression after 1wk of *in vitro* differentiation in OE-128 ESCs mirrored our miR-128a knockdown results (0.75wks, Figure16) by a significant downregulation of *Isl1* (p=0.0031), *Nkx2.5* (p=0.0286), *Mef2c* (p=0.0062) and *Sfrp5* (p=0.010) as well as significant enhancement of *Irx4* (p=0.0419) compared to OE-Ctr ESCs (Figure 37).

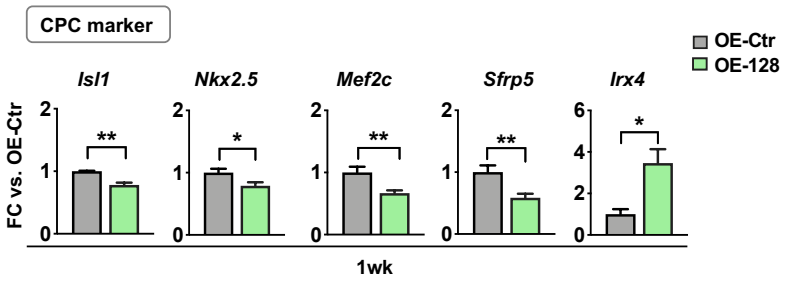

Figure 37 CPC marker expression in OE-ESC EBs at 1wk of *in vitro* differentiations. A. Panels of early CPC markers show that the expression of *Isl1* (p=0.0031, student's t-test), *Nkx2.5* (p=0.0286, student's t-test), *Mef2c* (p=0.0062, student's t-test) as well as *Sfrp5* (p=0.010, student's t-test), were significantly downregulated in OE-128 ESCs compared to OE-Ctr ESCs at 1wk of differentiation. *Irx4* expression was significantly upregulated (p=0.0419, student's t-test) upon miR-128a overexpression (OE-128) at 1wk compared to OE-Ctr. Data are represented as means ± SEM of two independent experiments with each three independent samples measured as singles ((OE-Ctr (clone4); OE-128 (clone 21/30 pooled); all n=6,9). Statistical significances were assessed by two-tailed student's t-test as stated. * p ≤ 0.05, ** p ≤ 0.01. Adapted from Figure 5E from Hoelscher *et al.* miR-128a Acts as a Regulator in Cardiac Development by Modulating Differentiation of Cardiac Progenitor Cell Populations. *Int. J. Mol. Sci.* 2020, *21*, 1158 (Hoelscher *et al*., 2020).

Some markers such as *Mef2c* (p=0.0316) *Sfrp5* (p=0.0122) and *Irx4* (p=0.0368) continued to be regulated until 1.5wks of *in vitro* differentiation in OE-128 ESCs (Figure 38A), a trend that we also observed, at least for *Sfrp5,* during miR-128a knockdown studies at 1wk (Figure18A).

However, after 2wks of *in vitro* differentiation expression of most of the selected markers was unaffected, indicating that regulatory actions of miR-128a seemed to be restricted to early cardiogenesis (Figure 38B, again, supporting the knockdown results (Figure 18B, C). Only *Sfrp5* was still significantly downregulated after 2wks (p=0.0391) in differentiating OE-128 ESCs in comparison to OE-Ctr ESCs (Figure 38B).

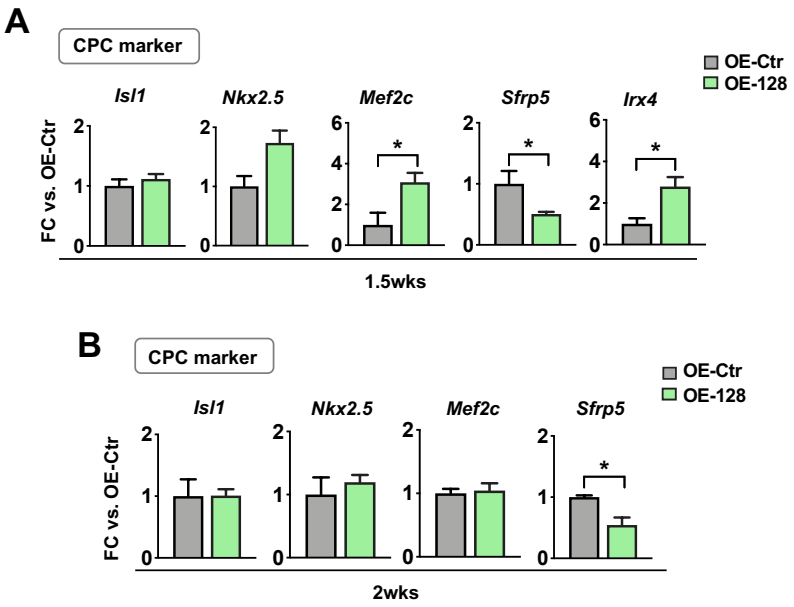

Figure 38 CPC marker expression in OE-ESC EBs at 1.5wk and 2wks of *in vitro* differentiations. A. The expression of some CPC markers including *Mef2c* (p=0.0316, student's t-test), *Sfrp5* (p=0.0122, student's t-test) as well as *Irx4* (p=0.0368, student's t-test) was significantly regulated in OE-128 ESCs at 1.5wks compared to OE-Ctr ESCs. **B.** Expression of *Isl1, Nkx2.5 and Mef2c* were not affected significantly after 2wks of *in vitro* differentiation upon miR-128 overexpression (OE-128). Only *Sfrp5* showed significant downregulation (p=0.0391, student's t-test) in differentiated OE-128 ESCs in comparison to OE-Ctr ESCs. Data are represented as means ± SEM (A, B) of one experiment with three independent samples measured as singles ((OE-Ctr (clone4); OE-128 (clone 21/30 pooled); all n=3,6). Statistical significances were assessed by two-tailed student's t-test as stated. * $p \leq 0.05$. Adapted from Figures 5F and S11A from Hoelscher *et al.* miR-128a Acts as a Regulator in Cardiac Development by Modulating Differentiation of Cardiac Progenitor Cell Populations. *Int. J. Mol. Sci.* 2020, *21*, 1158 (Hoelscher *et al*., 2020).

Next, we wanted to investigate if the enhancement of CPCs at 1.5wks in OE-128 ESC differentiations (Figure 36A) could be caused by retarded differentiation of CPCs into cardiac lineages. Thus, we monitored the expression of selected cardiac lineage markers by qRT-PCR (in accordance with miR-128a knockdown experiments (Figure 20B).

Surprisingly, we did not find any changes of expression of the ventricular CM marker *Myl2* in OE-128 ESCs compared to OE-Ctr ESCs during *in vitro* differentiation neither at 1.5 nor 2wks (Figure 39A, B). However, significant elevated levels of the general CM marker *Tnnt2* were observed after 1.5wks (p=0.0298) (Figure 39A) and 2wks (p=0.0057) (Figure 39B) accompanied by increased levels of *Myh6* at 2wks (p=0.0238) (Figure 39B) in OE-128 ESCs in comparison to OE-Ctr ESCs.

The expression levels of SMC marker *Acta2* and EC marker *Pecam1* were not affected by miR-128a overexpression after 2wks of *in vitro* differentiation (Figure 39B) indicating that neither SMCs nor ECs were influenced by miR-128a confirming the results of miR-128a knockdown (Figure 20).

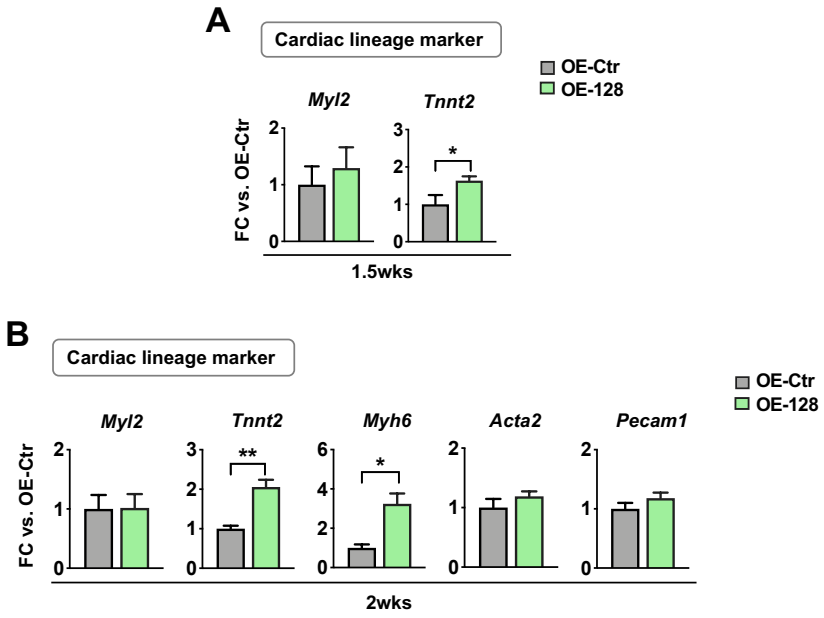

Figure 39 Cardiac lineage marker expression in OE-ESC EBs at 1.5wk and 2wks of *in vitro* differentiations. **A.** Panel show that the ventricular CM marker *Myl2* was not affected after 1.5wks in differentiating OE-128 ESCs in comparison to OE-Ctr ESCs. However, a significant higher expression of the general CM markers *Tnnt2* (p=0.0298, student's t-test) was observed in OE-128 ESCs compared to OE-Ctr ESCs. **B**. No regulation of *Myl2* expression was found after 2wks in OE-128 ESC differentiation, but *Tnnt2* (p=0.0057, student's t-test) and *Myh6* (p=0.0238, student's t-test) were significantly upregulated upon miR-128a overexpression (OE-128) compared to OE-Ctr ESCs. SMC as well as EC marker *Acta2* and *Pecam1* were unaffected after 2wks in differentiating OE-128 ESCs. Data are represented as means ± SEM (A, B) of one experiment with three independent samples measured as singles ((OE-Ctr (clone4); OE-128 (clone 21/30 pooled); all n=3,6). Statistical significances were assessed by two-tailed student's t-test as stated. * $p \leq 0.05$, ** $p \leq 0.01$. Adapted from Figures S11B, C and F from Hoelscher *et al.* miR-128a Acts as a Regulator in Cardiac Development by Modulating Differentiation of Cardiac Progenitor Cell Populations. *Int. J. Mol. Sci.* 2020, *21*, 1158 (Hoelscher *et al*., 2020).

Since *Tnnt2* and *Myh6* are typical CM markers, we assumed that, contrary to our hypothesis of retarded differentiation, miR-128a overexpression might rather favor the differentiation of CPCs into specific CM populations.

However, previously mentioned RNAseq results from cooperation partners (Nothjunge *et al.*, 2017) revealed that embryonic heart-derived NkxCE-GFP CPCs (E9 and E10) already expressed both CM markers at a relatively high level compared to adult CMs (P21) (Figure 40). Thus, the observed increase of *Tnnt2* and *Myh6* upon miR-128a overexpression might also reflect the observed enhancement of NkxCE-GFP CPCs at 1.5 and 2wks during OE-128 ESC *in vitro* differentiation as previously shown (Figure 36).

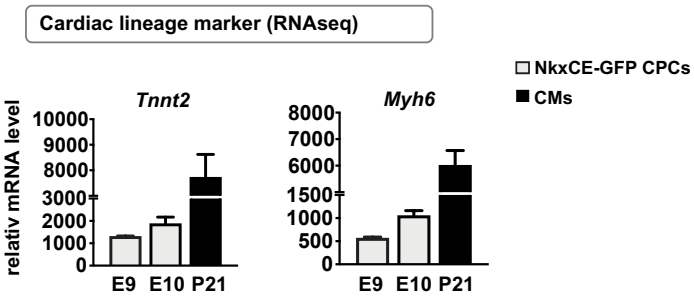

Figure 40 RNAseq data of CM marker expression in NkxCE-GFP CPCs. RNAseq data showed that embryonic heart-derived NkxCE-GFP CPCs (E9 and E10) expressed high levels of the general CM markers *Tnnt2* (left panel) and *Myh6* (right panel), although fairly not as high as CMs from adult mouse hearts (postnatal day 21; P21). Data are represented as means ± SEM of two to three independent CPC and CM populations (n=2-3). Data was obtained in context of another cooperation project published as (Nothjunge *et al.*, 2017). Adapted from Figure S11D from Hoelscher *et al.* miR-128a Acts as a Regulator in Cardiac Development by Modulating Differentiation of Cardiac Progenitor Cell Populations. *Int. J. Mol. Sci.* 2020, *21*, 1158 (Hoelscher *et al*., 2020).

Next, we evaluated the beating frequencies of early CMs throughout OE-ESC differentiations.

The beating frequencies (beats per minute (bpm)) were significantly increased in differentiating OE-128 ESCs when compared to the OE-Ctr ESCs at all timepoints including 1wk ($p<0.0001$), 1.5wks ($p=0.0067$), 1.75wks ($p=0.0004$) and 2wks ($p=0.050$) (Figure 41).

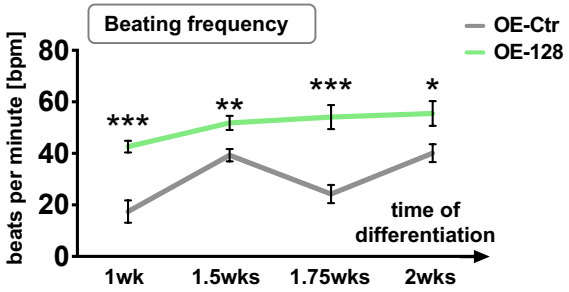

Figure 41 Beating frequency of early CMs during *in vitro* differentiations of OE-ESCs. Beating frequency (beats per minute, bpm) of early CMs was significantly upregulated during *in vitro* differentiation of the OE-128 ESCs in comparison to OE-Ctr ESCs; 1wk ($p<0.0001$, student's t-test), 1.5wks ($p=0.0067$, Mann-Whitney), 1.75wks ($p=0.0004$, student's t-test) and 2wks ($p=0.050$, student's t-test). Data are represented as means ± SEM of one experiment with each five to nine independently recorded videos per condition evaluated by three independent observers ((OE-Ctr (clone4); OE-128 (clone 21/30 pooled), 1wk n=5,17; 1.5wks (day 9/11 pooled) n=21,34; 1.75wks n=8,16; 2wks n=8,17). Statistical significances were assessed by Mann-Whitney Rank Sum test or two-tailed student's t-test as stated. * $p \leq 0.05$, ** $p \leq 0.01$, *** $p \leq 0.001$ Adapted from Figure 5G from Hoelscher *et al.* miR-128a Acts as a Regulator in Cardiac Development by Modulating Differentiation of Cardiac Progenitor Cell Populations. *Int. J. Mol. Sci.* 2020, *21*, 1158 (Hoelscher *et al*., 2020).

This reflected the results of LNA-treated ESCs (miR-128a knockdown) that showed a decreased beating frequency of early CMs throughout differentiation (Figure 21, Figure 30).

However, since we could not show an alteration of *Myl2* expression in differentiating OE-128 ESCs above (other than in knockdown experiments, Figure20B), we suggested that the increased beating frequencies might be caused by an enhancement of other CM populations that possibly co-express *Tnnt2* and *Myh6.*

As mentioned before, the frequency of the heartbeat is predominantly controlled by fast-firing nodal cells (that also express *Tnnt2* and *Myh6* as most CMs (Schiaffino and Reggiani, 1996; Wei and Jin, 2011). Thus, an enhancement of such a CM population might have caused the higher beating frequency in OE-128 EBs.

Therefore, we evaluated the expression of the nodal CM marker *Shox2* after 2wks of differentiation in OE-ESC lines and indeed found a significantly increased level in OE-128 EBs (p=0.0169) in comparison to OE-Ctr EBs (Figure 42) supporting the idea that miR-128a overexpression could favor the differentiation of CPCs into nodal cells expressing *Shox2, Tnnt2*, as well as *Myh6*.

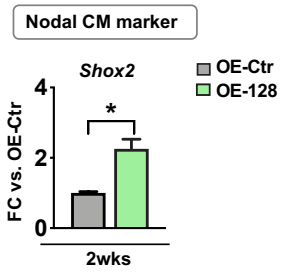

Figure 42 Nodal CM marker expression in OE-ESC EBs at 2wks of *in vitro* differentiations. The expression of *Shox2* was significantly upregulated (p=0.0169, student's t-test) after 2wks of *in vitro* differentiation of OE-128 ESCs compared to OE-Ctr ESCs. Data are represented as means ± SEM of one experiment with three independent samples measured as singles (OE-Ctr (clone4); OE-128 (clone 21/30 pooled); all n=3,6). Statistical significance was assessed by two-tailed student's t-test as stated. * p ≤ 0.05Adapted from Figure S11E from Hoelscher *et al.* miR-128a Acts as a Regulator in Cardiac Development by Modulating Differentiation of Cardiac Progenitor Cell Populations. *Int. J. Mol. Sci.* 2020, *21*, 1158 (Hoelscher *et al*., 2020)

5 Discussion

To date, over 2500 miRs have been detected in humans (Kozomara and Griffiths-Jones, 2014) and it is predicted that the expression of most mammalian mRNAs is regulated by at least one miR (Friedman *et al.*, 2009; Hoelscher *et al.*, 2020). Given this complexity, a complete picture of miR-dependent regulations in development, homeostasis and disease is still emerging (Hoelscher *et al.*, 2020).

Despite the fact that dozens of miRs have already been described as indispensable players in almost every facet of cardiac development (Cordes *et al.*, 2010), the exact roles of many cardiac-specific miRs remain elusive including those involved in early cardiogenesis.

Further characterization of those miRs may shed light on unknown regulatory networks and might also provide us with new diagnostic and therapeutic targets for diverse types of cardiac pathologies such as congenital heart diseases (CHD) where a dysregulation of a range of miRs has been already described as causal for disease development (Hoelscher *et al.*, 2017).

In this study we sought to complement the network of regulatory miRs by identifying miRs with so far unknown roles in early cardiac development. We finally identified miR-128a as a promising candidate and provide fundamental evidence that this miR is an indispensable player in early cardiogenesis by regulating CPC populations including their cardiac lineage differentiation.

5.1 Identification of miRs involved in early cardiac development

High-throughput approaches such as MicroRNA Arrays or RNA sequencing (RNAseq) made it possible to rapidly assess differentially expressed miRs in almost every tissue or cell type to further investigate their molecular function (Pritchard *et al.*, 2012).

So far numerous studies have analyzed the miR profiles of CPC populations or other cardiac cells as ECs, CMs or SMCs to characterize their functional relevance in more detail (Cordes and Srivastava, 2009; Malizia and Wang, 2011; Shen *et al.*, 2016). However, so far, no data existed for NkxCE-GFP CPCs, a distinct, multipotent cell population that is marked by an activated cardiac-specific *Nkx2.5* enhancer coupled with GFP expression.

NkxCE-GFP CPCs are able to evolve into all major cardiac cell types during cardiogenesis, namely ECs, CMs, SMCs or CFs (Li *et al.*, 2015; Wu *et al.*, 2006).

By comparative analysis of obtained MicroRNA Array data from isolated murine NkxCE-GFP CPCs as well as several other murine cell populations including GFP-negative fractions and fibroblast populations (CFs and TTFs) we were able to establish a miR profile of these CPCs for the first time.

We identified a total of 83 miRs that were differentially expressed in NkxCE-GFP CPCs, 40 of which were found to be significantly upregulated in comparison to either one or several of the above-mentioned cell populations. The identification of miR candidates for detailed functional studies during *in vivo* zebrafish development (in cooperation with Dr. David Hassel) as well as during *in vitro* murine ESC/iPSC differentiation, was then based on several criteria.

Initially, we focused on CPC-enriched miRs since it has been demonstrated before that miRs with essential developmental functions are in fact highly expressed in a range of CPC populations (Ivey *et al.*, 2008; Shen *et al.*, 2016). MiR-1 and miR-133 as major players of mesodermal formation, for instance, were found to be enriched in Nkx2.5-GFP^{+} CPCs (Ivey *et al.*, 2008). In addition, miR clusters as e.g. the miR-322/-503 cluster are highly expressed in *Mesp1*-CPCs facilitating important tasks in cardiomyocyte specification and cardiac fate (Shen *et al.*, 2016). Given that *Mesp1*-CPCs are one of the earliest CPC pool that develops during cardiac development (Brade *et al.*, 2013) and NkxCE-GFP CPCs occur at slightly later stages of cardiogenesis, this miR cluster was not found to be differentially expressed in our CPCs.

By this, most of cardiac-specific miRs (but also essential cardiac TFs as *Gata4, Nkx2.5* or *Hand2)* also show a typical kinetics throughout cardiogenesis where an increase of expression can be observed at the onset of cardiac development (e.g. CPC formation) (Ivey *et al.*, 2008). This typical kinetics behavior has also been nicely illustrated for above-mentioned miRs, miR-1 and miR-133 e.g. during ESC *in vitro* differentiation (Ivey *et al.*, 2008) and was therefore another important criterion for the selection of miR candidates upon the group of CPC-enriched miRs.

Furthermore, a wide range of those miRs with developmental impact usually also show a high cross-species sequence conservation, indicating its extraordinary revolutionary importance (Lin *et al.*, 2014). In fact, highly preserved functions during early cardiogenesis have already been described in mouse and human e.g. for conserved miRs like miR-1 and miR-133 (Ivey *et al.*, 2008).

Due to this, we additionally included preservation analysis as another selective tool to identify miRs that might harbor important functions.

Based on above mentioned criteria, in addition to extensive literature research, we finally selected four CPC-enriched miRs, namely miR-30b, miR-20b, miR-128a and miR-30a.

Besides showing highly conserved sequences as well as seed region/motifs across zebrafish *(Danio rerio),* mouse (*Mus musculus*), chicken (*Gallus gallus*) and human (*Homo sapiens*), all these miRs displayed typical kinetics throughout murine ESCs and human iPSC (hiPSC) differentiation. This supported their cardiogenic relevance and indicated possible preserved mechanisms of actions across several species.

In addition, a number of publications reported functions of the selected miRs in relation to cardiac or at least skeletal muscle development (Guess *et al.*, 2015; Huang *et al.*, 2018; Ketley *et al.*, 2013; Witman *et al.*, 2013; Zhu *et al.*, 2015)

MiR-20b, for instance, which is expressed in embryonic hearts of many species including zebrafish, rat and mouse (Ahn *et al.*, 2010; Chen *et al.*, 2005), has been attributed with a role in CM differentiation in the P19 cell model *in vitro* by regulating the BMP signaling pathway which is essential for cardiac development (Wang *et al.*, 2011; Zhu *et al.*, 2015).

The miR-30 family that includes miR-30a and miR-30b, has been associated with roles in myogenic specification processes. *In vitro* analysis showed that miR-30a/b/c gain-of-function was able to promote C_2C_{12} myoblast differentiation (Guess *et al.*, 2015). In addition, this miR family regulates early general muscle development by impacting Hedgehog signaling, another key pathway of embryonic development (Ketley *et al.*, 2013).

The role of miR-128a has so far mainly been studied in the context of cardiac regeneration (Huang *et al.*, 2018; Witman *et al.*, 2013). A very recent manuscript identified an involvement of miR-128 in adult CM proliferation and attributed miR-128a with a function in regeneration after myocardial infarction in mice (Huang *et al.*, 2018). However, it has been shown that miR-128a also targets *Isl1*, a key transcription factor during early heart formation that could indicate potential roles of miR-128a in early cardiogenesis (Witman *et al.*, 2013).

Despite this, the precise function of all four miRs in cardiogenesis remained elusive. However, we were confident that we identified miRs that could harbor relevant functional relevance for cardiogenesis.

5.2 Candidate miR function in zebrafish larvae *in vivo*

To get a first idea about functional involvement in cardiac development, we decided to further investigate the four candidate miRs in a transgenic zebrafish model. Therefore, our cooperation partner Dr. David Hassel conducted morpholino-(MO)-induced knockdown experiments for all miR candidates in (Tg(myl7:ras)-GFP (D'Amico *et al.*, 2007) zebrafish in which GFP expression is driven by the *myl7* promoter, an early cardiac marker. Morphological changes as well as functional cardiac outcomes including heart rate and fractional shortening were evaluated.

The survival of most vertebrates is highly dependent on a fully functional cardiovascular network. Accordingly, several rescue (compensatory) mechanisms, like genes with homologous function, exist in higher vertebrates such as mice, and might prevent that genetic manipulation with impact on heart development directly leads to an obvious phenotype or even embryonic lethality (Saga, 1998). Thus, studying vertebrates' cardiac development *in vivo* can be challenging.

Interestingly, however, zebrafish survival is not completely dependent on a functional cardiovascular system making them particularly well-suited for studying cardiac development *in vivo* (Stainier, 2001). In addition, zebrafish exhibit a wide range of practical advantages including fast external fertilization, optical transparency and easy genetic tractability (Tu and Chi, 2012).

And although obviously extensive differences of cardiac morphology exist between zebrafish and other vertebrates, a range of miRs that had been identified by MO studies to regulate heart development in zebrafish also showed overlapping functions during cardiogenesis in other vertebrates. For instance, miR-21 which was identified as a regulator of valvulogenesis in zebrafish has also been shown to be involved in similar developmental processes in humans and mice (Banjo *et al.*, 2013; Brown *et al.*, 2016; Chiavacci *et al.*, 2012). This can be explained by the fact that underlying molecular and morphological processes during heart development as well as other organ development are in fact very similar between all vertebrates (Choi *et al.*, 2008; Huisken *et al.*, 2004; Liu and Stainier, 2012; Nguyen *et al.*, 2008; Pierpont *et al.*, 2007; Stainier, 2001). Therefore, the scheduled zebrafish studies would provide us with information about functional involvement of the four miR candidates in cardiogenesis which we then aimed to investigate in more detail during murine ESC/iPSC differentiations.

First, Dr. Hassel aimed to analyze the kinetics of the selected miRs during zebrafish development. In fact, all of them were upregulated at the beginning of heart development at 24hpf in zebrafish larvae which confirmed the results obtained from murine and human ESC/iPSC *in vitro* differentiations and reflected the high conservation of the function of those miRs across several species.

However, despite the confirmed efficient knockdown of all miR candidates, only the MO-induced knockdown of miR-128a (MO-128a) induced a robust cardiac phenotype with pericardial edemas and blood congestion in front of the right outflow tract indicative of impaired heart function. In addition, zebrafish larvae developed abnormalities in heart looping, which led to incorrect positioning of the heart and larvae often had smaller ventricles accompanied by altered functional parameters including significantly reduced ventricular fractional shortening and heart rate.

Various gene-manipulating studies (including miR studies, e.g. miR-19b (M. Li *et al.*, 2014) have described similar cardiac abnormalities during zebrafish development and have later even been linked to the development of human CHDs (Grant *et al.*, 2017; Hoelscher *et al.*, 2017). Thus, we were highly confident that we identified a miR with important functional relevance in cardiogenesis.

In contrast, neither knockdown of miR-20 (MO-20b), miR-30a (MO-30a) nor miR-30b (MO-30b) led to changes in the cardiac phenotype or cardiac function of zebrafish larvae although all of these miRs, just like miR-128a, had been attributed with roles in muscle or even heart development (Wang *et al.*, 2011; Zhu *et al.*, 2015) as discussed above.

However, especially MO-20b and MO-30b morphants exhibited some non-cardiac phenotypes that, at least in part, could be explained by already characterized functions of those miRs. For instance, the observed severe brain hemorrhage and edema in the eye region at early stages of development after miR-20b knockdown could be linked to the described function of miR-20b during angiogenesis and vascular homeostasis (Cascio *et al.*, 2010; Wu *et al.*, 2009; Zhu *et al.*, 2019). For miR-30b, functions in neurological processes have been implicated before (Zhang *et al.*, 2018). Thus, this might explain the observed edema and enlarged hydrocephalus in MO-30b larvae. Further, the severely shortened body length as well as crimped tails in MO-30b larvae mirrored the above-mentioned role of this miR in general muscle development. In fact, similar phenotypes have already been described for MO-induced miR-30b knockdown in zebrafish (Ketley *et al.*, 2013). Nevertheless, given that none of these three miRs (miR-20b, miR-30a, miR-30b) directly impacted heart development in zebrafish larvae, we assumed that they might not be major players in cardiogenesis and therefore excluded them from further detailed analyses.

However, one must keep in mind that *in vivo* models remain highly complex. Despite the previously shown conserved sequence and similar kinetics behavior during development or differentiation of miR-128a across species that indicated conserved functions, miRs are in fact embedded in highly versatile networks that might also include species-specific regulation of mechanisms.

Interestingly, this might also hold true for miR-128a, for which contrary *in vivo* data exist about its involvements in postnatal proliferation of cardiac linages in newts and mice. Whereas inhibition of miR-128a in newts had no effect on CM proliferation but rather on hyperplasia of non-CMs (Witman *et al.*, 2013), the opposite effect has been described for CMs in mice (Huang *et al.*, 2018) indicating divergent functions of miR-128a in different species, at least in the postnatal heart. This does not exclude a conserved function of miR-128a during early cardiac development, although the possibility of species-specific mechanisms of actions must be considered.

Huang and colleagues (Huang *et al.*, 2018) also revealed that despite the impact of miR-128a on postnatal CM proliferation *in vivo*, neither changes in heart size nor functional changes (e.g. fractional shortening) were observed in newborn or adult mouse hearts when miR-128 was cardiac-specifically knocked out in Nkx2.5-Cre miR-128 floxed mice ($Nkx2.5^{Cre}$;$miR\text{-}128^{fl/fl}$ → $miR\text{-}128^{-/-}$). Though, postnatal cardiomyocytes were smaller and still highly proliferative compared to age-matched control mice as expected (Huang *et al.*, 2018). These results were contrary to our findings in MO-128a injected zebrafish larvae that showed severe cardiac malformations. This discrepancy might be possibly due to the different endpoints of experimental analysis (embryonic/larval vs. postnatal/adult) (Andres-Delgado and Mercader, 2016). It has been shown before that functions of miRs might not only vary between different species but also between different developmental stages (Ivey *et al.*, 2008). However, even if cardiac development of mouse and zebrafish closely resemble (Andres-Delgado and Mercader, 2016), species-specific differences cannot be excluded. In addition, the nonexistent penetrant phenotype in older $miR\text{-}128^{-/-}$ mice (Huang *et al.*, 2018) could be also attributed to previously mentioned compensatory mechanisms that have been activated to ensure proper cardiac development and thereby survival overall (Saga, 1998). Interestingly, the activation of such compensatory pathways has predominantly been observed after stable knockouts rather than transient transcriptional or translational knockdown (Rossi *et al.*, 2015). Thus, also the usage of different knockdown strategies in zebrafish and mouse could have contributed to the dramatic discrepancies in phenotypes.

While important progress was made in identifying the roles of miR-128a in pathophysiological processes especially in the postnatal and adult heart (W. Huang *et al.*, 2018; Witman *et al.*, 2013), we further aimed to define the role of this miR during early cardiogenesis on a cellular level *in vitro*.

5.3 Knockdown of miR-128a during *in vitro* differentiation of murine ESC/iPSCs

Over the last decade, ESCs and iPSCs have been widely used to study cardiac development *in vitro* (Doppler *et al.*, 2014; Dorn *et al.*, 2015; Ivey *et al.*, 2008; Pfeiffer *et al.*, 2018). The use of ESCs/iPSCs has fundamentally contributed to a deeper understanding of the highly complex networks of key players that guide early cardiogenesis including transcription factors and miRs (Mignone *et al.*, 2010).

This is predominantly due to their ability to precisely mimic early stages and basic mechanisms of *in vivo* cardiogenesis that include the formation of cardiac mesoderm, progenitor cell specification as well as their differentiation into cardiac linages (G. Li *et al.*, 2015; Van Vliet *et al.*, 2012; S. M. Wu *et al.*, 2006).

The cardiogenic mesoderm is one of the first structures formed during embryonic heart development that harbors a distinct source of multipotent mesodermal progenitors that will develop into the so-called first and second heart field (FHF and SHF) (Brade *et al.*, 2013). Around E7.5 of murine heart development those progenitors start to express cardiac transcription factors (TFs) such as *Isl1, Nkx2.5, Mef2c, Tbx5, Sfrp5, Hcn4* or *Irx4* that leads to their specification. Dependent on their unique expression profile, those CPCs will later contribute to specific structures of the heart by differentiating into all types of mature cardiac cells such as ECs, SMCs and several subtypes of CMs.

While murine ESCs/iPSCs nicely recapitulate all of these embryonic processes, the timing is usually slightly faster during *in vitro* differentiation than during *in vivo* embryogenesis (Van Vliet *et al.*, 2012), further explaining why ESCs/iPSCs are such an efficient and widely used tool to study heart development.

To study the role of miR-128a in more detail *in vitro*, we used the murine transgenic NkxCE-GFP ESC line in which a distinct, multipotent CPC population (NkxCE-GFP CPCs) (mainly resembling FHF progenitors) is marked by an activated cardiac-specific *Nkx2.5* enhancer that is coupled to GFP (Wu *et al.*, 2006). In addition, an *Isl1*-reporter iPSC line (iITG-iPSCs) was generated in which *Isl1*-CPCs (mainly resembling SHF progenitors) are marked by GFP upon Cre-mediated excision of membrane-tagged dimer Tomato (mT) (Muzumdar *et al.*, 2007; Yang *et al.*, 2006).

While both pools of CPCs start to occur around E8.5 during mouse heart development *in vivo,* the first GFP-positive CPCs can normally be observed as early as day 5/6 during ESC/iPSC *in vitro* differentiation. Unfortunately, for the self-generated *Isl1*-reporter iPSC line, a delayed differentiation capacity was observed that might be due to the Isl1Cre-R26^{mTmG} transgene itself. Since Cre was directly knocked in into the endogenous *Isl1* locus, actually replacing the *Isl1* ATG start codon, a general decrease in *Isl1* expression in iITG-iPSCs could have caused the observed delay (Muzumdar *et al.*, 2007; Yang *et al.*, 2006).

Comprising iITG-iPSC characterization of several clones all showed delayed timing while being fully reprogrammed. To ensure proper assessment, all performed experiments conducted with the iITG-iPSC line were accordingly adjusted in timing and the delay was factored in when results were interpreted.

Thus, for detailed functional studies of miR-128a, we conducted LNA-mediated knockdown on several timepoints during *in vitro* ESC/iPSC differentiation and tracked changes in CPC frequency, gene expression and functional outcomes such as the beating frequency.

And indeed, miR-128a regulated CPC frequency, gene expression of cardiac progenitor cell marker and beating frequency of early CMs.

LNA-mediated miR-128a knockdown in differentiating NkxCE-GFP ESC increased cardiac TFs including *Isl1, Sfrp5,* and *Hcn4*, but reduced *Irx4* at the onset of cardiogenesis indicating that miR-128a knockdown promoted the specification of an *Isl1/Sfrp5/Hcn4*-expressing CPC population as well as inhibited the specification of *Irx4*-expressing CPCs. We further verified the enhancement of *Isl1*-CPCs on a cellular level by flow cytometry analysis during iITG-iPSC *in vitro* differentiations. This might be due to previously mentioned ability of miR-128a to directly target the 3'UTR of *Isl1* (Witman *et al.*, 2013).

Furthermore, the idea of a promotion of mesodermal progenitors was supported by the fact that the ectodermal marker *Neurod1* was significantly reduced upon miR-128a knockdown. It could be that a favor of mesodermal or mesendodermal progenitors could be accompanied by reduced occurrence of other germ layer progenitors including those of the ectoderm. Although it seemed plausible that the reduction of *Neurod1* (and thereby possibly also *Neurod1*-expressing ectodermal progenitors) was a result of a miR-128a-dependent promotion of mesodermal CPCs, a direct involvement of miR-128a in the regulation of ectodermal cells has to be considered given its prominent role in neurogenesis that has been studied extensively before (Krichevsky *et al.*, 2003; Krichevsky *et al.*, 2006). Despite the involvement of miR-128 in the proliferation of postnatal CMs (Huang *et al.*, 2018), proliferation was not the mechanism of action for miR-128a during early cardiac development, since *Ki67* expression, a marker for proliferation, was not altered upon miR-128a knockdown.

Besides the impact on miR-128a in early stages of development, we further showed that miR-128a knockdown led to a reduction of NkxCE-GFP CPCs during progressing differentiation of NkxCE-GFP ESCs. We assumed that the seen CPC reduction might be due to earlier transdifferentiation of those CPCs into cardiac linages. And indeed, we found increased expression of the ventricular cardiomyocyte marker *Myl2* at this stage which was accompanied by significantly reduced beating frequencies of early CMs. This functional outcome was not only found during NkxCE-GFP ESC differentiations but was also reconfirmed after miR-128a knockdown during iITG-iPSC differentiations. Besides that, neither EC nor SMC marker were impacted by miR-128a knockdown.

The heart mainly consists of three cardiac cell types that include, besides ECs and SMCs, also distinct types of CMs that decisively define cardiac structure and function. Among those are nodal-like CMs that belong to the so-called "nodal myocardium" and are defined by the expression of several ion channels, e.g. *Shox2 or Hcn4,* as well as atrial- and ventricular-like CMs of the so-called "working myocardium" expressing genes such as e.g. *Myl2*. (He *et al.*, 2003).

Although most CMs exhibit pacemaking properties, fast-firing nodal-like cells that sit at the sinoatrial node (SAN), normally control the heart beat by overriding electrical impulses of other, slower firing cells (e.g. cells of the “working myocardium”) (He *et al.*, 2003; van Weerd and Christoffels, 2016; Zhu *et al.*, 2010).

However, we did not find any changes in the expression of above-mentioned nodal-like marker genes *Shox2 or Hcn4* that could explain the slower beating. Thus, we propose a model in which miR-128a knockdown promotes faster differentiation of cardiac progenitors into a distinct type of *Myl2*-expressing CMs as part of the “working myocardium” that might lead to the reduced beating capacity.

A potential relevance of miR128a in CM differentiation is additionally supported by the fact that miR-128a has not only been shown to regulate postnatal CMs proliferation (Huang *et al.*, 2018) but was also significantly higher expressed in adult mouse CMs when compared to other cardiac cells (Huang *et al.*, 2018).

Furthermore, it remained interesting from which pool of CPCs those *Myl2*-positive, ventricular CMs could have been derived from. As mentioned earlier, FHF and SHF progenitors that express specific marker genes, later contribute to distinct structures of the heart by differentiating into cardiac lineages. They contribute to the ventricular, atrial, and outflow tract (OFT) myocardium, the conduction system as well as aortic and even pulmonary cushions (Brade *et al.*, 2013; Fujii *et al.*, 2017). However, FHF-CPCs and SHF-CPCs contribute to different areas of the heart. Whereas cardiac lineages of the left ventricle predominantly derive from FHF-CPCs, parts of the OFT, right ventricle or inflow region and atria are rather built by SHF-derived lineages (Buckingham *et al.*, 2005; Colombo *et al.*, 2018; Domian *et al.*, 2009).

The reduction of NkxCE-GFP CPCs (FHF-CPC pool) which mainly contribute to ventricular structures of the heart (Domian *et al.*, 2009), let it appear likely that miR-128a knockdown promoted a faster differentiation of those FHF-CPCs into ventricular, *Myl2*-expressing CMs.

However, recently it was further demonstrated that *Isl1* which is a direct target of miR-128 (Witman *et al.*, 2013), also controls CPC differentiation, cardiomyocyte identity, and sarcomeric maturation by shaping the chromatin landscape of cardiac progenitor cells (Gao *et al.*, 2019). Thereby, a miR-128a/*Isl1*-dependent pathway that may include *Isl1* or even *Isl1*-expressing CPCs could be involved in the promotion of cardiac lineage specification.

Furthermore, the reduction of *Irx4* expression upon miR-128a knockdown and the fact that *Irx4*-expressing CPCs have been shown to exclusively contribute to ventricular structures of the heart (Nelson *et al.*, 2016), makes an involvement of such CPCs possible, even though the impact on *Irx4* expression was only found in earlier stages of differentiation.

Although we have strong evidence that a miR-128a knockdown promotes a faster differentiation of cardiac progenitors into a ventricular subtype of CMs, the direct contribution of a specific CPC population remains a matter of future investigation and could be evaluated e.g. by lineage tracing experiments.

Overall, results of *in vitro* and *in vivo* miR-128a knockdown studies coincided very well. While we showed that miR-128a *in vitro* knockdown led to changes of important cardiac TFs such as *Isl1, Sfrp5, Nkx2.5, Mef2c, Irx4, Hcn4* as well as the frequency of NkxCE-GFP- and *Isl1*-CPCs, MO-128a zebrafish larvae developed impaired cardiac phenotypes including abnormal heart looping. In fact, a wide range of gene manipulating studies have shown that changes of TF expression led to misguided heart development in zebrafish including abnormal cardiac looping (Brown *et al.*, 2016).

Further analogy can be found for the beating frequencies of early CMs that were reduced both *in vitro* and *in vivo* after miR-128a knockdown. In addition, neither *in vitro* nor *in vivo* knockdown of miR-128a led to any changes in atrial structures, shown by a normal appearance of the MO-128 zebrafish atria and unchanged expression levels of *Myl7* (atrial marker) during *in vitro* ESC differentiation.

However, although we propose a model in which miR-128a knockdown promotes faster differentiation of cardiac progenitors into specific ventricular CM in the murine model, MO-128a zebrafish larvae surprisingly showed smaller ventricles and reduced fractional shortening. Thus, despite the high transferability of results, species-specific factors might also impact miR-128a-dependent pathways and might explain this discrepancy.

5.4 Overexpression of miR-128a during *in vitro* differentiation of murine NkxCE-GFP ESCs

To get a more precise picture of the involvement of miR-128a in early cardiogenic processes, we further performed miR-128a overexpression (OE) experiments during *in vitro* differentiation of NkxCE-GFP ESCs.

So far, various gene delivery methods ranging from viral vectors to plasmid-based transient gene expressions have been applied to ESCs to ensure efficient and stable transgene expression (Kobayashi *et al.*, 2005).

However, especially lentiviral constructs have been proven to be one of the most effective tools for miR delivery in ESCs (Munoz *et al.*, 2012; Rothe *et al.*, 2013).

Given their ability to integrate in the host genome with a relatively low rate of insertional mutagenesis and the fact that they have been shown to be rather resistant to major silencing mechanisms that can occur during ESC differentiation (Pfeifer *et al.*, 2002) they have not only become the most reliable but also the most widely used tool to obtain stable overexpression in ESCs (Asano *et al.*, 2002; Gropp *et al.*, 2003; Kosaka *et al.*, 2004).

Thus, we established two stable OE-ESC lines by transducing the previously described NkxCE-GFP ESC line with doxycycline-inducible lentiviral particles that either expressed miR-128a (OE-128) or a non-targeting miR-Ctr (OE-Ctr) downstream of tRFP which was used as an indication for miR-expressing ESCs, respectively.

In particular, tetracycline-regulated (tet-on) viral systems have frequently been transduced in ESC/iPSCs (Masui *et al.*, 2005; Zhou *et al.*, 2007) since they allow spatiotemporal-controlled expression of the transgene. However, even though this feature clearly represents a major advantage, it is at the same time one of the main drawbacks of such systems. Due to basal regulations of tet-operated promoters such as the TRE3G-promoter used in this study, fair amounts of transgene expression have been reported even without the addition of tetracyclines (Garrick *et al.*, 1998; Meyer-Ficca *et al.*, 2004; Mizuguchi and Hayakawa, 2001). Unfortunately, this promoter “leakiness” occurred in our OE-128 ESC clones characterized by an already significantly elevated expression of miR-128a also in the absence of doxycycline.

In addition, miR-128a expression could not be further enhanced significantly upon doxycycline induction of the lentiviral system in OE-128 ESCs. This may be, at least in part, due to the above-mentioned leaking background expression of miR-128a which could make an additional overexpression after doxycycline induction even more challenging. However, it also has been shown that viral constructs, especially those in which the expression of polycistronic genes is controlled by the same inducible promoter, might lack sufficient expression of the gene located second downstream of the promoter (Kim *et al.*, 2004). Thus, the design of the used lentiviral construct (miR-128a co-expressed downstream of tRFP under the control of the TRE3G promoter) could also have contributed to that outcome. In addition, this would explain the sufficient tRFP expression, which was, other than miR-128a, significantly enhanced in OE-ESCs upon doxycycline induction.

Furthermore, we were aware that the use of tetracyclines in cell culture systems had been discussed controversially due to possible impacts on cell metabolism, proliferation as well as gene expression (Ahler *et al.*, 2013; Moullan *et al.*, 2015). It has been shown, for instance, that doxycycline alone is able to dramatically promote neuronal differentiation of stem cells when used for inducible systems (Cao *et al.*, 2019).

And although we were able to exclude that doxycycline changed the proliferation rates of the OE-ESCs, we identified significant impact on ESC *in vitro* differentiation mirrored by an increase of NkxCE-GFP CPC frequency and changes of gene expression of CPC markers such as *Isl1*, *Nkx2.5* and *Mef2c*.

Thus, we finally decided to conduct miR-128a overexpression experiments without doxycycline. However, due to the leakiness of the lentiviral OE-construct, we still achieved a fair overexpression of miR-128a during OE-128 ESC *in vitro* differentiation even without doxycycline induction. In fact, miR-128a expression was found to be continuously elevated throughout OE-128 ESC differentiation, though, not significantly at later stages. As mentioned above, most of the lentiviral systems should be resistant to major silencing mechanism during differentiation of ESCs. However, promoter methylations have nevertheless been commonly reported (Herbst *et al.*, 2012; Schlesinger and Goff, 2013) and might be one explanation for the non-efficient miR-128a overexpression.

Interestingly, when evaluating experimental outcomes of OE-ESC *in vitro* differentiations including gene expression, NkxCE-GFP CPC frequencies as well as beating frequencies of early CMs, we found profound analogies to miR-128 knockdown studies that complemented the previously established picture of miR-128a-dependent regulatory actions.

We were able to confirm the influence of miR-128a on early cardiac TF expression and by this possibly also an influence on CPC populations. Overexpression of miR-128a led, in opposition to knockdown studies, to significantly diminished expression of *Isl1, Sfrp5, Nkx2.5, Mef2c* as well as significantly increased *Irx4* expression at the onset of cardiogenesis.

In addition, we observed an enhanced abundance of NkxCE-GFP CPC upon miR-128a overexpression with progressing differentiation, again in compliance with the findings of the knockdown study. This supported our presumption that miR-128a overexpression smaller than 10-fold compared to the OE-Ctr ESC line can indeed induce a phenotype. In fact, other studies have confirmed that by showing that already a 2- to 5-fold artificial overexpression of a miR is sufficient to cause significant cellular impacts (Jin *et al.*, 2015).

We further aimed to confirm the role of miR-128a concerning the differentiation of cardiac progenitors into cardiac lineages. Again, miR-128a had no influence on EC or SMC marker gene expression supporting our knockdown data.

Since we hypothesized that miR-128a knockdown promoted faster differentiation of cardiac progenitors into *Myl2*-expressing, slower beating ventricular CMs, we proposed an opposite model of retarded differentiation for miR-128a overexpression. Interestingly, we did not observe the expected decrease of *Myl2* expression, but we found elevated levels of *Tnnt2, Myh6* and *Shox2* accompanied by increased beating frequencies of early CMs throughout OE-ESC differentiations. Thus, miR-128a overexpression might also promote the differentiation of cardiac progenitors into specific cardiac lineages.

Given that especially CMs of the “nodal myocardium” express *Shox2,* we concluded that miR-128a overexpression favored the differentiation of a distinct pool of CPCs into nodal-like CMs.

Moreover, an enhancement of fast-firing *Shox2*-expressing CMs (e.g. from the SAN) would coincide with the observed higher beating frequency during OE-128 ESC *in vitro* differentiation.

Tnnt2 and *Myh6* are basically expressed by all CMs (Schiaffino and Reggiani, 1996; Wei and Jin, 2011), thus, the increase of those genes might also mirror the enhancement of *Shox2*-expressing CMs. However, the other option is that higher levels of *Tnnt2* and *Myh6* reflected the observed accumulation of NkxCE-GFP CPCs since these also express a fair amount of those marker genes as shown by RNA sequencing data.

Based on the increase of NkxCE-GFP CPCs upon miR-128a overexpression what might reflect a retarded differentiation capacity of those CPCs as well as the fact that nodal-like, *Shox2*-expressing CMs at the SAN region predominantly derive from SHF progenitors (Zhu *et al.*, 2010), it appeared very likely that the *Shox2*-expressing CMs derived from another CPC pool upon miR-128a overexpression.

Interestingly, *Sfrp5*-expressing CPCs have recently been described to contribute to diverse areas of the heart including the sinus venosus (SV) as well as parts of the atria (Fujii *et al.*, 2017). Given the diminished expression of *Sfrp5* upon miR-128a overexpression that might indicate a reduction of *Sfrp5*-expressing CPCs, miR-128a overexpression could foster the differentiation of such CPCs into nodal-like CMs. However, the direct mechanistical link between CPCs and their contributions to cardiac linages remain elusive and would require further experimental evaluation by lineage tracing.

In general, overall results of gain- and loss-of-function experiments merge rather well. Especially, if we keep in mind that gene or miR overexpression by lentivirus always appears more artificial than a gene or miR knockdown e.g. by LNA probes. While an overexpression unphysiologically appears in every cell due to the integrative nature of the virus into the host genome, LNA-mediated knockdowns only block miRs transiently (miR-128a) in that cell where they are also physiologically expressed.

Finally, miR-dependent regulations are highly complex and can include many different target genes and a wide range of molecular pathways. They are “fine tuners” of transcriptional regulations whose expression in cells is precisely tuned in order to fulfill specific functions (Chen and Wang, 2012).

5.5 Conclusion

In this study we showed that morpholino (MO)-induced *in vivo* knockdown of miR-128a in zebrafish caused cardiac malformations including smaller ventricles and abnormal cardiac looping accompanied by reduced ventricular fractional shortening as well as heart rate. LNA-mediated *in vitro* miR-128a knockdown (KO) in differentiating murine ESCs/iPSCs increased cardiac TFs such as *Isl1*, *Sfrp5*, *and Hcn4* but reduced *Irx4* at the onset of cardiogenesis. MiR-128a overexpression (OE) caused opposite effects with diminished expression of *Isl1*, *Sfrp5*, *Nkx2.5*, and *Mef2c*, but increased expression of *Irx4*. Furthermore, miR-128a KO enhanced the frequency of *Isl1*-positive CPCs while the number of NkxCE-GFP CPCs was reduced. Upon miR-128a OE the NkxCE-GFP CPC frequency was increased. Later during *in vitro* differentiations, miR-128a KO led to increased expression of the ventricular CM marker *Myl2* accompanied by a reduced beating frequency of early CMs. Upon miR-128a OE, an increased expression of the nodal-type-like CM marker *Tnnt2*, *Myh6,* and *Shox2* was accompanied by increased beating frequencies. Neither ECs, nor SMCs were affected by miR-128a KO nor miR-128a OE (Figure 43).

Conclusively, our study demonstrated that miR-128a plays an important, so far unknown, role in early heart development and seemed to be involved in CPC specification and CPC differentiation into various CM subtypes. While important progress has been made in identifying the roles of miR-128a in physiological and pathophysiological processes in the postnatal heart, our results shed light on the regulatory functions of miR-128a during early cardiac development.

Deeper understanding of miR functions in embryonic heart development is of great interest since dysregulations of miRs have been linked to the development of congenital heart diseases (CHDs) (Hoelscher *et al.*, 2017) as well as acquired heart diseases (Zhou *et al.*, 2018). Thereby, miRs also represent promising targets for the treatment of many cardiac diseases. A detailed knowledge of cardiovascular development along with understanding homeostasis and disease will promote the invention of new agents to target miRs and enable safe application of cardiac regenerative therapies in the future.

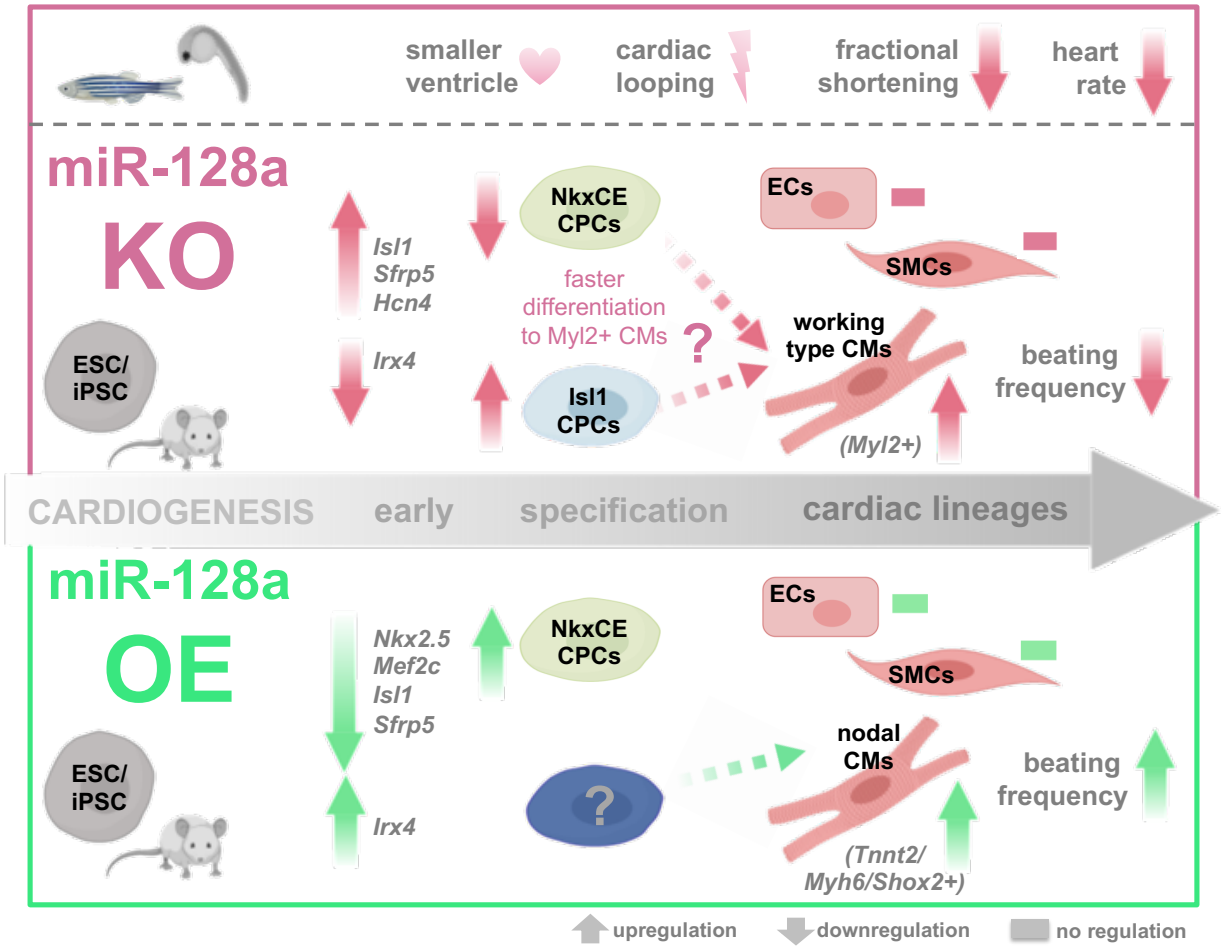

Figure 43 The role of miR-128a during *in vivo* and *in vitro* cardiac development. Morpholino (MO)-induced *in vivo* knockdown of miR-128a in zebrafish causes cardiac malformations including smaller ventricles and abnormal heart looping accompanied by reduced ventricular fractional shortening and heart rate. During murine *in vitro* differentiation, LNA-mediated miR-128a knockdown (KO) in differentiating ESCs/iPSCs increased cardiac transcription factors (TFs) such as *Isl1*, *Sfrp5*, and *Hcn4* but reduced *Irx4* at the onset of cardiogenesis; upregulated *Isl1*-positive CPCs, whereas NkxCE-GFP-positive CPCs were downregulated and increased the expression of the ventricular CM marker *Myl2* accompanied by a reduced beating frequency of early CMs. Overexpression (OE) of miR-128a diminished the expression of *Isl1, Sfrp5, Nkx2.5*, and *Mef2c*, but increased *Irx4*; enhanced the NkxCE-GFP CPC population as well as favored nodal-type-like CMs marked by *Tnnt2, Myh6,* and *Shox2* accompanied by increased beating frequencies. Neither EC nor SMC marker expression was affected by miR-128a KO and miR-128a OE. Parts of the figure were created with BioRender.com. Figure 6 from Hoelscher *et al.* miR-128a Acts as a Regulator in Cardiac Development by Modulating Differentiation of Cardiac Progenitor Cell Populations. Int. J. Mol. Sci. 2020, 21, 1158; doi:10.3390/ijms210311 (Hoelscher *et al.*, 2020).

6 References

Ahler, E., Sullivan, W. J., Cass, A., Braas, D., York, A. G., Bensinger, S. J., Graeber, T. G., and Christofk, H. R. (2013). Doxycycline alters metabolism and proliferation of human cell lines. *PLoS One, 8*(5), e64561. doi:10.1371/journal.pone.0064561

Ahn, H. W., Morin, R. D., Zhao, H., Harris, R. A., Coarfa, C., Chen, Z. J., Milosavljevic, A., Marra, M. A., and Rajkovic, A. (2010). MicroRNA transcriptome in the newborn mouse ovaries determined by massive parallel sequencing. *Mol Hum Reprod, 16*(7), 463-471. doi:10.1093/molehr/gaq017

Ai, F., Zhang, Y., and Peng, B. (2016). miR-20a regulates proliferation, differentiation and apoptosis in P19 cell model of cardiac differentiation by targeting Smoothened. *Biol Open, 5*(9), 1260-1265. doi:10.1242/bio.019182

Albinsson, S., Suarez, Y., Skoura, A., Offermanns, S., Miano, J. M., and Sessa, W. C. (2010). MicroRNAs are necessary for vascular smooth muscle growth, differentiation, and function. *Arterioscler Thromb Vasc Biol, 30*(6), 1118-1126. doi:10.1161/ATVBAHA.109.200873

Andersen, P., Tampakakis, E., Jimenez, D. V., Kannan, S., Miyamoto, M., Shin, H. K., Saberi, A., Murphy, S., Sulistio, E., Chelko, S. P., and Kwon, C. (2018). Precardiac organoids form two heart fields via Bmp/Wnt signaling. *Nat Commun, 9*(1), 3140. doi:10.1038/s41467-018-05604-8

Andres-Delgado, L., and Mercader, N. (2016). Interplay between cardiac function and heart development. *Biochim Biophys Acta, 1863*(7 Pt B), 1707-1716. doi:10.1016/j.bbamcr.2016.03.004

Asano, T., Hanazono, Y., Ueda, Y., Muramatsu, S., Kume, A., Suemori, H., Suzuki, Y., Kondo, Y., Harii, K., Hasegawa, M., Nakatsuji, N., and Ozawa, K. (2002). Highly efficient gene transfer into primate embryonic stem cells with a simian lentivirus vector. *Mol Ther, 6*(2), 162-168. doi:10.1006/mthe.2002.0655

Bakkers, J. (2011). Zebrafish as a model to study cardiac development and human cardiac disease. *Cardiovasc Res, 91*(2), 279-288. doi:10.1093/cvr/cvr098

Banjo, T., Grajcarek, J., Yoshino, D., Osada, H., Miyasaka, K. Y., Kida, Y. S., Ueki, Y., Nagayama, K., Kawakami, K., Matsumoto, T., Sato, M., and Ogura, T. (2013). Haemodynamically dependent valvulogenesis of zebrafish heart is mediated by flow-dependent expression of miR-21. *Nat Commun, 4*, 1978. doi:10.1038/ncomms2978

Bar, M., Wyman, S. K., Fritz, B. R., Qi, J., Garg, K. S., Parkin, R. K., Kroh, E. M., Bendoraite, A., Mitchell, P. S., Nelson, A. M., Ruzzo, W. L., Ware, C., Radich, J. P., Gentleman, R., Ruohola-Baker, H., and Tewari, M. (2008). MicroRNA discovery and profiling in human embryonic stem cells by deep sequencing of small RNA libraries. *Stem Cells, 26*(10), 2496-2505. doi:10.1634/stemcells.2008-0356

Barbuti, A., and Robinson, R. B. (2015). Stem cell-derived nodal-like cardiomyocytes as a novel pharmacologic tool: insights from sinoatrial node development and function. *Pharmacol Rev, 67*(2), 368-388. doi:10.1124/pr.114.009597

Bartel, D. P. (2004). MicroRNAs: genomics, biogenesis, mechanism, and function. *Cell, 116*(2), 281-297. doi:10.1016/s0092-8674(04)00045-5

Bem, J., Grabowska, I., Daniszewski, M., Zawada, D., Czerwinska, A. M., Bugajski, L., Piwocka, K., Fogtman, A., and Ciemerych, M. A. (2018). Transient MicroRNA Expression Enhances Myogenic Potential of Mouse Embryonic Stem Cells. *Stem Cells, 36*(5), 655-670. doi:10.1002/stem.2772

Berezikov, E., Chung, W. J., Willis, J., Cuppen, E., and Lai, E. C. (2007). Mammalian mirtron genes. *Mol Cell, 28*(2), 328-336. doi:10.1016/j.molcel.2007.09.028

Bhayani, M. K., Calin, G. A., and Lai, S. Y. (2012). Functional relevance of miRNA sequences in human disease. *Mutat Res, 731*(1-2), 14-19. doi:10.1016/j.mrfmmm.2011.10.014

Bober, E., Lyons, G. E., Braun, T., Cossu, G., Buckingham, M., and Arnold, H. H. (1991). The muscle regulatory gene, Myf-6, has a biphasic pattern of expression during early mouse development. *J Cell Biol, 113*(6), 1255-1265. doi:10.1083/jcb.113.6.1255

Bock, C., Kiskinis, E., Verstappen, G., Gu, H., Boulting, G., Smith, Z. D., Ziller, M., Croft, G. F., Amoroso, M. W., Oakley, D. H., Gnirke, A., Eggan, K., and Meissner, A. (2011). Reference Maps of human ES and iPS cell variation enable high-throughput characterization of pluripotent cell lines. *Cell, 144*(3), 439-452. doi:10.1016/j.cell.2010.12.032

Bohnsack, M. T., Czaplinski, K., and Gorlich, D. (2004). Exportin 5 is a RanGTP-dependent dsRNA-binding protein that mediates nuclear export of pre-miRNAs. *RNA, 10*(2), 185-191. doi:10.1261/rna.5167604

Bondue, A., Tannler, S., Chiapparo, G., Chabab, S., Ramialison, M., Paulissen, C., Beck, B., Harvey, R., and Blanpain, C. (2011). Defining the earliest step of cardiovascular progenitor specification during embryonic stem cell differentiation. *J Cell Biol, 192*(5), 751-765. doi:10.1083/jcb.201007063

Boni, A., Urbanek, K., Nascimbene, A., Hosoda, T., Zheng, H., Delucchi, F., Amano, K., Gonzalez, A., Vitale, S., Ojaimi, C., Rizzi, R., Bolli, R., Yutzey, K. E., Rota, M., Kajstura, J., Anversa, P., and Leri, A. (2008). Notch1 regulates the fate of cardiac progenitor cells. *Proc Natl Acad Sci U S A, 105*(40), 15529-15534. doi:10.1073/pnas.0808357105

Brade, T., Pane, L. S., Moretti, A., Chien, K. R., and Laugwitz, K. L. (2013). Embryonic heart progenitors and cardiogenesis. *Cold Spring Harb Perspect Med, 3*(10), a013847. doi:10.1101/cshperspect.a013847

Brennecke, J., Hipfner, D. R., Stark, A., Russell, R. B., and Cohen, S. M. (2003). bantam encodes a developmentally regulated microRNA that controls cell proliferation and regulates the proapoptotic gene hid in Drosophila. *Cell, 113*(1), 25-36. doi:10.1016/s0092-8674(03)00231-9

Brown, D. R., Samsa, L. A., Qian, L., and Liu, J. (2016). Advances in the Study of Heart Development and Disease Using Zebrafish. *J Cardiovasc Dev Dis, 3*(2). doi:10.3390/jcdd3020013

Bruneau, B. G., Logan, M., Davis, N., Levi, T., Tabin, C. J., Seidman, J. G., and Seidman, C. E. (1999). Chamber-specific cardiac expression of Tbx5 and heart defects in Holt-Oram syndrome. *Dev Biol, 211*(1), 100-108. doi:10.1006/dbio.1999.9298

Bruno, I. G., Karam, R., Huang, L., Bhardwaj, A., Lou, C. H., Shum, E. Y., Song, H. W., Corbett, M. A., Gifford, W. D., Gecz, J., Pfaff, S. L., and Wilkinson, M. F. (2011). Identification of a microRNA that activates gene expression by repressing nonsense-mediated RNA decay. *Mol Cell, 42*(4), 500-510. doi:10.1016/j.molcel.2011.04.018

Brutsaert, D. L. (2003). Cardiac endothelial-myocardial signaling: its role in cardiac growth, contractile performance, and rhythmicity. *Physiol Rev, 83*(1), 59-115. doi:10.1152/physrev.00017.2002

Buckingham, M., Meilhac, S., and Zaffran, S. (2005). Building the mammalian heart from two sources of myocardial cells. *Nat Rev Genet, 6*(11), 826-835. doi:10.1038/nrg1710

Burridge, P. W., Matsa, E., Shukla, P., Lin, Z. C., Churko, J. M., Ebert, A. D., Lan, F., Diecke, S., Huber, B., Mordwinkin, N. M., Plews, J. R., Abilez, O. J., Cui, B., Gold, J. D., and Wu, J. C.

(2014). Chemically defined generation of human cardiomyocytes. *Nat Methods, 11*(8), 855-860. doi:10.1038/nmeth.2999

Cai, C. L., Liang, X., Shi, Y., Chu, P. H., Pfaff, S. L., Chen, J., and Evans, S. (2003). Isl1 identifies a cardiac progenitor population that proliferates prior to differentiation and contributes a majority of cells to the heart. *Dev Cell, 5*(6), 877-889. doi:10.1016/s1534-5807(03)00363-0

Callis, T. E., Pandya, K., Seok, H. Y., Tang, R. H., Tatsuguchi, M., Huang, Z. P., Chen, J. F., Deng, Z., Gunn, B., Shumate, J., Willis, M. S., Selzman, C. H., and Wang, D. Z. (2009). MicroRNA-208a is a regulator of cardiac hypertrophy and conduction in mice. *J Clin Invest, 119*(9), 2772-2786. doi:10.1172/JCI36154

Cambier, L., Plate, M., Sucov, H. M., and Pashmforoush, M. (2014). Nkx2-5 regulates cardiac growth through modulation of Wnt signaling by R-spondin3. *Development, 141*(15), 2959-2971. doi:10.1242/dev.103416

Cao, D., Cheung, H. H., and Chan, W. Y. (2019). Doxycycline Masks the Genuine Effect of the Doxycycline-Inducible Transgene by Promoting Dopaminergic Neuron Differentiation from Human Pluripotent Stem Cells. *Stem Cells Dev, 28*(13), 833-845. doi:10.1089/scd.2018.0209

Cao, H., Yang, C. S., and Rana, T. M. (2008). Evolutionary emergence of microRNAs in human embryonic stem cells. *PLoS One, 3*(7), e2820. doi:10.1371/journal.pone.0002820

Cascio, S., D'Andrea, A., Ferla, R., Surmacz, E., Gulotta, E., Amodeo, V., Bazan, V., Gebbia, N., and Russo, A. (2010). miR-20b modulates VEGF expression by targeting HIF-1 alpha and STAT3 in MCF-7 breast cancer cells. *J Cell Physiol, 224*(1), 242-249. doi:10.1002/jcp.22126

Chen, C., Ridzon, D., Lee, C. T., Blake, J., Sun, Y., and Strauss, W. M. (2007). Defining embryonic stem cell identity using differentiation-related microRNAs and their potential targets. *Mamm Genome, 18*(5), 316-327. doi:10.1007/s00335-007-9032-6

Chen, C. Z., Li, L., Lodish, H. F., and Bartel, D. P. (2004). MicroRNAs modulate hematopoietic lineage differentiation. *Science, 303*(5654), 83-86. doi:10.1126/science.1091903

Chen, J., and Wang, D. Z. (2012). microRNAs in cardiovascular development. *J Mol Cell Cardiol, 52*(5), 949-957. doi:10.1016/j.yjmcc.2012.01.012

Chen, J. F., Mandel, E. M., Thomson, J. M., Wu, Q., Callis, T. E., Hammond, S. M., Conlon, F. L., and Wang, D. Z. (2006). The role of microRNA-1 and microRNA-133 in skeletal muscle proliferation and differentiation. *Nat Genet, 38*(2), 228-233. doi:10.1038/ng1725

Chen, J. F., Murchison, E. P., Tang, R., Callis, T. E., Tatsuguchi, M., Deng, Z., Rojas, M., Hammond, S. M., Schneider, M. D., Selzman, C. H., Meissner, G., Patterson, C., Hannon, G. J., and Wang, D. Z. (2008). Targeted deletion of Dicer in the heart leads to dilated cardiomyopathy and heart failure. *Proc Natl Acad Sci U S A, 105*(6), 2111-2116. doi:10.1073/pnas.0710228105

Chen, P. Y., Manninga, H., Slanchev, K., Chien, M., Russo, J. J., Ju, J., Sheridan, R., John, B., Marks, D. S., Gaidatzis, D., Sander, C., Zavolan, M., and Tuschl, T. (2005). The developmental miRNA profiles of zebrafish as determined by small RNA cloning. *Genes Dev, 19*(11), 1288-1293. doi:10.1101/gad.1310605

Chen, Z. Y., Chen, F., Cao, N., Zhou, Z. W., and Yang, H. T. (2017). miR-142-3p Contributes to Early Cardiac Fate Decision of Embryonic Stem Cells. *Stem Cells Int, 2017*, 1769298. doi:10.1155/2017/1769298

Chiavacci, E., Dolfi, L., Verduci, L., Meghini, F., Gestri, G., Evangelista, A. M., Wilson, S. W., Cremisi, F., and Pitto, L. (2012). MicroRNA 218 mediates the effects of Tbx5a over-expression on zebrafish heart development. *PLoS One, 7*(11), e50536. doi:10.1371/journal.pone.0050536

Choi, P. S., Zakhary, L., Choi, W. Y., Caron, S., Alvarez-Saavedra, E., Miska, E. A., McManus, M., Harfe, B., Giraldez, A. J., Horvitz, H. R., Schier, A. F., and Dulac, C. (2008). Members of the miRNA-200 family regulate olfactory neurogenesis. *Neuron, 57*(1), 41-55. doi:10.1016/j.neuron.2007.11.018

Ciafre, S. A., Galardi, S., Mangiola, A., Ferracin, M., Liu, C. G., Sabatino, G., Negrini, M., Maira, G., Croce, C. M., and Farace, M. G. (2005). Extensive modulation of a set of microRNAs in primary glioblastoma. *Biochem Biophys Res Commun, 334*(4), 1351-1358. doi:10.1016/j.bbrc.2005.07.030

Clark, C. D., Zhang, B., Lee, B., Evans, S. I., Lassar, A. B., and Lee, K. H. (2013). Evolutionary conservation of Nkx2.5 autoregulation in the second heart field. *Dev Biol, 374*(1), 198-209. doi:10.1016/j.ydbio.2012.11.007

Cohen, E. D., Tian, Y., and Morrisey, E. E. (2008). Wnt signaling: an essential regulator of cardiovascular differentiation, morphogenesis and progenitor self-renewal. *Development, 135*(5), 789-798. doi:10.1242/dev.016865

Cohen-Barak, O., Yi, Z., Hagiwara, N., Monzen, K., Komuro, I., and Brilliant, M. H. (2003). Sox6 regulation of cardiac myocyte development. *Nucleic Acids Res, 31*(20), 5941-5948. doi:10.1093/nar/gkg807

Colombo, S., de Sena-Tomas, C., George, V., Werdich, A. A., Kapur, S., MacRae, C. A., and Targoff, K. L. (2018). Nkx genes establish second heart field cardiomyocyte progenitors at the arterial pole and pattern the venous pole through Isl1 repression. *Development, 145*(3). doi:10.1242/dev.161497

Cordes, K. R., and Srivastava, D. (2009). MicroRNA regulation of cardiovascular development. *Circ Res, 104*(6), 724-732. doi:10.1161/CIRCRESAHA.108.192872

Cordes, K. R., Srivastava, D., and Ivey, K. N. (2010). MicroRNAs in cardiac development. *Pediatr Cardiol, 31*(3), 349-356. doi:10.1007/s00246-010-9639-3

D'Amico, L., Scott, I. C., Jungblut, B., and Stainier, D. Y. (2007). A mutation in zebrafish hmgcr1b reveals a role for isoprenoids in vertebrate heart-tube formation. *Curr Biol, 17*(3), 252-259. doi:10.1016/j.cub.2006.12.023

Davis, H. E., Morgan, J. R., and Yarmush, M. L. (2002). Polybrene increases retrovirus gene transfer efficiency by enhancing receptor-independent virus adsorption on target cell membranes. *Biophys Chem, 97*(2-3), 159-172. doi:10.1016/s0301-4622(02)00057-1

Davis, H. E., Rosinski, M., Morgan, J. R., and Yarmush, M. L. (2004). Charged polymers modulate retrovirus transduction via membrane charge neutralization and virus aggregation. *Biophys J, 86*(2), 1234-1242. doi:10.1016/S0006-3495(04)74197-1

de la Pompa, J. L., and Epstein, J. A. (2012). Coordinating tissue interactions: Notch signaling in cardiac development and disease. *Dev Cell, 22*(2), 244-254. doi:10.1016/j.devcel.2012.01.014

Desbaillets, I., Ziegler, U., Groscurth, P., and Gassmann, M. (2000). Embryoid bodies: an in vitro model of mouse embryogenesis. *Exp Physiol, 85*(6), 645-651.

Dodou, E., Verzi, M. P., Anderson, J. P., Xu, S. M., and Black, B. L. (2004). Mef2c is a direct transcriptional target of ISL1 and GATA factors in the anterior heart field during mouse embryonic development. *Development, 131*(16), 3931-3942. doi:10.1242/dev.01256

Domian, I. J., Chiravuri, M., van der Meer, P., Feinberg, A. W., Shi, X., Shao, Y., Wu, S. M., Parker, K. K., and Chien, K. R. (2009). Generation of functional ventricular heart muscle from mouse ventricular progenitor cells. *Science, 326*(5951), 426-429. doi:10.1126/science.1177350

Doppler, S. A., Werner, A., Barz, M., Lahm, H., Deutsch, M. A., Dressen, M., Schiemann, M., Voss, B., Gregoire, S., Kuppusamy, R., Wu, S. M., Lange, R., and Krane, M. (2014). Myeloid

zinc finger 1 (Mzf1) differentially modulates murine cardiogenesis by interacting with an Nkx2.5 cardiac enhancer. *PLoS One, 9*(12), e113775. doi:10.1371/journal.pone.0113775

Dorn, T., Goedel, A., Lam, J. T., Haas, J., Tian, Q., Herrmann, F., Bundschu, K., Dobreva, G., Schiemann, M., Dirschinger, R., Guo, Y., Kuhl, S. J., Sinnecker, D., Lipp, P., Laugwitz, K. L., Kuhl, M., and Moretti, A. (2015). Direct nkx2-5 transcriptional repression of isl1 controls cardiomyocyte subtype identity. *Stem Cells, 33*(4), 1113-1129. doi:10.1002/stem.1923

Duelen, R., and Sampaolesi, M. (2017). Stem Cell Technology in Cardiac Regeneration: A Pluripotent Stem Cell Promise. *EBioMedicine, 16*, 30-40. doi:10.1016/j.ebiom.2017.01.029

Fish, J. E., Wythe, J. D., Xiao, T., Bruneau, B. G., Stainier, D. Y., Srivastava, D., and Woo, S. (2011). A Slit/miR-218/Robo regulatory loop is required during heart tube formation in zebrafish. *Development, 138*(7), 1409-1419. doi:10.1242/dev.060046

Fishman, M. C., and Chien, K. R. (1997). Fashioning the vertebrate heart: earliest embryonic decisions. *Development, 124*(11), 2099-2117.

Friedman, R. C., Farh, K. K., Burge, C. B., and Bartel, D. P. (2009). Most mammalian mRNAs are conserved targets of microRNAs. *Genome Res, 19*(1), 92-105. doi:10.1101/gr.082701.108

Fujii, M., Sakaguchi, A., Kamata, R., Nagao, M., Kikuchi, Y., Evans, S. M., Yoshizumi, M., Shimono, A., Saga, Y., and Kokubo, H. (2017). Sfrp5 identifies murine cardiac progenitors for all myocardial structures except for the right ventricle. *Nat Commun, 8*, 14664. doi:10.1038/ncomms14664

Gao, R., Liang, X., Cheedipudi, S., Cordero, J., Jiang, X., Zhang, Q., Caputo, L., Gunther, S., Kuenne, C., Ren, Y., Bhattacharya, S., Yuan, X., Barreto, G., Chen, Y., Braun, T., Evans, S. M., Sun, Y., and Dobreva, G. (2019). Pioneering function of Isl1 in the epigenetic control of cardiomyocyte cell fate. *Cell Res, 29*(6), 486-501. doi:10.1038/s41422-019-0168-1

Garrick, D., Fiering, S., Martin, D. I., and Whitelaw, E. (1998). Repeat-induced gene silencing in mammals. *Nat Genet, 18*(1), 56-59. doi:10.1038/ng0198-56

Gessert, S., and Kuhl, M. (2010). The multiple phases and faces of wnt signaling during cardiac differentiation and development. *Circ Res, 107*(2), 186-199. doi:10.1161/CIRCRESAHA.110.221531

Graham, F. L., Smiley, J., Russell, W. C., and Nairn, R. (1977). Characteristics of a human cell line transformed by DNA from human adenovirus type 5. *J Gen Virol, 36*(1), 59-74. doi:10.1099/0022-1317-36-1-59

Grant, M. G., Patterson, V. L., Grimes, D. T., and Burdine, R. D. (2017). Modeling Syndromic Congenital Heart Defects in Zebrafish. *Curr Top Dev Biol, 124*, 1-40. doi:10.1016/bs.ctdb.2016.11.010

Gropp, M., Itsykson, P., Singer, O., Ben-Hur, T., Reinhartz, E., Galun, E., and Reubinoff, B. E. (2003). Stable genetic modification of human embryonic stem cells by lentiviral vectors. *Mol Ther, 7*(2), 281-287. doi:10.1016/s1525-0016(02)00047-3

Gu, H., Liu, Z., and Zhou, L. (2017). Roles of miR-17-92 Cluster in Cardiovascular Development and Common Diseases. *Biomed Res Int, 2017*, 9102909. doi:10.1155/2017/9102909

Guess, M. G., Barthel, K. K., Harrison, B. C., and Leinwand, L. A. (2015). miR-30 family microRNAs regulate myogenic differentiation and provide negative feedback on the microRNA pathway. *PLoS One, 10*(2), e0118229. doi:10.1371/journal.pone.0118229

Harrison, T., Graham, F., and Williams, J. (1977). Host-range mutants of adenovirus type 5 defective for growth in HeLa cells. *Virology, 77*(1), 319-329. doi:10.1016/0042-6822(77)90428-7

Harvey, R. P. (2002). Patterning the vertebrate heart. *Nat Rev Genet, 3*(7), 544-556. doi:10.1038/nrg843

He, J. Q., Ma, Y., Lee, Y., Thomson, J. A., and Kamp, T. J. (2003). Human embryonic stem cells develop into multiple types of cardiac myocytes: action potential characterization. *Circ Res, 93*(1), 32-39. doi:10.1161/01.RES.0000080317.92718.99

Herbst, F., Ball, C. R., Tuorto, F., Nowrouzi, A., Wang, W., Zavidij, O., Dieter, S. M., Fessler, S., van der Hoeven, F., Kloz, U., Lyko, F., Schmidt, M., von Kalle, C., and Glimm, H. (2012). Extensive methylation of promoter sequences silences lentiviral transgene expression during stem cell differentiation in vivo. *Mol Ther, 20*(5), 1014-1021. doi:10.1038/mt.2012.46

Hoelscher, S. C., Doppler, S. A., Dressen, M., Lahm, H., Lange, R., and Krane, M. (2017). MicroRNAs: pleiotropic players in congenital heart disease and regeneration. *J Thorac Dis, 9*(Suppl 1), S64-S81. doi:10.21037/jtd.2017.03.149

Hoelscher, S. C., Stich, T., Diehm, A., Lahm, H., Dressen, M., Zhang, Z., Neb, I., Aherrahrou, Z., Erdmann, J., Schunkert, H., Santamaria, G., Cuda, G., Gilsbach, R., Hein, L., Lange, R., Hassel, D., Krane, M., and Doppler, S. A. (2020). miR-128a Acts as a Regulator in Cardiac Development by Modulating Differentiation of Cardiac Progenitor Cell Populations. *Int J Mol Sci, 21*(3). doi:10.3390/ijms21031158

Holtzinger, A., Rosenfeld, G. E., and Evans, T. (2010). Gata4 directs development of cardiac-inducing endoderm from ES cells. *Dev Biol, 337*(1), 63-73. doi:10.1016/j.ydbio.2009.10.003

Hopfl, G., Gassmann, M., and Desbaillets, I. (2004). Differentiating embryonic stem cells into embryoid bodies. *Methods Mol Biol, 254*, 79-98. doi:10.1385/1-59259-741-6:079

Houbaviy, H. B., Murray, M. F., and Sharp, P. A. (2003). Embryonic stem cell-specific MicroRNAs. *Dev Cell, 5*(2), 351-358.

Huang, W., Feng, Y., Liang, J., Yu, H., Wang, C., Wang, B., Wang, M., Jiang, L., Meng, W., Cai, W., Medvedovic, M., Chen, J., Paul, C., Davidson, W. S., Sadayappan, S., Stambrook, P. J., Yu, X. Y., and Wang, Y. (2018). Loss of microRNA-128 promotes cardiomyocyte proliferation and heart regeneration. *Nat Commun, 9*(1), 700. doi:10.1038/s41467-018-03019-z

Huang, X., and Wu, S. M. (2010). Isolation and functional characterization of pluripotent stem cell-derived cardiac progenitor cells. *Curr Protoc Stem Cell Biol, Chapter 1*, Unit 1F 10. doi:10.1002/9780470151808.sc01f10s14

Huisken, J., Swoger, J., Del Bene, F., Wittbrodt, J., and Stelzer, E. H. (2004). Optical sectioning deep inside live embryos by selective plane illumination microscopy. *Science, 305*(5686), 1007-1009. doi:10.1126/science.1100035

Ivanovitch, K., Esteban, I., and Torres, M. (2017). Growth and Morphogenesis during Early Heart Development in Amniotes. *J Cardiovasc Dev Dis, 4*(4). doi:10.3390/jcdd4040020

Ivey, K. N., Muth, A., Arnold, J., King, F. W., Yeh, R. F., Fish, J. E., Hsiao, E. C., Schwartz, R. J., Conklin, B. R., Bernstein, H. S., and Srivastava, D. (2008). MicroRNA regulation of cell lineages in mouse and human embryonic stem cells. *Cell Stem Cell, 2*(3), 219-229. doi:10.1016/j.stem.2008.01.016

Jensen, B., Wang, T., Christoffels, V. M., and Moorman, A. F. (2013). Evolution and development of the building plan of the vertebrate heart. *Biochim Biophys Acta, 1833*(4), 783-794. doi:10.1016/j.bbamcr.2012.10.004

Jin, H. Y., Gonzalez-Martin, A., Miletic, A. V., Lai, M., Knight, S., Sabouri-Ghomi, M., Head, S. R., Macauley, M. S., Rickert, R. C., and Xiao, C. (2015). Transfection of microRNA Mimics Should Be Used with Caution. *Front Genet, 6*, 340. doi:10.3389/fgene.2015.00340

Johnston, R. J., and Hobert, O. (2003). A microRNA controlling left/right neuronal asymmetry in Caenorhabditis elegans. *Nature, 426*(6968), 845-849. doi:10.1038/nature02255

Jovicic, A., and Gitler, A. D. (2017). Distinct repertoires of microRNAs present in mouse astrocytes compared to astrocyte-secreted exosomes. *PLoS One, 12*(2), e0171418. doi:10.1371/journal.pone.0171418

Kamath, S. G., Chen, N., Enkemann, S. A., and Sanchez-Ramos, J. (2005). Transcriptional profile of NeuroD expression in a human fetal astroglial cell line. *Gene Expr, 12*(2), 123-136. doi:10.3727/000000005783992133

Kelly, R. G., Buckingham, M. E., and Moorman, A. F. (2014). Heart fields and cardiac morphogenesis. *Cold Spring Harb Perspect Med, 4*(10). doi:10.1101/cshperspect.a015750

Ketley, A., Warren, A., Holmes, E., Gering, M., Aboobaker, A. A., and Brook, J. D. (2013). The miR-30 microRNA family targets smoothened to regulate hedgehog signalling in zebrafish early muscle development. *PLoS One, 8*(6), e65170. doi:10.1371/journal.pone.0065170

Khvorova, A., Reynolds, A., and Jayasena, S. D. (2003). Functional siRNAs and miRNAs exhibit strand bias. *Cell, 115*(2), 209-216. doi:10.1016/s0092-8674(03)00801-8

Kim, K. J., Kim, H. E., Lee, K. H., Han, W., Yi, M. J., Jeong, J., and Oh, B. H. (2004). Two-promoter vector is highly efficient for overproduction of protein complexes. *Protein Sci, 13*(6), 1698-1703. doi:10.1110/ps.04644504

Kim, V. N., Han, J., and Siomi, M. C. (2009). Biogenesis of small RNAs in animals. *Nat Rev Mol Cell Biol, 10*(2), 126-139. doi:10.1038/nrm2632

Kobayashi, N., Rivas-Carrillo, J. D., Soto-Gutierrez, A., Fukazawa, T., Chen, Y., Navarro-Alvarez, N., and Tanaka, N. (2005). Gene delivery to embryonic stem cells. *Birth Defects Res C Embryo Today, 75*(1), 10-18. doi:10.1002/bdrc.20031

Kosaka, Y., Kobayashi, N., Fukazawa, T., Totsugawa, T., Maruyama, M., Yong, C., Arata, T., Ikeda, H., Kobayashi, K., Ueda, T., Kurabayashi, Y., and Tanaka, N. (2004). Lentivirus-based gene delivery in mouse embryonic stem cells. *Artif Organs, 28*(3), 271-277. doi:10.1111/j.1525-1594.2004.47297.x

Kozomara, A., and Griffiths-Jones, S. (2014). miRBase: annotating high confidence microRNAs using deep sequencing data. *Nucleic Acids Res, 42*(Database issue), D68-73. doi:10.1093/nar/gkt1181

Krichevsky, A. M., King, K. S., Donahue, C. P., Khrapko, K., and Kosik, K. S. (2003). A microRNA array reveals extensive regulation of microRNAs during brain development. *RNA, 9*(10), 1274-1281. doi:10.1261/rna.5980303

Krichevsky, A. M., Sonntag, K. C., Isacson, O., and Kosik, K. S. (2006). Specific microRNAs modulate embryonic stem cell-derived neurogenesis. *Stem Cells, 24*(4), 857-864. doi:10.1634/stemcells.2005-0441

Lagos-Quintana, M., Rauhut, R., Lendeckel, W., and Tuschl, T. (2001). Identification of novel genes coding for small expressed RNAs. *Science, 294*(5543), 853-858. doi:10.1126/science.1064921

Lagos-Quintana, M., Rauhut, R., Yalcin, A., Meyer, J., Lendeckel, W., and Tuschl, T. (2002). Identification of tissue-specific microRNAs from mouse. *Curr Biol, 12*(9), 735-739. doi:10.1016/s0960-9822(02)00809-6

Lau, N. C., Lim, L. P., Weinstein, E. G., and Bartel, D. P. (2001). An abundant class of tiny RNAs with probable regulatory roles in Caenorhabditis elegans. *Science, 294*(5543), 858-862. doi:10.1126/science.1065062

Laugwitz, K. L., Moretti, A., Caron, L., Nakano, A., and Chien, K. R. (2008). Islet1 cardiovascular progenitors: a single source for heart lineages? *Development, 135*(2), 193-205. doi:10.1242/dev.001883

Laurent, L. C., Chen, J., Ulitsky, I., Mueller, F. J., Lu, C., Shamir, R., Fan, J. B., and Loring, J. F. (2008). Comprehensive microRNA profiling reveals a unique human embryonic stem cell signature dominated by a single seed sequence. *Stem Cells, 26*(6), 1506-1516. doi:10.1634/stemcells.2007-1081

Lee, R. C., Feinbaum, R. L., and Ambros, V. (1993). The C. elegans heterochronic gene lin-4 encodes small RNAs with antisense complementarity to lin-14. *Cell, 75*(5), 843-854. doi:10.1016/0092-8674(93)90529-y

Lee, Y., Jeon, K., Lee, J. T., Kim, S., and Kim, V. N. (2002). MicroRNA maturation: stepwise processing and subcellular localization. *EMBO J, 21*(17), 4663-4670. doi:10.1093/emboj/cdf476

Lee, Y., Kim, M., Han, J., Yeom, K. H., Lee, S., Baek, S. H., and Kim, V. N. (2004). MicroRNA genes are transcribed by RNA polymerase II. *EMBO J, 23*(20), 4051-4060. doi:10.1038/sj.emboj.7600385

Li, G., Plonowska, K., Kuppusamy, R., Sturzu, A., and Wu, S. M. (2015). Identification of cardiovascular lineage descendants at single-cell resolution. *Development, 142*(5), 846-857. doi:10.1242/dev.116897

Li, M., Fu, W., Wo, L., Shu, X., Liu, F., and Li, C. (2013). miR-128 and its target genes in tumorigenesis and metastasis. *Exp Cell Res, 319*(20), 3059-3064. doi:10.1016/j.yexcr.2013.07.031

Li, M., Hu, X., Zhu, J., Zhu, C., Zhu, S., Liu, X., Xu, J., Han, S., and Yu, Z. (2014). Overexpression of miR-19b impairs cardiac development in zebrafish by targeting ctnnb1. *Cell Physiol Biochem, 33*(6), 1988-2002. doi:10.1159/000362975

Li, S., Chen, L. X., Peng, X. H., Wang, C., Qin, B. Y., Tan, D., Han, C. X., Yang, H., Ren, X. N., Liu, F., Xu, C. H., and Zhou, X. H. (2018). Overview of the reporter genes and reporter mouse models. *Animal Model Exp Med, 1*(1), 29-35. doi:10.1002/ame2.12008

Li, S., Flisikowska, T., Kurome, M., Zakhartchenko, V., Kessler, B., Saur, D., Kind, A., Wolf, E., Flisikowski, K., and Schnieke, A. (2014). Dual fluorescent reporter pig for Cre recombination: transgene placement at the ROSA26 locus. *PLoS One, 9*(7), e102455. doi:10.1371/journal.pone.0102455

Lien, C. L., Wu, C., Mercer, B., Webb, R., Richardson, J. A., and Olson, E. N. (1999). Control of early cardiac-specific transcription of Nkx2-5 by a GATA-dependent enhancer. *Development, 126*(1), 75-84.

Lin, C. C., Chang, Y. M., Pan, C. T., Chen, C. C., Ling, L., Tsao, K. C., Yang, R. B., and Li, W. H. (2014). Functional evolution of cardiac microRNAs in heart development and functions. *Mol Biol Evol, 31*(10), 2722-2734. doi:10.1093/molbev/msu217

Liu, J., and Stainier, D. Y. (2012). Zebrafish in the study of early cardiac development. *Circ Res, 110*(6), 870-874. doi:10.1161/CIRCRESAHA.111.246504

Maherali, N., Ahfeldt, T., Rigamonti, A., Utikal, J., Cowan, C., and Hochedlinger, K. (2008). A high-efficiency system for the generation and study of human induced pluripotent stem cells. *Cell Stem Cell, 3*(3), 340-345. doi:10.1016/j.stem.2008.08.003

Malizia, A. P., and Wang, D. Z. (2011). MicroRNAs in cardiomyocyte development. *Wiley Interdiscip Rev Syst Biol Med, 3*(2), 183-190. doi:10.1002/wsbm.111

Marvin, M. J., Di Rocco, G., Gardiner, A., Bush, S. M., and Lassar, A. B. (2001). Inhibition of Wnt activity induces heart formation from posterior mesoderm. *Genes Dev, 15*(3), 316-327. doi:10.1101/gad.855501

Masui, S., Shimosato, D., Toyooka, Y., Yagi, R., Takahashi, K., and Niwa, H. (2005). An efficient system to establish multiple embryonic stem cell lines carrying an inducible expression unit. *Nucleic Acids Res, 33*(4), e43. doi:10.1093/nar/gni043

Meyer-Ficca, M. L., Meyer, R. G., Kaiser, H., Brack, A. R., Kandolf, R., and Kupper, J. H. (2004). Comparative analysis of inducible expression systems in transient transfection studies. *Anal Biochem, 334*(1), 9-19. doi:10.1016/j.ab.2004.07.011

Mignone, J. L., Kreutziger, K. L., Paige, S. L., and Murry, C. E. (2010). Cardiogenesis from human embryonic stem cells. *Circ J, 74*(12), 2517-2526. doi:10.1253/circj.cj-10-0958

Mizuguchi, H., and Hayakawa, T. (2001). Characteristics of adenovirus-mediated tetracycline-controllable expression system. *Biochim Biophys Acta, 1568*(1), 21-29. doi:10.1016/s0304-4165(01)00195-7

Molkentin, J. D., Lin, Q., Duncan, S. A., and Olson, E. N. (1997). Requirement of the transcription factor GATA4 for heart tube formation and ventral morphogenesis. *Genes Dev, 11*(8), 1061-1072. doi:10.1101/gad.11.8.1061

Moretti, A., Caron, L., Nakano, A., Lam, J. T., Bernshausen, A., Chen, Y., Qyang, Y., Bu, L., Sasaki, M., Martin-Puig, S., Sun, Y., Evans, S. M., Laugwitz, K. L., and Chien, K. R. (2006). Multipotent embryonic isl1+ progenitor cells lead to cardiac, smooth muscle, and endothelial cell diversification. *Cell, 127*(6), 1151-1165. doi:10.1016/j.cell.2006.10.029

Morin, R. D., O'Connor, M. D., Griffith, M., Kuchenbauer, F., Delaney, A., Prabhu, A. L., Zhao, Y., McDonald, H., Zeng, T., Hirst, M., Eaves, C. J., and Marra, M. A. (2008). Application of massively parallel sequencing to microRNA profiling and discovery in human embryonic stem cells. *Genome Res, 18*(4), 610-621. doi:10.1101/gr.7179508

Moses, K. A., DeMayo, F., Braun, R. M., Reecy, J. L., and Schwartz, R. J. (2001). Embryonic expression of an Nkx2-5/Cre gene using ROSA26 reporter mice. *Genesis, 31*(4), 176-180. doi:10.1002/gene.10022

Moullan, N., Mouchiroud, L., Wang, X., Ryu, D., Williams, E. G., Mottis, A., Jovaisaite, V., Frochaux, M. V., Quiros, P. M., Deplancke, B., Houtkooper, R. H., and Auwerx, J. (2015). Tetracyclines Disturb Mitochondrial Function across Eukaryotic Models: A Call for Caution in Biomedical Research. *Cell Rep, 10*(10), 1681-1691. doi:10.1016/j.celrep.2015.02.034

Munoz, P., Toscano, M. G., Real, P. J., Benabdellah, K., Cobo, M., Bueno, C., Ramos-Mejia, V., Menendez, P., Anderson, P., and Martin, F. (2012). Specific marking of hESCs-derived

hematopoietic lineage by WAS-promoter driven lentiviral vectors. *PLoS One, 7*(6), e39091. doi:10.1371/journal.pone.0039091

Muzumdar, M. D., Tasic, B., Miyamichi, K., Li, L., and Luo, L. (2007). A global double-fluorescent Cre reporter mouse. *Genesis, 45*(9), 593-605. doi:10.1002/dvg.20335

Nakashima, Y., Yanez, D. A., Touma, M., Nakano, H., Jaroszewicz, A., Jordan, M. C., Pellegrini, M., Roos, K. P., and Nakano, A. (2014). Nkx2-5 suppresses the proliferation of atrial myocytes and conduction system. *Circ Res, 114*(7), 1103-1113. doi:10.1161/CIRCRESAHA.114.303219

Naldini, L., Blomer, U., Gage, F. H., Trono, D., and Verma, I. M. (1996). Efficient transfer, integration, and sustained long-term expression of the transgene in adult rat brains injected with a lentiviral vector. *Proc Natl Acad Sci U S A, 93*(21), 11382-11388. doi:10.1073/pnas.93.21.11382

Nelson, D. O., Lalit, P. A., Biermann, M., Markandeya, Y. S., Capes, D. L., Addesso, L., Patel, G., Han, T., John, M. C., Powers, P. A., Downs, K. M., Kamp, T. J., and Lyons, G. E. (2016). Irx4 Marks a Multipotent, Ventricular-Specific Progenitor Cell. *Stem Cells, 34*(12), 2875-2888. doi:10.1002/stem.2486

Newman, A. M., and Cooper, J. B. (2010). Lab-specific gene expression signatures in pluripotent stem cells. *Cell Stem Cell, 7*(2), 258-262. doi:10.1016/j.stem.2010.06.016

Nguyen, C. T., Lu, Q., Wang, Y., and Chen, J. N. (2008). Zebrafish as a model for cardiovascular development and disease. *Drug Discov Today Dis Models, 5*(3), 135-140. doi:10.1016/j.ddmod.2009.02.003

Nguyen, H. T., Bodmer, R., Abmayr, S. M., McDermott, J. C., and Spoerel, N. A. (1994). D-mef2: a Drosophila mesoderm-specific MADS box-containing gene with a biphasic expression profile during embryogenesis. *Proc Natl Acad Sci U S A, 91*(16), 7520-7524. doi:10.1073/pnas.91.16.7520

Noseda, M., Peterkin, T., Simoes, F. C., Patient, R., and Schneider, M. D. (2011). Cardiopoietic factors: extracellular signals for cardiac lineage commitment. *Circ Res, 108*(1), 129-152. doi:10.1161/CIRCRESAHA.110.223792

Nothjunge, S., Nuhrenberg, T. G., Gruning, B. A., Doppler, S. A., Preissl, S., Schwaderer, M., Rommel, C., Krane, M., Hein, L., and Gilsbach, R. (2017). DNA methylation signatures follow preformed chromatin compartments in cardiac myocytes. *Nat Commun, 8*(1), 1667. doi:10.1038/s41467-017-01724-9

Pedrazzini, T. (2007). Control of cardiogenesis by the notch pathway. *Trends Cardiovasc Med, 17*(3), 83-90. doi:10.1016/j.tcm.2007.01.003

Persengiev, S. P., Kondova, II, and Bontrop, R. E. (2012). The Impact of MicroRNAs on Brain Aging and Neurodegeneration. *Curr Gerontol Geriatr Res, 2012*, 359369. doi:10.1155/2012/359369

Pfeifer, A., Ikawa, M., Dayn, Y., and Verma, I. M. (2002). Transgenesis by lentiviral vectors: lack of gene silencing in mammalian embryonic stem cells and preimplantation embryos. *Proc Natl Acad Sci U S A, 99*(4), 2140-2145. doi:10.1073/pnas.251682798

Pfeiffer, M. J., Quaranta, R., Piccini, I., Fell, J., Rao, J., Ropke, A., Seebohm, G., and Greber, B. (2018). Cardiogenic programming of human pluripotent stem cells by dose-controlled activation of EOMES. *Nat Commun, 9*(1), 440. doi:10.1038/s41467-017-02812-6

Picot, J., Guerin, C. L., Le Van Kim, C., and Boulanger, C. M. (2012). Flow cytometry: retrospective, fundamentals and recent instrumentation. *Cytotechnology, 64*(2), 109-130. doi:10.1007/s10616-011-9415-0

Pierpont, M. E., Basson, C. T., Benson, D. W., Jr., Gelb, B. D., Giglia, T. M., Goldmuntz, E., McGee, G., Sable, C. A., Srivastava, D., Webb, C. L., and American Heart Association Congenital Cardiac Defects Committee, C. o. C. D. i. t. Y. (2007). Genetic basis for congenital heart defects: current knowledge: a scientific statement from the American Heart Association Congenital Cardiac Defects Committee, Council on Cardiovascular Disease in the Young: endorsed by the American Academy of Pediatrics. *Circulation, 115*(23), 3015-3038. doi:10.1161/CIRCULATIONAHA.106.183056

Poon, K. L., and Brand, T. (2013). The zebrafish model system in cardiovascular research: A tiny fish with mighty prospects. *Glob Cardiol Sci Pract, 2013*(1), 9-28. doi:10.5339/gcsp.2013.4

Pritchard, C. C., Cheng, H. H., and Tewari, M. (2012). MicroRNA profiling: approaches and considerations. *Nat Rev Genet, 13*(5), 358-369. doi:10.1038/nrg3198

Rana, M. S., Christoffels, V. M., and Moorman, A. F. (2013). A molecular and genetic outline of cardiac morphogenesis. *Acta Physiol (Oxf), 207*(4), 588-615. doi:10.1111/apha.12061

Razak, S. R., Ueno, K., Takayama, N., Nariai, N., Nagasaki, M., Saito, R., Koso, H., Lai, C. Y., Murakami, M., Tsuji, K., Michiue, T., Nakauchi, H., Otsu, M., and Watanabe, S. (2013). Profiling of microRNA in human and mouse ES and iPS cells reveals overlapping but distinct microRNA expression patterns. *PLoS One, 8*(9), e73532. doi:10.1371/journal.pone.0073532

Reifers, F., Walsh, E. C., Leger, S., Stainier, D. Y., and Brand, M. (2000). Induction and differentiation of the zebrafish heart requires fibroblast growth factor 8 (fgf8/acerebellar). *Development, 127*(2), 225-235.

Rodriguez, A., Griffiths-Jones, S., Ashurst, J. L., and Bradley, A. (2004). Identification of mammalian microRNA host genes and transcription units. *Genome Res, 14*(10A), 1902-1910. doi:10.1101/gr.2722704

Rossi, A., Kontarakis, Z., Gerri, C., Nolte, H., Holper, S., Kruger, M., and Stainier, D. Y. (2015). Genetic compensation induced by deleterious mutations but not gene knockdowns. *Nature, 524*(7564), 230-233. doi:10.1038/nature14580

Rothe, M., Modlich, U., and Schambach, A. (2013). Biosafety challenges for use of lentiviral vectors in gene therapy. *Curr Gene Ther, 13*(6), 453-468. doi:10.2174/15665232113136660006

Saga, Y. (1998). Genetic rescue of segmentation defect in MesP2-deficient mice by MesP1 gene replacement. *Mech Dev, 75*(1-2), 53-66.

Sakula, A. (1979). Robert Koch (1843--1910): founder of the science of bacteriology and discoverer of the tubercle bacillus. A study of his life and work. *Br J Dis Chest, 73*(4), 389-394.

Schiaffino, S., and Reggiani, C. (1996). Molecular diversity of myofibrillar proteins: gene regulation and functional significance. *Physiol Rev, 76*(2), 371-423. doi:10.1152/physrev.1996.76.2.371

Schlesinger, S., and Goff, S. P. (2013). Silencing of proviruses in embryonic cells: efficiency, stability and chromatin modifications. *EMBO Rep, 14*(1), 73-79. doi:10.1038/embor.2012.182

Schmittgen, T. D., and Livak, K. J. (2008). Analyzing real-time PCR data by the comparative C(T) method. *Nat Protoc, 3*(6), 1101-1108.

Schneider, V. A., and Mercola, M. (2001). Wnt antagonism initiates cardiogenesis in Xenopus laevis. *Genes Dev, 15*(3), 304-315. doi:10.1101/gad.855601

Schultheiss, T. M., Burch, J. B., and Lassar, A. B. (1997). A role for bone morphogenetic proteins in the induction of cardiac myogenesis. *Genes Dev, 11*(4), 451-462. doi:10.1101/gad.11.4.451

Schuster, J., Halvardson, J., Pilar Lorenzo, L., Ameur, A., Sobol, M., Raykova, D., Anneren, G., Feuk, L., and Dahl, N. (2015). Transcriptome Profiling Reveals Degree of Variability in

Induced Pluripotent Stem Cell Lines: Impact for Human Disease Modeling. *Cell Reprogram, 17*(5), 327-337. doi:10.1089/cell.2015.0009

Sedmera, D., and McQuinn, T. (2008). Embryogenesis of the heart muscle. *Heart Fail Clin, 4*(3), 235-245. doi:10.1016/j.hfc.2008.02.007

Shen, X., Soibam, B., Benham, A., Xu, X., Chopra, M., Peng, X., Yu, W., Bao, W., Liang, R., Azares, A., Liu, P., Gunaratne, P. H., Mercola, M., Cooney, A. J., Schwartz, R. J., and Liu, Y. (2016). miR-322/-503 cluster is expressed in the earliest cardiac progenitor cells and drives cardiomyocyte specification. *Proc Natl Acad Sci U S A, 113*(34), 9551-9556. doi:10.1073/pnas.1608256113

Sklepkiewicz, P., Shiomi, T., Kaur, R., Sun, J., Kwon, S., Mercer, B., Bodine, P., Schermuly, R. T., George, I., Schulze, P. C., and D'Armiento, J. M. (2015). Loss of secreted frizzled-related protein-1 leads to deterioration of cardiac function in mice and plays a role in human cardiomyopathy. *Circ Heart Fail, 8*(2), 362-372. doi:10.1161/CIRCHEARTFAILURE.114.001274

Sluijter, J. P., van Mil, A., van Vliet, P., Metz, C. H., Liu, J., Doevendans, P. A., and Goumans, M. J. (2010). MicroRNA-1 and -499 regulate differentiation and proliferation in human-derived cardiomyocyte progenitor cells. *Arterioscler Thromb Vasc Biol, 30*(4), 859-868. doi:10.1161/ATVBAHA.109.197434

Sommer, C. A., Stadtfeld, M., Murphy, G. J., Hochedlinger, K., Kotton, D. N., and Mostoslavsky, G. (2009). Induced pluripotent stem cell generation using a single lentiviral stem cell cassette. *Stem Cells, 27*(3), 543-549. doi:10.1634/stemcells.2008-1075

Spater, D., Abramczuk, M. K., Buac, K., Zangi, L., Stachel, M. W., Clarke, J., Sahara, M., Ludwig, A., and Chien, K. R. (2013). A HCN4+ cardiomyogenic progenitor derived from the first heart field and human pluripotent stem cells. *Nat Cell Biol, 15*(9), 1098-1106. doi:10.1038/ncb2824

Sperling, S. R. (2011). Systems biology approaches to heart development and congenital heart disease. *Cardiovasc Res, 91*(2), 269-278. doi:10.1093/cvr/cvr126

Stainier, D. Y. (2001). Zebrafish genetics and vertebrate heart formation. *Nat Rev Genet, 2*(1), 39-48. doi:10.1038/35047564

Stewart, S. A., Dykxhoorn, D. M., Palliser, D., Mizuno, H., Yu, E. Y., An, D. S., Sabatini, D. M., Chen, I. S., Hahn, W. C., Sharp, P. A., Weinberg, R. A., and Novina, C. D. (2003). Lentivirus-

delivered stable gene silencing by RNAi in primary cells. *RNA, 9*(4), 493-501. doi:10.1261/rna.2192803

Stockert, J. C., Blazquez-Castro, A., Canete, M., Horobin, R. W., and Villanueva, A. (2012). MTT assay for cell viability: Intracellular localization of the formazan product is in lipid droplets. *Acta Histochem, 114*(8), 785-796. doi:10.1016/j.acthis.2012.01.006

Suh, M. R., Lee, Y., Kim, J. Y., Kim, S. K., Moon, S. H., Lee, J. Y., Cha, K. Y., Chung, H. M., Yoon, H. S., Moon, S. Y., Kim, V. N., and Kim, K. S. (2004). Human embryonic stem cells express a unique set of microRNAs. *Dev Biol, 270*(2), 488-498. doi:10.1016/j.ydbio.2004.02.019

Sun, X., and Kaufman, P. D. (2018). Ki-67: more than a proliferation marker. *Chromosoma, 127*(2), 175-186. doi:10.1007/s00412-018-0659-8

Takahashi, K., and Yamanaka, S. (2006). Induction of pluripotent stem cells from mouse embryonic and adult fibroblast cultures by defined factors. *Cell, 126*(4), 663-676. doi:10.1016/j.cell.2006.07.024

Tam, P. P., and Behringer, R. R. (1997). Mouse gastrulation: the formation of a mammalian body plan. *Mech Dev, 68*(1-2), 3-25. doi:10.1016/s0925-4773(97)00123-8

Tang, F., Hajkova, P., Barton, S. C., Lao, K., and Surani, M. A. (2006). MicroRNA expression profiling of single whole embryonic stem cells. *Nucleic Acids Res, 34*(2), e9. doi:10.1093/nar/gnj009

Thum, T., Galuppo, P., Wolf, C., Fiedler, J., Kneitz, S., van Laake, L. W., Doevendans, P. A., Mummery, C. L., Borlak, J., Haverich, A., Gross, C., Engelhardt, S., Ertl, G., and Bauersachs, J. (2007). MicroRNAs in the human heart: a clue to fetal gene reprogramming in heart failure. *Circulation, 116*(3), 258-267. doi:10.1161/CIRCULATIONAHA.107.687947

Tu, S., and Chi, N. C. (2012). Zebrafish models in cardiac development and congenital heart birth defects. *Differentiation, 84*(1), 4-16. doi:10.1016/j.diff.2012.05.005

Tucker, K. L., Wang, Y., Dausman, J., and Jaenisch, R. (1997). A transgenic mouse strain expressing four drug-selectable marker genes. *Nucleic Acids Res, 25*(18), 3745-3746. doi:10.1093/nar/25.18.3745

Tzahor, E., and Lassar, A. B. (2001). Wnt signals from the neural tube block ectopic cardiogenesis. *Genes Dev, 15*(3), 255-260. doi:10.1101/gad.871501

van Rooij, E., Quiat, D., Johnson, B. A., Sutherland, L. B., Qi, X., Richardson, J. A., Kelm, R. J., Jr., and Olson, E. N. (2009). A family of microRNAs encoded by myosin genes governs myosin expression and muscle performance. *Dev Cell, 17*(5), 662-673. doi:10.1016/j.devcel.2009.10.013

Van Vliet, P., Wu, S. M., Zaffran, S., and Puceat, M. (2012). Early cardiac development: a view from stem cells to embryos. *Cardiovasc Res, 96*(3), 352-362. doi:10.1093/cvr/cvs270

van Weerd, J. H., and Christoffels, V. M. (2016). The formation and function of the cardiac conduction system. *Development, 143*(2), 197-210. doi:10.1242/dev.124883

Wang, J., Cao, N., Yuan, M., Cui, H., Tang, Y., Qin, L., Huang, X., Shen, N., and Yang, H. T. (2012). MicroRNA-125b/Lin28 pathway contributes to the mesendodermal fate decision of embryonic stem cells. *Stem Cells Dev, 21*(9), 1524-1537. doi:10.1089/scd.2011.0350

Wang, J., Greene, S. B., Bonilla-Claudio, M., Tao, Y., Zhang, J., Bai, Y., Huang, Z., Black, B. L., Wang, F., and Martin, J. F. (2010). Bmp signaling regulates myocardial differentiation from cardiac progenitors through a MicroRNA-mediated mechanism. *Dev Cell, 19*(6), 903-912. doi:10.1016/j.devcel.2010.10.022

Wang, J., Greene, S. B., and Martin, J. F. (2011). BMP signaling in congenital heart disease: new developments and future directions. *Birth Defects Res A Clin Mol Teratol, 91*(6), 441-448. doi:10.1002/bdra.20785

Wang, X., and Yang, P. (2008). In vitro differentiation of mouse embryonic stem (mES) cells using the hanging drop method. *J Vis Exp*(17). doi:10.3791/825

Wei, B., and Jin, J. P. (2011). Troponin T isoforms and posttranscriptional modifications: Evolution, regulation and function. *Arch Biochem Biophys, 505*(2), 144-154. doi:10.1016/j.abb.2010.10.013

Wightman, B., Ha, I., and Ruvkun, G. (1993). Posttranscriptional regulation of the heterochronic gene lin-14 by lin-4 mediates temporal pattern formation in C. elegans. *Cell, 75*(5), 855-862. doi:10.1016/0092-8674(93)90530-4

Winter, J., Jung, S., Keller, S., Gregory, R. I., and Diederichs, S. (2009). Many roads to maturity: microRNA biogenesis pathways and their regulation. *Nat Cell Biol, 11*(3), 228-234. doi:10.1038/ncb0309-228

Witman, N., Heigwer, J., Thaler, B., Lui, W. O., and Morrison, J. I. (2013). miR-128 regulates non-myocyte hyperplasia, deposition of extracellular matrix and Islet1 expression during newt cardiac regeneration. *Dev Biol, 383*(2), 253-263. doi:10.1016/j.ydbio.2013.09.011

Wong, L. L., Wang, J., Liew, O. W., Richards, A. M., and Chen, Y. T. (2016). MicroRNA and Heart Failure. *Int J Mol Sci, 17*(4), 502. doi:10.3390/ijms17040502

Wu, F., Yang, Z., and Li, G. (2009). Role of specific microRNAs for endothelial function and angiogenesis. *Biochem Biophys Res Commun, 386*(4), 549-553. doi:10.1016/j.bbrc.2009.06.075

Wu, S. M., Fujiwara, Y., Cibulsky, S. M., Clapham, D. E., Lien, C. L., Schultheiss, T. M., and Orkin, S. H. (2006). Developmental origin of a bipotential myocardial and smooth muscle cell precursor in the mammalian heart. *Cell, 127*(6), 1137-1150. doi:10.1016/j.cell.2006.10.028

Yang, L., Cai, C. L., Lin, L., Qyang, Y., Chung, C., Monteiro, R. M., Mummery, C. L., Fishman, G. I., Cogen, A., and Evans, S. (2006). Isl1Cre reveals a common Bmp pathway in heart and limb development. *Development, 133*(8), 1575-1585. doi:10.1242/dev.02322

Zaffran, S., and Frasch, M. (2002). Early signals in cardiac development. *Circ Res, 91*(6), 457-469. doi:10.1161/01.res.0000034152.74523.a8

Zhang, D., Liu, Z., Zheng, N., Wu, H., Zhang, Z., and Xu, J. (2018). MiR-30b-5p modulates glioma cell proliferation by direct targeting MTDH. *Saudi J Biol Sci, 25*(5), 947-952. doi:10.1016/j.sjbs.2018.02.015

Zhang, L., Nomura-Kitabayashi, A., Sultana, N., Cai, W., Cai, X., Moon, A. M., and Cai, C. L. (2014). Mesodermal Nkx2.5 is necessary and sufficient for early second heart field development. *Dev Biol, 390*(1), 68-79. doi:10.1016/j.ydbio.2014.02.023

Zhang, Y., Chao, T., Li, R., Liu, W., Chen, Y., Yan, X., Gong, Y., Yin, B., Liu, W., Qiang, B., Zhao, J., Yuan, J., and Peng, X. (2009). MicroRNA-128 inhibits glioma cells proliferation by targeting transcription factor E2F3a. *J Mol Med (Berl), 87*(1), 43-51. doi:10.1007/s00109-008-0403-6

Zhao, Y., Samal, E., and Srivastava, D. (2005). Serum response factor regulates a muscle-specific microRNA that targets Hand2 during cardiogenesis. *Nature, 436*(7048), 214-220. doi:10.1038/nature03817

Zhou, B. Y., Ye, Z., Chen, G., Gao, Z. P., Zhang, Y. A., and Cheng, L. (2007). Inducible and reversible transgene expression in human stem cells after efficient and stable gene transfer. *Stem Cells, 25*(3), 779-789. doi:10.1634/stemcells.2006-0128

Zhou, S. S., Jin, J. P., Wang, J. Q., Zhang, Z. G., Freedman, J. H., Zheng, Y., and Cai, L. (2018). miRNAS in cardiovascular diseases: potential biomarkers, therapeutic targets and challenges. *Acta Pharmacol Sin, 39*(7), 1073-1084. doi:10.1038/aps.2018.30

Zhu, K., Hu, X., Chen, H., Li, F., Yin, N., Liu, A. L., Shan, K., Qin, Y. W., Huang, X., Chang, Q., Xu, G. Z., and Wang, Z. (2019). Downregulation of circRNA DMNT3B contributes to diabetic retinal vascular dysfunction through targeting miR-20b-5p and BAMBI. *EBioMedicine, 49*, 341-353. doi:10.1016/j.ebiom.2019.10.004

Zhu, S., Hu, X., Yu, Z., Peng, Y., Zhu, J., Liu, X., Li, M., Han, S., and Zhu, C. (2015). Effect of miR-20b on Apoptosis, Differentiation, the BMP Signaling Pathway and Mitochondrial Function in the P19 Cell Model of Cardiac Differentiation In Vitro. *PLoS One, 10*(4), e0123519. doi:10.1371/journal.pone.0123519

Zhu, W. Z., Xie, Y., Moyes, K. W., Gold, J. D., Askari, B., and Laflamme, M. A. (2010). Neuregulin/ErbB signaling regulates cardiac subtype specification in differentiating human embryonic stem cells. *Circ Res, 107*(6), 776-786. doi:10.1161/CIRCRESAHA.110.223917

Acknowledgments

First and foremost, I would like to thank my first advisor apl. Prof. Dr. med. Markus Krane, as well as Prof. Dr. med Rüdiger Lange, for giving me the opportunity to join the lab and work at the German Heart Center Munich.

I would like to express my appreciation to Dr. Krane for his immense support throughout my Ph.D. studies. In addition, I also would like to thank Prof. Angelika Schnieke, Ph.D. for being my second advisor and providing me insightful comments on the project. Furthermore, I would like to thank PD Dr. Harald Lahm for being my mentor and a tremendous source of motivation and support over the past few years.

A special thanks goes to Dr. Stefanie Doppler for not only being involved in closely supervising, organizing, and structuring my Ph.D. project and all the related research, but also for her critical insight and feedback. She taught me how to scrutinize scientific protocols, workflows, as well as establish experimental setups and report outcomes. In the end, her expertise, commitment and expectations shaped me personally and made me a better scientist and critical thinker.

Furthermore, I would like to acknowledge and express my appreciation to all my German Heart Center colleagues who supported me throughout this project in a variety of ways. I would like to thank all the members of the hiPSCs lab including Zhong Zhang and Irina Neb, and would especially like to thank Martina Dreßen for being there as an indispensable Ph.D. partner in crime. Additionally, I would like to thank Theresia Stich and Anne Diehm for being supportive of my efforts and this project by conducting essential lab work.

I would like to extend my sincerest appreciation to all our cooperation partners including David Hassel, Heribert Schunkert, Jeanette Erdmann, Zouhair Aherrahrou, Giovanni Cuda, Gianluca Santamaria, Lynette Henkel, Matthias Schiemann, Lutz Hein, Ralf Gilsbach, Cesar A. Sommer, Sean M. Wu, and Sylvia Evans.

Last, but certainly not least, my greatest thanks goes to my family, Gisela, Ulrich, and David, as well as my fiancé, Matthew, who were always supportive and a source of strength and encouragement throughout all my years of study. I could not have done it without you!

Appendices

A Appendix Figures

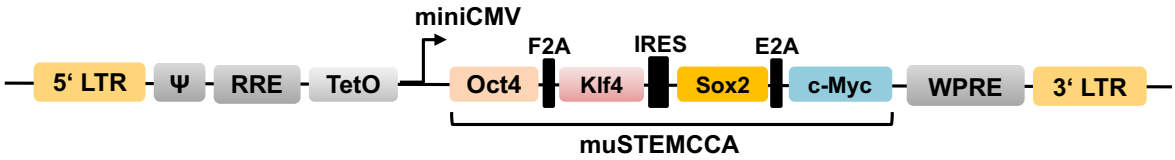

Appendix Figure A1 pHAGE-STEMCCA vector scheme. The “murine stem cell cassette” (muSTEMCCA) contains the four “Yamanaka factors” *Oct4, Klf4, Sox2* and *c-Myc* separated by self-cleaving 2A peptides (F2A and E2A) and IRES driven by a miniCMV promoter. This doxycycline-inducible polycistronic lentiviral vector was used to generate the Isl1Cre-R26^{mTmG} iPSC line (iITG-iPSCs). The vector was kindly provided by Sommer and colleagues from the Section of Gastroenterology, Department of Medicine, Boston University School of Medicine, MA, USA (Sommer et al., 2009). *Abbreviations: LTR, long terminal repeats; RRE, Reverse Response Element; TetO, tetracycline operator; miniCMV, mini-Cytomegalovirus Promoter; IRES, internal ribosome entry site; WPRE, Woodchuck Hepatitis Posttranscriptional Regulatory Element.* Reprinted from Figure S7B from Hoelscher et al. miR-128a Acts as a Regulator in Cardiac Development by Modulating Differentiation of Cardiac Progenitor Cell Populations. Int. J. Mol. Sci. 2020, 21, 1158 (Hoelscher et al., 2020).

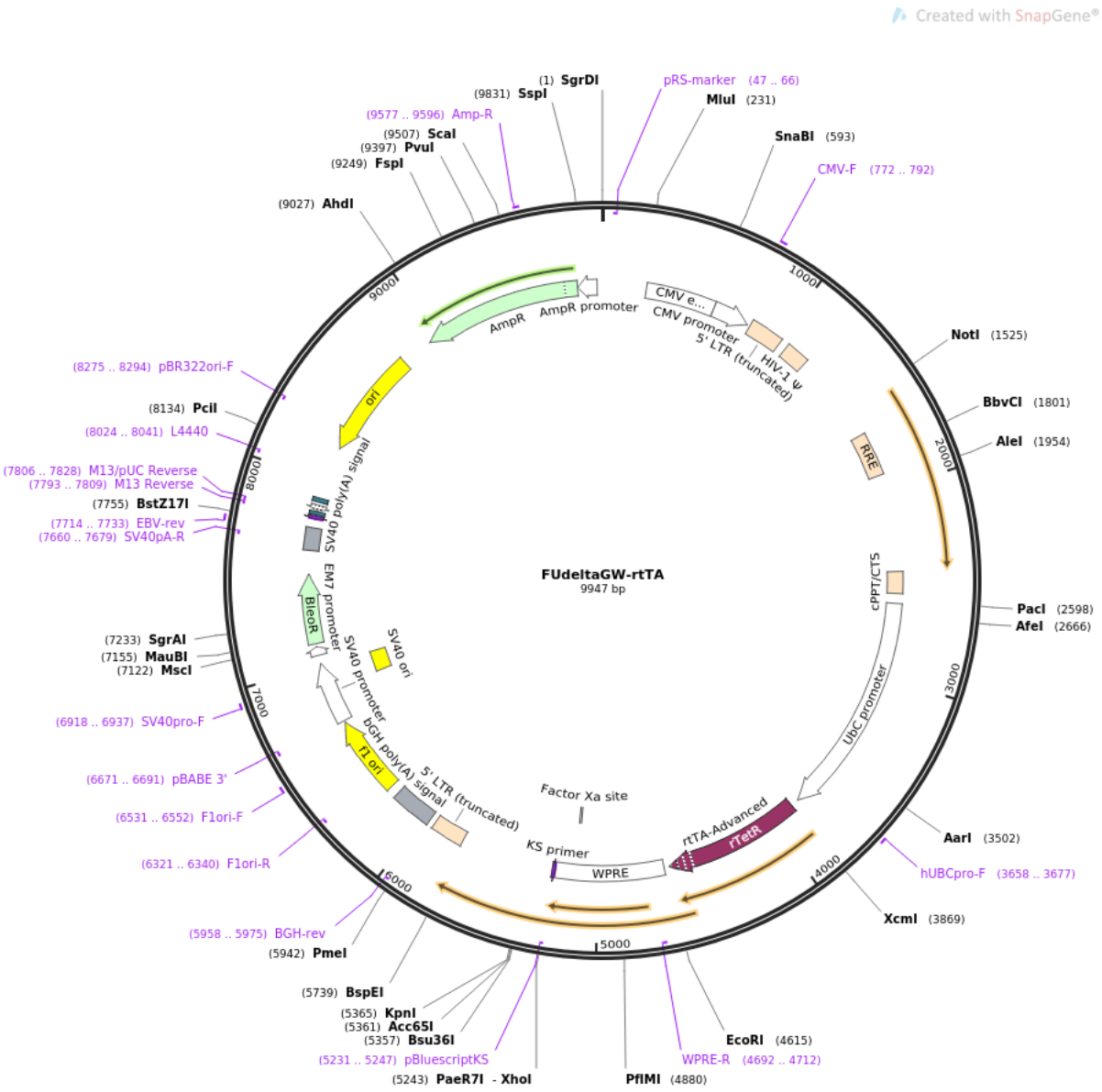

Appendix Figure A2 FudeltaGW-rtTA vector map. The vector was used to produce lentiviruses to generate the Isl1Cre-R26^{mTmG} iPSC line (iITG-iPSCs). It constitutively expresses the reverse tetracycline transcriptional activator (rtTA) which can bind to the tetO operator of the muSTEMCCA vector construct. The FUdeltaGW-rtTA was a gift from Konrad Hochedlinger (Addgene plasmid #19780; http://n2t.net/addgene:19780; RRID: Addgene_19780). Reprinted from https://www.addgene.org/19780 (Maherali et al., 2008).

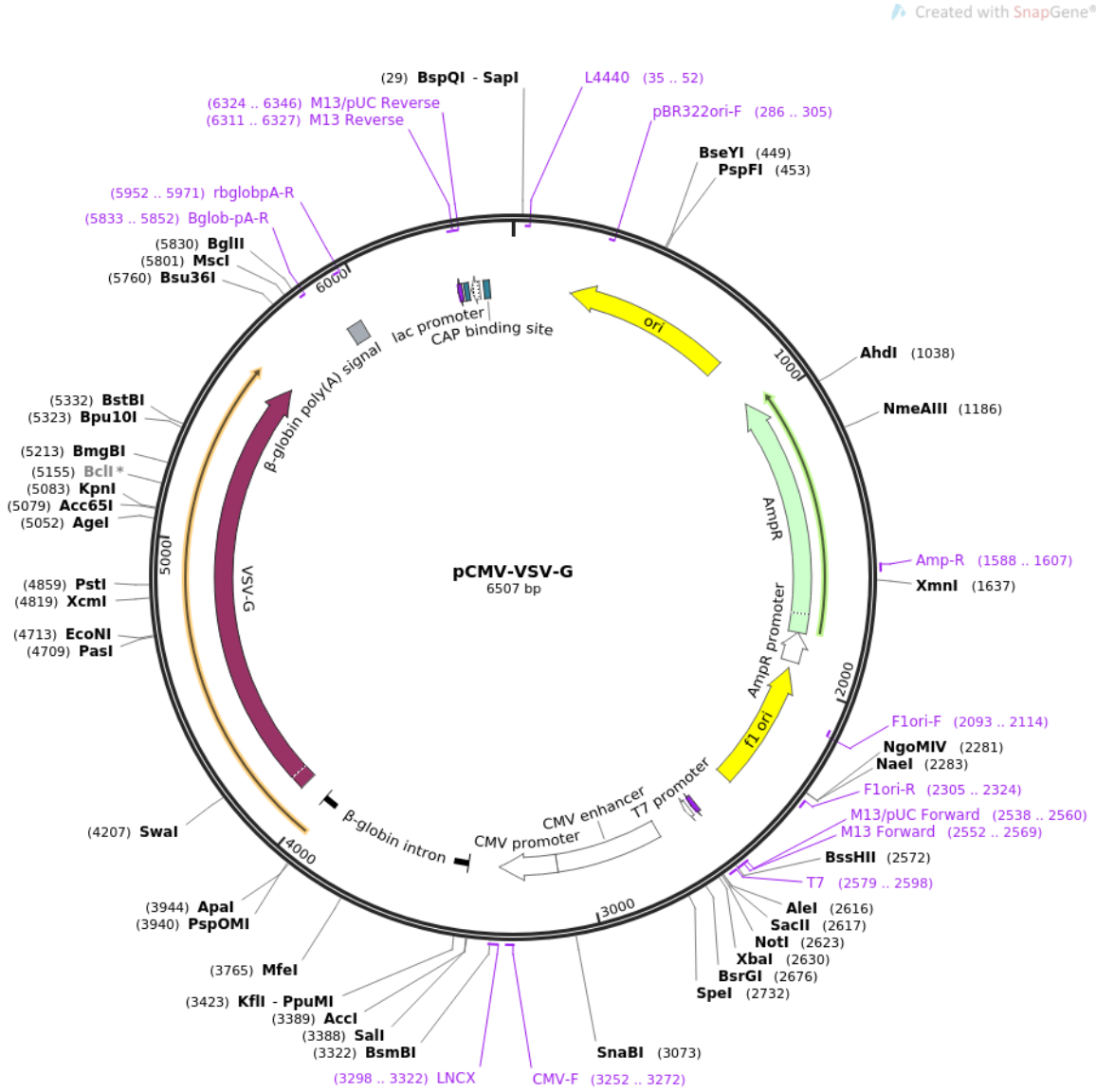

Appendix Figure A3 pCMV-VSV-G vector map. The vector was used to produce lentiviruses to generate the Isl1Cre-R26^{mTmG} iPSC line (iITG-iPSCs) and encodes the viral envelope protein. The pCMV-VSV-G was a gift from Bob Weinberg (Addgene plasmid # 8454; http://n2t.net/ addgene:8454; RRID: Addgene_8454). Reprinted from https://www.addgene.org/8454 (Stewart et al., 2003).

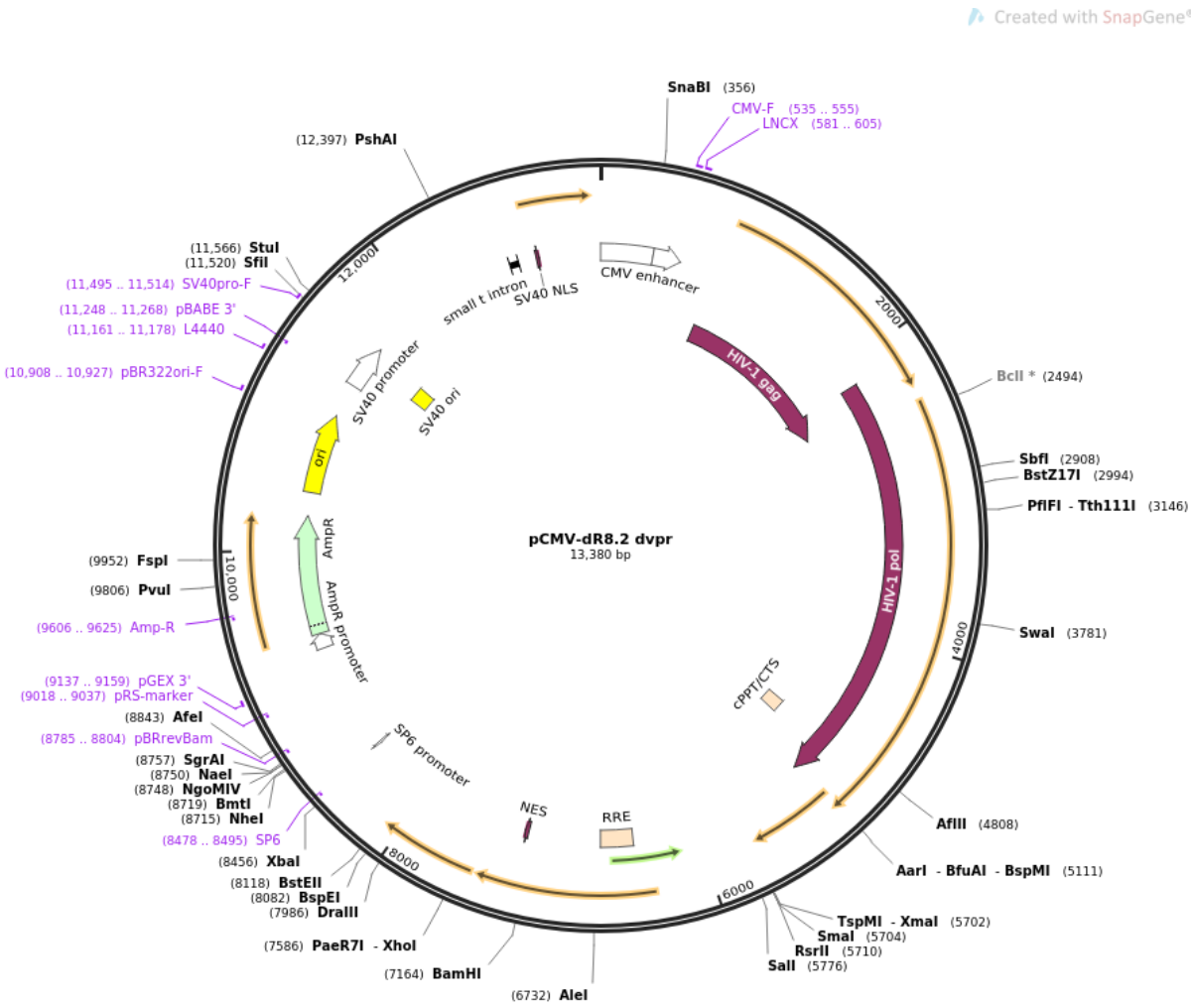

Appendix Figure A4 pCMV-dR8.2 dvpr vector map. The vector was used to produce lentiviruses to generate the Isl1Cre-R26^{mTmG} iPSC line (iITG-iPSCs) and encodes the viral packaging protein. The pCMV-dR8.2 dvpr was a gift from Bob Weinberg (Addgene plasmid # 8455; http://n2t.net/addgene:8455; RRID: Addgene_8455). Reprinted from https://www.addgene.org/8455 (Stewart et al., 2003).

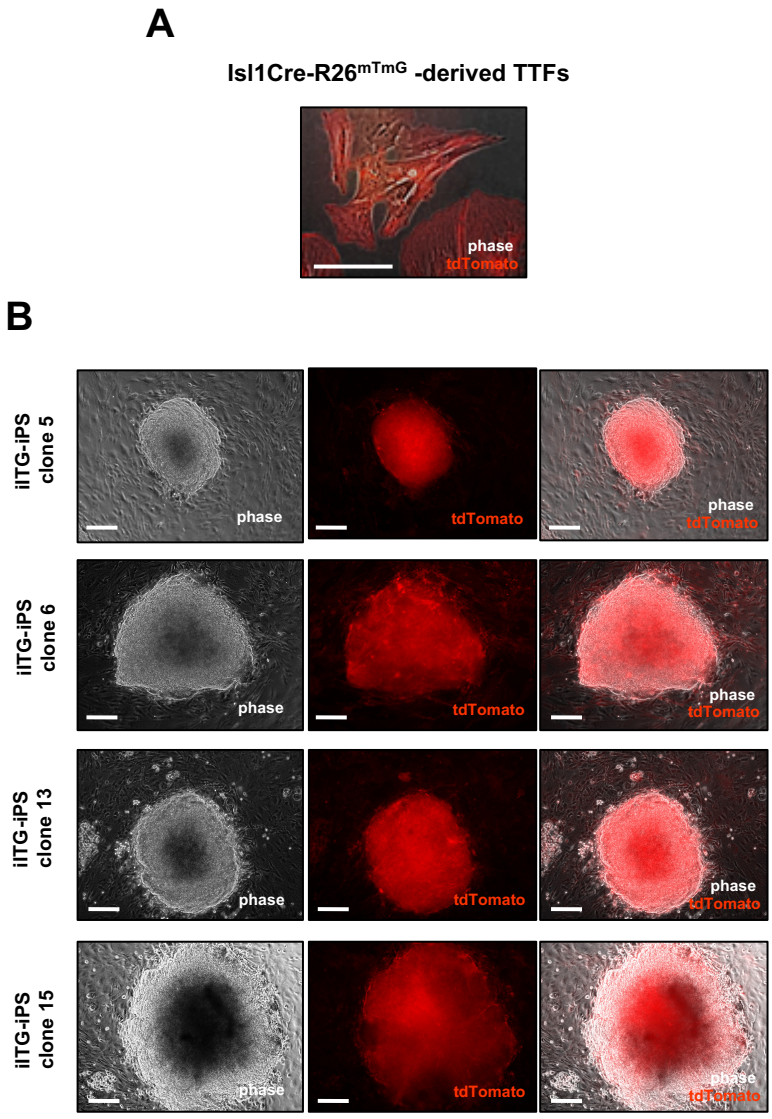

Appendix Figure A5 Generation of Isl1Cre-R26^{mTmG} iPSC line (iITG-iPSCs). A. Isl1Cre-R26^{mTmG}-derived TTFs that were used for the generation of iITG-iPSCs. Scale bar is 100µm. **B.** Panels show several iITG-iPSC clones after reprogramming before picking. iITG-iPSC clone 5 upper panel, iITG-iPSC clone 6 (second from top), iITG-iPSC clone 13 (second from bottom) and iITG-iPSC clone 15 (lower panel). Images are shown as single phase contrast and fluorescent pictures as well as an overlay between phase and fluorescent microscopic pictures. Scale bars are 200µm. iITG-iPSC clone 15 was used for further *in vitro* differentiation experiments.

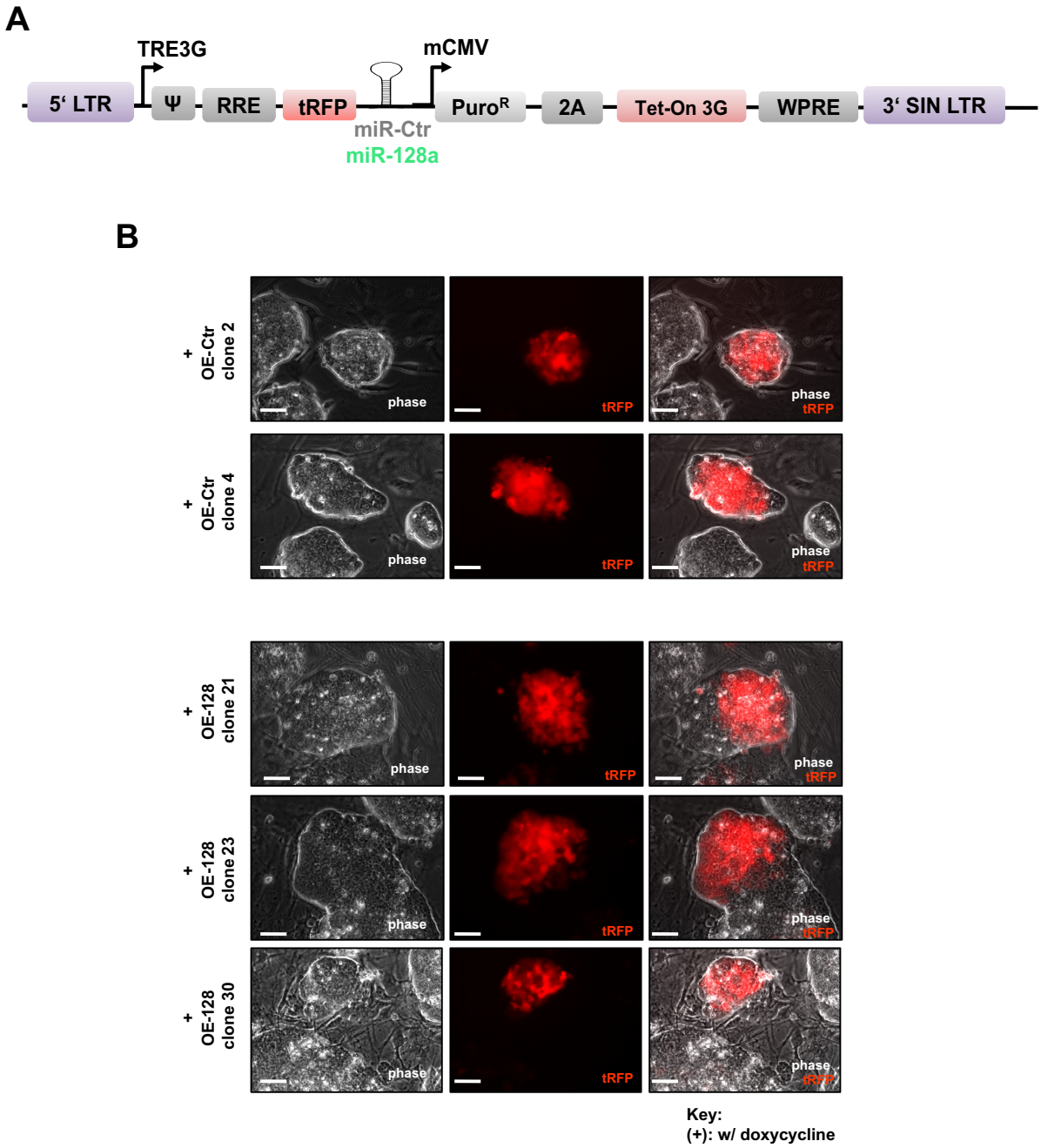

Appendix Figure A6 Generation of NkxCE-GFP miR overexpressing ESC line (OE-ESCs). A. Dharmacon™ shMIMIC inducible Lentiviral microRNA construct. The doxycycline-inducible, puromycin resistant (Puro^R) lentiviral particles that co-express tRFP with either miR-Ctr or miR-128a were used for the generation of NkxCE-GFP miR overexpressing ESC lines (OE-Ctr, OE-128). **B.** Panels of RFP-positive OE-Ctr and OE-128 ESC clones before picking cultured with (w/) doxycycline. OE-Ctr clone 2 and 4 (upper two panels) and OE-128 ESC clones 21, 23 and 30 (lower three panels). Images are shown as single phase and fluorescent pictures as well as an overlay between phase and fluorescent microscopic pictures. Scale bars are 200µm. OE-Ctr clone 4 as well as two of the OE-128 clones (21 and 30) were used for final OE experiments. *Abbreviations: 5'LTR, 5' long terminal repeats; TRE3G, Tetracycline Response Element 3G; RRE, Reverse Response Element; tRFP, turbo Red Fluorescent Protein; mCMV, murine Cytomegalovirus Promoter; 2A, 2A peptide; Tet-On 3G, Tet-On 3G transactivator protein; WPRE, Woodchuck Hepatitis Posttranscriptional Regulatory Element; 3' SIN LTR, 3' Self-inactivating Long Terminal Repeat.* Figure A6A is reprinted from Figure S9A from Hoelscher et al. miR-128a Acts as a Regulator in Cardiac Development by Modulating Differentiation of Cardiac Progenitor Cell Populations. Int. J. Mol. Sci. 2020, 21, 1158 (Hoelscher et al., 2020).

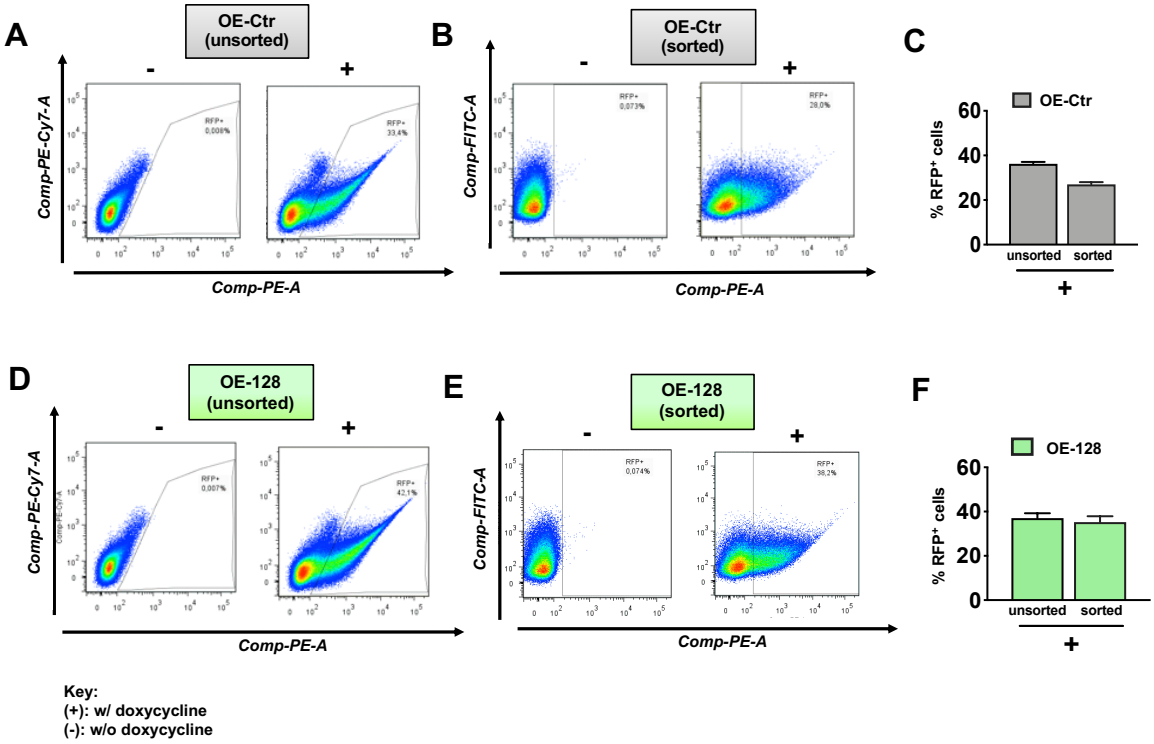

Appendix Figure A7 Flow cytometry of RFP-positive cells in OE-ESCs clones after sorting. A-B. Panels show dot plots of flow cytometry analysis of RFP-positive cells in unsorted (A) as well as sorted (B) OE-Ctr ESCs after culture without doxycycline (each left panel, used as reference for gate selection) or with doxycycline (each right panel). **C.** Quantification of RFP-positive cells in unsorted and sorted OE-Ctr ESCs cultured with doxycycline showed no significant enhancement of RFP-positive cells after sorting. **D-E.** Panels show dot plots of flow cytometry analysis of RFP-positive cells in unsorted (A) as well as sorted (B) OE-128 ESCs after culture without doxycycline (each left panel, used as reference for gate selection) or with doxycycline (each right panel). **F.** Quantification of RFP-positive cells in unsorted and sorted OE-128 ESCs cultured with doxycycline showed no significant enhancement of RFP-positive cells after sorting. RFP-positive cells in OE-Ctr and OE-128 were detected with the use of the PE-A filter on a BD LSR Fortessa™ 7.6.5.

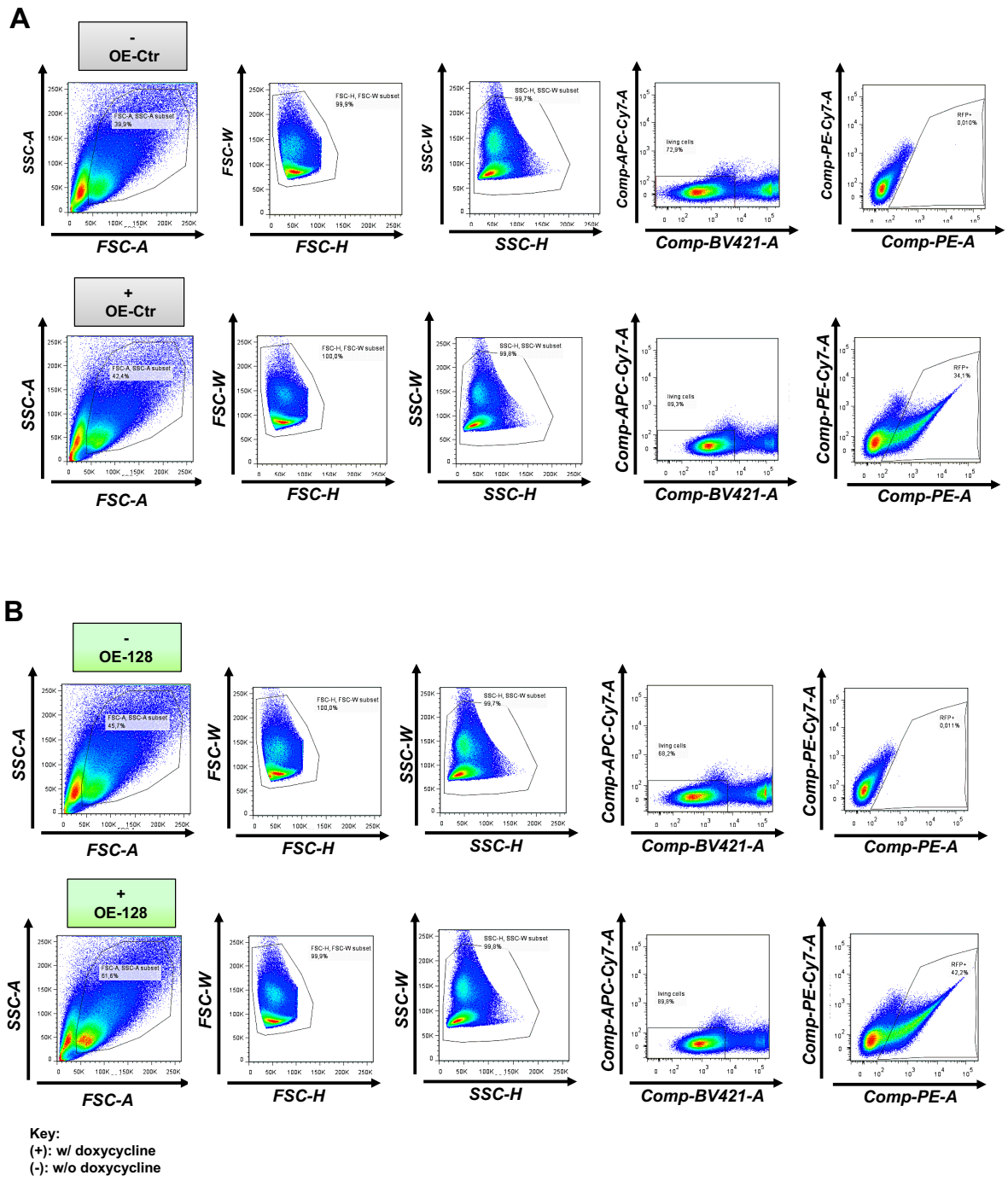

Appendix Figure A8: Exemplary flow cytometry dot plots and gate selection of OE-ESC clones. A-B. Panels show dot plots of flow cytometry analysis and detailed gate selection in OE-Ctr ESCs (A) and OE-128 (B) cultured with doxycycline (lower panels). Gate selection was based on the correspondent OE-ESC (OE-Ctr or OE-128) cultured without doxycycline (upper panels). First gate selections were based on cell size and granularity and were done with the help of forward and side scatter (FSC, SSC) created dot plots. Further, the exclusion of dead cells was done with the filter BV421 that detects cells with DAPI incorporation. Finally, RFP-positive cells were detected with the use of the PE-A filter on a BD LSR Fortessa™ 7.6.5.

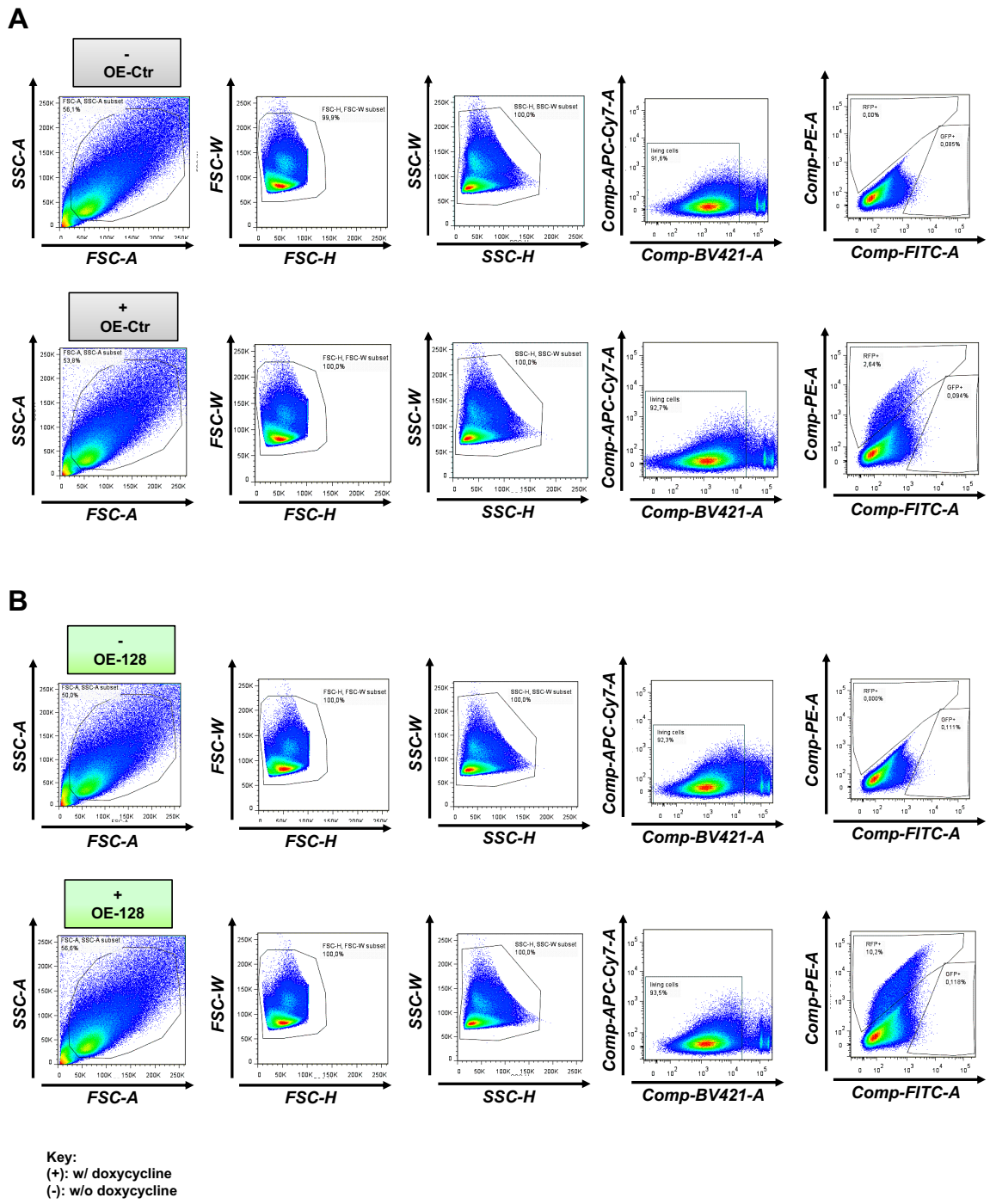

Appendix Figure A9: Exemplary flow cytometry dot plots and gate selection of OE-ESCs after 0.75wks of *in vitro* differentiation. A. Panels show dot plots of flow cytometry analysis and detailed gate selection of 0.75wks *in vitro* differentiated OE-Ctr ESCs cultured without doxycycline (upper panel, reference for gate selection) and with doxycycline (lower panel). **B.** Panels show dot plots of flow cytometry analysis and detailed gate selection of 0.75wks *in vitro* differentiated OE-128 ESCs without doxycycline (upper panel) and with doxycycline (lower panel). The flow cytometry data from OE-128 ESC during *in vitro* differentiation with doxycycline (B, lower panel), however, was not included in the final results due to influences of doxycycline that we demonstrated during differentiation of OE-Ctr ESCs (also see results, Figure 34A). First gate selections were based on cell size and granularity and were done with the help of forward and side scatter (FSC, SSC) created dot plots. Further, the exclusion of dead cells was done with the filter BV421 that detects cells with DAPI incorporation. Finally, GFP-positive cells were detected with the use of the FITC- filter and RFP-positive cells with the PE filter on a BD LSR Fortessa™ 7.6.5.

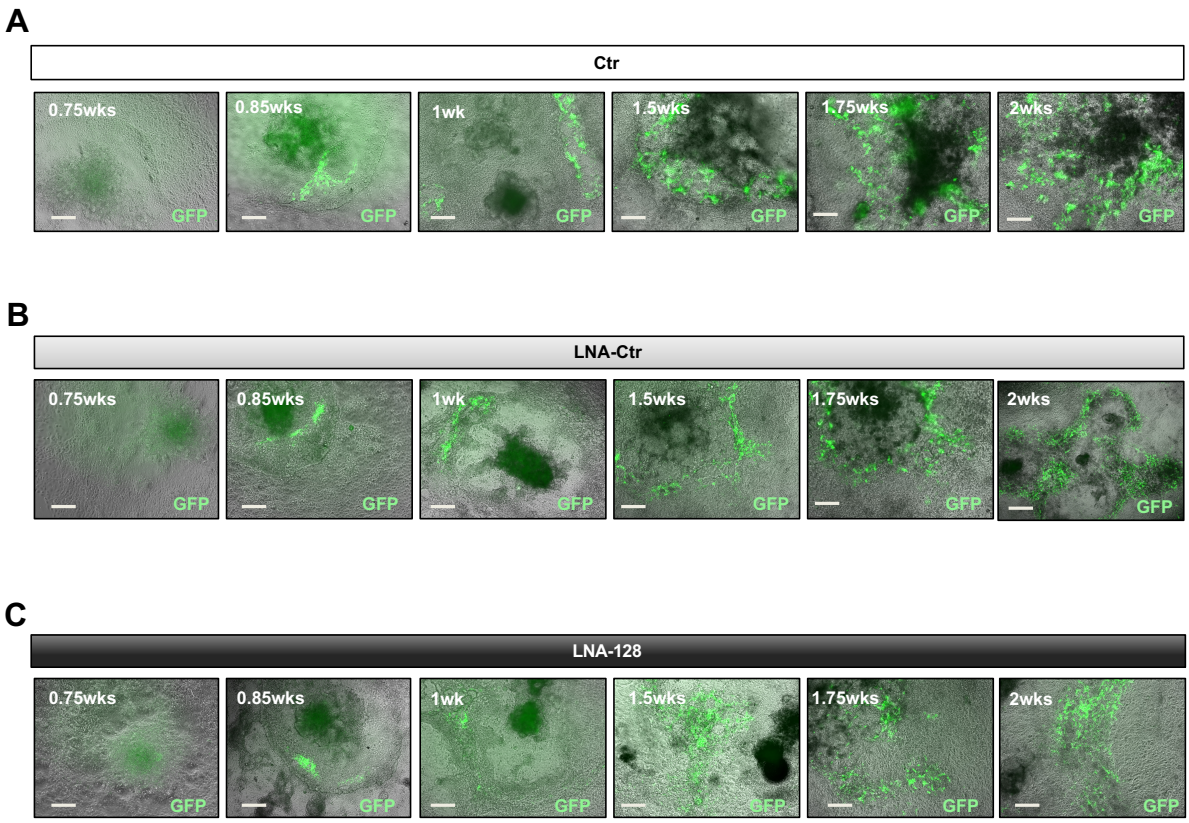

Appendix Figure A10 Fluorescence images of NkxCE-GFP ESC during *in vitro* differentiation under the three conditions of LNA-mediated knockdown. A-C. Panels show exemplary fluorescence images of the NkxCE-GFP ESC line which was treated either as (A) Ctr, transfected with (B) LNA-Ctr or transfected with (C) LNA-128. Images were taken from 0.75wks to 2wks of *in vitro* differentiation and show the occurrence of GFP-positive CPCs with progressing differentiation under all three conditions. Images are shown as overlay between phase and fluorescent microscopic pictures. Scale bars are 200µm.

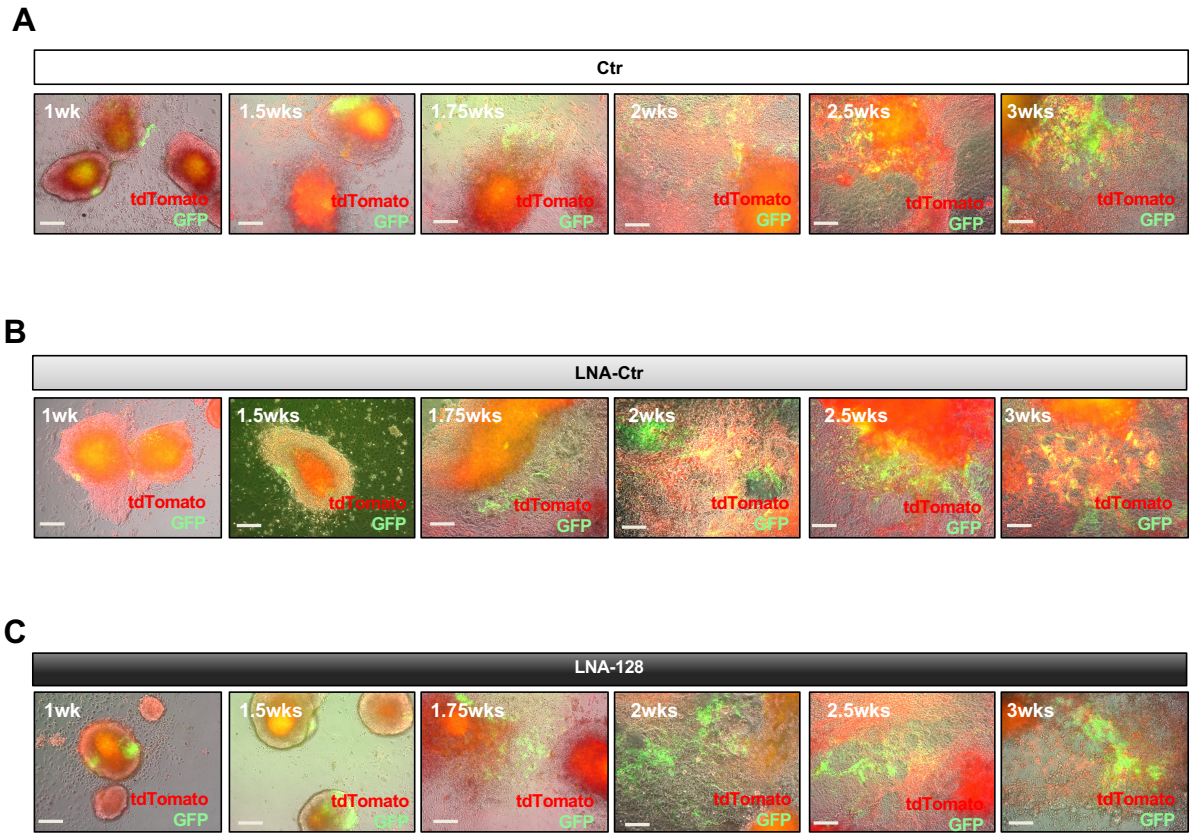

Appendix Figure A11 Fluorescence images of Isl1Cre-R26^{mTmG} iPSCs (iITG-iPSCs) during *in vitro* differentiation under the three conditions of LNA-mediated knockdown. A-C. Panels show exemplary fluorescence images of the iITG-iPSC line which was treated either as (A) Ctr, transfected with (B) LNA-Ctr or transfected with (C) LNA-128. Images were taken from 1wk to 3wks of *in vitro* differentiation and show permanently membrane-targeted tandem dimer Tomato (mT)-labelled iITG-iPSCs as well as the occurrence of GFP-positive CPCs with progressing differentiation under all three conditions. Images are shown as overlay between phase and fluorescent microscopic pictures. Scale bars are 200µm.

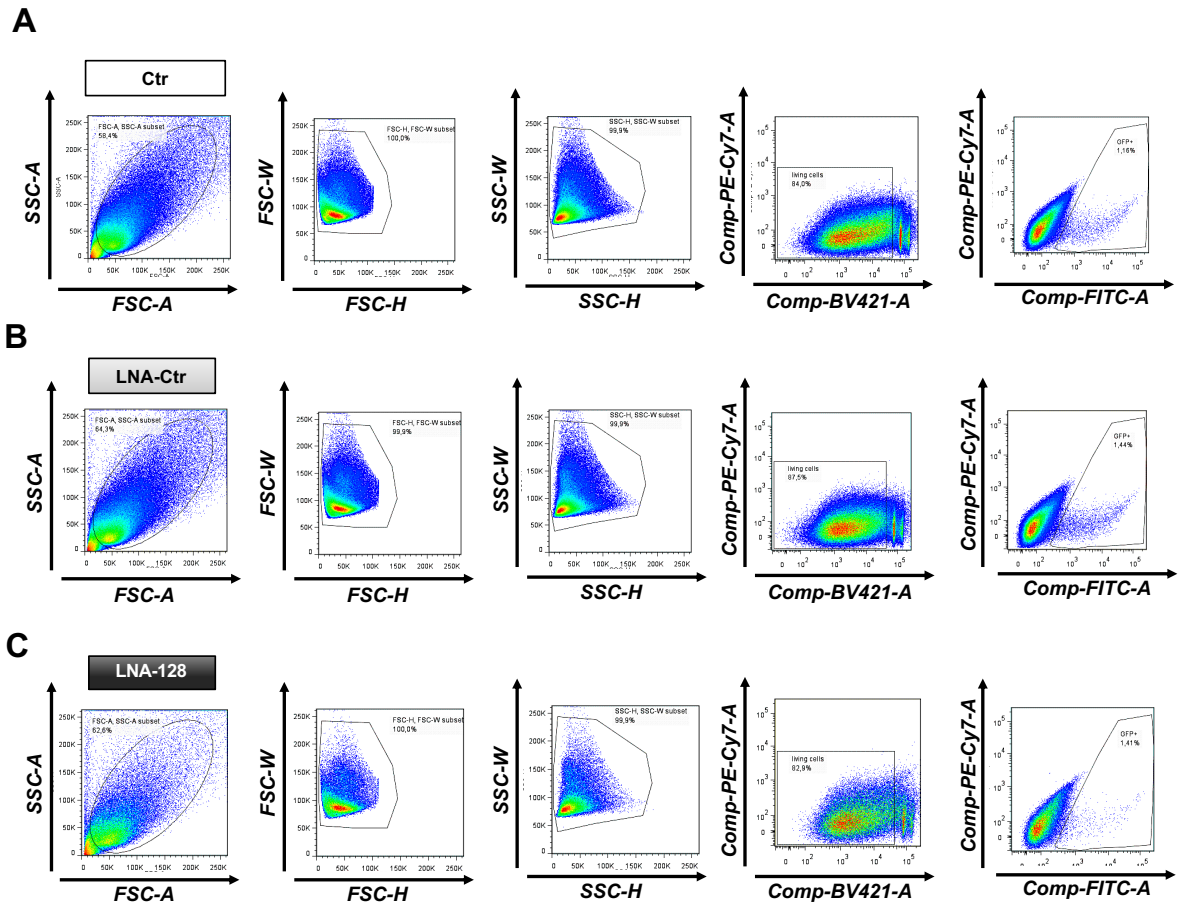

Appendix Figure A12 Exemplary flow cytometry dot plots and gate selection of NkxCE-GFP ESCs after 1wk of *in vitro* differentiation under the three conditions of LNA-mediated knockdown. **A-C.** Panels show exemplary dot plots of flow cytometry analysis and detailed gate selection of the NkxCE-GFP ESC line which was treated either as (A) Ctr, transfected with (B) LNA-Ctr or transfected with (C) LNA-128 after 1wk of *in vitro* differentiation. Gate selection was based on the correspondent NkxCE-GFP ESC Ctr line (A). First gate selections were based on cell size and granularity and were done with the help of forward and side scatter (FSC, SSC) created dot plots. Further, the exclusion of dead cells was done with the filter BV421 that detects cells with DAPI incorporation. Finally, GFP-positive cells were detected with the use of the FITC-A filter on a BD LSR Fortessa™ 7.6.5.

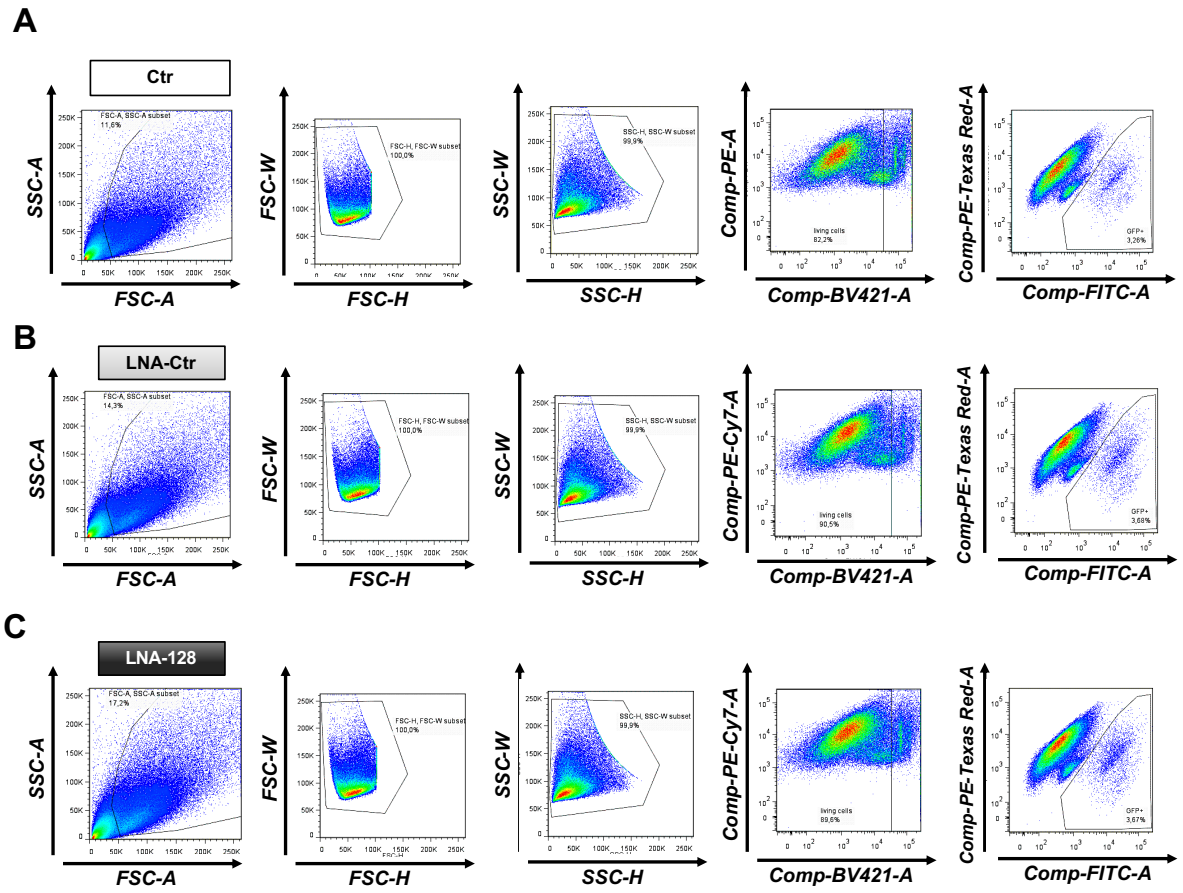

Appendix Figure A13: **Exemplary flow cytometry dot plots and gate selection of Isl1Cre/R26^{mTmG} iPSCs (iITG-iPSCs) after 3wks of *in vitro* differentiation under the three conditions of LNA-mediated knockdown**. **A-C.** Panels show exemplary dot plots of flow cytometry analysis and detailed gate selection of the iITG-iPSC line which was treated either as (A) Ctr, transfected with (B) LNA-Ctr or transfected with (C) LNA-128 after 3wks of *in vitro* differentiation. Gate selection was based on the correspondent iITG-iPSC Ctr line (A). First gate selections were based on cell size and granularity and were done with the help of forward and side scatter (FSC, SSC) created dot plots. Further, the exclusion of dead cells was done with the filter BV421 that detects cells with DAPI incorporation. Finally, GFP-positive cells were detected with the use of the FITC-A filter on a BD LSR Fortessa™ 7.6.5.

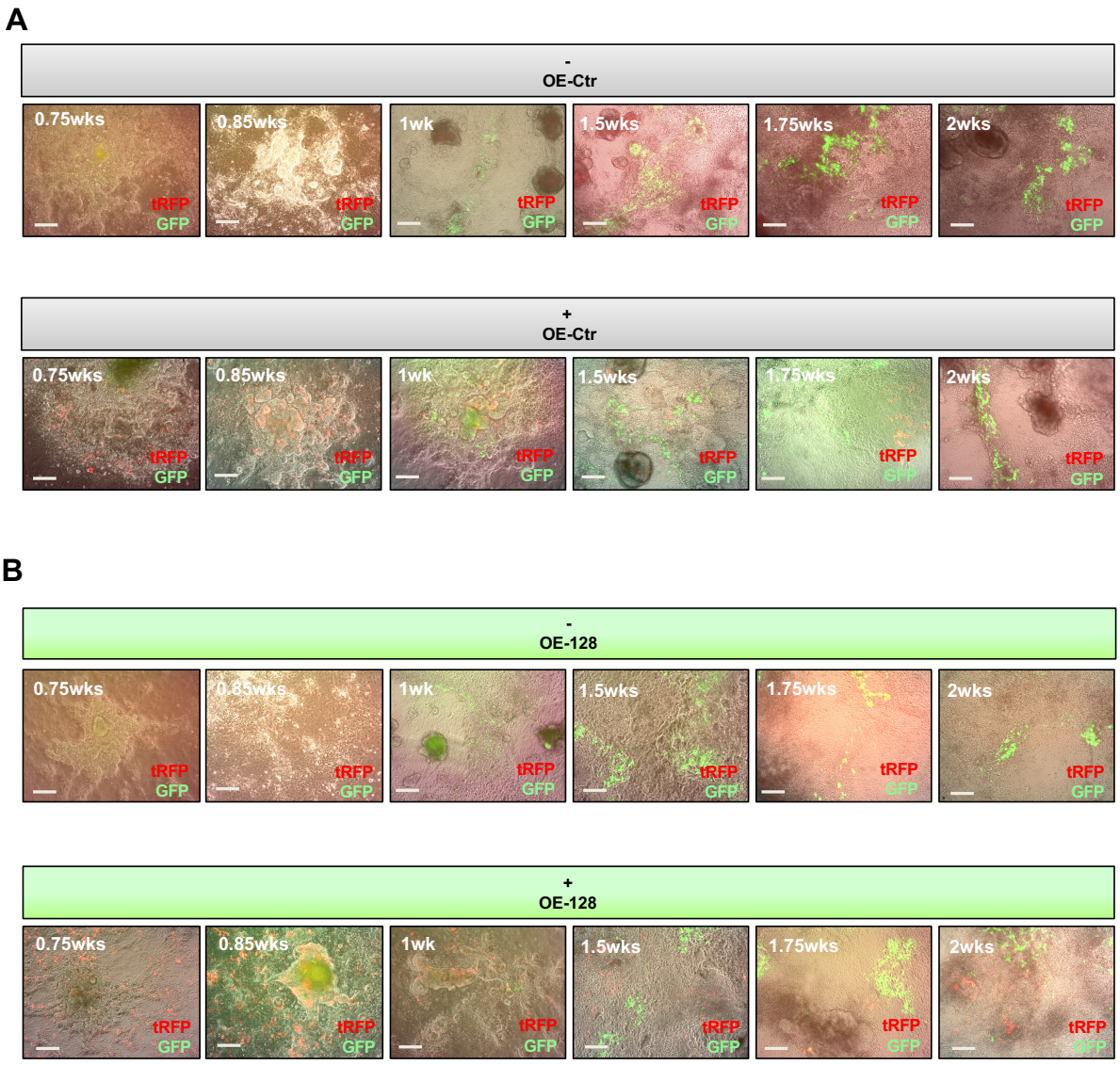

Appendix Figure A14: Fluorescence images of miR overexpression NkxCE-GFP ESCs (OE-Ctr, OE-128) during *in vitro* differentiation with or without doxycycline. A-B. Panels show exemplary fluorescence images of the miR overexpression NkxCE-GFP ESCs, OE-Ctr (A) and OE-128 (B) either cultured without doxycycline (upper panels) and with doxycycline (lower panels). Data from OE-128 ESC during *in vitro* differentiation with doxycycline (B, lower panel), however, was not included in the final results due to influence of doxycycline alone that we demonstrated during differentiation of OE-Ctr ESCs (also see results, Figure 34A). Images were taken from 0.75wks to 2wks of *in vitro* differentiation and show the occurrence of GFP-positive CPCs with progressing differentiation under both conditions. Images are shown as overlay between phase and fluorescent microscopic pictures. Scale bars are 200µm.

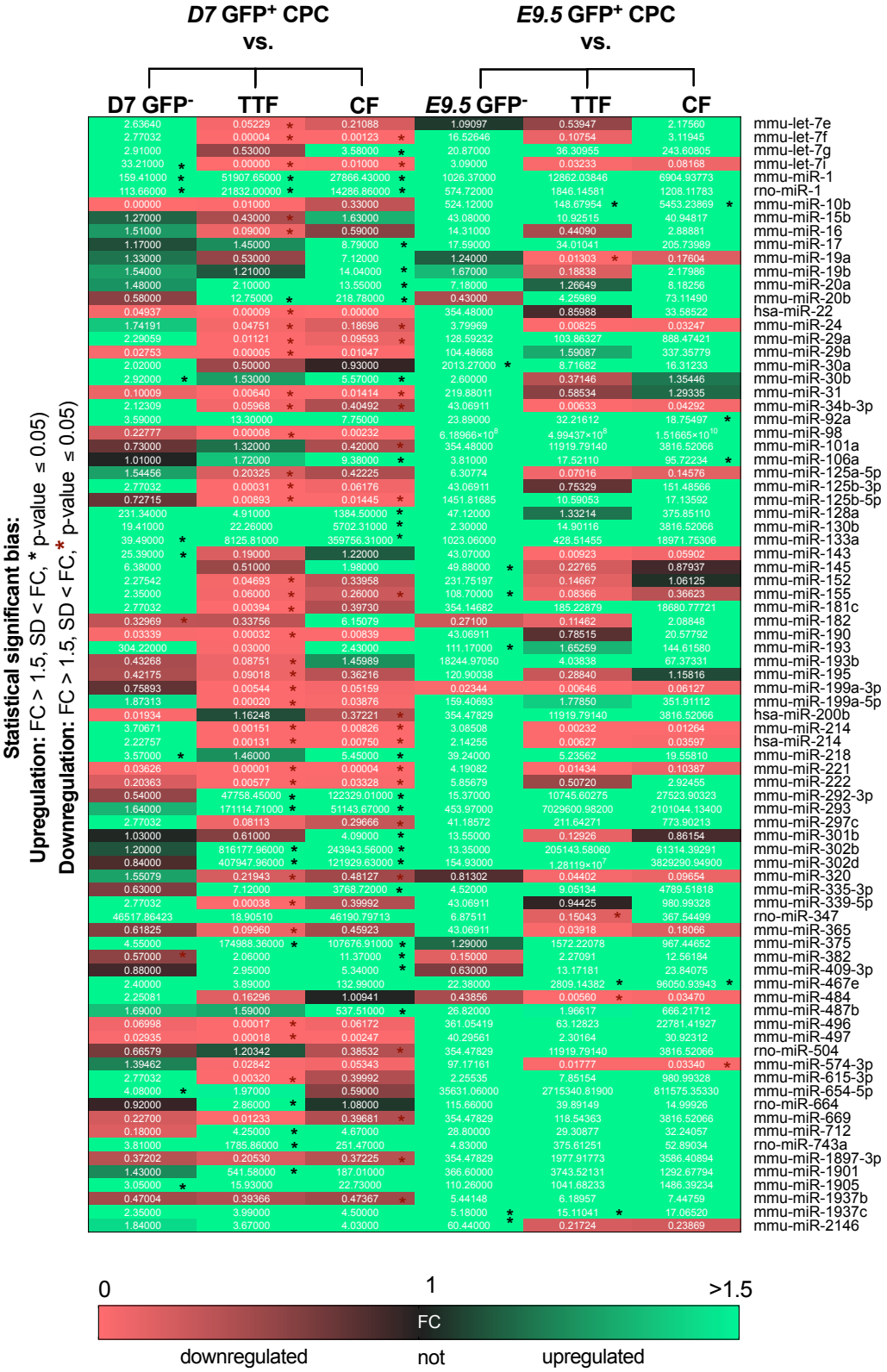

Appendix Figure A15 MicroRNA Array results of up- and downregulated miRs in NkxCE-GFP CPCs. Heat map shows a total of 83 miRs differentially regulated in D7 and E9.5 isolated NkxCE-GFP CPCs (GFP$^+$ CPC) in comparison to their corresponding GFP-negative fractions (GFP$^-$), TTFs and CFs. Among those, 43 miRs were found significantly downregulated whereas 40 were significantly upregulated in GFP+ CPC. Bias upregulated: FC > 1.5, SD < FC, $p \leq 0.05$; Bias downregulated: FC > 1.5 SD < FC, $p \leq 0.05$ (two-sided Student's t-test). Significant values are marked with * (green* for up, red* for down). *Abbreviations: FC, fold change; SD, standard deviation*

B Publications

Hoelscher, S. C., Doppler, S. A., Dreßen, M., Lahm, H., Lange, R., & Krane, M. (2017). MicroRNAs: pleiotropic players in congenital heart disease and regeneration. *Journal of thoracic disease*, 9(Suppl 1), S64 (Hoelscher *et al*., 2017)

Hoelscher SC, Stich T, Diehm A, Lahm H, Dreßen M, Zhang Z, Neb I, Aherrahrou Z, Erdmann J, Schunkert H, Santamaria G, Cuda G, Gilsbach R, Hein L, Lange R, Hassel D, Krane M, Doppler SA. miR-128a Acts as a Regulator in Cardiac Development by Modulating Differentiation of Cardiac Progenitor Cell Populations. *International Journal of Molecular Sciences*. 2020; 21(3):1158 (Hoelscher *et al.*, 2020)

C Oral presentation

47th Annual Meeting of the German Society for Thoracic and Cardiovascular Surgery (DGTHG), *Leipzig, 17.–20.02.2018*: “miR-128: Pleiotropic Player in Cardiac Development”

D Poster presentations

MHA Summer meeting 2017, Bernried, Germany, 03.07.2017: “microRNA-128 in cardiac development”

E Memberships

Young-DZHK (Deutsches Zentrum für Herz-Kreislauf-Forschung e.V.)

F Grants

Visiting Scientist Programme PY.2-B; Mobility program (University of Wisconsin-Madison – 81X3600504) by Munich Heart Alliance (MHA) (Deutsches Zentrum für Herz-Kreislauf-Forschung (DZHK).